Candidate loci in a threshold model of malignant hyperthermia.

Rohan Paranjpe

Submitted in accordance with the requirements for the degree of

Doctor of Philosophy

The University of Leeds

Faculty of Medicine and Health

Leeds Institute of Medical Research at St James's

May 2024

The candidate confirms that the work submitted is their own, except where work which has formed part of jointly authored publications has been included. The contribution of the candidate and the other authors to this work has been explicitly indicated below. The candidate confirms that appropriate credit has been given within the thesis where reference has been made to the work of others.

Chapter 3 includes work featured in the following jointly authored publication;

• Rohan Paranjpe, Christine Diggle, Vikas Kaura, Marie-Anne Shaw, Phil Hopkins. Investigating candidate modifier loci in malignant hyperthermia susceptibility using CRISPR/Cas gene editing. British Journal of Anaesthesia, Volume 130, Issue 2. 2023. https://doi.org/10.1016/j.bja.2022.10.012.

Phil Hopkins and Marie-Anne Shaw were responsible for the conceptual design. Vikas Kaura and Christine Diggle aided the conducting of experiments. Rohan Paranjpe conducted the experiments and was responsible for data collection, analysis and drafting the manuscript. All authors reviewed the drafts of the manuscript and approved the final version.

Acknowledgements

I would like to thank the Royal College of Anaesthetists and the British Journal of Anaesthesia for jointly funding my PhD. I would also like to thank my supervisors; Prof Phil Hopkins, Dr Marie-Anne Shaw, Dr Christine Diggle, and Dr Vikas Kaura. Their unwavering support, guidance and encouragement have been instrumental in my development as a research scientist. I am incredibly grateful to have received their mentorship, for the opportunities to present my research both domestically and internationally, and for my time at the lab.

Thank you to all the members of the MH unit, past and present, for their support and advice during my research. In particular, Ms Catherine Daly who has always been there when I needed help and is essential to the smooth running of the lab. Dr Xiaochen Liu for the troubleshooting and support with western blots. Ms Sarah Hobson and Ms Nickla Fisher for their support and for preparing patient DNA from the MH unit, alongside Catherine, for my case-control study. I would also like to thank Dr Basudha Basu for her technical advice on using CRISPR technologies and Mrs Liz Straszynski for performing FACS.

Finally, I would like to also thank my family, friends and partner for their support over the course of my PhD, without which my studies would have been infinitely more difficult. My mum and brothers' willingness to hear about all my research, and celebrate my accomplishments encouraged me throughout my studies. My partners support through all the challenges I faced throughout my research enabled me to face them head on. I've had an enjoyable experience pursuing my PhD, and this would not have been possible without all the wonderful people who had my back.

Abstract

Malignant Hyperthermia is an inherited pharmacogenetic skeletal muscle disorder, resulting in a hypermetabolic reaction under exposure to volatile anaesthetics or succinylcholine. The most common diagnostic variant for the UK MH cohort is the *RYR1* p.(G2434R) mutation. Previous studies have indicated more than one gene may be involved in susceptibility, suggesting the disorder may adhere to a threshold model of inheritance. Muscle samples from MH patients have shown mitochondrial deficits, and downregulation of metabolic genes has been observed in a mouse model. Additionally, pathogenic variants in *CPT2* and *PYGM* have been identified in susceptible individuals.

CRISPR/Cas gene editing was used to knock-out *Cpt2* and *Pygm* in *Ryr1* heterozygous p.(G2435R mouse myoblasts. Lentivirus transduction was used to introduce pathogenic *CPT2* (p.(S113L), p.(P50H)) and *PYGM* variants (p.(R50X), p.(A193S)) into the knock-out clones. The sensitivity to triggering agents in the genetically modified cells was assessed via live cell calcium imaging. A case-control study was also conducted to identify regions of interest and incidence of pathogenic variants in 10 candidate genes (*ACADVL*, AMPD1, *ATP2A1*, *CACNA1S*, *CACNA2D1*, *CASQ1*, *CPT2*, *PYGM*, *STAC3*, *TRPV1*).

The *Pygm* knock-out clone exhibited increased sensitivity to triggering excitation contraction coupling (ECC) via KCl. The introduction of the p.(R50X) variant led to increased sensitivity to KCl and caffeine, indicating increased RYR1 sensitivity. The introduction of *CPT2* variant p.(S113L) led to increased KCl sensitivity. The introduction of p.(P50H) led to increased caffeine sensitivity. The case-control study revealed several regions of interest across genes involved in ECC, calcium homeostasis and metabolism. Pathogenic variants in *ACADVL* and *PYGM* were also significantly over-represented in MH susceptible individuals.

These results suggest the possible contribution of candidate variants to a threshold model of MH, using a gene editing pipeline novel to MH research, alongside the identification of new candidates for investigation.

Table of Contents

List of Figures

List of tables

List of abbreviations

°C	Degree centigrade
7-AAD	7-Aminoactinomycin D
95% CI	95% confidence interval
aa	Amino acid
ACADVL	Human very long-chain acyl-CoA dehydrogenase gene
Ach	Acetylcholine
ADP	Adenosine diphosphate
AID	Alpha-1 interacting domain
AMPD1	Human adenosine monophosphate (AMP) deaminase 1 gene
ANOVA	Analysis of variance
ATP	Adenosine triphosphate

ATP2A1	Human sarco(endo)plasmic reticulum calcium-ATPase 1 gene
AUC	Area under the curve
BCA	Bicinchoninic acid assay
bp	Base pair
BSA	Bovine serum albumin
c.	Coding sequence number
Ca^{2+}	Calcium ion
CACNA1S	Human alpha-1 subunit of the dihydropyridine receptor gene
CACNA2D1	Human calcium voltage-gated channel auxiliary subunit alpha2delta 1 gene
CADD	Combined Annotation Dependent Depletion tool
Cas	CRISPR associated proteins
CASQ1	Human calsequestrin-1 gene
CASQ1	Human calsequestrin-1 protein
Cav1.1	Alpha-1 subunit of the dihydropyridine receptor
CBA	chicken beta actin promoter
CBh	combined chicken beta actin and cytomegalovirus promoter
cDNA	Complementary DNA
CK	Creatine kinase
cm	Centimetre
CMV	cytomegalovirus promoter
CoA	Coenzyme A
CPT II	Carnitine palmitoyltransferase 2 protein
Cpt2	Mouse carnitine palmitoyltransferase 2 gene
CPT2	Human carnitine palmitoyltransferase 2 gene
CRISPR	Clustered Regularly Interspaced Short Palindromic Repeats
crRNAs	Precursor CRISPR RNAs
Cryo-EM	Cryogenic electron microscopy
Ct	Cycle threshold
C-terminal	Carboxy-terminal
DAPI	4',6-diamidino-2-phenylindole
dCas9	Catalytically inactive Cas9
DEAE-D	Diethylaminoethyl dextran
DHPR	Dihydropiridine receptor
DMEM	Dulbecco's modified
DMSO	Dimethyl sulfoxide

DNA	Deoxyribonucleic acid
dNTPs	Deoxynucleotides
DSB	Double stranded break
E.coli	Escherichia coli
ECC	Excitation contraction coupling
ECL	Entactin-collagen-laminin
ECM	Extracellular matrix
EDTA	Ethylenediaminetetraacetic acid
EGTA	Ethylene glycol tetraacetic acid
EHI	Exertional heat illness
EMHG	European Malignant Hyperthermia Group
EPP	Endplate potential
FACS	Fluorescence activated cell sorting
FBS	Fetal bovine serum
fps	Frames per second
g	Force of gravity
GAPDH	Glyceraldehyde 3-phosphate dehydrogenase protein
GFP	Green fluorescent protein
gnomAD	Genome Aggregation Database
gRNA	Guide RNA
H+	Hydrogen ion
H2O	Water
HCl	Hydrochloric acid
HDR	Homology directed repair
HEK293 FT	Human embryonic kidney 293 cells with SV40 large T antigen
HET	Heterozygous
hFGF	Human fibroblast growth factor
HOM	Homozygous
HRP	Horse radish peroxidase
IDT	Integrated DNA Technologies
IFC	Integrated fluidic circuit
IPTG	Isopropyl β-D-1-thiogalactopyranoside
IVCT	In-vitro contracture test
kb	Kilobase
KCl	Potassium chloride
kDa	Kilodalton

LB	Lysogeny Broth
LD	Linkage disequilibrium
L-type	Long-lasting type calcium channels
Mg^{2+}	Magnesium ion
MH	Malignant hyperthermia
MHN	Malignant hyperthermia normal
MHS	Malignant hyperthermia susceptible
MHSc	Malignant hyperthermia susceptible to caffeine
MHSh	Malignant hyperthermia susceptible to halothane
MHShc	Malignant hyperthermia susceptible to caffeine and halothane
mRNA	Messenger RNA
nAChR	Nicotinic acetylcholine receptor
NAM	Native American Myopathy
NEB	New England Biolabs
NFQ	Non-fluorescent quencher
NGS	Next generation sequencing
NHEJ	Non-homologous end joining
NLS	Nuclear localisation signal
nM	Nanomolar
nm	Nanometre
nt	Nucleotide
N-terminal	Amine terminal
ORAI1	Calcium release-activated calcium channel 1
OXPHOS	Oxidative phosphorylation
p.	Primary amino acid sequence number
P/S	Penicillin-streptomycin
PAGE	Polyacrylamide gel electrophoresis
PAM	Protospacer adjacent motif
PBS	Phosphate buffered saline
PCR	Polymerase chain reaction
psi	Pounds per square inch
PYGM	Human muscle glycogen phosphorylase gene
Pygm	Mouse glycogen phosphorylase gene
RFLP	Restriction fragment length polymorphism
RIN	RNA integrity number
RNA	Ribonucleic acid

RNS	Reactive nitrogen species
ROI	Region of interest
ROS	Reactive oxygen species
RT-qPCR	Real time quantitative pcr
RYR	Ryanodine receptor protein
RYR1	Human ryanodine receptor 1 gene
RYR1	Human ryanodine receptor 1 protein
Ryr1	Mouse ryanodine receptor 1 gene
RYR1	Mouse ryanodine receptor 1 protein
S.pyogenes	Streptococcus pyogenes
S1	RYR1 transmembrane domain helices 1
S2	RYR1 transmembrane domain helices 2
S3	RYR1 transmembrane domain helices 3
S4	RYR1 transmembrane domain helices 4
S5	RYR1 transmembrane domain helices 5
S6	RYR1 transmembrane domain helices 6
SD	Standard deviation
SDS	Sodium dodecyl sulfate
SDS-PAGE	Sodium dodecyl sulfate polyacrylamide gel electrophoresis
SERCA	Human sarco/endoplasmic reticulum Ca2+-ATPase
SERCA1	Human sarco(endo)plasmic reticulum calcium-ATPase isoform 1
SNARE	Soluble NSF attachment protein receptor
SNP	Single nucleotide polymorphism
SR	Sarcoplasmic reticulum
STAC3	SH3 And Cysteine Rich Domain 3 gene
STIM1	Stromal interaction molecule 1
SV40	Polyomavirus Simian Virus 40
T tubule	Transverse tubule
TBE	Tris-borate-EDTA buffer
TBS	Tris buffered saline
TBST	Tris buffered saline with tween
TE	Tris EDTA
TEMED	N,N,N',N'-tetramethylethane-1,2-diamine

1 Introduction

1.1 Malignant hyperthermia

Malignant hyperthermia is an inherited disorder characterised by Ca^{2+} dysregulation, affecting excitation-contraction coupling and ultimately leading to uncontrolled metabolism (Rosenberg et al., 2015). The vast majority of functionally characterised causative variants for MH occur in *RYR1*, with few diagnostic variants also found in *CACNA1S* (Miller et al., 2018, European Malignant Hyperthermia Group). Another gene suggested to play a role in pathogenesis is *STAC3*, due to the high incidence of MH among patients with SH3 and cysteine rich domain 3 (STAC3) disorder (Stamm et al., 2008) and a zebrafish model indicating decreased excitation contraction coupling (ECC) (Horstick et al., 2013). Calsequestrin 1 has also been suggested as playing a potential role in MH due to experiments in knock-out mice indicating MH phenotypes, such as mortality upon anaesthetic exposure (Protasi et al., 2009).

Mitochondrial disorders, such as Luft's disease and *MT-ND3* associated mitochondrial myopathy, have also been linked to MH, with patients exhibiting MH-like reactions or abnormal *in vitro* contracture test (IVCT) results (Finsterer et al., 2009). Recent experimental studies have also indicated mitochondrial dysfunction in MHS human muscle and knock-in mice. Specifically, human MH susceptible (MHS) muscle fibres have significantly decreased flux control ratios in complexes I and II, both before and after exposure to halothane, compared to MH normal (MHN) fibres, despite an increased mitochondrial mass (Chang et al., 2019). In a knock-in mouse model of the most common causative variant for MH in the UK, metabolic defects were indicated in the form of reduced expression of genes associated with fatty acid oxidation, such as *CPT2* and *ACADVL*, alongside an increase in the production of reactive oxygen species under basal conditions (Chang et al., 2020). These studies

indicate the potential in investigating candidate genes related to metabolism and mitochondrial function for contribution to MH pathogenesis.

1.1.1 Clinical characteristics of malignant hyperthermia

Malignant hyperthermia is a potentially fatal pharmacogenetic disorder, which presents as a hypermetabolic reaction upon exposure to volatile anaesthetics or succinylcholine (Hopkins, 2011). An MH crisis may occur any time under anaesthesia and up to 60 minutes after discontinuation of triggering agents (Litman et al., 2008). Signs of an MH reaction include tachycardia, muscle rigidity, a rise in end-tidal carbon dioxide and hyperthermia (Rosenberg et al., 2015). The uncontrolled hypermetabolic reaction may also lead to rhabdomyolysis, leading to increased serum creatine kinase levels, and respiratory and metabolic acidosis. Untreated rhabdomyolysis may result in life-threatening hyperkalaemia and myoglobinuria (Rosenberg et al., 2015). Additional fatal complications may also include dysfunction in vital organs, such as congestive heart failure, and disseminated intravascular coagulation (DIC). In particular, DIC is typically the cause of death in an MH crisis, especially if patient temperature exceeds 41ºC (Rosenberg et al., 2015).

The only currently known treatment for all MH crises is the administration of dantrolene (Glahn et al., 2020). Dantrolene reduces the voltage-induced Ca^{2+} release from the sarcoplasmic reticulum (SR) in an MH crisis (Ellis & Bryant, 1972). Specifically, it has been found to bind to ryanodine receptor isoform 1 (RYR1) at amino acids 590-609 (Paul-Pletzer et al., 2002). Dantrolene alters the interaction between RYR1 and the dihydropyridine receptor (DHPR) in an inhibitory manner, and is dependent on RYR1 expression (Bannister, 2013).

1.1.2 Diagnosing malignant hyperthermia

Susceptibility to MH can be diagnosed using the IVCT in which the contractile responses of muscle biopsies challenged with halothane and caffeine are used to diagnose the individual (European Malignant Hyperpyrexia Group, 1984). The IVCT remains the gold standard of diagnosis (figure 1.4), with a specificity of 94% (95% confidence interval 89.2-96.5) and sensitivity of 99% (95% confidence interval 94.8-100) (Hopkins et al., 2015; Ording et al., 1997). Alternatively the caffeine-halothane contracture test may also be used, such as in North America, where susceptibility is determined based on response to 3% halothane or 2mM caffeine (Allen et al., 1998). Although, this test has an estimated sensitivity of 97% and specificity of 78% in optimal conditions, and may range to 62% sensitivity and 87% specificity depending on which combination of measurements are used to determine susceptibility (Allen et al., 1998).

For the IVCT, muscle biopsies are taken from either the *vastus medialis* or *vastus lateralis* and must be 20-25mm in length, 2-3mm in thickness, and 100-200mg in weight. Muscle specimens are subsequently placed in precarboxygenated Krebs-Ringer solution and electrically stimulated to assess viability and record baseline tension. Muscle is then exposed to increasing concentrations of halothane (0.11, 0.22 and 0.44 mmol/L; equivalent to 0.5, 1.0 and 2.0 Vol%) and caffeine (0.5, 1.0, 1.5, 2.0, 3.0, 4.0, and 32 mmol/L) (EMHG, 1984). A tension of ≥0.2g from the baseline in response to 2% halothane and/or 2mM caffeine is used as the threshold for determining an MH null (MHN) or susceptible (MHS) status. The MHS status is further subcategorised into whether susceptibility was determined based on both halothane and caffeine (MHShc), halothane only (MHSh) or caffeine only (MHSc) (Hopkins et al., 2015), with IVCT phenotype correlating with the severity of clinical phenotype (Carpenter, Robinson, et al., 2009) and observable differential

expression of genes associated with mitochondrial bioenergetics between MHS subtypes (Chang et al., 2024).

Typically, an index case will be referred to for an IVCT, however, DNA screening is an alternative method of diagnosis, should they carry one of 68 pathogenic variants that are sufficiently functionally characterised to be used diagnostically. Relatives of individuals with a known diagnostic variant may also be referred for genetic testing instead (figure 1.5). This diagnostic approach however is limited due to the need for further research into the genetic basis of MH. For example, many more variants have been associated with MH susceptibility however have not been sufficiently functionally characterised for diagnostic use. Typically this is due to the identification of variants in MHS patients, but lacking models for functional characterisation, such as *in vitro* cell models, or lacking genetic characterisation, such as family studies showing co-segregation with the disease (Hopkins et al., 2015). Therefore, currently the IVCT remains the gold standard of diagnosis.

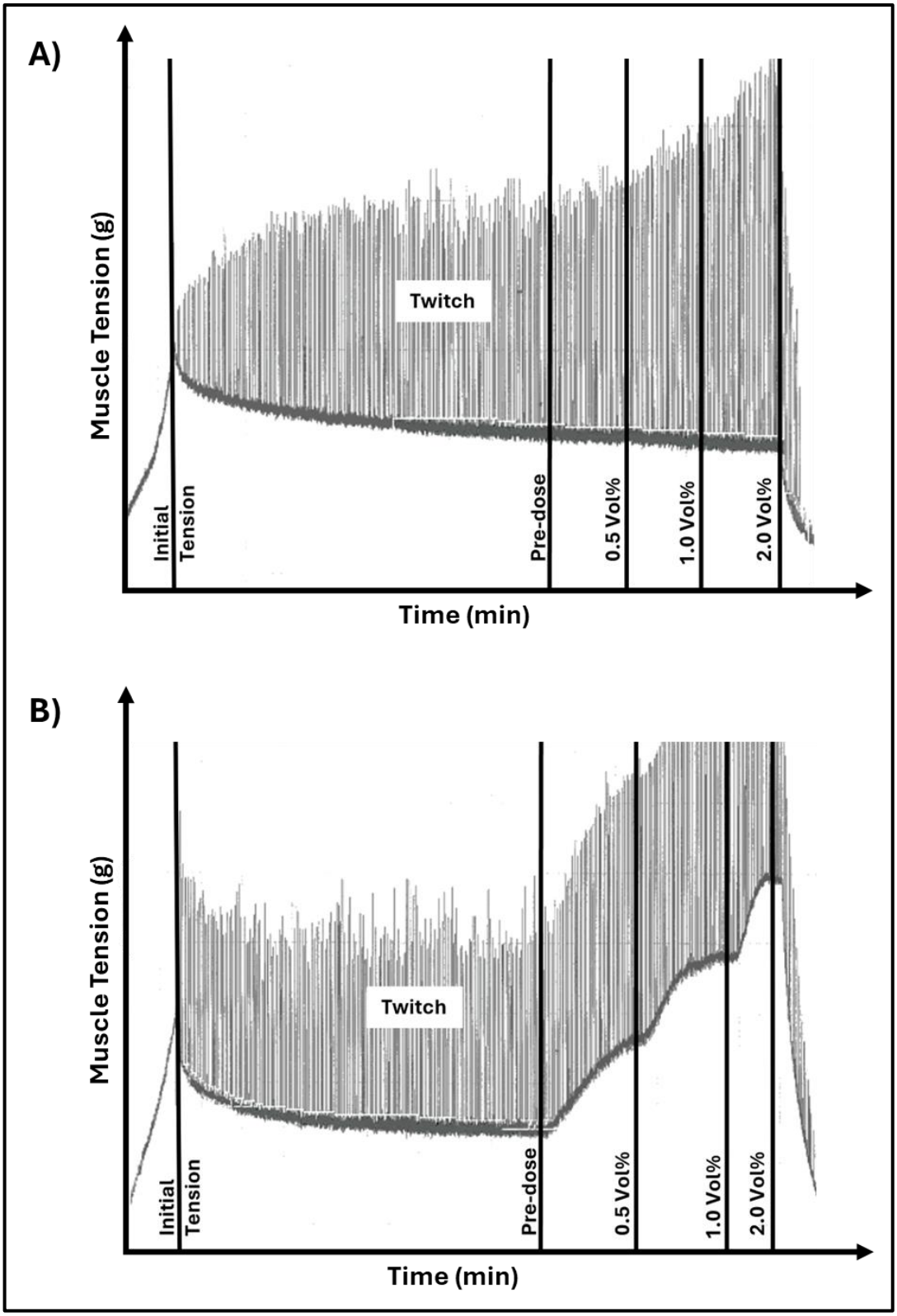

Figure 1.1: *In vitro* contracture test traces for halothane. Representative IVCT traces showing a halothane test for A) MHN and B) MHS individuals. Twitch is generated by applying electrical stimulation to muscle biopsy and indicates the viability of the sample. An initial tension is applied, after which the muscle is allowed to relax. Pre-dose indicates the baseline tension measurement taken prior to successive exposure to 0.5, 1.0 and 2.0 Vol% of halothane. Halothane lines on trace indicate the point at which the tension has plateaued, and a measurement can be made.

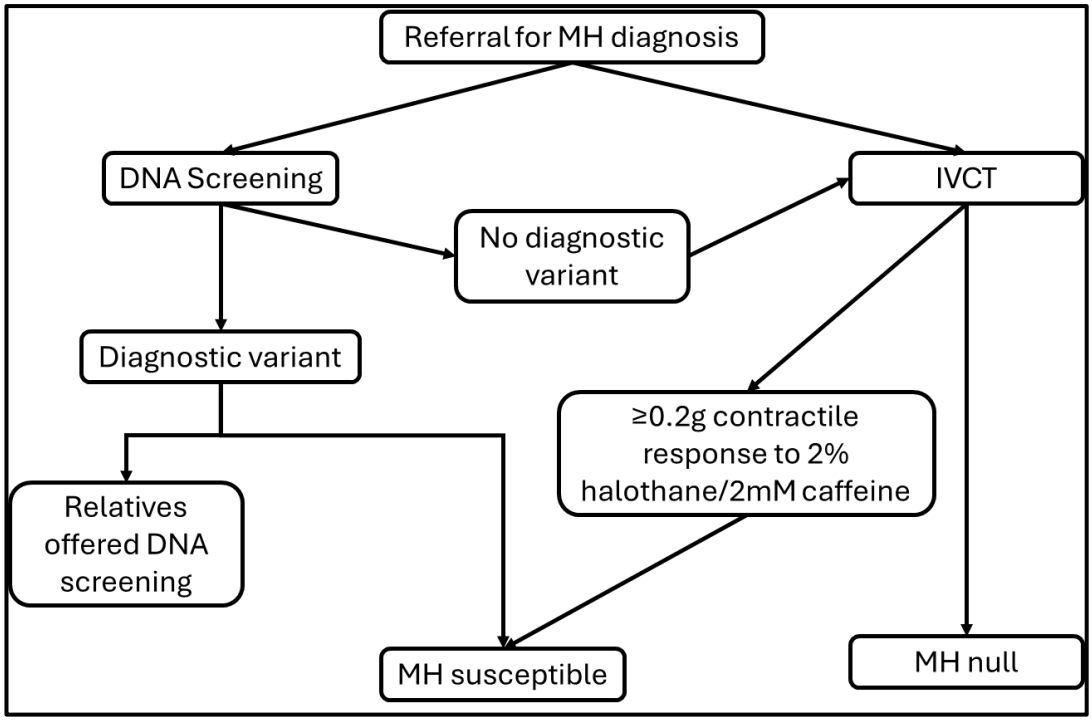

Figure 1.2: Diagnostic flowchart for investigating malignant hyperthermia susceptibility. Choice of diagnosis via DNA screening or IVCT is made on a case-by-case basis. Those identified as MH susceptible will also be considered candidates for further research.

1.1.3 Malignant hyperthermia genetics

Calcium dysregulation is at the centre of MH pathogenesis, and it follows that pathogenic variants in *RYR1*, *CACNA1S* and *STAC3* have been associated with disorder (see sections 1.3.1 -1.3.3). The majority of susceptible individuals in the UK have a pathogenic variant in *RYR1* (~73%), whilst pathogenic variants in *CACNA1S* and *STAC3* combined account for <2%. Additionally, it was also shown that around ~10% of MH susceptible families had more than one potentially pathogenic variant across the three genes (Ibarra Moreno et al., 2019; Miller et al., 2018; Robinson et al., 2006).

RYR1 is a ~15kb gene with 106 exons at chromosomal location 19q13.2, and was originally linked to MH following the observation of co-segregation of *RYR1* restriction fragment length polymorphisms (RFLP) with the MH phenotype (MacLennan et al., 1990). Hundreds of pathogenic variants in this gene have been associated with malignant hyperthermia, however only 66 meet the functional

characterisation criteria and are currently accepted for diagnostic use by the EMHG. The most common causative variant for MH in the UK is the *RYR1* c.7300C>G: p.(G2434R) variant, accounting for ~16% of susceptible families (Miller et al., 2018). Pathogenic variants in *RYR1* lead to a gain-of-function effect, thus increasing the sensitivity to activation and ultimately resulting in Ca^{2+} dysregulation. Specifically, a mouse model of the p.(G2434R) variant exhibited increased sensitivity to triggering agents and increased intracellular [Ca^{2+}] both at before and after challenge (Lopez et al., 2018).

CACNA1S is a ~6kb gene with 44 exons at chromosomal location 1q32.1, and was first linked to MH in a French family exhibiting co-segregation of the c.3333A>G: p.(R1086H) variant with the susceptible phenotype (Monnier et al., 1997). 11 potentially pathogenic variants were observed across 12 (~1.7%) MHS families in the UK, of which only 2 (p.(R1086H) and p.(R174W)) are classified as diagnostic by the EMHG (Miller et al., 2018). The c.520C>T: p.(R147W) variant was associated with MH in UK families, and thought to affect voltage sensing due to residing in the S4 domain of the alpha-1-subunit of the DHPR (Carpenter, Ringrose, et al., 2009). The p.(R1086H) variant is located in the III-IV loop and disrupts the negative regulator role of the loop (Weiss et al., 2004). Both diagnostic variants, alongside other functionally characterised pathogenic variants in *CACNA1S* (Kaura et al., 2022; Pirone et al., 2010), have been shown to increase RYR1 sensitivity.

STAC3 is a ~1.1kb gene with 12 exons at chromosomal location 12q13.3, and is linked to STAC3 myopathy (Native American Myopathy) (Horstick et al., 2013). This is an autosomal recessive disorder which has been linked to malignant hyperthermia susceptibility (Bailey & Bloch, 1987). Specifically, an assessment patients with the myopathy showed a 29% incidence of MH susceptibility (Stamm et al., 2008) and 55% incidence of adverse MH-like reactions under general anaesthetic (Zaharieva et al., 2018). The most common pathogenic variant in this

gene is c.851C>G: p.(W28S), and in a corresponding zebrafish model decreased excitation-contraction coupling was observed (Horstick et al., 2013). Only one MH susceptible proband was found to be homozygous for a pathogenic *STAC3* variant (p.(W284S)) in a UK study (Miller et al., 2018), and there are currently no diagnostic *STAC3* variants for MH as classified by the EMHG due to the lack of functional characterisation.

1.1.4 Malignant hyperthermia epidemiology

MH is a rare intraoperative event, with an estimated incidence ranging from 1:3000 to 1:100,000 in the UK, with an increased sex prevalence in males (2:1) (Gupta & Hopkins, 2017) and children (Rosenberg et al., 2015). However, the prevalence of MH susceptible individuals may actually be much higher, estimated at around 1:1500 based on those that may carry a *RYR1* variant that predisposes to MH (Shaw & Hopkins, 2019). The difference between these estimates is likely due to the fact that an MH crisis may not always occur in an MH susceptible individual upon exposure to triggering agents (Ibarra Moreno et al., 2019), and compounded by the occurrence of individuals that may never receive triggering agents.

Clinically, the risk of developing an MH reaction when considering genetics has been seen as an all or nothing occurrence (Hopkins, 2000a). Furthermore, the heterogeneity in clinical phenotypes, such as triggering on a second or later anaesthetic exposure, variation in onset time and serum CK, has been assumed to be due to environmental factors. This has not been thoroughly investigated, and as such it remains unclear whether the clinical heterogeneity is truly due to environmental factors or genetic contributors as of yet unidentified. There have been case reports of individuals suffering stress, trauma or heat induced hyperthermia (Feuerman et al., 1988; Gibbs et al., 2019; Gronert et al., 2011), however these are rare, with limited reports of such cases over the years. Additionally, the grade or classification of an MH reaction is largely dependent on

the time to diagnosis and the treatment implementation, as well as being influenced by the availability of complete clinical data, which is not commonly present (Carpenter, Robinson, et al., 2009; Gupta & Hopkins, 2017). This makes it difficult to establish individual environmental contributions and their importance in an MH crisis, alongside factors such as stress, fever and trauma. In particular, the rarity of the disease means data is limited, which combined with only partly complete clinical patient data limits the power and possibility of analyses even in larger datasets to discern environmental contributions. However, it has been proposed that the rate of development of clinical symptoms may be dependent on the rate of Ca^{2+} accumulation in skeletal muscle, which in turn may be dependent on specific genetic defects (Carpenter, Robinson, et al., 2009). Further work is required within the field to identify consistent quantifiable clinical symptoms that could be used to elucidate the extent of possible environmental contributions to the disorder and the rate of Ca^{2+} accumulation.

Furthermore, pathogenic variants in *RYR1*, *CACNA1S*, and *STAC3* only account for ~75% of MH susceptible UK families (Miller et al., 2018), highlighting a gap in our knowledge of the genetic basis of malignant hyperthermia. Additionally, segregation analysis of MH susceptible UK families revealed that ~25% had at least one case of genotype-phenotype discordance. Specifically, ~75% of discordant families with a pathogenic or likely pathogenic had at least one case of an individual with a positive phenotype but didn't have the familial variant, and ~34% had at least one case of an individual with the familial variant but a negative phenotype (Miller et al., 2018). The rate of discordance was also shown to be significantly more than the false positive rate of the IVCT.

This highlights two important aspects of the current understanding of the genetic epidemiology and basis of MH. Firstly, the high incidence of individuals that do not carry a familial variant but test positive for MH indicates the gap in knowledge of

variants associated with the disorder. Secondly, the high incidence of individuals that do carry a familial variant, but do not test positively for MH alludes to the possible need for additional contributory factors to meet the threshold of triggering. Indeed, this has also been suggested previously where other additional loci were suggested to be implicated in 77 MH susceptible UK families with a major gene effect (ROBINSON et al., 2000), as well as in the study assessing the genetic epidemiology of MH in the UK (Miller et al., 2018).

1.1.5 Variation in MH phenotypes

A 2009 study assessed the quantitative phenotypes of malignant hyperthermia in a total of 504 susceptible individuals from 203 families with a *RYR1* variant associated with MH (Carpenter et al., 2009). The findings showed that the specific *RYR1* variant of an individual was a significant determinant of the severity of laboratory phenotype. Furthermore, there was a significant correlation between the IVCT contracture response and the onset time of a clinical MH event. Specifically, it was noted that c.487C>T: p.(R163C), c.6488G>A: p.(R2163H), c.7304G>A: p.(R2435H) and c.14477C>T: p.(T4826I) variants presented relatively severe IVCT phenotypes with stronger contractures and shorter response times to triggering agents, whilst the relatively common p.(G2434R) variant was associated with a relatively mild IVCT phenotype. These results showed the genotype-phenotype correlation of *RYR1* variants and the corresponding MH clinical variation. In fact, it was suggested that these results would allude to a non-mendelian threshold model for malignant hyperthermia. Additionally, for disorders that overlap with MH, see section 1.4.

1.1.6 Threshold model

Malignant Hyperthermia has historically been modelled as autosomal dominant, and due to the phenotype-genotype discordance, with incomplete penetrance (Ibarra Moreno et al., 2019; Shaw & Hopkins, 2019). However, as the wealth of studies alluding to additional contributory genetic factors suggest, it may better be explained with an alternative non-mendelian threshold model. In fact this is not unique to MH, and has been suggested that the observation of reduced penetrance in disorders presumed to have Mendelian inheritance may better be explained by non-Mendelian models (Scriver & Waters, 1999). The combination of observed genotype-phenotype discordance in MH susceptible families, the correlation between *RYR1* variants and clinical MH phenotypes, and the potential contribution of additional loci in susceptible families with a major gene effect, all make the prospect of a non-mendelian threshold model for MH much more likely. This model would suggest that there is a threshold of dysfunction that must be met in order to confer a MH phenotype. In the case of 'strong' variants, these alone may be enough to meet the threshold, as is seen in the case of the p.(R163C) variant for example. However, 'weaker' variants may require additional contributors, potentially in the form of genetic modifier loci, that may compound in order to meet the required threshold for triggering. It is in fact in the relatively mild and common p.(G2434R) variant that we see a comparatively higher number of families with an individual with the variant but a negative phenotype (Miller et al., 2018). It would seem likely that in this case the difference between a relative with the variant and positive IVCT, and an individual with the variant but a negative IVCT, would possibly be additional genetic contributors as of yet untested for. This is a current avenue for investigation, particularly whether the number of *RYR1* variants correlates with any clinical phenotypes (personal communications Phil Hopkins, UK MH unit). However, individuals carrying multiple pathogenic *RYR1* variants are very rare. Therefore, the scope for meaningful statistical analysis is limited. However, widening the

investigation for multiple genes may enable meaningful insights into the potential contributions of additional variants and a threshold model of MH.

Although the threshold model has been suggested in the several studies regarding malignant hyperthermia, there is a requirement for the further identification of candidate modifier loci. Additionally, there is no functional data investigating the contributory effects of candidate variants. Thus, there is a need for further genetic epidemiological studies assessing the prevalence of additional candidate variants in MHS individuals as well as exploration into over-represented genetic regions in the MHS population. Additionally, direct functional studies utilising recent gene editing technologies, such as CRISPR/Cas, in concert with models of MH and established functional assays to assess the contribution of additional candidate variants would be novel and useful in establishing functional evidence of a threshold model.

1.1.7 Models of malignant hyperthermia

Malignant hyperthermia occurs not only in humans, but various other mammals as well, and early research consisted of studying porcine models of MH (Fujii et al., 1991). Unlike in humans, MH in pigs is inherited in an autosomal recessive fashion and leads to stress-induced MH events that mimic the anaesthetic-triggered reactions in humans, with symptoms including tachycardia, muscle rigidity, hyperthermia and metabolic acidosis (Mitchell & Heffron, 1982).

Modern MH research focuses on the use of mouse models, patient-derived cell lines, both patient and mouse muscle biopsies, and RYR1 induction in human embryonic kidney (HEK) cells (Chang et al., 2019, 2020; Lopez et al., 2018; R. White et al., 2022). The first HEK293 model induced heterologous expression of cDNAs containing rabbit *RYR1* and investigated the caffeine and halothane sensitivity of 15 pathogenic mutations (Tong et al., 1997). Patient muscle samples were also used around this time to functionally characterise the pathogenic *RYR1*

p.(R163C) and p.(G2434R) variants (Brinkmeier et al., 1999; Censier et al., 1998). The generation of *RYR1*-null (dyspedic) mice was also achieved previously via the insertion of a neomycin cassette into exon 2 of the *RYR1* gene to disrupt gene function during mouse embryonic development (Takeshima et al., 1994). These were subsequently used to introduce *RYR1* mutations, generated via site directed mutagenesis of rabbit *RYR1* cDNA constructs, seen in central core disease and MH for functional characterisation (Avila & Dirksen, 2001; Yang et al., 2003).

Of particular interest are mouse models of MH, as *in vivo*, *ex vivo* and *in vitro* characterisations of the disorder could be made, enabling comprehensive investigation of MH phenotypes. The phylogenetic relatedness, physiological similarity to humans and the controlled genetic background of mouse models which reduces variability when characterising variants can make mouse models a useful tool in the research of rare diseases (Perlman, 2016). The first MH mouse model developed was a *Ryr1* p.(Y522S) knock-in model using site directed mutagenesis, which led to adoption of this technique for MH research (Chelu et al., 2006). In total, 7 knock-in mouse models with pathogenic variants associated with MH currently exist (table 1.1). All four RYR1 knock-in models typically exhibit increased sensitivity to RYR1 agonists *in vitro*, onset of hyperthermia upon exposure to triggering agents *in vivo*, and elevated intracellular calcium levels (Chelu et al., 2006; Lopez et al., 2018; Yang et al., 2006; Yuen et al., 2012). A STAC3 p.(W280S) knock-in mouse model has also been generated to investigate the corresponding STAC3 myopathy associated human variant associated for MH susceptibility (personal communications, Christine Diggle). Of the two *CACNA1S*knock-in models, the p.(T1009K) mice also exhibit similar phenotypes to the RYR1 knock-in mice (Kaura et al., 2022). The *CACNA1S* p.(R174W) knock-in mice, however, did not develop fulminant malignant hyperthermia in response to halothane or heat stress (see sections 1.1.2 and 1.4) (Feng et al., 2023). The p.(R174W) mice were

developed based on the identification of this variant in an MHS patients (Carpenter, Ringrose, et al., 2009) and the previous work showing increased sensitivity to caffeine and halothane in primary mouse myotubes dysgenic for *CACNA1S* that had the p.(R174W) variant introduced (Eltit et al., 2012).

The case of the p.(R174W) mouse models highlights some of the issues that can crop up when using mice to model human disease. Despite the high genetic homology between humans and mice (Mouse Genome Sequencing Consortium et al., 2002), there are often phenotypic differences in modelling genetic disorders in mice relative to humans (Elsea & Lucas, 2002). This also seems to be the case for the p.(R174W) mice. Another interesting point to note is the discrepancy between p.(R174W) mouse and the dysgenic myoblasts that have had the same variant transduced, highlighting that different ways of modelling in mice may also produce different results. Ultimately, mouse models can provide a powerful tool for elucidating the aetiology of MH, but they are not without their drawbacks, and these should be considered when utilising them.

Table 1.1: Knock-in mouse models of MH. A summary of the knock-in mouse models developed based on pathogenic variants associated with malignant hyperthermia.

Gene	Exon	Amino Acid change	DNA change	Reference
RYR1	14	p.(Y522S)	c.1565A>C	Chelu et al., 2006
RYR1	6	p.(R163C)	c.487C>T	Yang et al., 2006
RYR1	100	p.(T4826I)	c.14477C>T	Yuen et al., 2016
RYR1	45	p.(G2435R)	c.7300G>A	Lopez et al., 2018
CACNA1S	4	p.(R174W)	c.520C>T	Feng et al., 2023
CACNA1S	7	p.(T1009K)	c.3026C>A	Kaura et al., 2022
STAC3	3	p.(W280S)	c.851G>C	Pers. Comms., C.Diggle

Although the above detailed developments in MH have enabled the characterisation of pathogenic variants, there is a lack of investigation into a threshold model. The research has typically focused on utilising established gene editing techniques to

generate new animal models that exhibit a major gene effect. The utilisation of current gene editing technologies and the investigation of animal models of modifier loci is an avenue not yet explored. These studies do however provide the established models of MH which may form the foundation for the investigation of modifier loci and investigation of the threshold model of MH.

1.2 Skeletal muscle structure

Skeletal muscle is composed of ~75% water, ~20% protein, and ~5% fat and carbohydrates, representing ~40% of total human body weight (Frontera & Ochala, 2015). Skeletal muscle structure consists of three layers of connective tissue (epimysium, perimysium, and endomysium) that separate muscle fibres and fibre bundles (fascicles) (figure 1.1). Each mature muscle fibre is a post-mitotic, multinucleated cell surrounded by the sarcolemma.

Due to the presence of satellite cells, muscle tissue is also capable of regeneration. Satellite cells, once activated, differentiate into myoblasts which go on to differentiate and merge into the final multinucleated muscle fibres. This can also be observed *in vitro* where myoblasts will differentiate and merge to form myotubes (Yin et al., 2013).

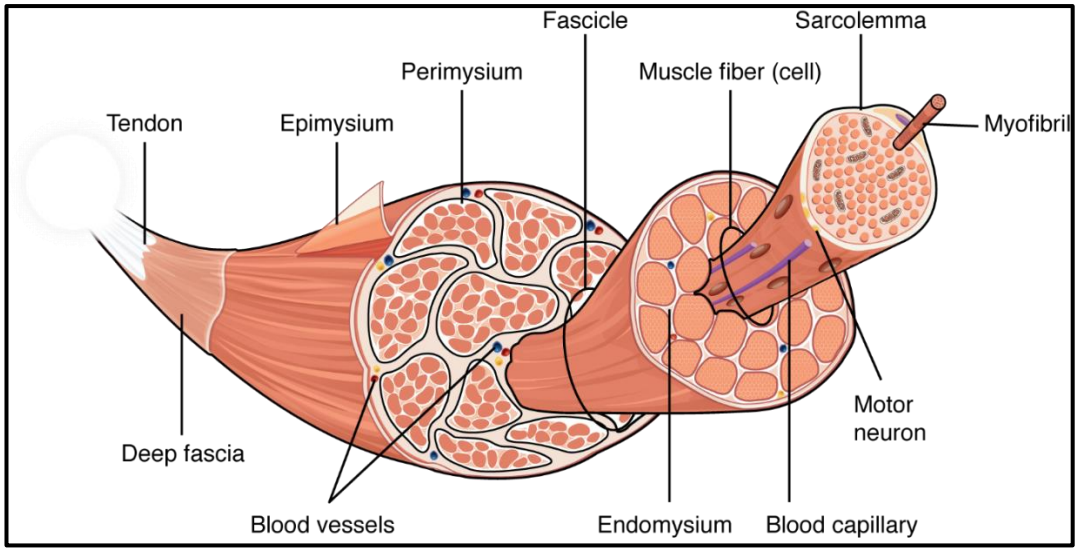

Figure 1.3: Skeletal muscle structure. The epimysium is the outer most layer of connective tissue that surrounds skeletal muscle, holding numerous fascicles within it. The perimysium is the next layer that surrounds each fascicle. Finally, the endomysium separates individual fibres within a fascicle. Each fibre is single, post-mitotic, multinucleated cell with rod-like contractile organelles called myofibrils (Frontera & Ochala, 2015). This image is an adaptation from (OpenStax, 2013), available under the terms of the Creative Commons Attribution 4.0 international license (https://creativecommons.org/licenses/by/4.0/deed.en).

Mammalian skeletal muscle fibres may also be categorized into subtypes. Broadly, slow-twitch type I fibres are specialised in oxidative metabolism, and fast-twitch type II fibres are generally specialised in glycolytic metabolism (Schiaffino & Reggiani, 2011). Type II fibres may be further subcategorised into IIA (fast-twitch, oxidative metabolism), which act as a hybrid between type I and II fibres, and types IIX and IIB (fast-twitch, glycolytic metabolism). The *vastus lateralis* and *vastus medialis* muscles biopsied for IVCT are largely composed of types I and IIA, indicating their specialisation in oxidative metabolism (Staron et al., 2000; Stockmar et al., 2006). The main difference between the use of oxidative and glycolytic metabolism in muscle is based on their energy needs and the resulting fatiguability. Oxidative metabolism generates more ATP by utilising oxidative phosphorylation and aerobic pathways, whilst glycolytic metabolism produces less ATP and relies on anaerobic pathways such as glycolysis (Schiaffino & Reggiani, 2011). It is important to note that both oxidative and glycolytic metabolism utilise glycolysis, however glycolytic metabolism essentially stops at this point, whilst oxidative metabolism goes further

as well as being able to utilise other substrates such as fats and protein for energy production.

Furthermore, muscle fibres are comprised of repeating units called sarcomeres, which is the basic effective unit of skeletal muscle tissue (figure 1.2). The sliding filament theory explains skeletal muscle contraction through the shortening of sarcomeres via cross bridge cycling (A. F. Huxley & Niedergerke, 1954; H. Huxley & Hanson, 1954).

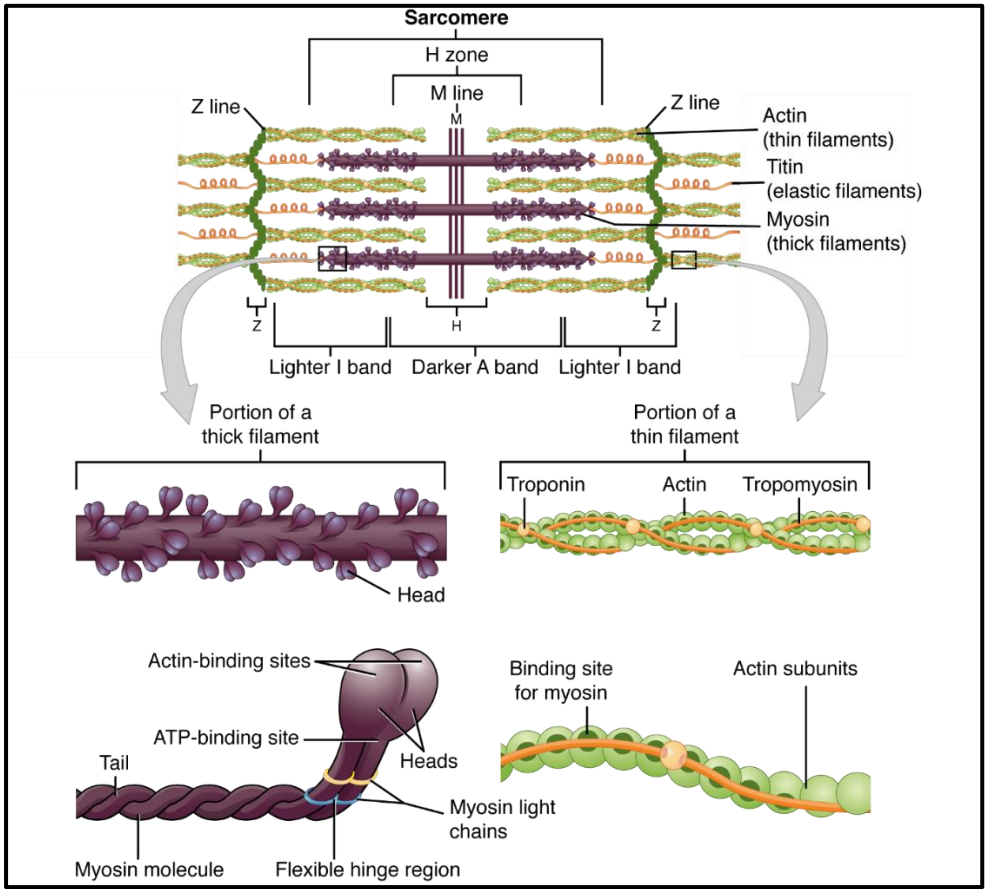

Figure 1.4: Sarcomere structure. The lighter I band in a sarcomere contains the actin filaments, whilst the darker A band contains myosin filaments. Troponin and Tropomyosin control the binding of myosin to actin. Tropomyosin blocks the myosin binding site on actin, at rest, thus preventing contraction. However, when Ca^{2+} binds to troponin, it undergoes a conformational shape change, shifting the position of the tropomyosin and allowing myosin to bind. This subsequently initiates cross bridge cycling leading to sarcomere shortening, due to the tethering of actin to the Z lines, and thus muscle contracture. During cross-bridge cycling ATP is bound to myosin and is catalysed into ADP and phosphate to generate energy for the contraction. Titin maintains the structural integrity of the sarcomere during contraction and relaxation. This image is an adaptation from (OpenStax, 2013), available under the terms of the Creative Commons Attribution 4.0 international license (https://creativecommons.org/licenses/by/4.0/deed.en).

1.3 Excitation contraction coupling

The stimulation of muscle fibres by motor neurons, resulting in muscle contraction via sarcomere shortening is known as excitation contraction coupling (Sandow, 1952). An action potential travels towards the neuromuscular junction and depolarises the terminal bouton. This results in activation of voltage gated calcium channels, leading to an influx of Ca^{2+} into the presynaptic cytosol. The increase in Ca^{2+} levels causes intracellular vesicles of acetylcholine (ACh) to fuse to the cell membrane through soluble N-ethylmaleimide-sensitive factor attachment protein receptor (SNARE) proteins, releasing the neurotransmitter into the synaptic cleft. ACh binds to nicotinic acetylcholine receptors (nAChR) on the motor endplate, causing an influx of Na^{+} ions and generating the endplate potential (EPP) (Shishmarev, 2020).

This depolarisation travels along the sarcolemma and into transverse tubules (T-tubules) resulting in Ca^{2+} release and muscle contraction (figure 1.3) (Calderón et al., 2014). Key components of Ca^{2+} release in myocytes include the L-type voltage gated Ca^{2+} channel, DHPR, the Ca^{2+} release channel RYR1, and STAC3. The DHPR is located within the sarcolemma in T-tubules and is crucial to sensing the voltage change (Rios & Brum, 1987) caused by the travelling action potential. The DHPR signals RYR1, situated in sarco-endoplasmic reticulum (SR) membrane, to release Ca^{2+} from the SR lumen in an orthograde manner (Lanner et al., 2010), whilst STAC3 mediates the retrograde signalling between RYR1 and DHPR (Horstick et al., 2013).

Additional to the key components of ECC above, many other proteins also play roles in this process. Junctophillin is key to forming junctions between the plasma membrane and SR at T-tubules (Takeshima et al., 2000). Calsequestrin 1 is a Ca^{2+} binding protein in the SR that acts as a calcium buffer and sensor (Kumar et al., 2013). In concert with junctin and triadin, transmembrane proteins in the SR,

calsequestrin 1 has also been shown to inhibit RYR1 (Györke et al., 2004). Sarco-endoplasmic reticulum calcium-ATPase 1 (SERCA1), encoded by *ATP2A1*, is the fast isoform of the Ca^{2+} ATPase that sequesters cytosolic calcium back into the SR lumen to replenish calcium stores (Zhang et al., 1995). Transient receptor potential cation channel subfamily V member 1 (TRPV1) was also identified as a functional SR calcium leak channel, associated with the SR membrane and was suggested to cross-talk with RYR1 (Lotteau et al., 2013).

Aside from the canonical role of ECC in muscle contracture, other methods of calcium entry also exist. Store-operated calcium entry describes the mechanism of replenishment of Ca^{2+} stores in the SR upon depletion, and is thought to occur via the interactions between stromal interaction molecule 1 (STIM1) and the calcium release-activated calcium channel 1 (ORAI1) (Roos et al., 2005). Excitation coupled calcium entry is also shown to occur upon depolarisation of the sarcolemma, regardless of calcium depletion, and is absent in mice without RYR1 or DHPR (Cherednichenko et al., 2004). Finally, calcium induced calcium release also occurs whereby Ca^{2+} released from the SR triggers further release by RYR1, and appears to be important in caffeine contracture and MH (Endo, 2009).

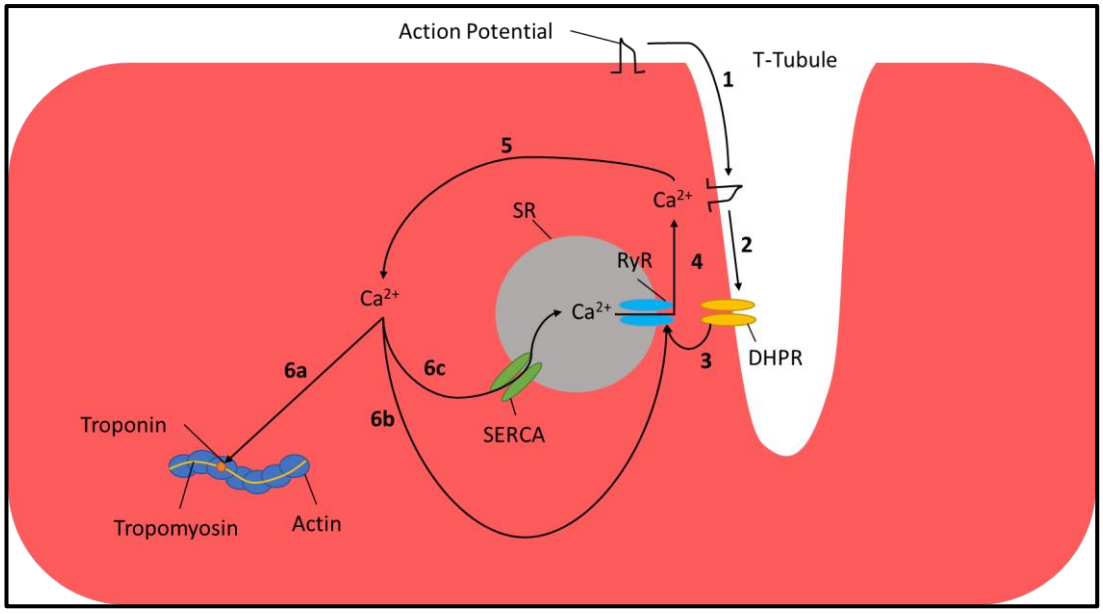

Figure 1.5: Diagrammatic representation of excitation contraction coupling. 1) the depolarisation caused by acetylcholine binding, travels across the sarcolemma and down the t-tubule. 2) dihydropyridine receptor (DHPR) senses the voltage change. 3) DHPR undergoes a conformational shape change and acts as an allosteric activator of the ryanodine receptor (RyR), mediated by STAC3. 4) RyR releases calcium stored in the sarco-endoplasmic reticulum (SR). 5) The release of calcium increases the cytosolic calcium concentration. 6a) calcium binds to troponin, causing a conformational shape change of tropomyosin, allowing myosin to bind to actin and resulting in sarcomere shortening and muscle contraction. 6b) the decrease in SR luminal calcium and increase in cytosolic calcium triggers further calcium release by RyR. 6c) cytosolic calcium is sequestered back into the SR lumen via sarco-endoplasmic reticulum Ca^{2+}-ATPase (SERCA) and bound by calsequestrin.

1.3.1 RYR1

There are three isoforms of ryanodine receptors, of which RYR1 is primarily expressed in skeletal muscle, RYR2 is primarily expressed in cardiac cells, and RYR3 is primarily expressed in brain tissue (Lanner et al., 2010). RYR1 has a homotetrameric tertiary structure, with each subunit approximately ~550kDa and ~5000 amino acid residues in size (Inui et al., 1987). The tetramer forms a large mushroom-like shape, with a cytoplasmic head and transmembrane stalk forming a pore structure, and is located on the SR (Van Petegem, 2012). Using cryo-electron microscopy of rabbit RYR1, three major regions have been elucidated; the transmembrane domain which forms the pore, the cytosolic central domain, and the cytosolic ligand-binding domain (Yan et al., 2015).

Ca^{2+}, caffeine and ATP are activating ligands of RYR1, and have been shown to bind at the C-terminal interdomain regions to activate the channel (des Georges et al., 2016). Ca^{2+}, specifically, binds in a concentration-dependent manner, with both high affinity (activating) and low affinity (inactivating) sites to regulate RYR1. The channel may also be inhibited by Mg^{2+}, which competes with Ca^{2+} at high affinity sites or binding to the less selective low affinity Ca^{2+} sites (Laver et al., 1997). Finally, the channel may also be modulated through post-translational modifications and interactions with Ca^{2+}-handling proteins, such as calsequestrin or calmodulin, or with the DHPR (Lanner et al., 2010).

Due to the size and complexity of RYR1, elucidating binding sites for regulatory elements can be difficult. Further work into the interactions with STAC3 and halothane in particular would be useful for understanding the aetiology of MH. Additionally, the changes in architecture as a result of pathogenic variants would be useful to elucidate.

1.3.2 DHPR

The DHPR is a ~450kDa channel, consisting of five subunits (α1, α2, β, δ, and γ) (Catterall, 2011). The α1 subunit is 176kDa, encoded by *CACNA1S*, and forms the Ca^{2+} channel and voltage sensor domains. The α2 (147kDa) and δ (24kDa) subunits, encoded by *CACNA2D1*, are linked by disulphide bonds and improve membrane trafficking and increasing the amplitude of the current (Dolphin, 2013). The β (56kDa) subunit, encoded by *CACNB1*, affects the channel gating and trafficking of the α1 subunit (Dolphin, 2012). The γ (34kDa) subunit, encoded by *CACNG1*, acts as Ca^{2+} antagonist, and maintains the inactive state of the DHPR (Andronache et al., 2007). Of particular interest, are the 4 repeat units (I-IV) of the α1 subunit, each containing 6 transmembrane domains (S1-6), which form the II-III loop thought to interact with RYR1 directly (Tanabe et al., 1990). Additionally I-II loop contains the alpha-1 interacting domain that allows for the transmission of

conformational shape changes from voltage sensing domains of α1 to the β subunit (Almagor et al., 2012) and enables the docking of the β subunit to RYR1 which brings the II-III loop within it's proximity (Hu et al., 2015).

1.3.3 STAC3

STAC3 is a 41kDa protein and has been shown in several studies to also be a key component of ECC in skeletal muscle, aside from RYR1 and DHPR. Specifically, a zebrafish model indicates that pathogenic variants in *STAC3* decrease excitation-contraction coupling (Horstick et al., 2013). A mouse model further elucidated that STAC3 facilitates α1 subunit of DHPR trafficking as well as having direct involvement with the conformational coupling between the α1 subunit and RYR1 (Polster et al., 2016). Specifically, it has been shown that the SH3 domain of STAC3 associates with the II-III loop of the α1 subunit, which is critical for activation of RYR1 mediated Ca^{2+} release (Polster et al., 2018).

1.4 Disorders associated with malignant hyperthermia

Many RYR1 related myopathies are associated with MH, such as central core disease (CCD) and multi-minicore disease (MMD) (Litman et al., 2018). CCD is characterised by regions devoid of mitochondria in predominantly type I muscle fibres, with symptoms ranging from asymptomatic to presenting with muscle rigidity, muscle atrophy and skeletal deformities (Jungbluth, 2007). MMD is characterised by regions of sarcomeric disorganization and reduced oxidative phosphorylation derived from a lack of mitochondria, with symptoms including ophthalmoplegia and rhabdomyolysis (Jungbluth, 2007). Both disorders are rare congenital myopathies that overlap with MH, and are caused by causative pathogenic variants in *RYR1* (Robinson et al., 2006).

Exertional heat illness (EHI) is another disorder that has been linked to malignant hyperthermia. Patients with EHI have previously been reported to be subsequently

diagnosed with MH (Hopkins et al., 1991; Thomas & Crowhurst, 2013). EHI is characterised by the inability to regulate body temperature during physical activity (Armstrong et al., 2007). Symptoms include elevated serum creatine kinase, rhabdomyolysis, tachycardia and metabolic acidosis amongst others, and can lead to death in severe cases (Capacchione & Muldoon, 2009). Variants in *RYR1* have been observed in both MH and EHI, lending evidence to the link between the two disorders (Dlamini et al., 2013; Snoeck et al., 2016; Zhao et al., 2014). Furthermore, 34% of individuals with EHI were observed to also be MH susceptible (Gardner et al., 2020).

1.5 Genetic Disorders associated with rhabdomyolysis

1.5.1 McArdle's disease

McArdle's disease, also known as glycogen storage disease V, is a metabolic myopathy caused by mutations in the *PYGM* gene (Lebo et al., 1984). The disorder is inherited in an autosomal recessive manner, and results in the loss of activity of the *PYGM* gene product, myophosphorylase, which is a skeletal muscle isoform of glycogen phosphorylase (Nogales-Gadea et al., 2015a). Myophosphorylase catalyses the initial reaction of muscle glycogenolysis, which is crucial for glucose availability for glycolytic and oxidative metabolism in skeletal muscle. The absence of myophosphorylase activity leads to symptoms of exercise intolerance (rapid fatigue and contractures, and in more severe cases, myoglobinuria and rhabdomyolysis) which are acute and reversible (Lucia et al., 2008). McArdle's disease may either be diagnosed by assessing myophosphorylase activity levels in muscle biopsy, using a forearm exercise test, or by identifying pathogenic variants using DNA sequencing (Pizzamiglio et al., 2021). The most common causative pathogenic variant for McArdle's disease is the c.148C>T: p.(R50X) mutation in the UK and northern Europe, which is estimated to have an allele frequency of 77% amongst British patients, with 96% of patients having at least one mutated allele

containing either the p.(R50X) or c.613G>A: p.(G205S) variants (Pizzamiglio et al., 2021; Quinlivan et al., 2010).

Previous case reports have indicated several patients with McArdle's disease have had subsequent diagnosis of MH susceptibility after an IVCT. Specifically, a 21yo male experienced tachycardia and hypotonia under exposure to anaesthesia, and testing later revealed a diagnosis of both McArdle's disease and Malignant Hyperthermia (Bollig, 2013). Similarly, a 6yo boy had complained of rapid fatigue and muscle weakness, which led to testing positive for McArdle's disease, and a family history of MH, which was investigated and the boy was also shown to be susceptible for MH after an IVCT (Isaacs et al., 1989). Finally, a 2yo boy who developed intraoperative non-cardiogenic pulmonary edema followed by hyperthermia and rhabdomyolysis was later confirmed to have McArdle's disease (Lobato et al., 1999). In this final case, MH could not be confirmed at the time. In an overview of 14 patients confirmed with McArdle's disease, three (~20%) were also confirmed to be MH susceptible using the IVCT (Bollig et al., 2005). Additionally, the pathogenic *PYGM* variants p.(R50X) and p.(A193S) have been observed in individuals that are MH susceptible to (Gardner et al., 2020). Ultimately, a definitive link between McArdle's disease and MH has not been made due to a lack of evidence. Case reports of McArdle's disease coinciding with MH phenotypes typically have small numbers of individuals and/or no genetic confirmation. Additionally, case reports may not take into account clinical decisions leading to overlapping symptoms with MH, such as the use of tourniquets in surgery that may lead to rhabdomyolysis in McArdle's patients (Kotha et al., 2023). This makes it unclear whether *PYGM* is the causative gene. Further evidence is required to elucidate the possible contribution of *PYGM*. Thus, it remains unclear whether defects in glycogenolysis contribute to the aetiology of malignant hyperthermia. However, due to the similarities in clinical presentation, the possibility of MH being

linked to McArdle disease cannot be ruled out and thus warrants further investigation.

1.5.2 CPT II deficiency

CPT II deficiency is a metabolic disorder where CPT II activity, a key enzyme in beta oxidation, is diminished resulting in disrupted fatty acid oxidation. The enzyme catalyses the conversion of acylcarnitines, transported into the mitochondrial matrix by the carnitine shuttle, to acyl-CoA metabolites (Violante et al., 2010). The disorder may present in one of three subtypes; lethal neonatal, severe infantile hepatocardiomuscular and myopathic (Wieser, 1993). The former two are severe multisystemic disorders, whilst the third is characterised by rhabdomyolysis, myalgia and myoglobinuria, which is induced by fasting, fever, stress or prolonged exercise (Deschauer et al., 2005). Beta oxidation is crucial to skeletal muscle fibres that exhibit oxidative metabolism, utilising fats as a substrate. CPT II deficiency is inherited in an autosomal recessive manner, with the most common causative variants being *CPT2* c.338C>T: p.(S113L), with an estimated allele frequency of 76% amongst patients and present in at least one allele of 95% of patients, and c.149C>A: p.(P50H), with an estimated allele frequency of 7% (Deschauer et al., 2005). The disorder is diagnosed by finding pathogenic causative variants via DNA sequencing (Wieser, 1993). The disorder may also be screened for using tandem mass spectrometry to detect serum acylcarnitines and looking for an elevated ratio of (C16:0 + C18:1)/C2 acylcarnitines in order to make a diagnosis (Gempel et al., 2002). Genotype-phenotype correlations show a strong association between the p.(S113L) variant and the myopathic form (Anichini et al., 2011), whilst the p.(P227L) is associated with the lethal neonatal isoform, and the severe infantile hepatocardiomuscular form frequently exhibits compound heterozygosity of variants associated with the previous two (Isackson et al., 2008).

A previous case report has observed MH-like symptoms in an individual heterozygous for the pathogenic *CPT2* p.(R503C) variant, exhibiting tachydysrhythmia and metabolic acidosis, amongst others, upon exposure to succinylcholine and halothane (Hogan & Vladutiu, 2009). Evidence linking CPT II deficiency and MH is lacking. However, pathogenic variants in *CPT2* have been identified in MHS patients within the unit, namely the p.(S113L) change, at a higher rate than the general population (UK MH Unit, unpublished data). Additionally, mitochondrial deficits have been observed in MHS muscle (Chang et al., 2019), as well as a shift to lipid metabolism in MHS muscle but with an accumulation of long chain acylcarnitines (Bojko et al., 2021), and the downregulation of genes associated with fatty acid metabolism in an MH mouse model (Chang et al., 2020). The combination of these observations certainly warrants further investigation into *CPT2* within the context of MH.

1.6 Thesis aims

This thesis aims to investigate candidate modifier loci that may be involved in a threshold model of malignant hyperthermia susceptibility. Previous studies have indicated the likelihood of additional genetic contributors to MH, the variation in MH phenotypes and the identification of a gap in the understanding of the genetic basis of MH. However, they have lacked in going so far as to specifically investigate the threshold model. This thesis will aim to fill this gap by generating a novel mouse model containing multiple pathogenic variants, via a gene editing pipeline new to the field and an established mouse model of MH. Due to the overlap between MH with McArdle's disease and CPT II deficiency, as well as pathogenic variants for these disorders being identified in MH susceptible individuals, this thesis will aim to characterise *CPT2* and *PYGM* for any potential contribution to a threshold model of MH susceptibility. Finally, this thesis also aims to identify additional over-

represented regions of interest for modifier loci across several genes through a case-control study, comparing MHS to MHN individuals within the UK MH cohort.

1.7 Thesis objectives

1.7.1 Investigate *CPT2* for potential contribution to a threshold model of MH.

CRISPR/Cas9 technology will be used to first knockout *Cpt2* in primary mouse myoblast heterozygous for *Ryr1* p.(G2435R). Myotubes from this novel line will be assessed for sensitivity to RyR1 agonists. Subsequently, lentiviral vectors will be used to introduce the *Cpt2* p.(S113L) and p.(P50H) variants into the knockout line and assessed as before. Finally, single nucleotide polymorphisms (SNPs) and rare pathogenic variants in CPT2 will be genotyped across ~1500 patient DNA samples consisting of MHS and MHN individuals to identify any alleles over-represented amongst the UK MH susceptible cohort.

1.7.2 Investigate *PYGM* for potential contribution to a threshold model of MH.

CRISPR/Cas9 technology will be used to first knockout *Pygm* in primary mouse myoblast heterozygous for *Ryr1* p.(G2435R). Myotubes from this novel line will be assessed for sensitivity to RYR1 agonists. Subsequently, lentiviral vectors will be used to introduce the *Pygm* p.(R50X) and p.(A193S) variants into the knockout line and assessed as before. Finally, SNPs and rare pathogenic variants in *PYGM* will be genotyped across ~1500 patient DNA samples consisting of MHS and MHN individuals to identify any alleles over-represented amongst the UK MH susceptible cohort.

1.7.3 Investigate additional candidate genes for potential modifier loci

An additional eight genes, chosen based on the identification of individuals with pathogenic variants in these genes within the MH unit or in the literature, as well as any associations with MH (section 5.1), (*ACADVL*, *AMPD1*, *ATP2A1*, *CACNA1S*, *CACNA2D1*, *STAC3*, *TRPV1*, and *CASQ1*) will also be investigated. For example,

many of these genes have been highlighted when looking at comparisons of gene expression between MHS and MHN muscle, after challenge by halothane or caffeine (Chang et al., 2019, 2020, 2024), as well as case reports of individuals with the related gene disorder also showing susceptibility to MH (Gardner et al., 2020; Odermatt et al., 1996; Zaharieva et al., 2018). SNPs and rare pathogenic variants from each gene will be genotyped across ~1500 patient DNA samples consisting of MHS and MHN individuals to identify any alleles over-represented amongst the UK MH susceptible cohort.

2 General Methods

2.1 Cell culture

2.1.1 Primary mouse myoblasts

Primary mouse myoblasts were cultured in a proliferation media on plates (Sarstedt) coated with rat tail collagen (First Link Ltd) at 37ºC and 5% CO_2. Collagen was diluted in acetic acid (0.1%) to make a working solution (46µg/ml) for plate coating. Plates were coated with 5ml of collagen working solution and incubated for 30 minutes at 37ºC and 5% CO_2. Plates were then washed with 7ml phosphate-buffered saline (PBS, Gibco). Proliferation media consisted of Ham's F-10 media (Gibco) supplemented with 20% (v/v) fetal bovine serum (Gibco) and 2x penicillin/streptomycin (P/S, final concentration 1mg/ml). Proliferation media was changed every 24-48 hours and supplemented with 10ng/ml of human fibroblast growth factor beta (FGF-β) (Peprotec). Myoblasts were not allowed to reach 70% confluency, unless in the case of differentiating into myotubes.

For differentiation, plates were coated with entactincollagen IV-laminin (ECL) or ECM cell attachment matrix (Sigma Aldrich) based on downstream application. ECL, diluted to a working concentration of 20µg/ml in serum-free Hams F-10 media, was applied (1.3µg/cm^2) for 1 hour at 37ºC and 5% CO_2 or overnight at 4ºC. ECM was diluted 1:3 in Hams F-10 media and applied (11.3µg/cm^2) for 30 minutes at 37ºC and 5% CO_2. Myoblasts were trypsinised for 3 minutes at at 37ºC and 5% CO_2 (1ml/25cm^2) (TrypLE, Gibco), resuspended in proliferation media and transferred to ECL or ECM coated plates. Media was changed to differentiation media at 70-90% confluency and replaced every 48 hours until mature myotubes had formed (3-5 days later). Differentiation media consisted of Dulbecco's modified eagle medium (DMEM) supplemented with 2% heat inactivated horse serum and 1x P/S (All from Gibco).

2.1.2 NIH/3T3 and HEK293T cells

NIH/3T3 and HEK293T cells were cultured on 10cm cell+ dishes at 37ºC and 5% CO_2 with media changed every 48 hours. Cells were not allowed to reach 70% confluency. Culture media consisted of DMEM supplemented with 10% FBS and 2x P/S. An addition of 500µg/ml Geneticin was also made specifically for the HEK293FT media.

2.1.3 Cell passage, counting and viability

Passage of cells was conducted by aspirating media from the culture dish and washing cells with PBS prior to the addition of trypsin. Cells were incubated at 37ºC and 5% CO_2 with trypsin until cells had lifted, after which culture media was added to inactivate the trypsin. Cells were then split either 1:2 or 1:4 into new culture dishes. When counting was required, cells were pelleted at 330*g*/6mins and resuspended in 1ml of culture media. 10µl of this suspension was mixed with 10µl of trypan blue (Gibco) and then 10µl of the mixture was loaded onto a haemocytometer for counting.

2.1.4 Cryostorage of cells

Cells were trypsinised, resuspended in culture media and pelleted at 330*g* / 6 minutes. Cell pellet was resuspended in FBS with 10% dimethylsulfoxide (DMSO) and stored in 1ml aliquots ($1x10^6$/ml) in cryovials, which were cooled slowly to -80ºC over 24 hours. Frozen cells were stored at -80ºC for short term use, or in liquid nitrogen (-196ºC) for long term storage.

2.2 Molecular methods

2.2.1 Polymerase chain reaction

Prior to gDNA extraction, cells were trypsinised, resuspended in media and pelleted by centrifuging at 330*g* / 6 minutes. The pellet was resuspended in PBS and re-pelleted as before, after which the PBS was disposed of. The Purelink Genomic DNA extraction kit (Thermofisher) was used, following the manufacturers protocol. Genomic DNA quality was checked on the nanodrop, where only samples with a 260/280 ratio of 1.7-1.9 and 260/230 ratio of 2.0-2.2 were used downstream. When dealing with smaller cell populations, such as in a 6-well dish or smaller, direct extraction was used in lieu of the genomic DNA extraction kit. In this case, the cell pellet was resuspended in 100ul of PBS and a 10ul aliquot was taken and diluted in 15ul of nuclease free water. The sample was then incubated at 99ºC for 5 mins to lyse cells prior to PCR. For bacterial DNA, a colony was picked using a pipette tip and swirled into 25µl of nuclease free water, which was incubated at 99ºC for 5 mins to lyse cells prior to PCR.

For PCR, a reaction consisted of 400µM forward and reverse primer, 12.5µl PCR mastermix (2X) (Thermofisher), 2.5µl of direct-extracted-gDNA or 25ng of kit-extracted-gDNA and made to a total volume of 25µl with nuclease-free water. The thermocycling program consisted of: 95ºC/3min, 30x (95ºC/30s, 62.4ºC/1min, 72ºC/1min), 72ºC/5min, 4ºC hold. 10µl of PCR product was mixed with 2µl Gel Loading Dye (6x) purple (New England Biolabs) and 10µl loaded onto a 2% agarose (Sigma Aldrich) gel alongside 10µl of Quick-Load 100bp DNA ladder (New England Biolabs) and run at 100V for 1 – 1.5 hours in TBE buffer. If band size was correct with minimal or no primer-dimer and additional bands, the PCR product was used for Sanger sequencing. A full primer list can be found in appendix 2, table A.1.

2.2.2 Sanger sequencing

For Sanger sequencing, the PCR product was treated with 1µl of ExoProStar (Cytiva) per 2.5µl of product and incubated at 37ºC for 15 minutes then 80ºC for 15 minutes. 1µl of cleaned product was added to sequencing mix of 10µl total reaction volume consisting of 1µl Big Dye (Applied Biosystems), 1µl Half Big Dye (Merck Millipore), 1µl of 400µM primer (separate forward and reverse reactions), topped up with nuclease-free water. The thermocycling program consisted of: 96ºC / 5 minutes, 25x (96ºC / 10 seconds, 50ºC / 5 seconds, 60ºC / 4 minutes), 4ºC hold. DNA was subsequently precipitated by adding 1µl ammonium acetate and 25µl of 95% ethanol and incubated at room temperature for 20 minutes. Samples were centrifuged at 4ºC / 2250g / 30 minutes to pellet the DNA, then inverted on a paper towel and centrifuged at 4º / 700g / 1 minute to aspirate the ethanol. Subsequently, 70µl of 70% ethanol was added and the DNA was re-pelleted, and ethanol aspirated as above. The DNA pellets were then incubated at room temperature for 20 minutes to air dry, after which 10µl of Hi-Di formamide (Applied Biosciences) was used to redissolve pellets. The samples were then sent to an in-house sequencing facility (LIMMSeq) to generate the read-outs. When sequencing was outsourced, PCR product was shipped to Source Bioscience for product cleaning and Sanger sequencing. Reads were analysed using Chromas software (Technelysium Pty Ltd).

2.2.3 Real Time quantitative Polymerase Chain Reaction

2.2.3.1 RNA extraction

Prior to RNA extraction, cells were pelleted as above. Subsequently, the RNeasy mini kit (Qiagen) was used, following the manufacturers protocol. RNA quality and concentration were checked on the Agilent TapeStation in the Leeds next generation sequencing (NGS) facility by Mrs Morag Raynor. RNA with RNA integrity (RIN) values of under 7.0 or a 28S:18S ratio of under 2.1 were not used.

2.2.3.2 cDNA synthesis

cDNA was made by following the manufacturers protocol for the High-Capacity cDNA reverse transcription kit (Applied Biosystems). For no reverse transcriptase controls, reverse transcriptase was substituted with an equal amount of nuclease-free water. The thermocycler program used consisted of: 25ºC / 10 minutes, 37ºC / 120 minutes, 85ºC / 5 minutes. cDNA was stored at -80ºC.

2.2.3.3 qPCR

Real time qPCR was conducted on the QuantStudio™ 5 real time PCR to investigate *PYGM* and *CPT2* expression across multiple genotypes of primary mouse myoblasts and myotubes. TaqMan® gene expression assays were used and *PYGM* (Mm00478582_m1 & Hs00989942_m1, Thermofisher) and *CPT2* (Mm00487202_m1 & Hs00988962_m1, Thermofisher) expression were normalised against *B2M, Ap3d1,* and *Csnk2a2* (Hildyard & Wells, 2014; Vandesompele et al., 2002). Each run had three technical replicates and three independent samples per genotype. A 20µl reaction volume was made consisting of; 1µl TaqMan probe, 1ng cDNA, 10ul TaqMan gene expression mastermix (Applied Biosystems) and topped up with nuclease-free water. The thermocycling program consisted of: 95ºC/ 10min, 40X (95ºC/15s, 60ºC/60s). C_q (C_t) values were averaged across technical replicates and used to calculate relative gene expression values using the $\Delta\Delta C_t$ method (Livak & Schmittgen, 2001). Differences between groups were assessed for significance

using the t-test or ANOVA, after testing data for normality using the Shapiro-Wilk test.

2.2.4 Western Blotting

2.2.4.1 Protein extraction

Cells were trypsinised, resuspended in media and pelleted by centrifuging at 330*g* / 6 minutes. The pellet was resuspended in PBS and re-pelleted as before, after which the PBS was disposed of.

For protein extraction, 1ml radioimmunoprecipitation assay (RIPA) lysis buffer (Thermofisher) with 10µl 100X Halt protease inhibitor (Thermofisher) was used to resuspend the cell pellet ($1x10^6$/ml RIPA). The solution was incubated on ice for 5 mins with intermittent vortexing, then spun at ~9800*g* for 15 minutes to pellet cell debris. Supernatant was removed and stored for downstream analysis. Protein concentration of samples was determined using a bicinchoninic acid (BCA) assay (Pierce BCA protein assay kit, Thermofisher) according to the manufactures microplate protocol.

2.2.4.2 SDS-PAGE

5µg Protein sample was boiled at 99ºC / 5 mins with 5x loading buffer (250mM Tris-HCl pH 6.8, 4% Sodium Dodecyl Sulfate (w/v), 0.06% bromophenol blue (w/v), 12.5% β-mercaptoethanol (v/v), 30% glycerol (v/v)) to a final concentration of 1x, then loaded into a SDS-Polyacrylamide gel electrophoresis gel consisting of a 5% stacking gel (5% acrylamide/bis-acrylamide (w/v, Sigma Aldrich), 126mM Tris-HCl pH 6.8, 0.1% SDS (w/v), 0.1% Ammonium Persulfate (w/v), 0.1% TEMED (v/v)) and 10% resolving gel (10% acrylamide/bis-acrylamide (w/v), 375mM Tris-HCl pH 8.8, 0.1% SDS (w/v), 0.1% Ammonium Persulfate (w/v), 0.1% TEMED (v/v)). Where a precast gel was required, a 10% Mini-PROTEAN TGX precast gel (Bio-Rad) was used. The samples were subsequently run at 100V for 2 hours in 1x SDS

electrophoresis buffer (25mM Tris base, 192mM Glycine, 1% Sodium dodecyl sulfate (w/v, SDS)).

2.2.4.3 Western blot

Proteins were transferred onto a 0.45µm Polyvinylidene fluoride (PVDF) membrane (Bio-Rad) overnight at 10mA / 4ºC in transfer buffer (25mM Tris base, 192mM Glycine, 1% SDS(w/v), 4% methanol (v/v)). The membrane was subsequently washed 3 times for 15 minutes in 1x Tris-Buffered-Saline-Tween (TBST) (25mM Tris-HCl pH 7.6, 150mM NaCl, 0.1% Tween 20 (v/v)) and then incubated in blocking buffer (5% skimmed milk powder (w/v) in TBST) for 1 hour at room temperature. Membrane was then incubated with primary antibody diluted in blocking buffer for 1 hour at room temperature. Primary antibodies included anti-PYGM (ab231963, abcam), anti-CPT2(ab181114, abcam) and anti-GAPDH (ab181602, abcam). The membrane was subsequently washed with TBST as before, followed by incubation with secondary antibody (ab6721, abcam) diluted 1:5000 in blocking buffer for 1 hour at room temperature and then washed again as before. Finally, membrane was incubated with chemiluminescent substrate (Pico West, Thermofisher) at room temperature in dark for 5 mins prior to imaging. To the strip the membrane, prior to re-probing, a mild stripping buffer (200mM Glycine, 0.1% SDS (w/v), 1% Tween 20) was used followed by 3 x 10-minute washes with TBST after which the membrane was ready for blocking and re-probing.

2.3 Live cell imaging

2.3.1 Perfusion and cell imaging system

The imaging rig (figure) consisted of a Nikon eclipse T2000 microscope with metal halide lamp, filter sets, neutral density filters (NDF) and a 12-bit intensified charge coupled device camera attachments to measure variations in myotube fluorescence during drug exposure. Eight 35ml syringes connect to a valvebank 8 pinch valve perfusion system (Automate Scientific, USA) were used to regulate cell exposure to variable drug concentrations. The pinch valves were connected via perfusion tubing to a borosilicate glass pipette. The pipette had been fitted to produce a 3mm longer inlet channel as compared to the outlet channel, resulting in a dead space to prevent cells drying out. A constantly running roller pump, connected to the outlet channel, enabled removal of solutions from wells and into a waste container. Solutions were perfused at a pressure of 2 pounds per square inch (psi).

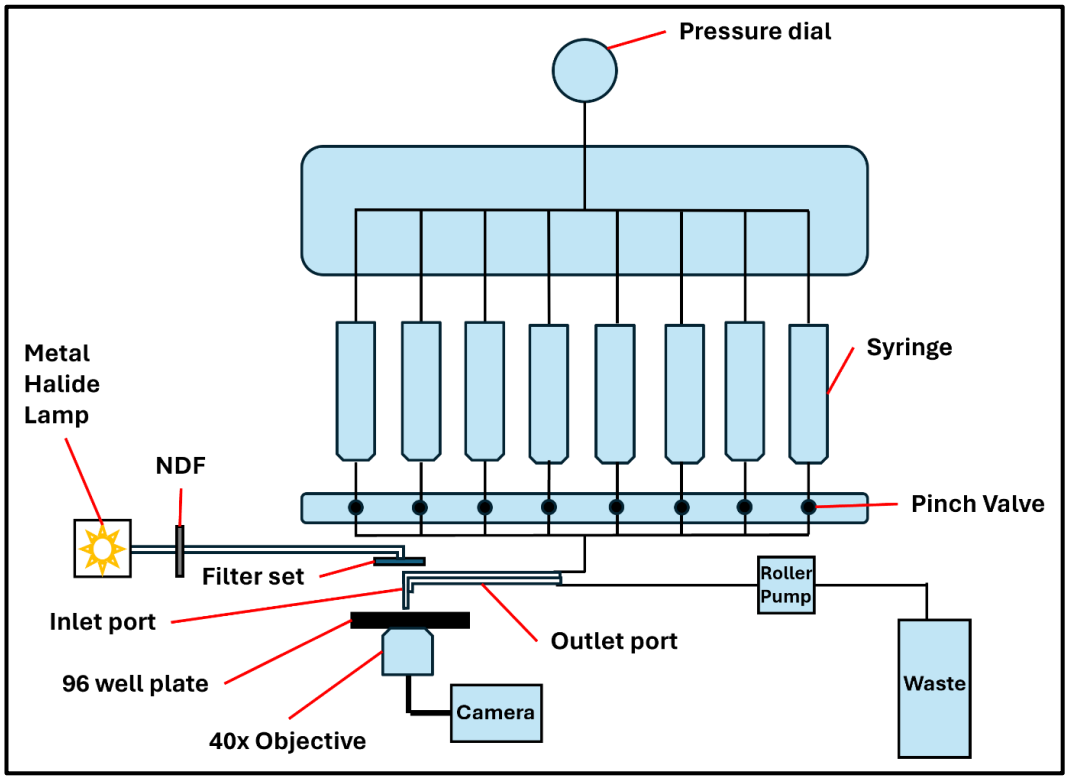

Figure 2.1: Diagrammatic representation of perfusion and imaging system used in live-cell imaging experiments. Multiple syringes enabled the sequential application of various drug concentrations and imaging buffer at a constant pressure as set by the pressure dial. Variations in fluorescence were measured via the camera connected to the 40x oil immersion objective lens.

2.3.2 Solutions

All solutions were made fresh on the day of imaging.

Imaging buffer (133mM NaCl, 5mM KCl, 1mM $MgCl_2$, 2mM $CaCl_2$, 5.5mM Glucose, 10mM 4-(2-hydroxyethyl)-1-piperazineethanesulfonic acid (HEPES), pH 7.4) was used for drug washout.

Caffeine was dissolved in imaging buffer to produce a 20mM stock solution. The stock solution was diluted to desired concentrations in imaging buffer for the caffeine response curves.

To produce various concentrations of KCl solution, for the KCl response curves, the concentrations of KCl in imaging buffer were altered. The concentration of NaCl was also reciprocally reduced, such that the total concentration of NaCl and KCl in the solution remained at a total of 138mM.

For dye loading, a 2.5mM stock of the calcium indicator dye Fluo-4AM (Thermofisher) was made by dissolving in DMSO and stored at -20ºC. A 20% weight by volume stock solution of pluronic F127 acid (Sigma Aldrich) was also made by dissolving in DMSO and stored in the dark at room temperature.

2.3.3 Epifluorescence imaging

On the day of the experiment, Fluo-4AM was mixed with the 20% pluronic F127 acid in a 1:1 ratio to aid with dye uptake, which was then diluted in imaging buffer to a final concentration of 5μM. Media was aspirated from the myotubes, which were subsequently washed twice with imaging buffer. The Fluo-4AM solution was then applied to the cells and incubated for 15 minutes at 37ºC/5% CO_2. The dye was subsequently discarded and the myotubes washed with imaging buffer twice again and incubated in imaging buffer for 30 minutes in the dark at room temperature. The myotubes were then imaged on the rig described above using a 40x 1.3 NA objective lens. Imaging buffer was applied for 10s, followed by the drug for 10s which was subsequently washed out with another 10s application of imaging buffer.

Fluo-4AM was excited using a metal halide lamp and excitation filter set at 480nm +/- 20nm, and emission was measured at 535nm +/- 25nm. Images were captured on IPlab software (BD Biosciences, USA) using a 4x4 bin rate and at 20fps for a total of 500-700 frames per concentration of drug. To prevent phototoxicity, neutral density filters were used to reduce light intensity. Furthermore, cells were allowed to recover for 3 minutes between drug concentrations during which the metal halide lamp was turned off. The recordings were suspended during recovery and additional 30s of imaging buffer was applied. 60mM KCl was included in each experiment to ascertain functioning excitation-contraction coupling.

2.3.4 Data analysis

Images were imported in ImageJ for analysis. Regions of interest were drawn within myotubes and the mean grey value per slice was measured to determine the changes in fluorescence intensity over time. This data was then exported to Microsoft Excel (version 2312 for Windows, Microsoft, USA) and Prism 10 (GraphPad, USA) for further analysis. The area under the curve for each concentration response was determined using the average response during drug application minus the average baseline fluorescence over the 3s prior to challenge. AUC values were then normalised using the response to the maximum drug concentration for each myotube to account for the variability across cells. Normalised values for each myotube were used to plot a concentration-response curve by fitting a four-parameter variable slope non-linear regression on a semi-log axis. This was used to calculate a half maximal effective concentration (EC_{50}) for each myotube. The geometric mean of the EC_{50}'s per genotype was calculated and used for further statistical analysis. Geometric means were compared for statistical significance using parametric or non-parametric tests based on the distribution of data and were also corrected for multiple comparisons. A p-value below 0.05 was accepted significant.

2.4 Bacterial methods

2.4.1 Transformations

Prior to transformation, *Escherichia.coli* (E.coli) cells were thawed on ice for 20 minutes. 2µl of plasmid was added to 50µl of cells which was then gently mixed by flicking the tube and incubated on ice for 30 minutes. Cells were then heat shocked at 42ºC for 30s and immediately transferred back on ice. 250µl room temperature S.O.C medium (Invitrogen) was added to the cells and vials were subsequently incubated at 37ºC for 1 hour with shaking at 225rpm. 50µl - 250µl of the transformation reaction was then plated on a Lysogeny Broth (LB) agar (3% w/v in dH_2O, Invitrogen) plate containing 100ug/ml ampicillin and incubated overnight at 37ºC. Plates were subsequently stored at 4ºC until colonies were picked.

For TA cloning transformations, One Shot TOP10F' chemically competent E.coli (Invitrogen) were used. Transformation reaction protocol was same as above. LB agar plates in this case contained 50µg/ml kanamycin alongside ampicillin, as well as coated with 40µl each of 100mM Isopropyl-β-d-1-thiogalactopyranoside (IPTG, Invitrogen) and 40mg/ml X-Gal (Invitrogen) and left to soak into the plates for 1 hour at room temperature after equilibrating plates to 37ºC. Transformed cultures were then plated as before.

2.4.2 Starter cultures

Single colonies were picked from plated transformed cultures using a sterile pipette tip and transferred to 5ml LB media (1.8% w/v in dH_2O, Invitrogen) containing the relevant antibiotics, which were subsequently incubated at 37ºC overnight with shaking at 200rpm.

For long term storage, 500µl of starter culture (following overnight incubation) was mixed with 500µl 50% glycerol (v/v in dH_2O, Sigma Aldrich) and vortexed to form glycerol stocks, which were stored at -80ºC in cryovials.

2.4.3 Plasmid Maxi prep

For plasmid Maxi prep, 200µl of starter culture was added to 200ml of LB media (1.8% w/v) containing 100µg/ml ampicillin and incubated at 37ºC overnight with shaking at 200rpm. Plasmid was isolated using the Qiagen-tip 500 plasmid maxi kit according to the manufacturers protocol and subsequently quantified using the NanoDrop 1000 spectrophotometer.

3 The use of CRISPR/Cas9 to Knock-out *Pygm* and *Cpt2* in the heterozygous p.(G2435R) mouse model of *RYR1*

3.1 Introduction

The similarities in clinical presentation of McArdle's disease and CPT II deficiency with MH (section 1.5) warrant further investigation. Additionally, coupled with the mitochondrial deficiencies observed in both MHS mouse (Chang et al., 2020) and human samples (Chang et al., 2019) suggest that metabolic genes would be ideal candidates for the investigation of candidate modifier variants. These two genes were specifically considered above others due to the observation of pathogenic alleles of either gene within the MHS UK cohort at a relatively increased rate (personal communications Phil Hopkins, UK MH unit). For example, the identification of *PYGM* p.(R50X) and *CPT2* p.(S113L) pathogenic variants in several MHS patients. Thus, the gene editing pipeline across this chapter and the next will focus on the investigation of *CPT2* and *PYGM*.

3.1.1 Muscle glycogen phosphorylase

The skeletal muscle isoform of glycogen phosphorylase is encoded by *PYGM*, which catalyses the first and rate-limiting step of glycogenolysis (figure 3.1) by breaking α-1,4,-glycosidic bonds resulting in the release of glucose-1-phosphate (G1P) (Di Mauro, 2007). *PYGM* is 14.3kb with 20 exons and located at the chromosomal location 11q13.1. The coding sequence amounts to 2.5kb and encodes a 97kDa protein with 842 amino acids, which forms a homodimer in the cytosol (Lukacs et al., 2006). Myophosphorylase is regulated by both phosphorylation and allosteric regulators. Allosteric activators include AMP, inorganic phosphate, G1P, and glycogen, whilst inhibitors consist of ATP, glucose-6-phosphate, glucose and purine (Madsen et al., 1973). Most allosteric regulators bind to the N-terminal domain (residues 1-484) of the monomer, whilst the C-terminal domain (residues 485-842) contains the Lys 681 residue which is the binding site for

the pyridoxal phosphate cofactor (Withers et al., 1981). The glycogen binding site is towards the surface of the enzyme around residues 398-438, relatively distanced from the catalytic and allosteric binding sites (Johnson, 1992). Residues in the N-terminal contribute to the C-terminus domain leading to the formation of the catalytic site of the enzyme, as a crevice between the domains of the protein (Nogales-Gadea et al., 2015b). Furthermore, the enzyme contains a gate like domain called the 280's loop, formed by the residues 281-289, which opens and closes in response to allosteric regulators to control access to the catalytic site (Buchbinder & Fletterick, 1996). As a key enzyme in glycogenolysis, naturally its function is crucial to carbohydrate metabolism and ATP production downstream, both anaerobically and aerobically.

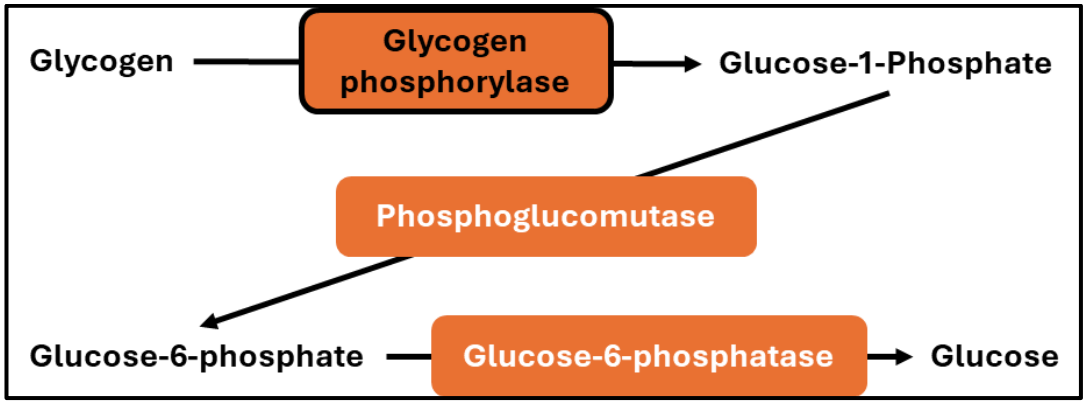

Figure 3.1: Glycogenolysis pathway schematic. Glycogen phosphorylase (outlined) catalyses the rate-limiting initial step of glycogen into glucose-1-phosphate. The pathway enables downstream anaerobic and aerobic respiration, through the generation of glucose that is now free to be metabolised.

3.1.2 Carnitine Palmitoyl Transferase II

CPT II is located on the inner mitochondrial membrane and is encoded by the *CPT2* gene. The enzyme catalyses the conversion of acylcarnitines, transported into the mitochondrial matrix by the carnitine shuttle, to acyl-Coenzyme A metabolites (figure 3.2), which is a rate limiting step in the beta-oxidation pathway (Violante et al., 2010). The gene spans 17.3kb with 5 exons and is located at the chromosomal location 1p32.2. The coding sequence amounts to 2kb and encodes a 74kDa

protein with 658 amino acids. The crystal structure of rat CPT II, which has 95.2% similarity to its human homologue, was determined and showed some key domains. Specifically, the enzyme could be separated into the N-terminal domain (residues 111-440) and C-terminal domain (residues 441-658 and 32-111). Two β sheets mediate the interface between the two domains, where a y-shaped tunnel forms the active site, with binding sites for acyl, carnitine and CoA (Rufer et al., 2006). Furthermore, residues 464-479 and 488-496 are predicted to form a α helix turn helix structure that inserts into the inner mitochondrial membrane and loosely anchor the enzyme (Wieser et al., 2003). CPT II is a key enzyme in fatty acid metabolism associated with the mitochondria and crucial to ATP production downstream.

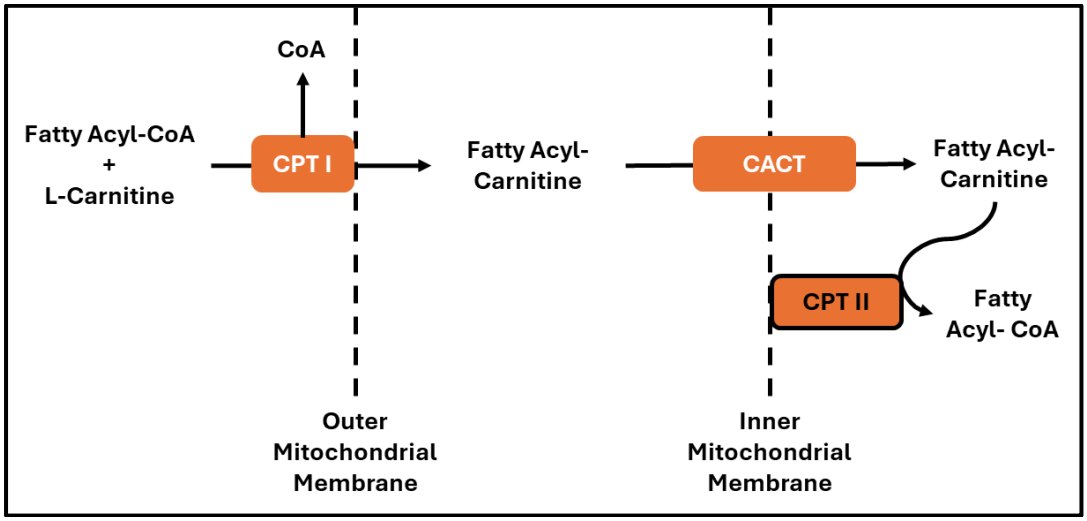

Figure 3.2: Carnitine shuttle and CPT II function schematic. CPT II (outlined) catalyses the rate-limiting step in the beta-oxidation pathway, directly after the carnitine shuttle. Fatty Acyl-CoA is generated for use in the TCA cycle downstream, enabling energy production from fatty acids.

3.1.3 CRISPR/Cas9 system

The manipulation of the prokaryotic CRISPR/Cas (clustered regularly interspaced palindromic repeats / CRISPR-associated proteins) proved to revolutionize the genetic modification landscape, and the concept was initially laid out in 2012 (Jinek et al., 2012). There are three subtypes of the CRISPR/Cas system (S. Makarova et al., 2011). Type I and III both feature Cas endonucleases processing pre-CRISPR RNA (pre-crRNA). Mature crRNAs then assemble with multiple Cas proteins in a ribonucleoprotein complex capable of targeting DNA that is complementary to crRNAs for cleavage. The type II system differs from this in that a trans-activating-crRNA (tracrRNA), which is complementary to repeat sequences in the pre-crRNA, triggers the processing of pre-crRNA by RNase III when Cas9 is present. The tracrRNA and crRNA then form a ribonucleoprotein complex with Cas9 to target and cleave DNA complementary to the crRNA. The first use of this type II system for genome editing was documented in 2013, whereby the *Streptococcus pyogenes* system was manipulated and crRNA was designed to target specific sections of DNA (Cong et al., 2013; Ran, Hsu, Wright, et al., 2013). However, when using the *S.pyogenes* system, the protospacer-adjacent motif (PAM) must also be considered when designing a guide RNA. The PAM sequence denotes a motif that is recognisable by the Cas9 itself when binding, and in *S.pyogenes* consists of the nucleotides NGG. Additionally, the HNH and RuvC Cas9 nuclease domains were shown to cleave the DNA. HNH cleaves the strand complementary to the crRNA, whilst RuvC cleaves the opposite strand. It was shown that, for editing in mammalian cells, only the crRNA, tracrRNA and Cas9 were required (Ran, Hsu, Wright, et al., 2013). The tracrRNA and crRNA sequences could also be fused to form a single guide RNA (sgRNA) to further simplify the gene editing tool. Further modifications to the Cas9 were also made to enhance specificity, dubbing the modified variant as eSpCas9, where the amino acid changes made were p.(K848A), p.(K1003A) and p.(R1060A) (Slaymaker et al., 2016).

The result of these advances is a programmable CRISPR/Cas gene editing system that provides high specificity (figure 3.3). Once a double strand break (DSB) is caused by Cas9, two mechanisms of DNA repair are available; homology-directed repair (HDR) and non-homologous end joining (NHEJ). The gene editing strategy must take this into account when considering the desired outcome. Typically, HDR is promoted *in vitro* when the goal is to produce a specific variant of interest and requires further components and design considerations. However, if the goal is to simply knock-out the gene and render it non-functional then the use of Cas9 and sgRNA suffice. Wild-Type Cas9 produces blunt ends when cleaving DNA, leading to NHEJ being largely favoured over HDR when repairing the DSB (Bothmer et al., 2017). NHEJ typically results in the insertion or deletion of random nucleotides at the break site which may cause frameshifts and/or premature stop codons, usually leading to gene knock-out.

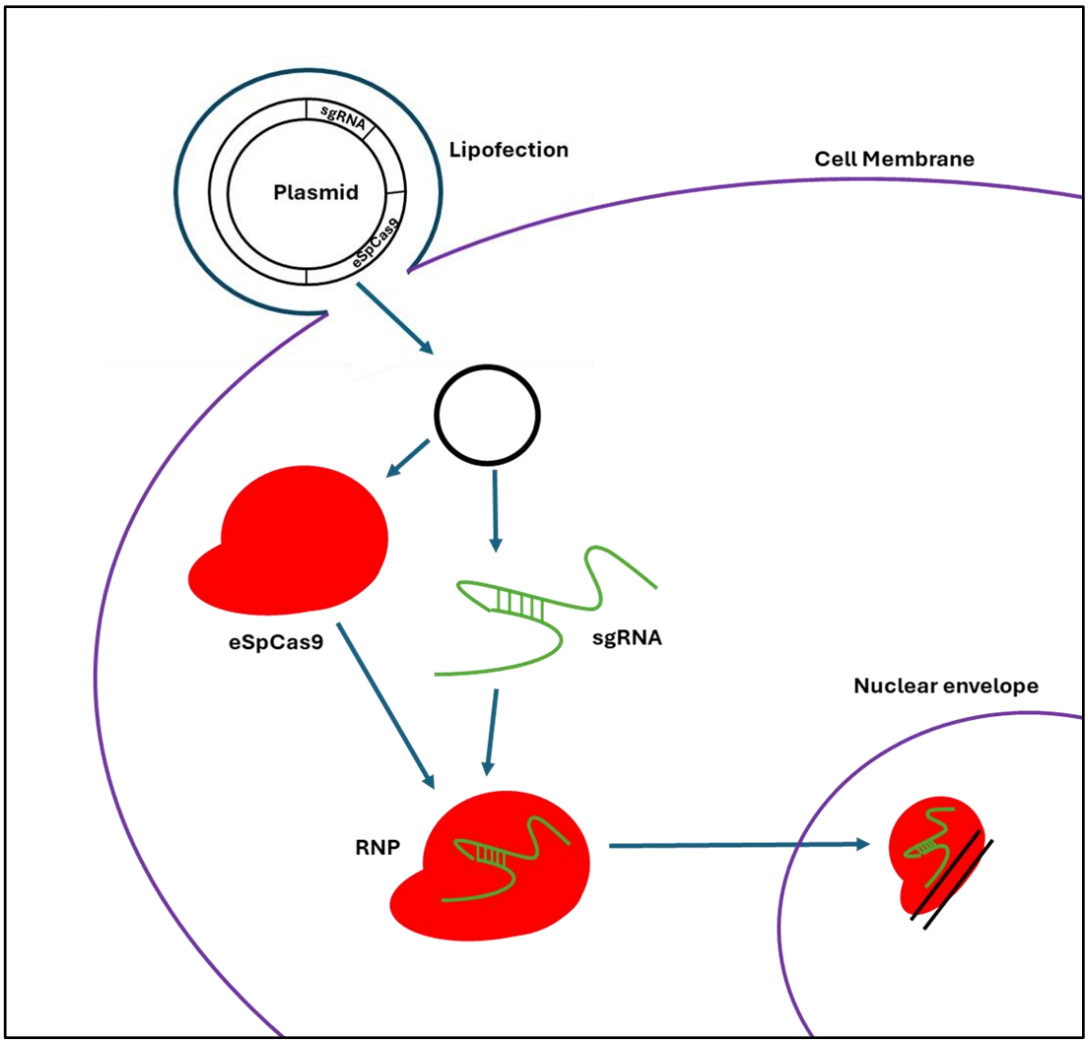

Figure 3.3: A programmable CRISPR/Cas9 gene editing system. Plasmid construct containing a chosen Cas9 variant (eSpCas9 in this case) and the sgRNA guide sequence is transfected into target cells. Transcription of the plasmid in the cytosol results in the production of the Cas9 protein and mature sgRNA, which go on to form the ribonucleoprotein (RNP). The RNP enters the nuclear envelope using nuclear localisation signal sequences enabling access to the genome. The sgRNA guides Cas9 to the programmed target site, where Cas9 can induce a double strand break through cleavage of the DNA via HnH and RuvC domains.

When using CRISPR/Cas9 as gene editing tool, certain design considerations may be taken into account. In particular, guide design and transfection methodology are important. When considering guide design, the primary question is the purpose of gene editing; knock-in or knock-out. In the generation of knock-out lines, it is important to consider regions that are more likely to have a high success rate of rendering the gene non-functional, such as exons across multiple transcripts that may be expressed, and with a favour towards earlier exons. By selecting a common

exon among transcripts, you ensure all transcripts are knocked out, and by aiming for earlier regions of the gene you increase the likelihood of nonsense mediated decay (Brogna & Wen, 2009). Another viable strategy may be targeting regions that are crucial to the genes function, such that even if transcripts are translated to protein, the protein is not functional, but this may not be as successful, especially if the protein is not well characterised and estimates can only be based on *in silico* modelling. Another important factor of guide design is the on target and off target efficiency. Ideally you want both scores to be as high possible ensuring only your selected gene is targeted and with high efficiency (Hsu et al., 2013). However, this depends on the target sequence, its similarity with other regions in the genome and how efficiently a guide RNA may be able to bind to it. Furthermore, the PAM motif must be considered as the target can only be a region adjacent to this motif. The considerations of PAM and on/off target scores may ultimately limit the regions which can be targeted. Ideally, you would want to target at least the transcript(s) of interest and avoid targets in the last exon to optimise knock-down of mRNA products via nonsense mediated decay.

When considering the transfection strategy, ultimately the choice lies in deciding how the RNP construct is formed and delivered. There is a discrete, but sliding scale in how many components are made *in vitro* vs encoded in a plasmid. A plasmid vector encoding the guide and cas9 together may be coupled with lipofection. The benefits here are the continuous expression of the components and RNP formation as long as the plasmid is present, alongside the relatively lower cytotoxicity of lipofection. However, the expression of the construct adds extra steps, alongside nuclear entry, which may decrease the efficiency of editing events. This strategy also results in increased exposure to the RNP, potentially resulting in more off-target events. On the other end of the scale, you could form the RNP *in vitro* completely (Farboud et al., 2018), but transfecting this construct may be more

difficult due its shape and size. This method would also have a shorter window of editing due to the half-life of the RNP, which may reduce efficiency in return for decreased likelihood of off-target editing events. In this case, the RNP may be introduced via nucleofection to direct it straight into the nucleus in an attempt to increase efficiency with the trade-off that it may also be more cytotoxic. An approach somewhere in between may also be utilised with certain components encoded in a plasmid, whilst others are prepared *in vitro*. However, ultimately the choice may depend on the ability of the cells to withstand stress and damage, limiting options.

3.1.4 Chapter aims

This chapter aims to develop a CRISPR pipeline for the investigation of candidate genes, specifically in a threshold model of malignant hyperthermia. This will be achieved by knocking-out genes of interest in an established mouse model of MH. The use of a mouse model enables a controlled genetic background on which comparisons between additional genetic contributors can be made. Additionally, using an established mouse model means that the MH phenotypes for the model are already well established, allowing robust comparisons. This pipeline will ideally be flexible to use in various cell models of MH, and lead to the creation of novel cell lines specific to the threshold model of inheritance. These cell lines will subsequently be functionally assessed using established live-cell calcium imaging assays to deduce their sensitivity to various triggering agents.

Specifically, this chapter will aim to investigate the effects of disrupting *PYGM* and *CPT2* function in the *Ryr1* p.(G2435R) heterozygous primary mouse myoblasts (Lopez et al., 2018). This mouse model is well characterised, and exhibits the mouse equivalent of the most common causative mutation for MH in the UK (Miller et al., 2018). The *RYR1* p.(G2434R) heterozygous phenotype is relatively mild (Carpenter et al., 2009), and thus differences in MH phenotypes should in theory be easier to distinguish.

3.2 Methods

3.2.1 CRISPR guide design

CRISPR guide RNAs were designed to target common exons amongst the majority, if not all, transcript variants expressed in mice for each gene. The entire exonic sequence for chosen exons as potential targets (mouse PYGM reference sequence: NC_000085.7, mouse CPT2 reference sequence: NC_000070.7) were entered into Benchlings (Benchling, biology software, 2021) design tool. The guide RNA design tool searched for candidate sequences, of around 20 nucleotides, that were adjacent to a PAM sequence of NGG required for Cas9 from *streptococcus pyogenes*. Candidate guide sequences were subsequently cross-checked for on-target and off-target scores on IDTs guide check tool ((https://eu.idtdna.com/site/order/designtool/index/CRISPR_SEQUENCE, 2021). On-target scores predict the cleavage efficiency of Cas9, whilst off-target scores predict the likelihood of Cas9 cleaving non-intended sites. Candidate guide sequences were filtered for on-target scores and off-target scores above 50. The three highest scoring guides were chosen, if there were more than 3 (table 3.1).

Table 3.1: Chosen CRISPR guide sequences for *PYGM* and *CPT2*. Strand indicates the targeting of sense (+) or antisense (-) strands. On and Off target scores generated using IDTs guide checker tool and scale from 0 – 100. A higher on/off target score indicates higher targeting efficiency and lower probability of off-target perturbations respectively.

Gene	Exon	Strand	Sequence	PAM	IDT on target score	IDT off target score
PYGM	1	+	ACTGTCCGGGACCACCTCGT	GGG	76	89
	5	-	ACTCGGCCATAGAAGTGCAC	AGG	78	84
	16	+	GTCAACCACGACCCTGCGGT	AGG	76	93
CPT2	5	+	ACAAGTGTCGGTCAAAGCCC	TGG	81	77
	5	-	CGTATGCTGTTCACGATGAC	TGG	56	88

3.2.2 CRISPR/Cas9 Ribonucleoprotein Nucleofection

Initially a ribonucleoprotein nucleofection strategy in concert with a fluorescent tag for fluorescence activated cell sorting was chosen. Chosen guide sequences were first tested for efficiency in NIH/3T3 cells, due to higher transfection efficiencies in this cell line, before conducting transfection in heterozygous *RYR1* p.(G2435R) mouse myoblasts. This enabled efficiency testing for each candidate guide sequence, before narrowing down to a chosen sequence for downstream application. The crRNA for candidate guide sequences and ATTO-550 conjugated tracrRNA were sourced from IDT. These were combined to form a guide RNA duplex by combining to final concentration of 100μM of each and subsequently annealed by heating to 95ºC for 5 minutes. The solution was left to cool to room temp and subsequently stored at -20ºC for long term storage. To form ribonucleoprotein complexes, 120pmol of guide duplex was combined with 104pmol of Cas9 to a final volume of 5ul. The solution was incubated at room temperature for 20 minutes, prior to log sterm storage at -80ºC.

For nucleofection, cells were trypsinised and pelleted as before (section 2.1). Cell pellet was resuspended in 1ml of media and counted using a haemocytometer using a 1:1 ratio of trypan blue. 1.5 x 10^6 cells were re-pelleted and resuspended in 100μl of nucleofector solution (Nucleofector kit V, Lonza) and 5μl of RNP solution was added. Cell solution was transferred to a cuvette and inserted into the Amaxa Nucleofector II (Lonza). Program A-024 was used for NIH/3T3 cells, and program B-032 was used for myoblasts. Cells were immediately plated onto the appropriate tissue culture dish and incubated at 37ºC and 5% CO2 for 24 hours.

3.2.3 TIDE

To check for editing efficiency, the frequency of insertion and deletions in a mixed pool of NIH/3T3 cells, each transfected with a different candidate guide sequence, were checked using Tracking of Indels by Decomposition (TIDE software)

(Brinkman et al., 2014). In order to do this, direct extraction of DNA from transfected NIH/3T3 cells was conducted and PCR amplified as described before (section 2.3). PCR products were sent for clean up and Sanger sequencing to Source Bioscience. AB1 files were subsequently imported into the TIDE software. The guide with greatest frequency was taken forward for subsequent transfections.

3.2.4 Fluorescent activated cell sorting

Following 24 hours incubation, myoblasts were trypsinised and pelleted as before. Cell pellet was resuspended in 500µl sorting buffer (10% v/v FBS, 2x P/S, 1µg/ml 7-AAD (Thermofisher), in PBS) before transferring through a 70µm cell strainer to FACS tubes (352063, Falcon®, Corning) that were pre-coated with sorting buffer, and kept on ice until sorting. FACS was conducted on the Beckton Dickinson Influx™ by Ms. Liz Straszynski, gating for both 7-AAD for live cells and the ATTO-550 dye for successfully transfected cells. Cells were sorted into one cell per well in a 96 well plate coated with ECL. 96 well plate contained 100µl of a 1:1 mix of warm fresh and spent media. Spent media was collected from heterozygous *RYR1* p.(G2435R) cells and sterile filtered using a 0.22µm filter prior to use. Colonies were trypsinised and progressively transferred to larger well sizes up to a 10cm dish, prior to direct DNA extraction for sequencing and freezing down.

3.2.5 CRISPR/Cas9 plasmid lipofection

Chosen CRISPR guide sequences were inserted into a commercial eSpCas9-2A-puro-(PX459) V2.0 plasmid by GenScript. This plasmid contained eSpCas9, a modified variant of Cas9 used increase cleavage efficiency, the chosen sgRNA sequence and a puromycin selection cassette (figure 3.4). An empty-vector control was also transfected, where plasmid did not contain any guide sequence.

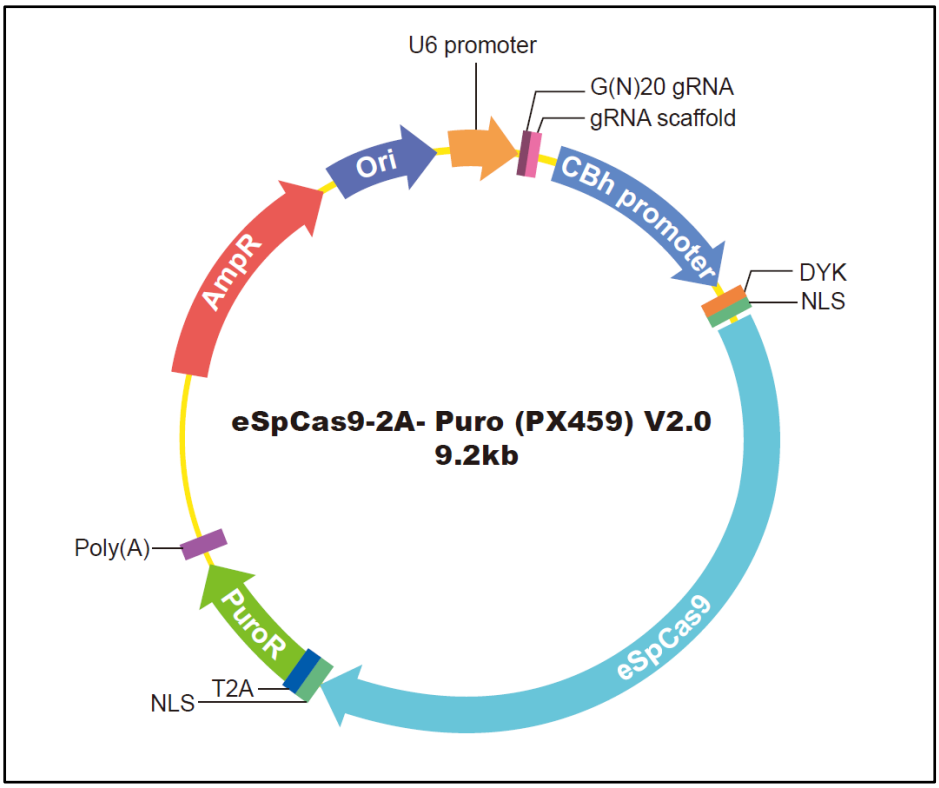

Figure 3.4: PX459 Plasmid vector map from GenScript. Plasmid construct contains eSpCas9 variant and scaffold for the insertion of guide sequences for the sgRNA. Ampicillin resistance cassette (AmpR) and origin of replication (Ori) included for plasmid prep. U6 promoter used for sgRNA expression, hybrid CMV and CBA promoter (CBh) used for eSpCas9 expression. DYK tag included for purification of eSpCas9, T2A sequence included in case of insertion of additional protein sequences. Nuclear localisation signal (NLS) sequences enable eSpCas9 to enter nuclear envelope. Puromycin resistance cassette (PuroR) included for selection in transfected cells.

2.5µg of plasmid was mixed with 7.5µl Lipofectamine 3000 (Thermofisher) for transfection into heterozygous *RYR1* p.(G2435R) primary mouse myoblasts. The mixture was added drop-wise to media and incubated at 37ºC and 5% CO2 for 24 hours. Lipofectamine was subsequently removed and media supplemented with 5µg/ml puromycin (Thermofisher) added. Purmoycin concentration for selection was determined using a kill assay in *Ryr1* p.(G2435R) heterozygous myoblasts over 48 hours with concentrations ranging from 1-10 µg/ml. Selection took place over 48 hours and transfected cells were trypsinised and counted as before, on the condition that control cells were all dead. Cells were diluted and plated in 96 well plate at a concentration of 0.5 cells per 200µl per well in a 1:1 mix of fresh and spent media. Empty vector control cells were plated at 100 cells per well. Colonies

were grown in progressively larger wells up to a 10cm dish, at which point DNA was extracted via direct extraction for sequencing and colonies were frozen down and stored at -80ºC. DNA was PCR amplified as described before, and PCR product was sent to Source Bioscience for clean up and Sanger sequencing.

3.2.6 TA cloning

TA cloning was used to confirm homozygosity of mutations suspected to lead to knock-out in candidate colonies. The TA cloning kit pCR®2.1 with One Shot® TOP10F' chemically competent *E.coli* (Thermofisher) was used following the manufacturers protocol. Briefly, PCR products were inserted into the pCR®2.1 vector (figure 3.5) in a 1:1 ratio using T4 DNA ligase and incubated at room temperature for 15 minutes. Ligation reaction was then used in transformations of TOP10F' chemically competent E.coli as described before. Following plating, 10 white colonies were picked per transformation and DNA was extracted using direct extraction, followed by PCR amplification of the insert using M13 primers. PCR products were sent to Source Bioscience for clean up and Sanger sequencing.

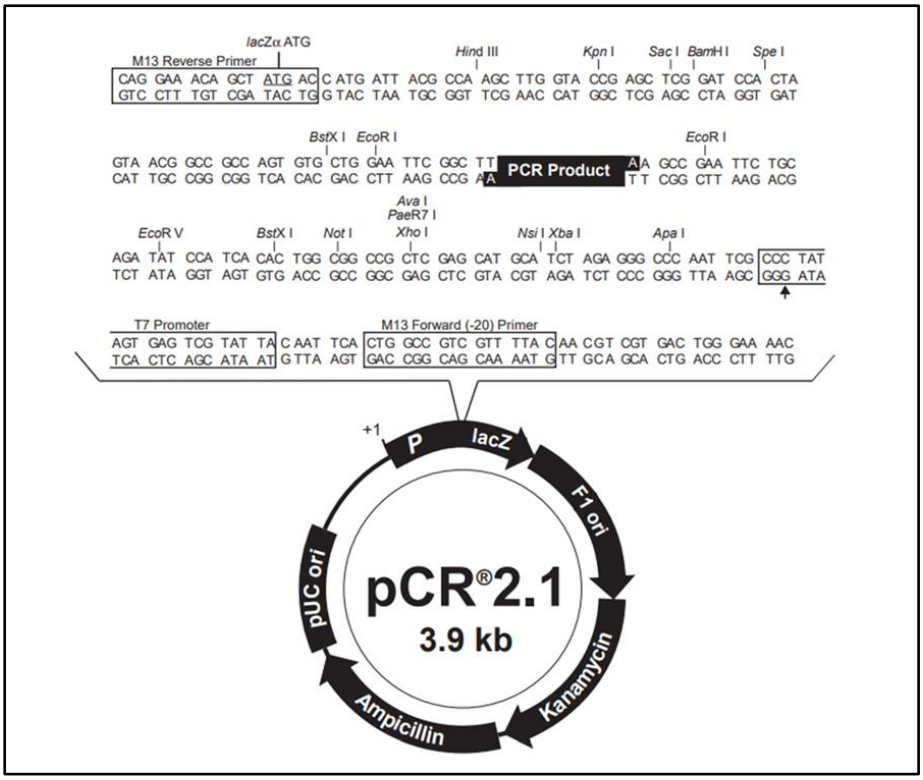

Figure 3.5: pCR®2.1 vector map from Thermofisher.

3.3 Results

The nucleofection and FACS strategy did not yield any successful knock-out clones. This was postulated to be due to the cytotoxicity of the combination of nucleofection and FACS, resulting in a lack of successful primary mouse myoblast knock-out colonies that could grow from a single cell. Based on this the strategy was shifted to lipofection of a single plasmid containing eSpCas9 and a single-guideRNA, followed by puromycin selection and serial dilution to single cells in order to reduce cytotoxicity in primary mouse myoblasts as much as possible.

3.3.1 TIDE and gRNA selection

TIDE provides a few different statistics and outputs as part of its modelling of indel spread. A total editing efficiency is provided which is the sum of all proportions of indels up to 10bp, which show significant difference ($p<0.001$) as compared to a reference trace. This is represented as a bar graph showing the proportion of the mixed pool of NIH/3T3 cells with different indel sizes. This is the primary output in deciding between guide sequences. However, an R^2 value also indicates how well its model fits and therefore the confidence that one can have in the total editing efficiency. This must also be considered, when selecting a guide sequence. In order to get the best possible fit, parameters in the model are tweaked, such as number of bases used to align sequences and the number of bases after the cut site. However, repetitive regions and noise in the trace can also affect how well its able to model indel decomposition. Another output is the quality control aberrant sequence signal chart, which allows you to visualise the proportion sequence discrepancies along the base positions. In this output you should be able to see low discrepancy prior to the cut site and high discrepancy after. This is also useful in deciding the guide sequence to use.

3.3.1.1 CPT2

TIDE analysis of the editing efficiency and INDEL decomposition showed the CPT2 crRNA sequence “ACAAGTGTCGGTCAAAGCCC” to be more efficient of the two, with higher confidence in the finding as represented by a higher R^2 value (figures 3.6 and 3.7). Specifically, this guide had a total editing efficiency of ~13.2% with an $R^2 = 0.96$, whilst the guide sequence of “CGTATGCTGTTCACGATGAC” had a total editing efficiency of ~6.7% with an $R^2 = 0.89$. The aberrant sequence signal also confirmed the increased efficiency of the first guide sequence over the latter with larger discrepancies noticed in sequence “ACAAGTGTCGGTCAAAGCCC”. The results also match the differences of the *in silico* predictions of the on target scores for each guide sequence. Based on this, the first guide sequence was taken forward for knock-out generation.

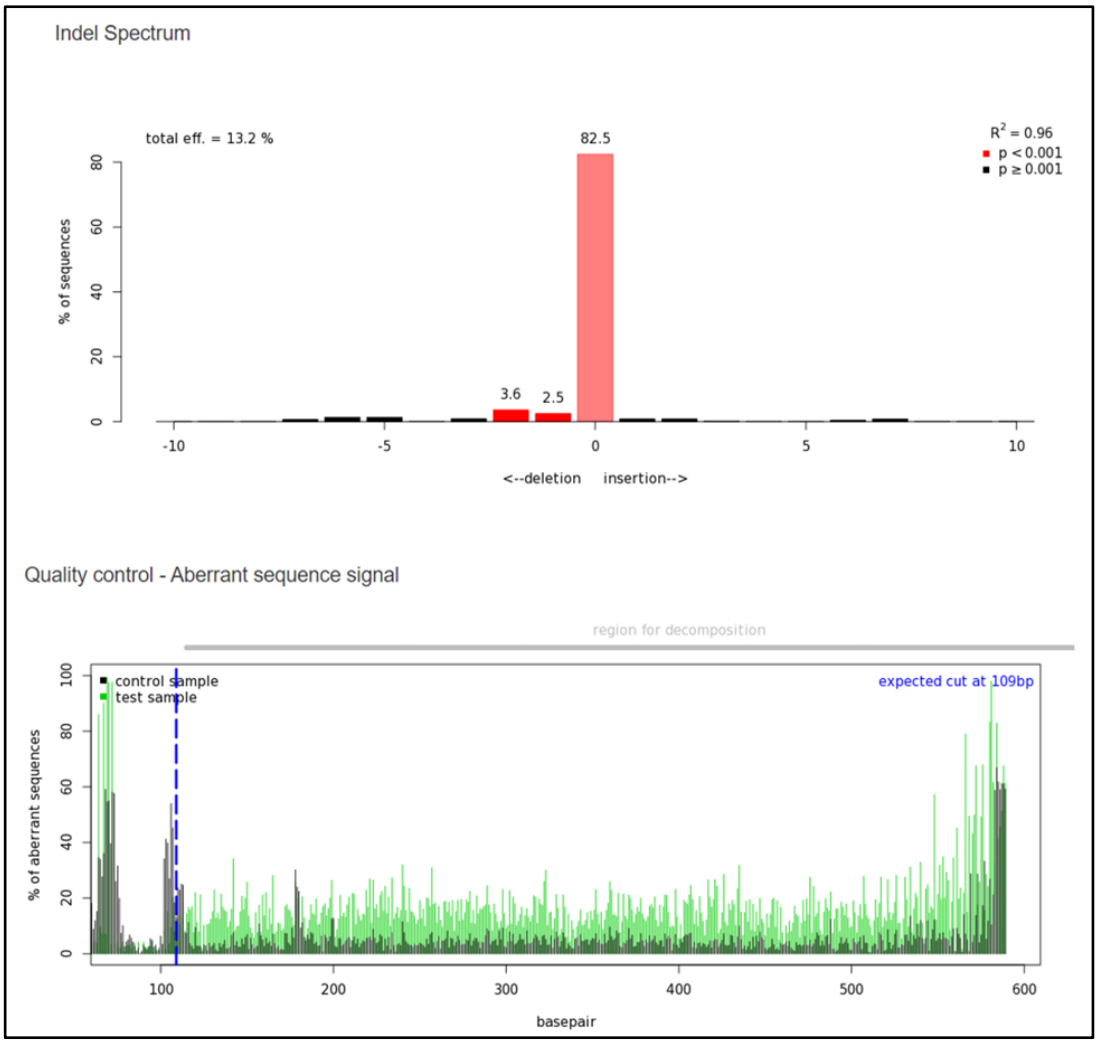

Figure 3.6: TIDE analysis of *CPT2* guide sequence "ACAAGTGTCGGTCAAAGCCC". Indel spectrum shown on top representing spread of proportions of insertions and deletions of up to 10bp in size in mixed pool of NIH/3T3 cells based on Sanger sequence surrounding cut site. Red bars represent those with p<0.001, indicating the proportion represented is significantly different to the background noise in the sequence trace. Aberrant sequence signal shown below, indicating the discrepancy between control (dark green) and test sample (light green) at each sequence position and the cut site represented with dashed blue line.

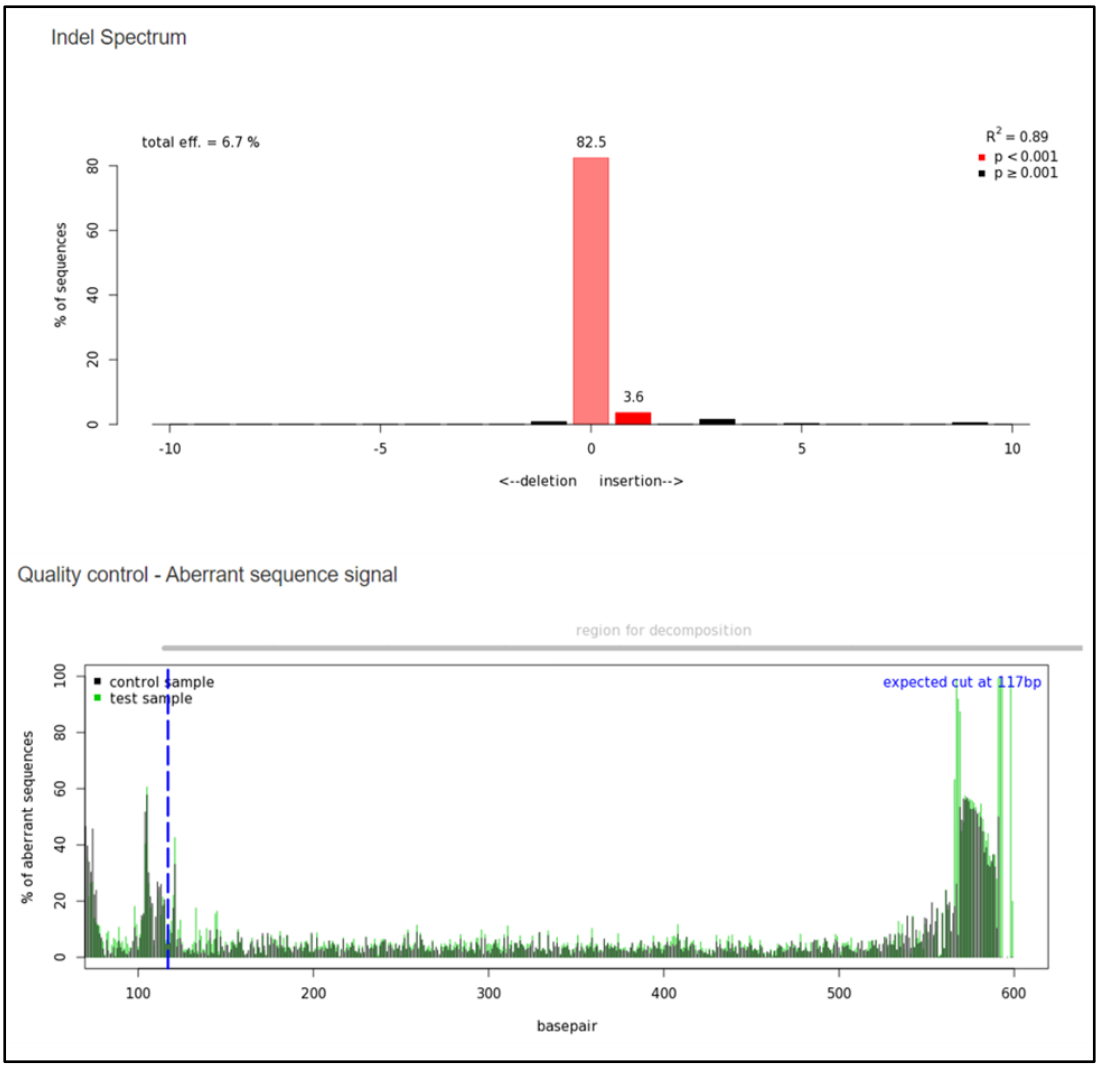

Figure 3.7: TIDE analysis of *CPT2* guide sequence "CGTATGCTGTTCACGATGAC". Indel spectrum shown on top representing spread of proportions of insertions and deletions of up to 10bp in size in mixed pool of NIH/3T3 cells based on Sanger sequence surrounding cut site. Red bars represent those with a p-value below 0.001, indicating the proportion represented is significantly different from background noise in the sequence trace. Aberrant sequence signal shown below, indicating the discrepancy between control (dark green) and test sample (light green) at each sequence position and the cut site represented with dashed blue line.

3.3.1.2 PYGM

TIDE analysis showed varying efficiencies for the three PYGM guide sequences. Sequence “GTCAACCACGACCCTGCGGT” showed ~37.7% editing efficiency and had an R^2 = 0.97 indicating good fit for the model (figure 3.8). Sequence “ACTCGGCCATAGAAGTGCAC” showed higher efficiency at ~52.6%, however an R^2 = 0.62 suggested that model fit was poor, and therefore confidence in the higher efficiency was much lower (figure 3.9). Sequence “ACTGTCCGGGACCACCTCGT” showed an editing efficiency of ~30.6% and an R^2 = 0.89 (figure 3.10). Based on this, sequence “GTCAACCACGACCCTGCGGT” was chosen due to the compromise between editing efficiency and confidence in finding as compared to the other two candidate guide sequences. When looking at the aberrant sequence signal for the three guides, a similar output is seen, with sequence “GTCAACCACGACCCTGCGGT” showing a level of discrepancy in between the other two, matching the spread in editing efficiency between the guide sequences.

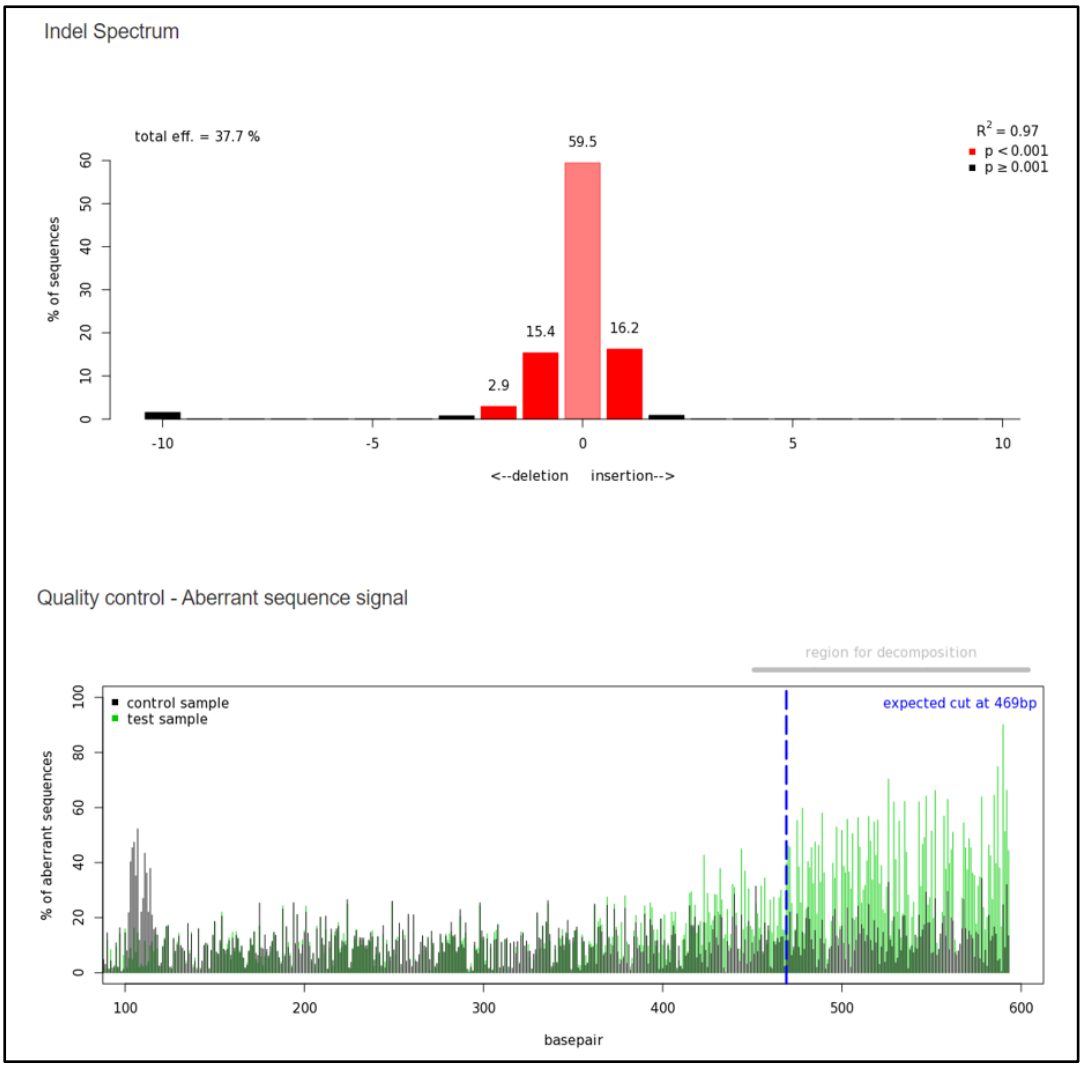

Figure 3.8: TIDE analysis of *PYGM* guide sequence "GTCAACCACGACCCTGCGGT". Indel spectrum shown on top representing spread of proportions of insertions and deletions, of up to 10bp in size, in a mixed pool of NIH/3T3 cells based on Sanger sequence surrounding cut site. Red bars represent those with a p-value below 0.001, indicating the proportion represented is significantly different from background noise in the sequence trace. Aberrant sequence signal shown below, indicating the discrepancy between control (dark green) and test sample (light green) at each sequence position and the cut site represented with dashed blue line.

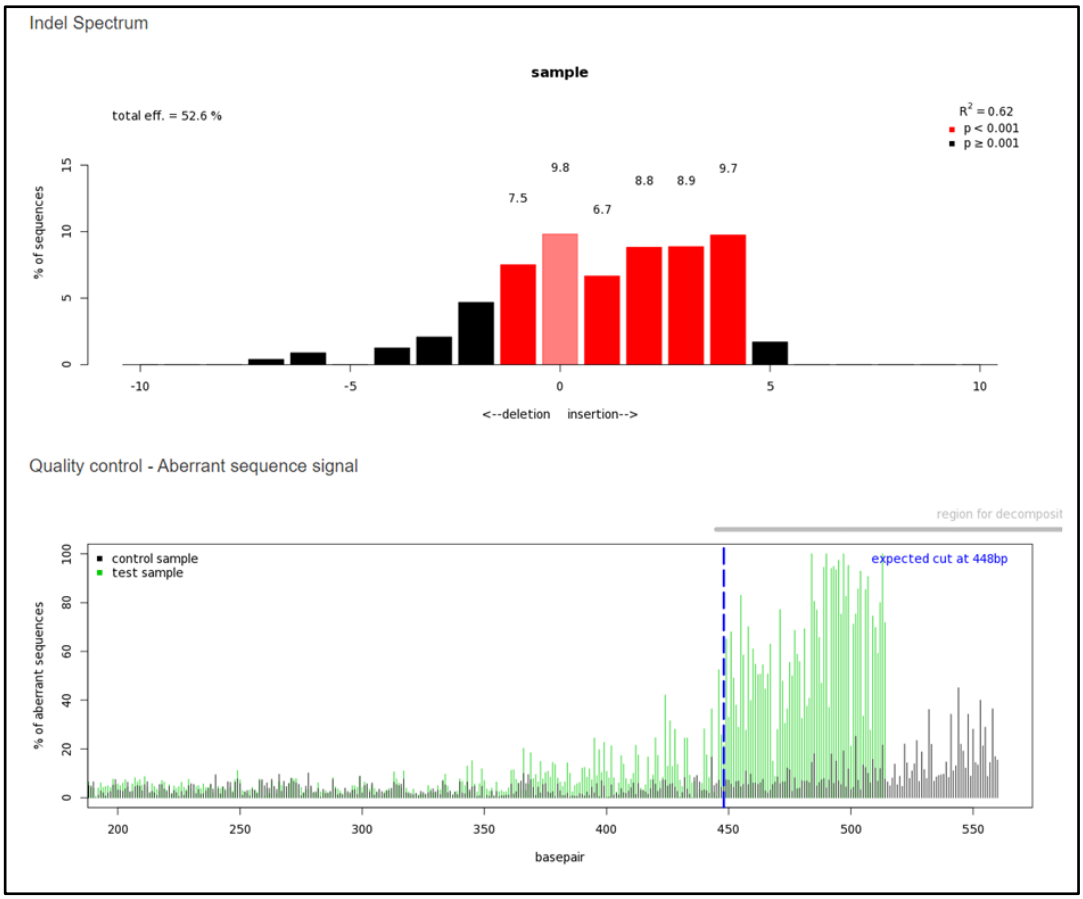

Figure 3.9: TIDE analysis of *PYGM* guide sequence "ACTCGGCCATAGAAGTGCAC". Indel spectrum shown on top representing spread of proportions of insertions and deletions, of up to 10bp in size, in a mixed pool of NIH/3T3 cells based on Sanger sequence surrounding cut site. Red bars represent those with a p-value below 0.001, indicating the proportion represented is significantly different from background noise in the sequence trace. Aberrant sequence signal shown below, indicating the discrepancy between control (dark green) and test sample (light green) at each sequence position and the cut site represented with dashed blue line.

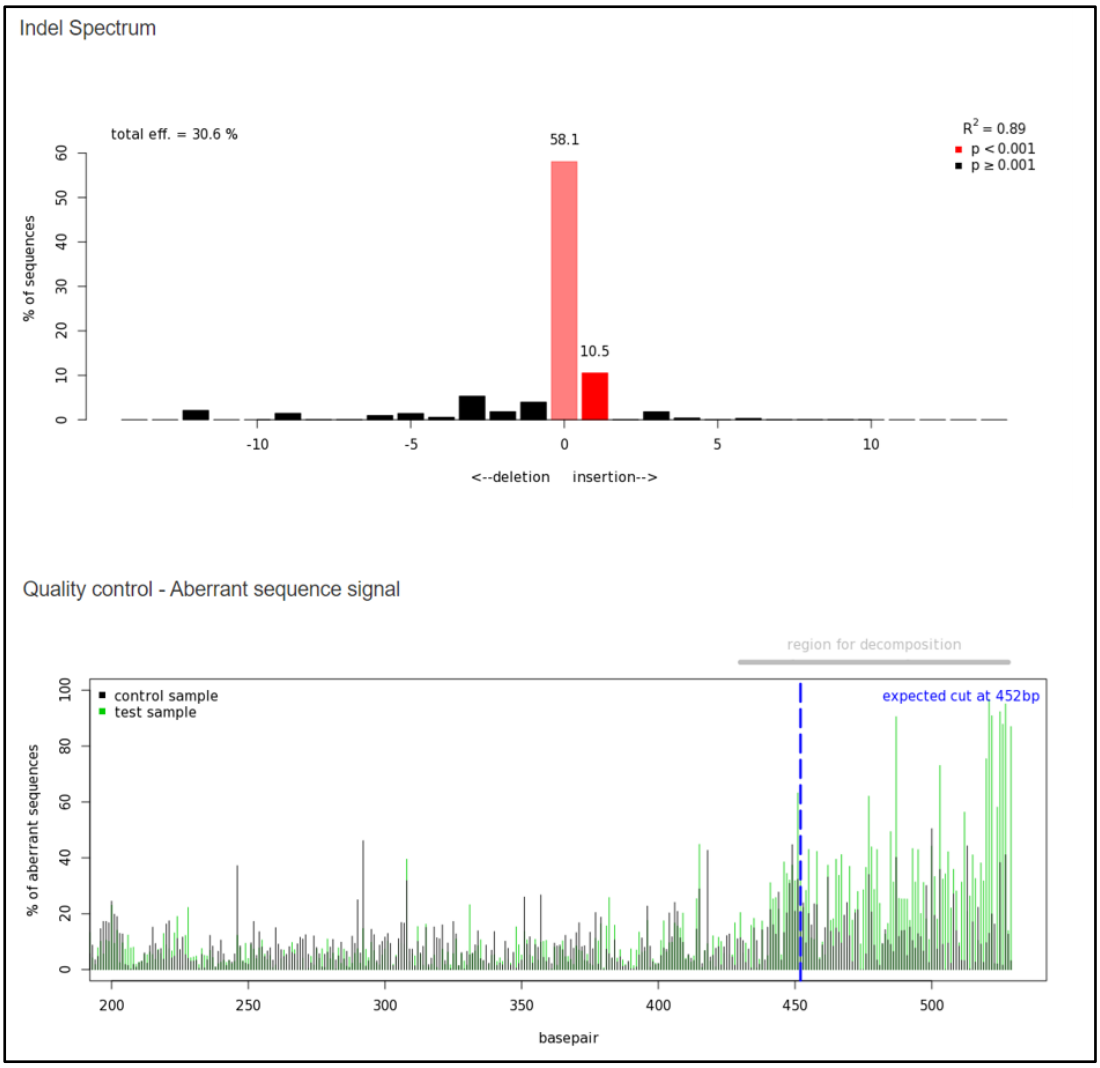

Figure 3.10: TIDE analysis of *PYGM* guide sequence "ACTGTCCGGGACCACCTCGT". Indel spectrum shown on top representing spread of proportions of insertions and deletions, of up to 10bp in size, in a mixed pool of NIH/3T3 cells based on Sanger sequence surrounding cut site. Red bars represent those with a p-value below 0.001, indicating the proportion represented is significantly different from background noise in the sequence trace. Aberrant sequence signal shown below, indicating the discrepancy between control (dark green) and test sample (light green) at each sequence position and the cut site represented with dashed blue line.

3.3.2 Sanger sequencing of myoblast clones

3.3.2.1 *Cpt2*

Out of 576 single cell wells plated following lipofection, a total of 25 survived to 10cm dishes for sequencing. Out of 25 clones, 2 showed successful mutagenesis at the target site, of which only clone 11 (figure 3.11) had a homozygous mutation predicted to result in knock-out. Homozygosity was confirmed with TA cloning. The sanger trace indicated a deletion of a single cytosine base (c.C1653del) in the coding sequence of the gene. This would be predicted to lead to a frameshift change in the coding sequence.. This was in turn predicted to result in nonsense mediated decay of the resulting mRNA and ultimately knock-out. This clone was taken forward for further validation.

3.3.2.2 *Pygm*

Out of 576 single cell wells plated following lipofection, a total of 25 survived to 10cm dishes for sequencing. Out of 25 clones, 2 showed successful mutagenesis at the target site. Clone 3 showed a homozygous T insertion that was predicted to lead to a frameshift and downstream premature stop codon. Clone 13 showed compound heterozygote mutations (figure 3.12); a G deletion predicted to lead to the formation of a premature stop codon immediately after and a 28bp insertion also predicted to include a premature stop codon. Homozygosity and compound heterozygosity were confirmed using TA cloning.

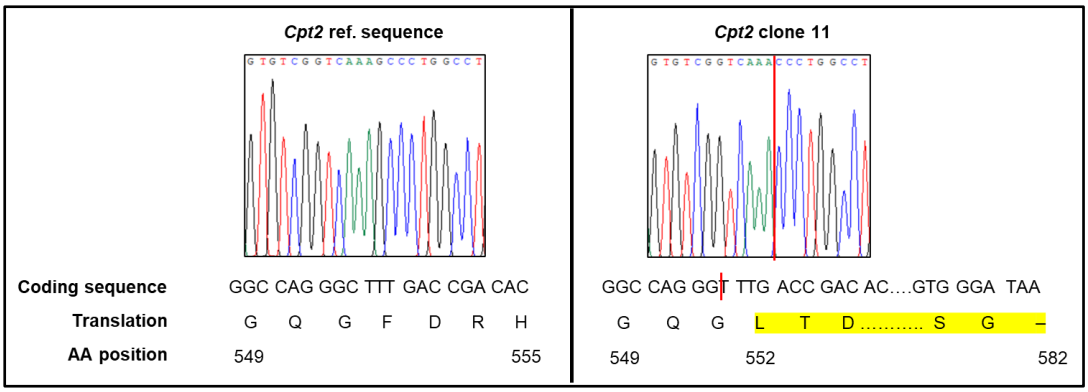

Figure 3.11: Sanger sequence trace of control sample and *Cpt2* clone 11. Red line over clone 11 trace indicates site of deletion. Coding sequence transcribed underneath traces, with corresponding amino acids and their position indicated further below. Yellow highlighted amino acids indicate the changes from reference sequence, with dash indicating premature stop codon.

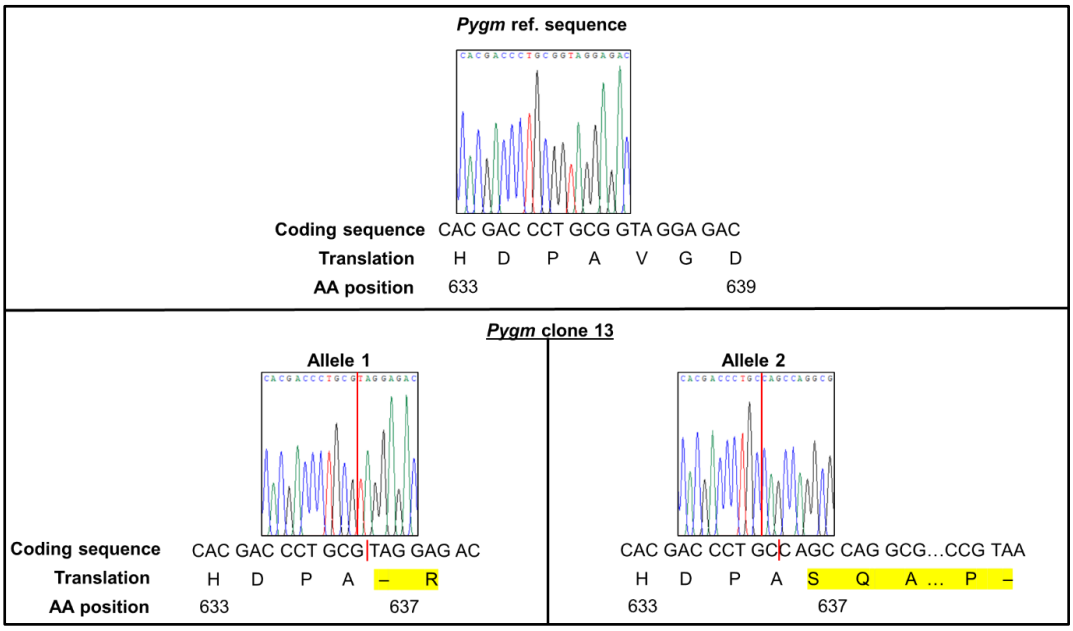

Figure 3.12: Sanger sequence trace of control sample and both alleles of *Pygm* clone 13. Red line over clone 13 traces indicates sites of indel. Coding sequence transcribed underneath traces, with corresponding amino acids and their position indicated further below. Yellow highlighted amino acids indicate the changes from reference sequence, with dash indicating premature stop codon.

3.3.3 Validation of gene expression in myoblast clones

RT-qPCR was used to assess mRNA levels, followed by western blot to assess protein expression in order to confirm predicted gene knock-out. Transcript and protein expression were assessed in myotubes after differentiating cells for 4 days on ECL and extracting RNA and protein. Knock-out clones were compared to control heterozygous *RYR1* p.(G2435R) myotubes.

3.3.3.1 *Cpt2*

Transcript levels in clone 11 were ~12% relative to *Ryr1* p.(G2435R) heterozygous myotubes (figure 3.13A), which was a significant knock-down of mRNA expression, which may be due to the premature stop codon potentially resulting in nonsense mediated decay of the transcripts. Protein expression via western blot confirmed knock-out of the gene as clone 11 had an absence of bands. A GAPDH control was used to verify protein loading did not differ between wells (figure 3.13B). Full blots can be viewed in the appendices.

3.3.3.2 *Pygm*

Transcript levels in clone 13 were ~2% relative to *Ryr1* p.(G2435R) heterozygous myotubes (figure 3.14A), which was a significant knockdown of the mRNA, which may be due to the premature stop codons in both alleles potentially resulting in nonsense mediated decay of the transcripts. Protein expression via western blot confirmed knock-out of the gene as clone 13 had an absence of bands. A GAPDH control was used to verify protein loading did not differ between wells (figure 3.14B). Full blots can be viewed in the appendices.

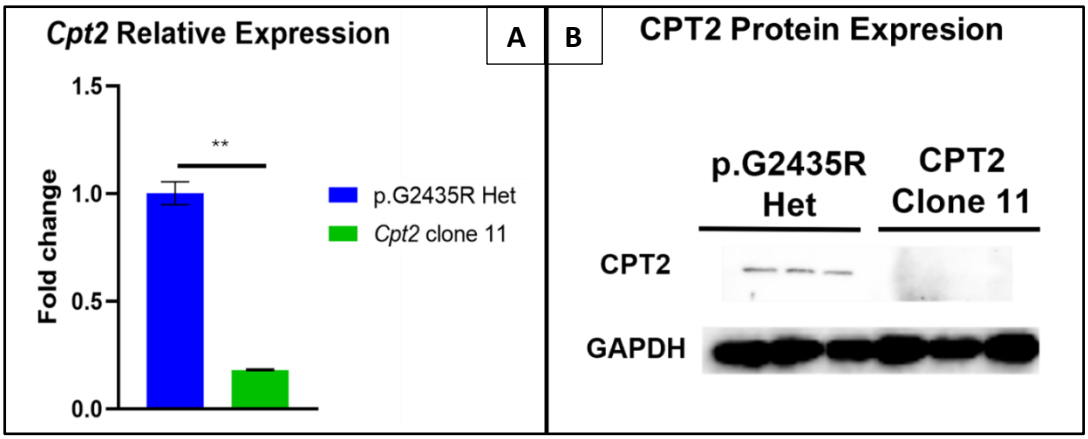

Figure 3.13: *Cpt2* expression in knock-out clone 11. A) Relative mRNA level, as compared to control *Ryr1* p.(G2435R) Heterozygous genotype, showing mean relative transcript level (fold change) and SEM error bars. "**" indicates p<0.01 generated from a two-tailed t-test. B) Western blot showing CPT2 and GAPDH protein levels in clone 11 and control genotype. Both conducted at passage 33 from 3 independent samples. Full western blot displayed in Appendix 2, figure A.1.

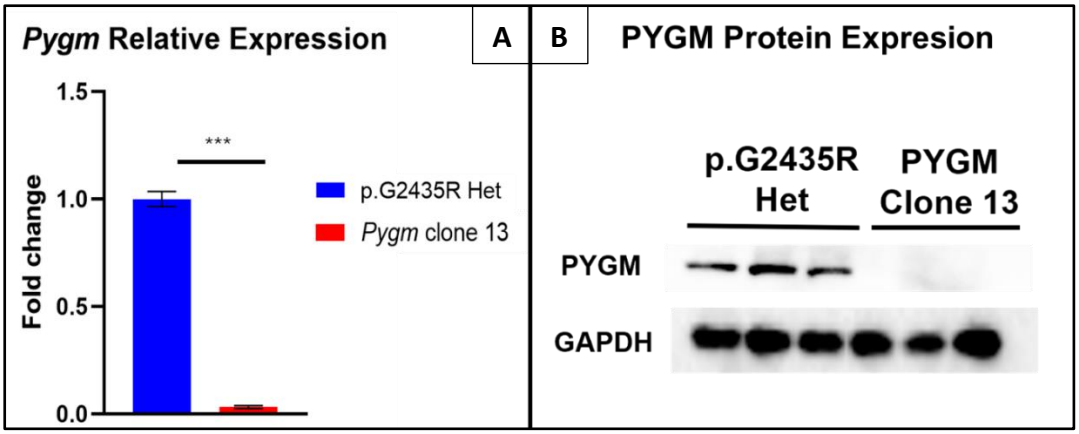

Figure 3.14: *Pygm* expression in knock-out clone 13. A) Relative mRNA level, as compared to control *Ryr1* p.(G2435R) Heterozygous genotype, showing mean relative transcript level (fold change) and SEM error bars. "***" indicates p<0.001 generated from a two tailed t-test. B) Western blot showing CPT2 and GAPDH protein levels in clone 13 and control genotype. Both conducted at passage 33 from 3 independent samples. Full western blot displayed in Appendix 2, figure A.2.

3.3.4 Myotube formation

Formation of multinucleated myotubes was confirmed using immunofluorescence. DAPI and an anti-Myosin Heavy Chain primary antibody with an Alexa-fluor 488 conjugated secondary antibody were used. Myosin heavy chain is an established marker for myogenesis and myotube formation and so was chosen as a target for validation, alongside multinucleated cells. Myotube formation was necessary for downstream applications as an *in vitro* model for skeletal muscle. Knock-out clones *Cpt2* clone 11 and *Pygm* clone 13 were shown to produce multinucleated structures that express myosin heavy chain, confirming the formation of myotubes. The *Ryr1* p.(G2435R) heterozygous mouse myotubes were used as a positive control for reference and the empty vector control cell line was also validated for myotube formation (figure 3.15). Brightfield images are also shown adjacent to fluorescent images for reference.

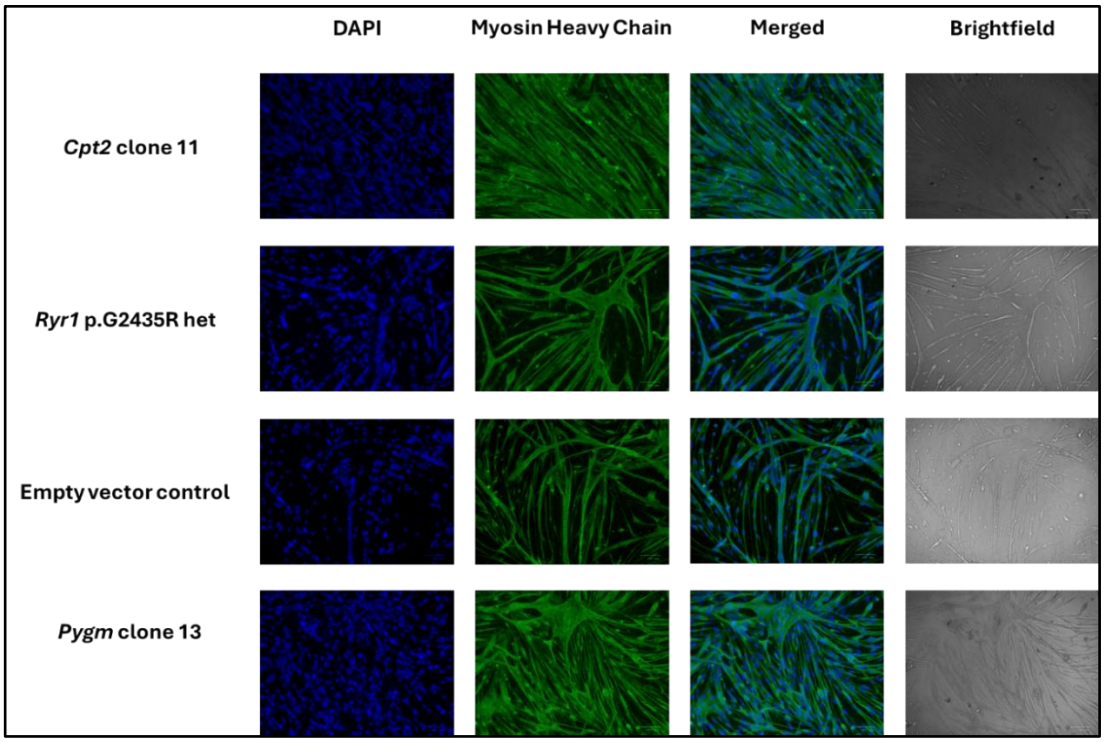

Figure 3.15: Immunofluorescence assay in knock-out clones. *Cpt2* clone 11, *Pygm* clone 13, Empty vector control and *Ryr1* p.(G2435R) heterozygous mouse myotube formation confirmed by using DAPI and anti-Myosin Heavy Chain antibody with Alexa-fluor 488 conjugated secondary antibody. Brightfield images also shown adjacent to fluorescent images.

3.3.5 Functional assessment of clones by investigating sensitivity to KCl

KCl is a depolarizing agent and, by using a concentration response assay, determining the sensitivity to this reagent sheds light on the variation in threshold for broadly triggering excitation-contraction coupling across genotypes. Myotubes were exposed to a range of KCl concentrations from 5mM to 40mM (figure 3.16). 60mM was also used prior to dose response assay to check for functional ECC. The *Ryr1* p.(G2435R) heterozygous myotubes were used as a reference for the analysis to assess whether knock-out changed sensitivity to KCl relative to this genotype. The empty vector control was also used as a control to assess whether the CRISPR/Cas9 gene editing process may have had any affect. *Cpt2* clone 11 (17.3mM, 95% CI:16.0-18.6) did not show any significant difference from the reference genotype (17.3mM, 95% CI:16.6-18.0), suggesting no change in sensitivity. *Pygm* clone 13 showed a significant increase in sensitivity to KCl (13.4mM, 95% CI:12.6-14.2), which may suggest a generally lower threshold to triggering ECC. The empty vector control (15.8mM, 95% CI:14.6-17.1) did show a significant increase in sensitivity. Both knock-out clones also showed a significant difference to the empty vector control ($p<0.0001$).

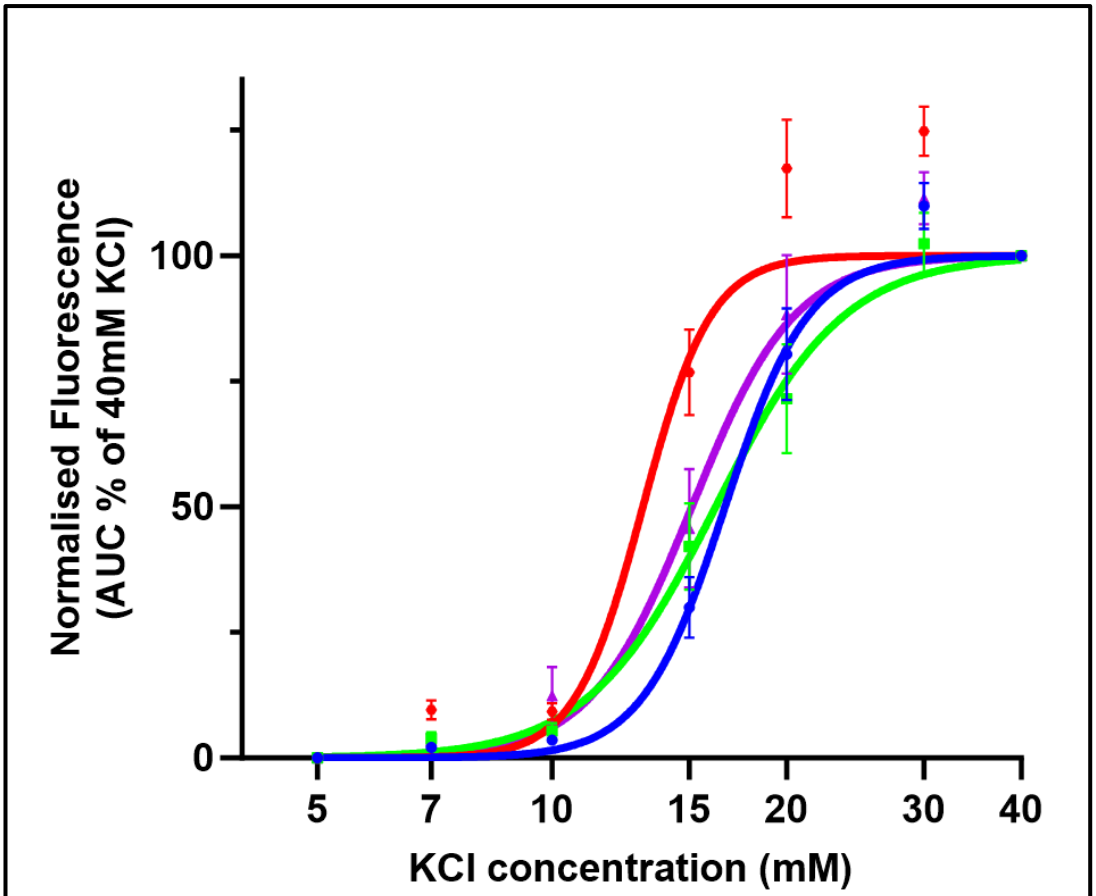

Key	Genotype	EC_{50} (mM)	p-value	n
	p.G2435R Het	17.3	Ref.	41
	Cpt2 clone 11	17.3	ns	52
	Pygm clone 13	13.4	<0.0001	55
	Empty Vector Control	15.8	<0.0001	42

Figure 3.16: Knock-out clone KCl-dose response. Data points shown are mean with 95% confidence intervals of area-under the curve at each concentration. Table on right shows key for graph and corresponding EC_{50} (mM) values with n-number and p-value. P-values based on Brown-Forsythe and Welchs ANOVA, with Tukeys correction for multiple comparisons, comparing to reference *RYR1* p.(G2435R) heterozygous genotype.

3.3.6 Functional assessment of clones by investigating sensitivity to caffeine

Caffeine is an RYR1 agonist and is used diagnostically as part of the IVCT to challenge muscle tissue and assess susceptibility for MH. Myotubes were exposed to a range of caffeine concentrations from 1mM to 20mM (figure 3.17). However, 60mM KCl was also used prior to dose response assay to check for functional ECC. The *Ryr1* p.(G2435R) heterozygous myotubes were used as a reference for the analysis to assess whether knock-out changed sensitivity to KCl relative to this genotype. The empty vector control was also used as control to assess whether the CRISPR/Cas9 gene editing process may have had any affect. The empty vector control (4.7mM, 95% CI:4.2-5.4) did not show any significant difference to the reference genotype (4.1mM, 95% CI:3.5-4.8), which was expected. *Pygm* clone 13 (4.5mM, 95% CI:3.9-5.2) also did not show any significant difference to the *Ryr1* p.(G2435R) heterozygous myotubes. *Cpt2* clone 11 (6.4mM, 95% CI:5.8-7.2) showed a decrease in sensitivity to caffeine. When compared to the empty vector control, *Pygm* clone 13 did not show a significant difference, whilst *Cpt2* clone 11 exhibited a decrease in sensitivity ($p<0.0001$).

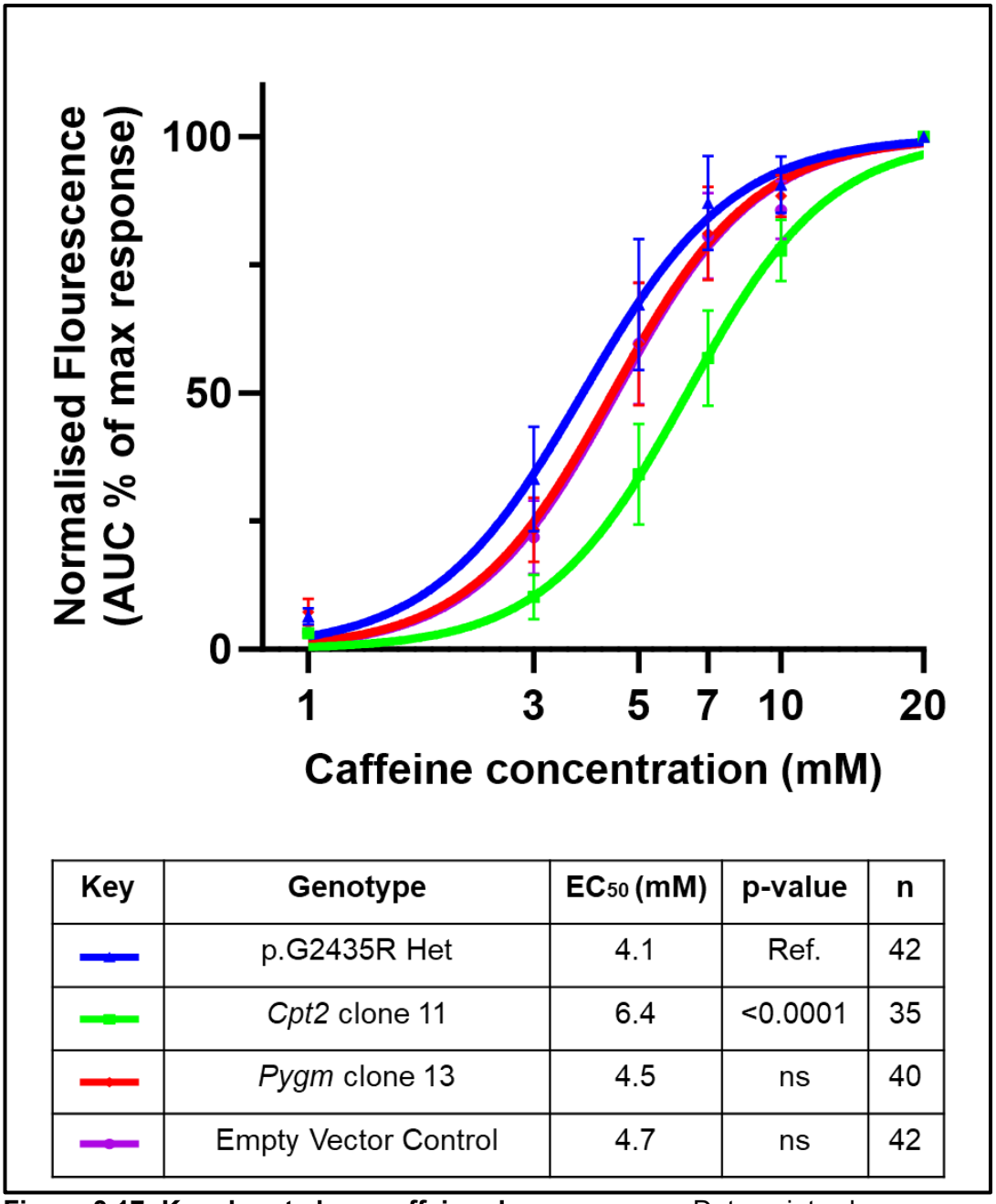

Key	Genotype	EC_{50} (mM)	p-value	n
	p.G2435R Het	4.1	Ref.	42
	Cpt2 clone 11	6.4	<0.0001	35
	Pygm clone 13	4.5	ns	40
	Empty Vector Control	4.7	ns	42

Figure 3.17: Knock-out clone caffeine-dose response. Data points shown are mean with 95% confidence intervals of area-under the curve at each concentration. Table on right shows key for graph and corresponding EC_{50} (mM) values with n-number and p-value. P-values based on Brown-Forsythe and Welchs ANOVA, with Tukeys correction for multiple comparisons, comparing to the reference *RYR1* p.(G2435R) heterozygous genotype.

3.4 Discussion

The generation of knock-out clones posed certain challenges and limitations in the execution of this chapters aims. Firstly, the transfection method had to be adjusted part way through due to the cytotoxicity of the nucleofection/RNP strategy. The initial strategy was chosen for the increase in efficiency this may confer. This worked with the NIH/3T3 cell line, however, proved problematic with primary mouse myoblasts. The nucleofection coupled with attempts to single cell sort via FACS soon after proved to cause too much damage, that single cell colonies could not recover from. This was compounded when considering that a metabolic gene may have been knocked out, increasing the difficulty of recovery for cells with successful editing events. Based on this, a change to a less cytotoxic strategy was employed, using a plasmid coupled with lipofection and serial dilution to single cells. Additionally, the puromycin selection for successfully transfected cells, between transfection and serial dilution, may have provided a brief rest period in a mixed pool of cells enabling better recovery upon establishing single cell colonies.

Expectedly still, efficiency was low. Around 4% of single cell colonies survived, of which again only ~8% had a successful editing event, resulting in a final success rate of ~0.35%. This is likely due to the efficiency of plasmid transfection coupled with the use of primary cells. Using primary cells naturally meant they were more sensitive to any damage induced from the CRISPR strategies. As a result, few clonal lines with successful knock-out were generated. This was a limitation of this chapter, as the results could not be bolstered by validating across multiple knock-out clones for each gene, providing more robust findings. Thus, a useful next step would be to generate additional knock-out clones that could be used to validate the results of this chapter.

The resulting passage number after completion of the CRISPR strategy also posed a limitation. Starting at passage 10 *Ryr1* p.(G2435R) heterozygous myoblasts, given

a starting passage of P8 after successful isolation from muscle, was as low as possible after thawing cells and letting them acclimatise prior to transfection. The subsequent process of growing a 60% confluent 10cm dish from a single cell added ~20 doublings, and as such successful clonal colonies were effectively P30 by the time they could be used experimentally. Therefore, there is a potential accumulation of background variation that must be considered as well.

Interestingly, similar limitations in passage number and transduction efficiency were noted in a preliminary abstract attempting *RYR1* knockout in human myoblasts (Beaufils et al., 2022). The protocol utilised lentivirus mediated transduction of CRISPR components, noting the cytotoxicity and issues with generation of clonal populations. Although, they were able to generate some representative results of 4-Chloromethcathinone, a RYR1 agonist, in a single immortalised line that circumvented passage limitations. Whilst CRISPR efficiency is well documented (Cong et al., 2013; Ran, Hsu, Lin, et al., 2013; Ran, Hsu, Wright, et al., 2013; Seki & Rutz, 2018), the documentation of passage limits of myoblasts is lacking. Anecdotally, myoblasts are typically interrogated at passages around 10-16, with isolation from muscle resulting in a starting passage of 8. The results in this chapter show that it is possible to culture primary mouse myoblasts for much longer, with an anecdotal limit of passage ~40. However, further investigation into the cell health, such as investigating markers of senescence and the percentage of cells that may have entered this phase in a late passage population, would be useful in determining their robustness. It would also be useful to interrogate late passage cells for accumulation of mutations, in order to deduce the degree of drift.

The strong reduction in transcript level observed in *Pygm* clone 13, may be explained by the exon-junction-complex model of NMD (Brogna & Wen, 2009). This model dictates that the EJC bound to the mRNA during the initial round of translation leads to the recruitment and activation of NMD-promoting factors, such

as UPF1, on the ribosome upon the termination of translation. Therefore, a premature stop codon prior to the final exon-exon junction would lead to mRNA degradation. However, as the target for *Cpt2* was exon 5, the EJC model would not apply here. if the premature stop codon is in the last exon, then the EJC has already detached, and therefore based on this model it is less likely that mRNA is degraded. Instead the faux 3'-UTR model (Brogna & Wen, 2009) may be what led to the reduction in transcript levels in *Cpt2* clone 13. This model relies on the distance between the premature stop codon and the 3' UTR to explain NMD. In this model, the poly(A) binding protein is the key influence in whether mRNA is degraded. In a canonical termination of translation, PABP binds to the terminating ribosome. However, if the premature stop codon is far enough from the 3' UTR, NMD-promoting factors are able to bind instead leading to mRNA degradation. Ultimately the difference in transcript level knock-down observed between the two genes did not carry over to protein expression, with both clones exhibiting clear knock-out.

Sensitivity to potassium chloride was higher in the *Pygm* knock-out line than the controls. This suggests that loss of function in *Pygm* may broadly affect excitation contraction coupling as predicted, given the reduced metabolic capacity this may result in. Skeletal muscle from McArdles patients show higher levels of oxidative stress (Kaczor et al., 2017) and it was hypothesised that perhaps the increase in ROS may act on RYR1, increasing its sensitivity. However, *Pygm* clone 13 did not exhibit increased sensitivity to caffeine, an RYR1 agonist, relative to the *Ryr1* p.(G2435R) heterozygous myotubes or the empty vector control. This may suggest that the mechanism of action is not related directly to RYR1, but perhaps other pathways involved. A possible alternative may be that the reduction in ATP production that may result from this knock-out may instead affect SERCA, which actively sequesters calcium back into the SR. A reduction in ATP would possibly result in diminished SERCA activity, which may lead to longer recovery times after

challenge to the myotube or even increased intracellular calcium levels. Investigating the intracellular calcium levels in this knock-out line, relative to controls, would be useful in determining whether this is viable theory. The live-cell imaging protocol could also be altered to accommodate the investigation of SERCA activity.

Sensitivity to potassium chloride was not significantly different in *Cpt2* clone 11, relative to the *Ryr1* p.(G2435R) heterozygous myotubes, but did show significant increase relative to the empty vector control. Furthermore, the clone showed decreased sensitivity to caffeine relative to both control lines. It would be useful to investigate the mechanisms by which CPT II deficiency may have an impact on RYR1 function and ECC. A possible explanation could be the lack of palmitoyl-CoA production as a result of CPT II knock-out. S-palmitoylation is a post-translational modification of RYR1 that regulates Ca^{2+} release from the SR, and it has been shown that the reduction in this modification also leads to reduced RYR1 function, including Ca^{2+} release when stimulated (Chaube et al., 2014). This could explain the decrease in both caffeine KCl sensitivities observed.

An alternative explanation for observations seen in both clones may be genetic compensation (El-Brolosy & Stainier, 2017). This explanation stems from the observed differences between gene knock-down and knock-out, whereby a knock-out may not exhibit the expected level of dysfunction based on the results of a knock-down model, as seen in both zebrafish and mouse studies (Kok et al., 2015; J. K. White et al., 2013). Possible explanations for compensation include the genetic robustness from either redundant genes overlapping in function with the target (Wang et al., 1996) or tightly regulated networks maintaining overall phenotype (Davidson & Levin, 2005). Investigating the expression of other genes in the same metabolic pathways as *PYGM* and *CPT2* may shed light on whether this is the case in these clones. Additionally, the investigation of specific disease-causing variants

may also elucidate whether genetic compensation is truly taking place, or this is a common feature of dysfunction in these genes. Specific disease-causing variants in these genes will be explored in the following chapter.

These results suggest that both *PYGM* and *CPT2* variants may have an impact on malignant hyperthermia susceptibility. The knock-out models represent a severe model of dysfunction in these enzymes, and as such may represent a worst-case scenario when considering the impact of variants in these genes. The observations in this chapter alone would suggest that *Cpt2* perturbations may decrease the severity of the *Ryr1* p.(G2435R) heterozygous phenotype, whilst *Pygm* may modify ECC triggering in pathways other than RYR1. However, the mechanism of action and the modification of MH phenotype requires further investigation. The investigation of the metabolic profile of these clones would be useful in deducing a more detailed picture of the phenotypic changes in these cells, enabling the generation of more targeted assays. Additional generation of clones would also enable the validation of these results. Furthermore, the investigation of specific disease-causing variants may also shed light on the likelihood of genetic compensation in these clones. Future research may also include the expression levels of gene networks involving *PYGM* and *CPT2*, the investigation of SERCA activity and the elucidation intracellular calcium levels.

This chapter also fulfils the aims of investigating threshold models of MH in more detail. The results present the generation of a novel mouse model, and ability to functionally investigate the contribution of multiple pathogenic variants in a single model to pathogenesis. This forms the foundation upon which further functional studies involving a threshold model may take place in the future, a sub-area of MH research that is still lacking. Considerations of the limitations of the use of CRISPR technologies in mouse myoblasts may also inform the development of threshold model research and the use of novel gene editing techniques in MH.

4 Investigating *PYGM* and *CPT2* pathogenic variants for association with Malignant Hyperthermia

4.1 Introduction

This chapter will explore the potential of specific variants in the candidate genes *PYGM* and *CPT2* as modifier loci in the context of a threshold model of malignant hyperthermia. The identification of mitochondrial deficiency (Chang et al., 2019) and the downregulation of genes associated with mitochondrial function (Chang et al., 2020) have led to the interest in the role of metabolic genes in MH. Additionally, metabolic disorders such as McArdle's disease, which affects glycolysis, (Bollig et al., 2005) and CPT II deficiency, which affects fatty acid oxidation, (Hogan & Vladutiu, 2009) have been shown to have some overlap with malignant hyperthermia. By generating knock-outs in the previous chapter and reintroducing specific variants of interest in this chapter, a two-step model of knock-out and rescue is able to be investigated for comprehensive characterisation of candidate genetic contributors in the context of potential modification of MH phenotypes.

4.1.1 Pathogenic variants in *CPT2*

Pathogenic variants in *CPT2* typically lead to CPT II deficiency in an autosomal recessive manner. The most common variant causative for the adult myopathic form of CPT II deficiency is the p.(S113L) mutation, accounting for around 70% of alleles in patients with the disorder (Deschauer et al., 2005). Serine is a neutral polar amino acid, whereas leucine is hydrophobic. This change can result in differential tertiary structure of the enzyme and can therefore influence how it interacts with molecules in the mitochondrial matrix, as well as the substrate given its proximity to the active site (Amino acid site372) based on the predictive structure of the enzyme in the tool AlphaFold (AlphaFold; Jumper et al., 2021). The p.(S113L) variant has a minor allele frequency of 0.002 in the non-Finnish European population (GnomAD), with a CADD score of 32. The second most common causative variant is p.(P50H)

(7% of patients) (Wieser et al., 2003). Proline is smaller in comparison to histidine and more hydrophilic, thus a change at this site is also likely to alter tertiary folding. The above variants are located in exon 3 and 1 respectively, and lead to diminished enzyme activity (Motlagh et al., 2016; Olpin et al., 2003). The p.(P50H) variant has a minor allele frequency of 0.0002 in the non-Finnish European population (GnomAD), with a CADD score of 28.7.

Previous sequencing of 50 candidate genes in 139 MHS individuals within the UK MH unit has revealed the presence of the p.(S113L) variant in the heterozygous state in 2 MHS patients (UK MH Unit, unpublished data). Based on this, investigating causative variants for CPT II deficiency as candidate modifier loci in MH could be prudent in identifying additional genetic contributors in the context of a threshold model of malignant hyperthermia. Given the pathogenicity and frequency of the p.(S113L) and p.(P50H) variants in CPT II deficiency, these may be potential candidate variants for investigation, and would also provide the most scope in screening CPT II patients for MH down the line, should these variants be identified to contribute to MH phenotypes.

4.1.2 Pathogenic variants in *PYGM*

Pathogenic variants in *PYGM* typically lead to glycogen storage disease V (McArdle's) in an autosomal recessive manner. The most common variant amongst those with the disease is the p.(R50X) nonsense variant, with an allele frequency of 77% in British patients (Pizzamiglio et al., 2021; Quinlivan et al., 2010). The second most common variant causative for McArdle's disease, in European populations, is the p.(G205S) change with a ~10% allele frequency. The vast majority of pathogenic variants are in exons (~91%), with exons 1 and 17 being the most dense (Nogales-Gadea et al., 2015b). Furthermore, the variants p.(R50X) and p.(A193S) have both been observed in exertional heat illness patients testing positively for MH via the IVCT (1 and 2 MHSh respectively), with reported CADD scores of 35 and 25.6

respectively (Gardner et al., 2020). The p.(A193S) variant, however, has not been found in McArdles patients. The p.(A193S) variant has a minor allele frequency of 0.003 in the non-Finnish European population (GnomAD), and leads to the substitution of the non-polar alanine to a polar serine, which may alter the structure of the enzyme. The position of the p.(A193S) variant is near the site of subunit association and in the N-terminus which also provides residues to form the active site of glycogen phosphorylase. Thus, alterations at this site may lead to diminished enzyme activity. The p.(R50X) variant has a minor allele frequency of 0.003 in the non-Finnish European population (GnomAD), and the change results in premature termination of translation and nonsense mediated decay of the transcript, leading to diminished enzyme and disruption of glycogenolysis (Nogales-Gadea et al., 2008)

Additionally, in a separate sequence analysis of 50 candidate genes across 139 MHS patients within the unit, both p.(A193S) and p.(R50X) have been observed in 2 and 1 MHS patients respectively (Gardner et al., 2020). Given the frequency that these variants are observed within the MHS cohort, their pathogenicity and the association of the p.(R50X) variant with McArdle's disease (Nogales-Gadea et al., 2015b), patients of which have previously also been identified as MHS after IVCT testing (Bollig et al., 2005), they would make ideal candidate variants for the investigation of potential modifier loci in a threshold model of malignant hyperthermia.

4.1.3 Introducing specific variants using lentiviral transduction

Lentiviral vectors for transgene expression have been developed from the human immunodeficiency virus 1 (Delenda, 2004). Lentiviruses are a genus of retroviruses, and the use of these as vectors enabled stable transgene expression due to integration into the target genome. Lentiviral vectors in particular, as compared to other retroviral vectors, are able to translocate across the nuclear envelope enabling the transduction of non-dividing cells (Naldini et al., 1996). Furthermore, the long

terminal repeat component of the lentiviral vectors also decrease the risk of insertional mutagenesis, as compared to other retroviral vectors (Montini et al., 2009). These attributes make them attractive choices for stable transgene expression. However, the trade-off is random integration of the transgene. This could result in the integration at less optimal sites, such as those not expressed very well, or could even lead to multiple integration events which would require further controls to normalise expression data.

Current lentiviral vectors utilise a four-plasmid system, denoted 3rd generation vectors, that provide enhanced user safety from recombinant viruses (Dull et al., 1998). The 3rd generation system separates the viruses necessary packaging and envelope proteins into three plasmids alongside a fourth plasmid carrying the transgene (figure 4.1). The packaging elements *gag*, *pol* and *rev* are split across two plasmids, with one containing the former two, whilst the *env* element is in the third plasmid. *Gag* encodes the retroviral core (matrix, capsid and nucleocapsid), *pol* encodes the reverse transcriptase, *env* encodes the viral envelope and *rev* encodes a necessary regulatory element (Poletti & Mavilio, 2021). The transgene encoded in the fourth plasmid also contains the LTR sequences, necessary for integration, of which the 5' LTR is chimeric and fused to a heterologous promoter (Dull et al., 1998). By transfecting these four plasmids into a host cell, it may be utilised for virus production. HEK293T cells are ideal for this due to the presence of the SV40 T antigen improving the efficiency of vector production (Gama-Norton et al., 2011).

Specifically, transfecting human vector constructs, due to the fact that the variants described in *CPT2* and *PYGM* are human disease-causing mutations, onto the knock-out background generated in chapter 3 would enable the investigation of their contribution to MH phenotypes. Additionally, the sequence conservation between mouse and human for both *CPT2* and *PYGM* is quite high, thus enabling the

transduction of human constructs without interfering with cell function. Specifically, for *CPT2* the transcript has 86.2% similarity with the mouse orthologue and 87.2% similarity between primary amino acid sequences, with 94% of residues with a positive alignment score. The *PYGM* transcript has 87.7% similarity with the mouse orthologue and 97% similarity between primary amino acid sequences, with 99% of residues with a positive alignment score.

4.1.4 Chapter aims

This chapter aims to develop the CRISPR pipeline from chapter 3 further, to enable the characterisation of specific pathogenic variants in genes that potentially could be linked to MH, in the context of a threshold model. This will enable the functional assessment of additional variants identified in MHS individuals to deduce their potential contribution to malignant hyperthermia pathogenesis. Furthermore, development of a gene editing pipeline novel to MH will enable greater scope to investigate pathogenic variants *in vitro*. This pipeline may be applied to any candidate gene, both for the investigation of a major gene effect and modifier loci. This will be achieved by the use of lentivirus vectors to transduce candidate variants in *PYGM* and *CPT2* into the knock-out clones developed in chapter 3. Thus, one may investigate the potential modification of MH phenotypes as a result of pathogenic variants previously identified, in the context of a threshold model.

4.2 Methods

4.2.1 Lentiviral vector plasmids

A 3rd generation lentivirus system was utilized which included 3 packaging plasmids and one transfer plasmid containing the coding sequence for *CPT2* or *PYGM*. Packaging plasmids included pRSV-Rev (#12253, Addgene), pMDLg/pRRE (#12251, Addgene) and pMD2.G (#12259, Addgene) all of which were high-copy number plasmids and included an ampicillin cassette for selection in bacteria prior to plasmid purification (figure A.3 – A.5 in appendix 3). Transfer plasmids with human wild-type coding sequence for each gene and variants *CPT2* p.(P50H), *CPT2* p.(S113L), *PYGM* p.(R50X) and *PYGM* p.(A193S) were ordered from GenScript using the pGenLenti vector (figure 4.1) which also included both puromycin and ampicillin selection cassettes. As a control, pLenti CMV GFP Puro (658-5) plasmid was used (#17448, Addgene) to determine successful transduction easily, optimise for multiplicity of infection and determine viral titre easily, as compared to using puromycin selection (figure A.6 in appendix 3).

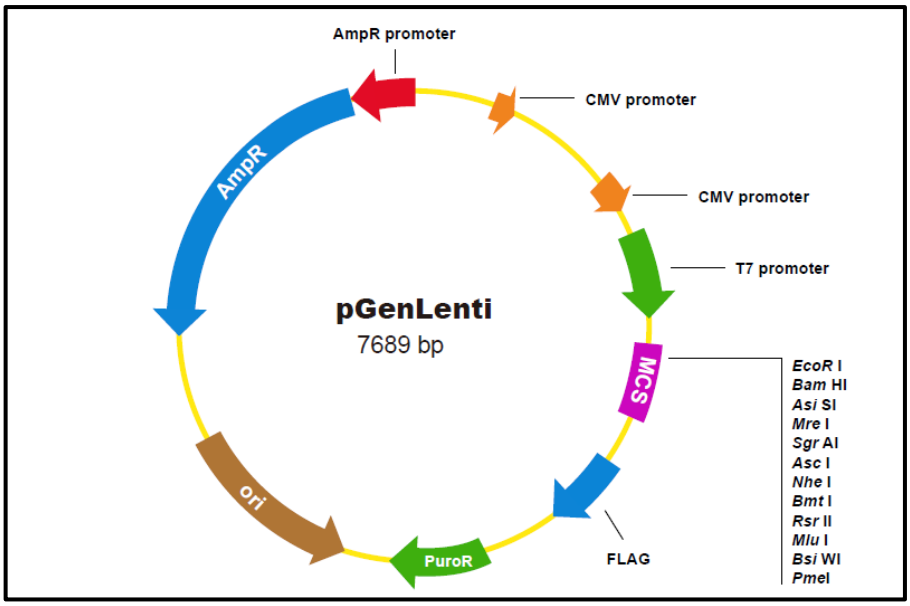

Figure 4.1: Vector map of pGenLenti lentivirus transfer plasmid from GenScript. Multiple cut site (MCS) indicates region of insert for transfer sequence; *PYGM* between EcoR I and Nhe I sites, *CPT2* between Nhe I and Mlu I sites. Puromycin resistance (PuroR) and ampicillin resistance (AmpR) cassettes used for selection in mammalian and bacterial cells respectively. DDYK flag site included for protein purification.

4.2.2 Lentivirus vector generation

HEK293FT cells were plated on a 15cm+ culture dish (Sarstedt) and grown until ~90% confluent and cultured in antibiotic-free growth media for 24 hours prior to transfection. A packaging plasmid mix was prepared to a final amount of 15µg of total plasmid by mixing p.MDLg/p.RRE, p.RSV-Rev and p.MD2.G in a 4:1:1 µg ratio respectively. The packaging plasmid mix was combined with 15µg of transfer plasmid, 1ml of DMEM and 90µl of Fugene HD transfection reagent (Promega) and incubated at room temperature for 15 minutes to allow transfection complexes to form. Complexes were distributed to cells over fresh antibiotic-free media and cells were incubated for 72 hours at 37ºC and 5% CO_2. Subsequently, media was harvested and spun at 300g for 5 minutes to pellet any HEK293FT cells. The supernatant was then filtered through a 0.45µm PVDF filter to ensure no cells remained, before combining with 5x PEG-it™ virus precipitation solution (Systems Bioscience) and gently mixed. The solution was incubated overnight at 4ºC prior to centrifugation at 1500g for 30 minutes at 4ºC to pellet the virus particles. Supernatant was discarded, and pellet was resuspended in 1ml of PBS to concentrate virus by 30x. Virus solution was aliquoted into cryovials and stored at -80ºC until use.

4.2.3 Titre determination

To determine the amount of virus in the stock solution a viral titre assay was conducted. 24 hours prior to transfection 75,000 HEK293FT cells were seeded in a 6 well dish. Cells were incubated for 48 hours with a serial dilution of stock GFP control virus; neat, 1 in 10, 1 in 100, 1 in 1000, 1 in 10,000, and 1 in 100,000. Dilutions were made in antibiotic-free medium with 6µg/ml of DEAE-Dextran (Thermofisher Scientific) to a final volume of 1.5ml. Dilutions were added to cells directly and incubated at 37ºC and 5% CO_2 for 48 hours, prior to imaging on the ZOE fluorescent cell imaging system (Bio-Rad). The dilution with ~15% of cells that

were fluorescent was chosen for calculating the titre, to mitigate the risk of counting cells with multiple integration events. The percentage area of fluorescence was calculated using ImageJ (Schneider et al., 2012) from five fields of view per well. This percentage was compared with total cell count obtained using haemocytometer from a control well to calculate an absolute number of fluorescent cells. This number was multiplied by the dilution factor to get a final number of transduction units per aliquot. This titre for the GFP virus was used as an indirect estimate for other transfer plasmids that did not contain a fluorescent protein.

4.2.4 Multiplicity of infection determination

MOI describes the number of virus particles required to infect a cell. To determine the amount of virus required to transduce knock-out cells generated in the previous chapter, an MOI assay was conducted. 24 hours prior to transduction, $1x10^5$ myoblasts were seeded in a 6 well dish on ECL. Once ~20% confluence was reached, a serial dilution calculated using the viral titre was prepared with the control GFP virus to represent a range of MOI's from 0 to 200 virus particles per cell in a final volume of 2ml of antibiotic-free growth media with 6µg/ml of DEAE-dextran. Virus dilutions were applied directly to the cells, which were then incubated at 37ºC and 5% CO_2 for 48 hours. Cells were then imaged on the ZOE imager as before and fluorescent cells estimated for each well and cytotoxicity noted. A balance of transduction efficiency and cytotoxicity was considered when selecting the MOI and incubation time (24,48 and 72 hours) to carry forward.

4.2.5 Viral transduction

24 hours prior to transduction, $1x10^5$ myoblasts were seeded in a 6 well dish on ECL. Once ~20% confluence was reached, an MOI of 25 and 50 were used to transduce 3 wells per viral vector per MOI over 48 hours as before. Subsequently, media was replaced with fresh growth media and cells were allowed to rest for 24 hours. Cells were then subjected to puromycin selection at 0.5µg/ml in fresh media,

for 14 days with media changes every 48 hours. Puromycin concentration was determined by a kill assay in primary p.(G2435R) heterozygous mouse myoblasts using concentrations ranging from 0 – 2 µg/ml. Ideally cells in non-transduced control wells would all be dead by day 7, serving as an indirect indicator for other wells, however regardless selection was continued till day 14 as a pre-caution. Cells were then grown until 60% confluent and frozen down, along with DNA extracted via direct extraction for sequencing as in section 2.2.1.

4.2.6 Lentiviral vector integration

Lentiviral vector integration was tested on kit-extracted gDNA as in section 2.2.1. The human TaqMan gene expression assays for *PYGM* and *CPT2* were used and normalised against mouse *GAPDH* (Mm05724508_g1, Thermofisher) copy number. Assays were conducted using the same plate considerations and thermocyling program as section 2.2.2. Relative integration differences were calculated using the ΔΔCt method in section 2.2.2, after which data was tested for normality using the Shapiro-Wilk test, and differences assessed using an ANOVA in GraphPad Prism 10.

4.3 Results

4.3.1 MOI determination

Fluorescent cells were estimated as a percentage of total plated by contrasting GFP fluorescence with brightfield images and were observed to increase with MOI as expected (figure 4.2). However, cytotoxicity also grew with increasing virus particles per cell, as estimated by the observable amount of cell death and debris. An MOI of 125 virus particles per cell was the lowest concentration at which 100% transduction efficiency was observed, where all observed cells were fluorescent, but also showed notable cell death and debris. Given the subsequent puromycin selection, cytotoxicity was given more weight in the consideration of MOI, as non-transduced cells would be selected against later. Based on this an MOI of 50 was chosen, given the 60% transduction efficiency which provided enough cells to not hinder subsequent colony growth whilst also have much lower cytotoxicity. An additional MOI of 25 was used as a precautionary measure, in case cells transduced at MOI 50 did not survive.

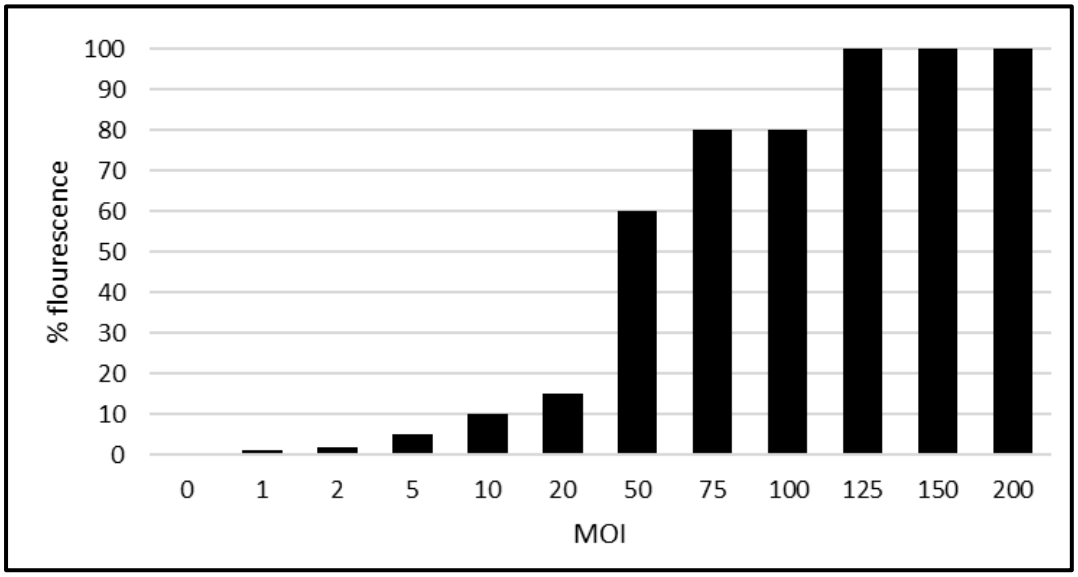

Figure 4.2: MOI assay. Percentage of GFP fluorescent cells observed plotted against virus particles per cell (MOI). N = 1 well.

4.3.2 Puromycin concentration determination

Primary mouse p.(G2435R) heterozygous myoblasts were plated at 30% confluency and exposed to final puromycin concentrations in growth media ranging from 0 – 2 µg/ml (figure 4.3). Changes in confluency were observed over 14 days to determine downstream concentration. Ideally, the selected concentration would cause death of the entire population of cells by day 7, as this would provide more certainty of selection of puromycin resistant cells downstream, especially when the assay is still carried forward to the full 14 days. Concentrations of 0.2 and 0.1 µg/ml impeded cell growth, but ultimately did not fully stop proliferation or cause sufficient cell death. At 0.3µg/ml cells did eventually die, however this was around day 10 which was later than desired. Concentrations of 0.4µg/ml and above all caused complete cell death by day 5. Based on this a concentration of 0.5µg/ml was selected for downstream puromycin selection.

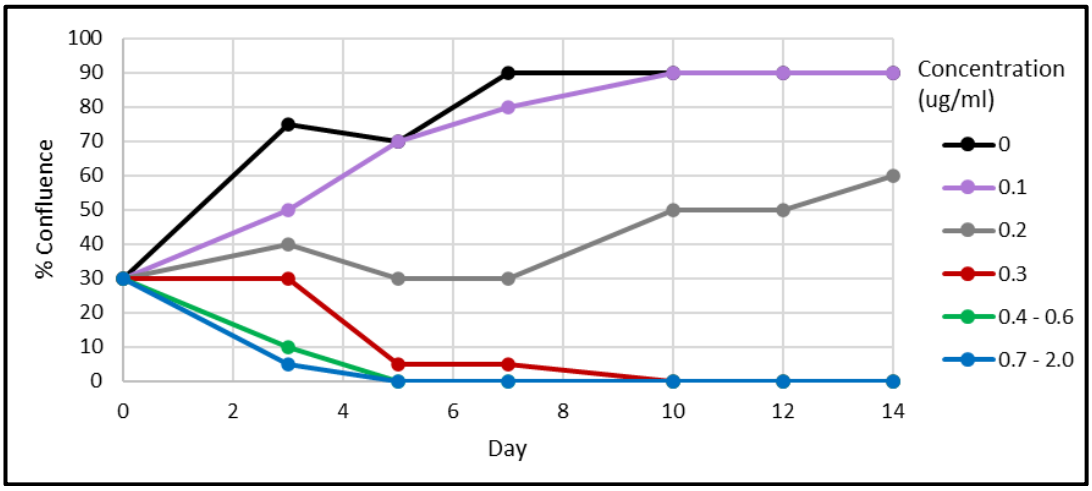

Figure 4.3: Puromycin kill curve. Cell confluence plotted against day of selection for final puromycin concentrations ranging from 0 – 2 µg/ml in growth media. Some concentrations plotted together where changes in cell confluence were the same. Specifically, 0.4/0.5/0.6µg/ml 0.7/0.8/0.9/1.0/2.0µg/ml were grouped together. N = 1 well.

4.3.3 Variant pool generation

3 independent cell pools per variant and control were generated at an MOI of 25 and MOI of 50. GFP transduced cells were used as an indirect control to confirm successful transduction and to monitor puromycin selection. GFP transduced wells expectedly died under puromycin by day 5, however selection was maintained until day 14 as a precautionary measure to ensure pools of cells contained only those successfully transduced. One mixed pool per variant and control at MOI 50 was carried forward for downstream applications. MOI 50 was chosen over MOI 25 due to better growth rates after puromycin selection. As MOI 25 wells had fewer cells transduced, they naturally took longer to grow to a usable population after selection, and so an MOI 50 pool was progressed in the meantime.

4.3.4 Lentiviral vector integration

Sanger sequencing was conducted on gDNA from myotubes to validate vector integration for all six cell pools (figure 4.4 & 4.5). Wild-type trace shows reintroduced wild-type vector used as a control cell line, with the trace indicating the reference region for each variant to confirm wild-type had neither pathogenic variant. Relative differences in integration were also determined to assess the contribution of copy number on downstream differences in gene expression (figure 4.6). Reintroduced wild-type was used as a control to compare relative differences in fold change against. Amongst *CPT2* vectors, p.(P50H) vector integration was determined to be around 50% ($p<0.001$) higher than the WT, whilst p.(S113L) vector integration was around 28% ($p<0.01$) higher. Amongst *PYGM* vectors, both p.(A193S) and p.(R50X) vector integration was around 35% higher than the WT ($p<0.01$). Significance was assessed using the Brown-Forsythe and Welchs ANOVA with Dunnet T3 correction for multiple comparisons.

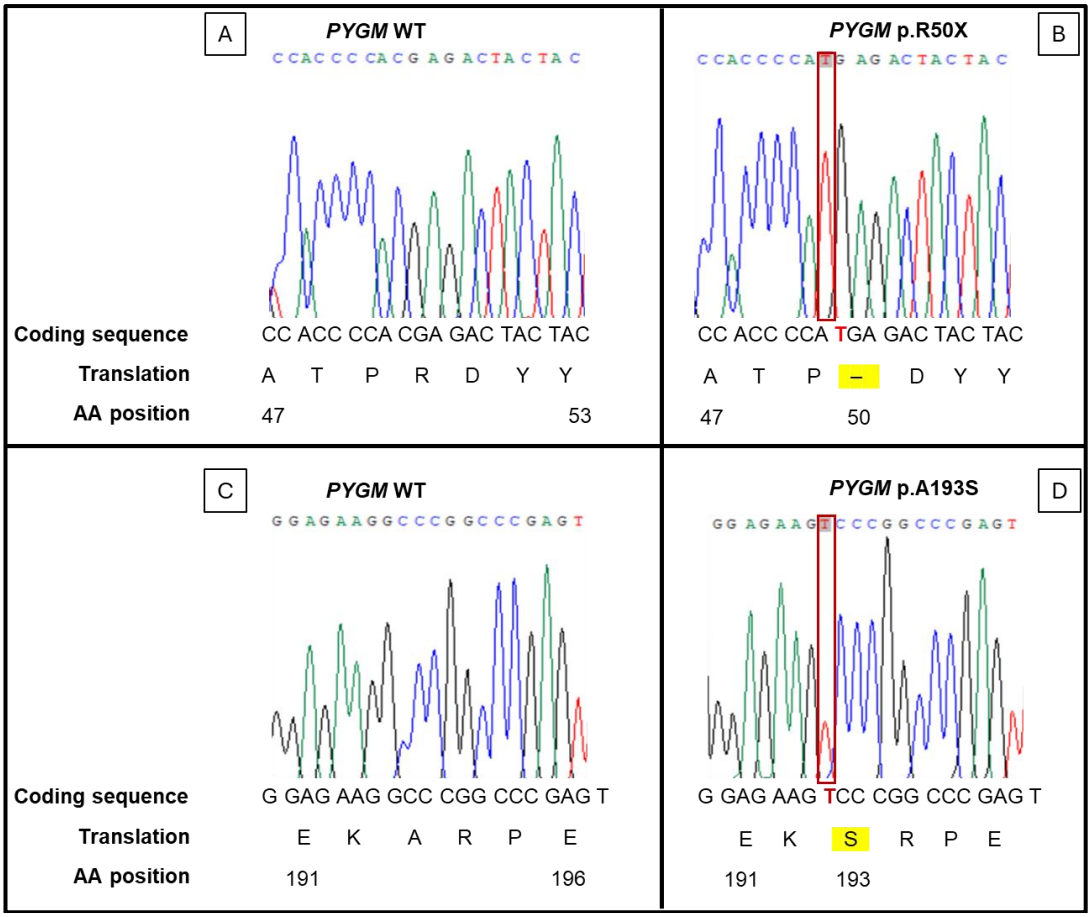

Figure 4.4: Sanger sequence traces for *PYGM* Lentiviral transduced variants. Sanger sequence traces with coding sequence, amino acid translation and amino acid position transcribed below. A) *PYGM* WT trace showing region corresponding to the site of p.(R50X) mutation for reference. B) *PYGM* p.(R50X) trace with c.148C>T change in red and corresponding amino acid translation change highlighted in yellow. C) *PYGM* WT trace showing region corresponding to the site of p.(A193S) mutation for reference. D) *PYGM* p.(A193S) trace with c.577G>T change in red and corresponding amino acid translation change highlighted in yellow.

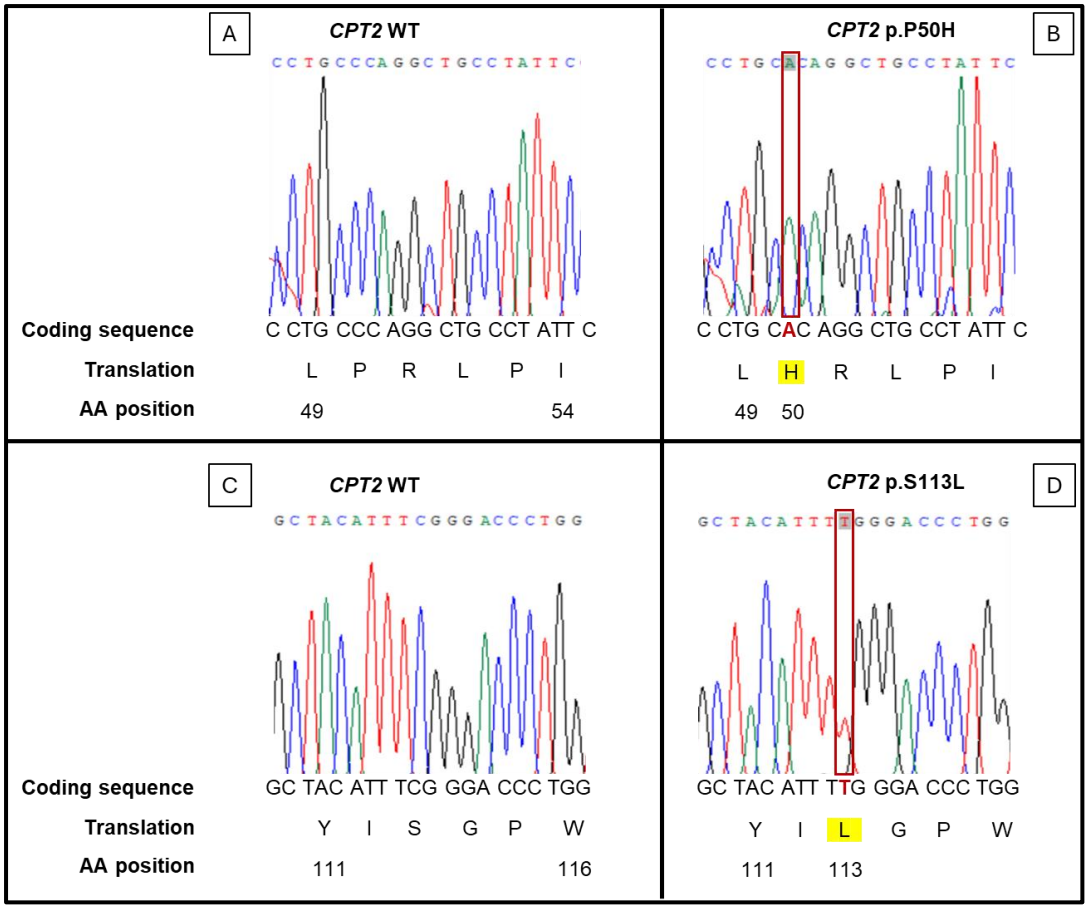

Figure 4.5: Sanger sequence traces for *CPT2* Lentiviral transduced variants. Sanger sequence traces with coding sequence, amino acid translation and amino acid position transcribed below. A) *CPT2* WT trace showing region corresponding to the site of p.(P50H) mutation for reference. B) *CPT2* p.(P50H) trace with c.149C>A change in red and corresponding amino acid translation change highlighted in yellow. C) *CPT2* WT trace showing region corresponding to the site of p.(S113L) mutation for reference. D) *CPT2* p.(S113L) trace with c.338C>T change in red and corresponding amino acid translation change highlighted in yellow.

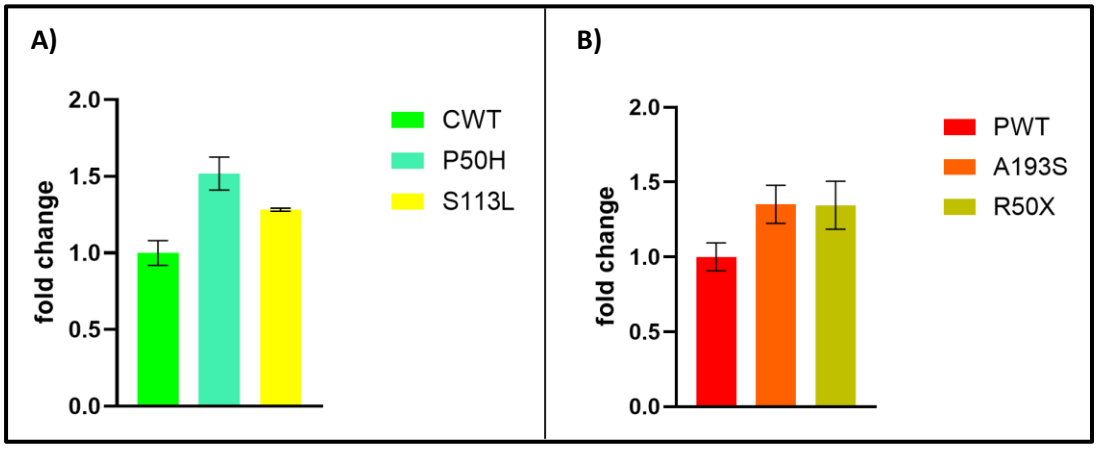

Figure 4.6: Relative viral vector integration. A) *CPT2* vector integration. CWT indicates *CPT2* wild-type vector. B) *PYGM* vector integration. PWT indicates *PYGM* wild-type vector. TaqMan™ gene expression assays used on gDNA to assess viral vector integration relative to wild type controls for each gene. Mean fold change over 3 independent samples with 95% CI relative to wild type vector, assessed using the ΔΔCt method.

4.3.5 Gene expression

Gene expression of viral vectors was assessed via measuring relative transcript levels as before in section 3.3.3. Variant pools were compared to the wild-type variant for each gene and the p.(G2435R) heterozygous myotubes. Significance was assessed using the Brown-Forsythe and Welchs ANOVA with Dunnet T3 correction for multiple comparisons.

4.3.5.1 *CPT2*

Transcript levels were assessed relative to the wild-type variant pool (figure 4.7). The p.(P50H) variant pool showed a 15% increase ($p<0.05$) in transcript levels whilst p.(S113L) showed a 55% decrease ($p<0.0001$) in transcript levels. When normalising with relative vector integration levels, p.(P50H) showed a 25% decrease ($p<0.01$) and p.(S113L) showed a 65% decrease ($p<0.0001$) in transcript levels relative to the wild-type vector. Transcript levels for all variant pools were greater than the p.(G2435R) heterozygous myotubes. Specifically, CWT exhibited around 16x ($p<0.0001$), p.(P50H) around 18x ($p<0.01$) and p.(S113L) around 7x ($p<0.0001$) the transcript level relative to the p.(G2435R) heterozygous myotubes.

4.3.5.2 *PYGM*

Transcript levels were assessed relative to the wild-type variant pool (figure 4.8). The p.(A193S) variant pool showed a 32% increase ($p<0.0001$) and p.(R50X) an 86% increase ($p<0.0001$) in transcript levels. When normalising with relative vector integration levels, the p.(A193S) vector showed no difference and the p.(R50X) vector showed a 40% increase ($p<0.0001$) in transcript levels relative to the wild-type vector. Transcript levels were all lower than the p.(G2435R) heterozygous myotubes. Specifically, the wild-type variant pool exhibited a 75% decrease ($p<0.01$), p.(A193S) a 68% decrease ($p<0.01$) and p.(R50X) a 55% decrease ($p<0.01$) in transcript levels relative to the p.(G2435R) heterozygous myotubes.

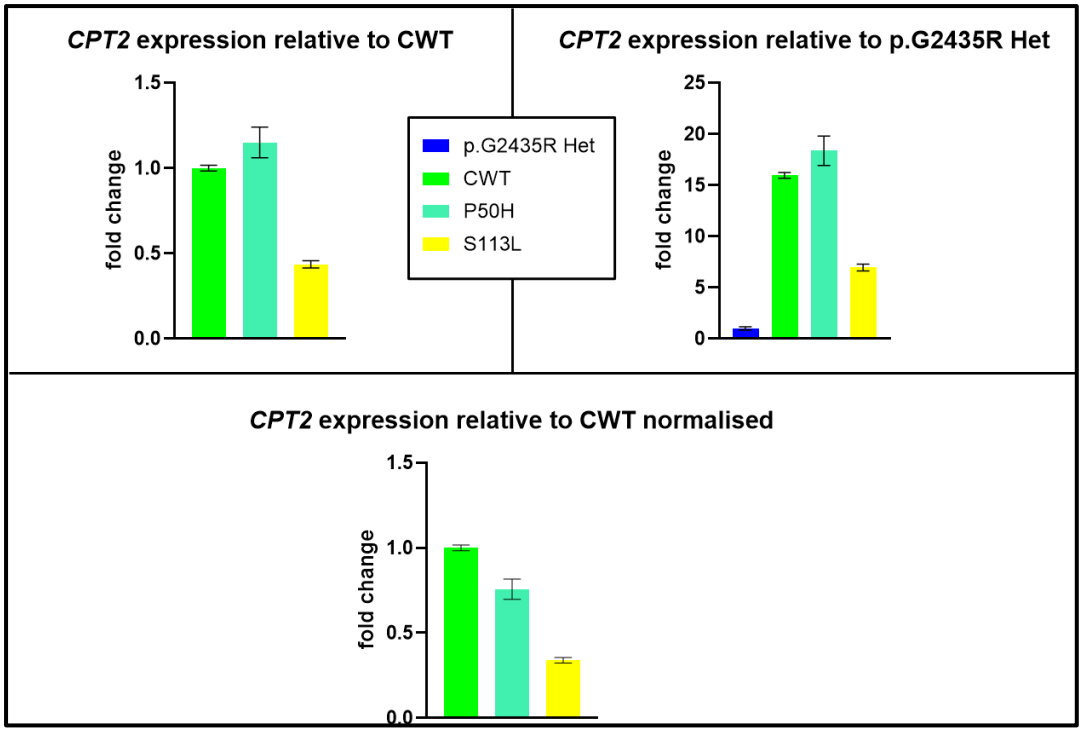

Figure 4.7: *CPT2* mRNA expression in lentivirus transduced colonies. Mean with 95% CI represented for relative fold change over 3 independent samples, assessed using the ΔΔCt method. Genotypes include *RYR1* p.(G2435R) Het, *CPT2* reintroduced wild-type (CWT), *CPT2* p.(P50H) and p.(S113L). Expression shown relative to *CPT2* wild-type with and without normalisation to vector integration, as well as relative to p.(G2435R) heterozygous myotubes.

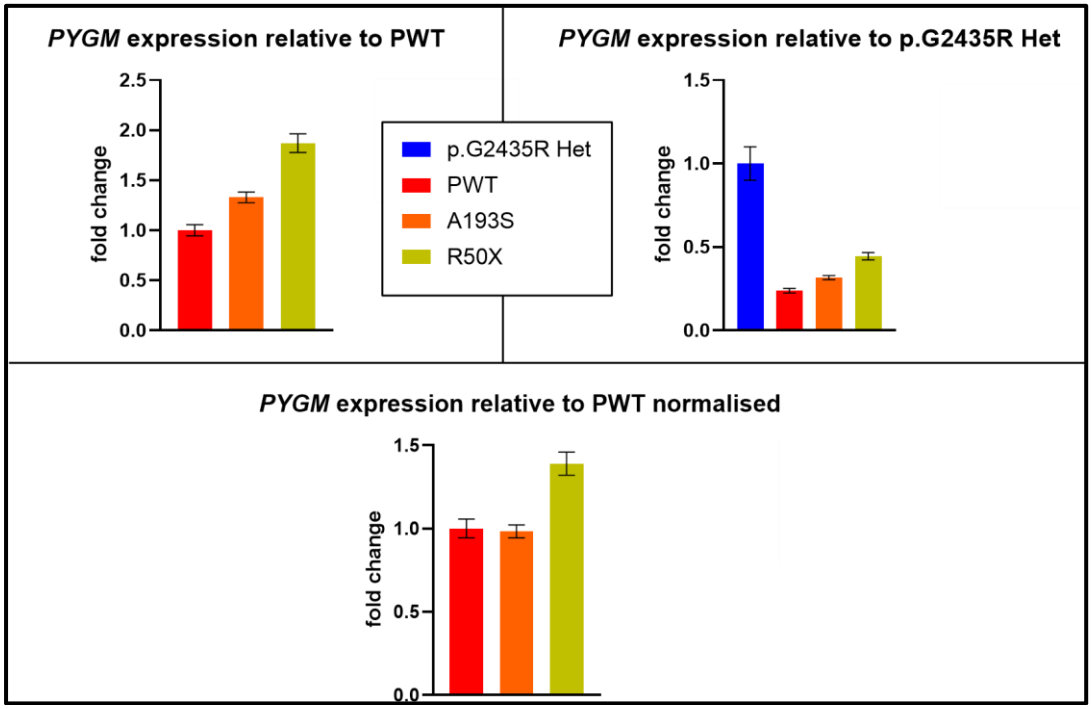

Figure 4.8: *PYGM* mRNA expression in lentivirus transduced colonies. Mean with 95% CI represented for relative fold change over 3 independent samples, assessed using the ΔΔCt method. Genotypes include *RYR1* p.(G2435R) Het, *PYGM* reintroduced wild-type (PWT), *PYGM* p.(A193S) and p.(R50X). Expression shown relative to *PYGM* wild-type with and without normalisation to vector integration, as well as relative to p.(G2435R) heterozygous myotubes.

4.3.6 Myotube formation

Formation of myotubes were confirmed using immunofluorescence studies as before in section 3.3.4. Myotube formation was necessary as an *in vitro* model of skeletal muscle for downstream applications. All viral vector transduced clones were shown to produce multinucleated structures that express myosin heavy chain confirming the formation of myotubes (figure 4.9). Brightfield images are also shown adjacent to the fluorescent images to show cell structure relative to stains.

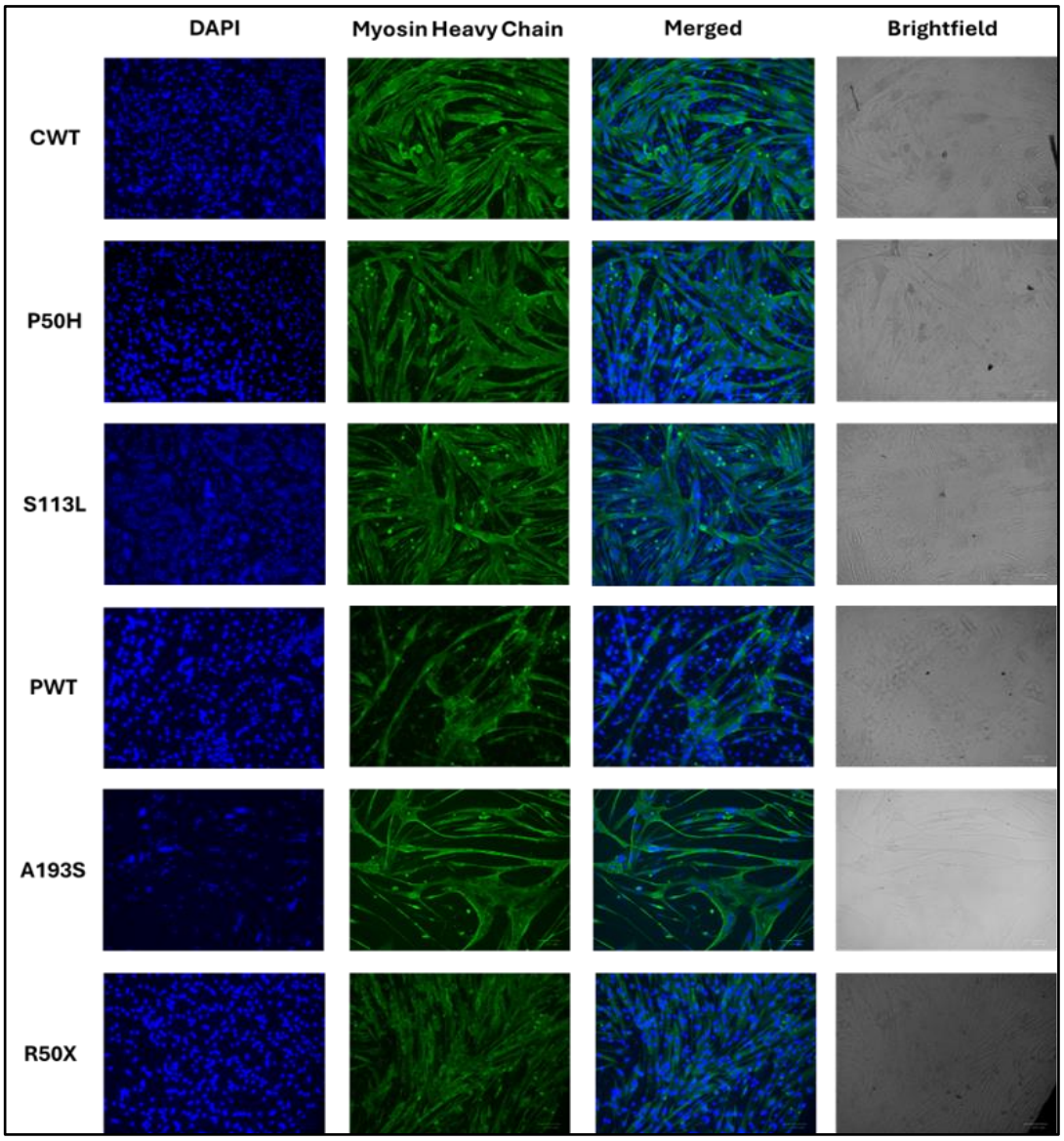

Figure 4.9: Immunofluorescence assay in viral vector transduced clones. *CPT2* wild type (CWT), *CPT2* p.(P50H), *CPT2* p.(S113L), *PYGM* wild type (PWT), *PYGM* p.(A193S), *PYGM* p.(R50X) myotube formation confirmed using DAPI nuclear stain (blue) and anti-Myosin Heavy Chain antibody with Alexa-Fluor 488 conjugated secondary antibody (green). Brightfield images also shown adjacent to fluorescent images.

4.3.7 Sensitivity to KCl

Variant pools were exposed to a range of KCl concentrations between 5 to 40 mM, as before in section 3.3.5. This was used to assess changes in ECC triggering as a result of the specific pathogenic variants introduced onto the *RYR1* p.(G2345R) heterozygous + knock-out background. Reintroduced human wild-type was used as a control to compare EC_{50} (mM) against. Comparisons were also made to the p.(G2435R) heterozygous myotubes to assess differences due to human/mouse orthologues and lentiviral transduction.

4.3.7.1 *CPT2* viral vector clones

The p.(S113L) variant (14.0mM) exhibited a significant increase in sensitivity to KCl as compared to the *CPT2* wild type (15.1mM), whilst the p.(P50H) (14.7mM) was not significantly different (figure 4.10). The p.(G2435R) heterozygous myotubes (17.4mM) exhibited lower sensitivity than the *CPT2* wild type. This would suggest a baseline difference in sensitivity due to lentivirus transduction of human orthologues, and an additional effect of the p.(S113L) variant in ECC triggering sensitivity.

4.3.7.2 *PYGM* viral vector clones

The p.(A193S) variant (16.7mM) exhibited a significant decrease in sensitivity to KCl as compared to the *PYGM* wild type (13.1mM), whilst the p.(R50X) (10.9mM) exhibited a significant increase in sensitivity (figure 4.11). The p.(G2435R) heterozygous myotubes (17.4mM) exhibited lower sensitivity than the *PYGM* wild type. This would suggest a baseline difference in sensitivity due to lentivirus transduction of human orthologues. Additionally, the p.(R50X) variant resulted in heightened ECC triggering sensitivity, whilst the p.(A193S) variant led to reduced triggering sensitivity.

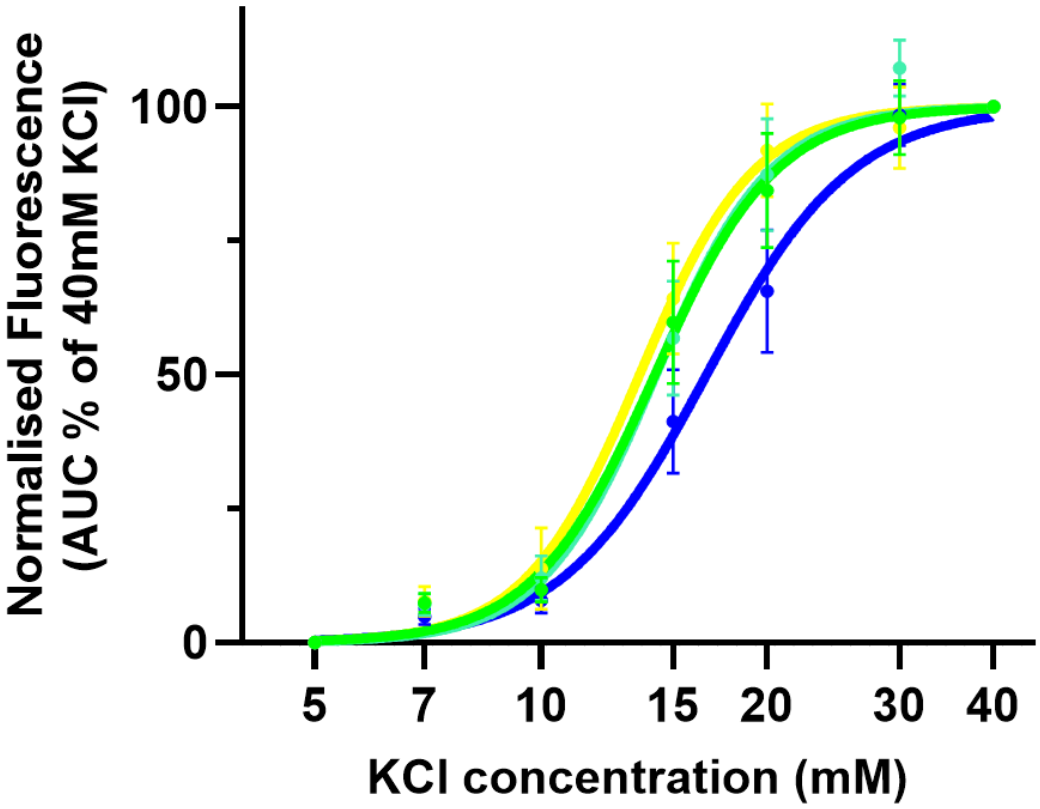

Key	Genotype	EC_{50} (mM)	p-value	n
	CPT2 wild type	15.1	Ref.	41
	CPT2 p.P50H	14.7	ns	31
	CPT2 p.S113L	14.0	0.007	32
	p.G2435R Het	17.4	<0.0001	40

Figure 4.10: *CPT2* viral vector transduced clones KCl-dose response. Data points shown are mean with 95% confidence intervals of area under the curve for each concentration. Table below shows key for graph with corresponding EC_{50} (mM), p-value and n-number. P-values based on Brown-Forsythe and Welch's ANOVA with Tukey's correction for multiple comparisons.

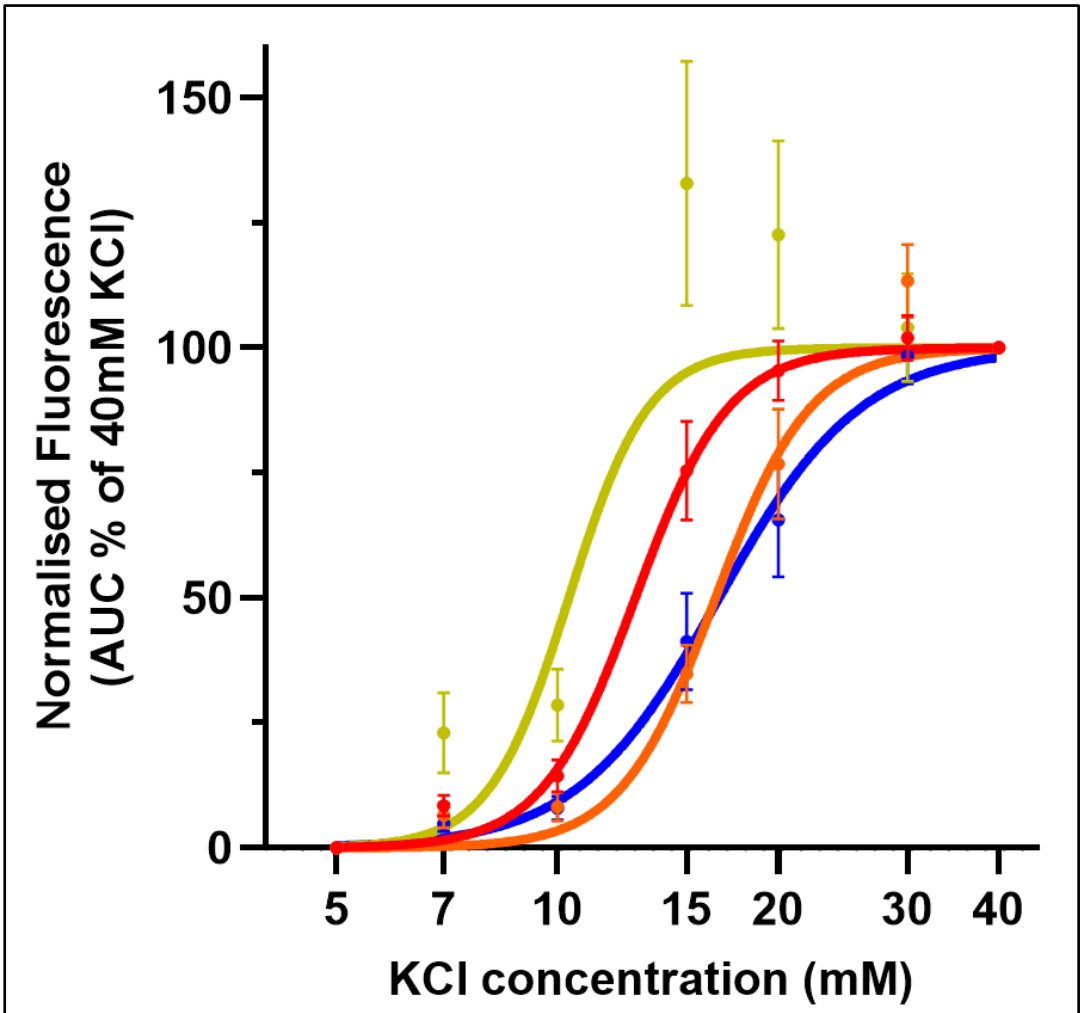

Key	Genotype	EC_{50} (mM)	p-value	n
	PYGM wild type	13.1	Ref.	43
	PYGM p.A193S	16.7	<0.0001	23
	PYGM p.R50X	10.9	<0.0001	22
	p.G2435R Het	17.4	<0.0001	40

Figure 4.11: *PYGM* viral vector transduced clones KCl-dose response. Data points shown are mean with 95% confidence intervals of area under the curve for each concentration. Table below shows key for graph with corresponding EC_{50} (mM), p-value and n-number. P-values based on Brown-Forsythe and Welch's ANOVA with Tukey's correction for multiple comparisons.

4.3.8 Sensitivity to Caffeine

Variant pools were exposed to a range of caffeine concentrations between 1 to 20 mM, as before in section 3.3.6. This was used to assess changes in RYR1 sensitivity specifically as a result of specific the pathogenic variants that were introduced on the *RYR1* p.(G2435R) heterozygous and knock-out background. The reintroduce human wild-type line was used as a control to compare EC_{50} (mM) against. Additionally, the p.(G2435R) heterozygous myotubes were used to determine differences due to human/mouse orthologues and lentivirus transduction as before.

4.3.8.1 *CPT2* viral vector clones

The p.(S113L) variant (3.6mM) exhibited no significant difference in sensitivity to caffeine as compared to the *CPT2* wild type (5.0mM), whilst the p.(P50H) (3.0mM) exhibited a significant increase in sensitivity (figure 4.12). The p.(G2435R) heterozygous myotubes (4.3mM) exhibited no significant difference to the *CPT2* wild type. These results would suggest that decreases in CPT II function increase the sensitivity of RYR1 triggering.

4.3.8.2 *PYGM* viral vector clones

The p.(A193S) variant (5.4mM) exhibited no significant difference in sensitivity to caffeine as compared to the *PYM* wild type (5.3mM), whilst the p.(R50X) (2.7mM) exhibited a significant increase in sensitivity (figure 4.13). The p.(G2435R) heterozygous myotubes (4.3mM) exhibited no significant difference to the *PYGM* wild type. This would suggest that the p.(R50X) variant results in increasing RYR1 sensitivity to triggering.

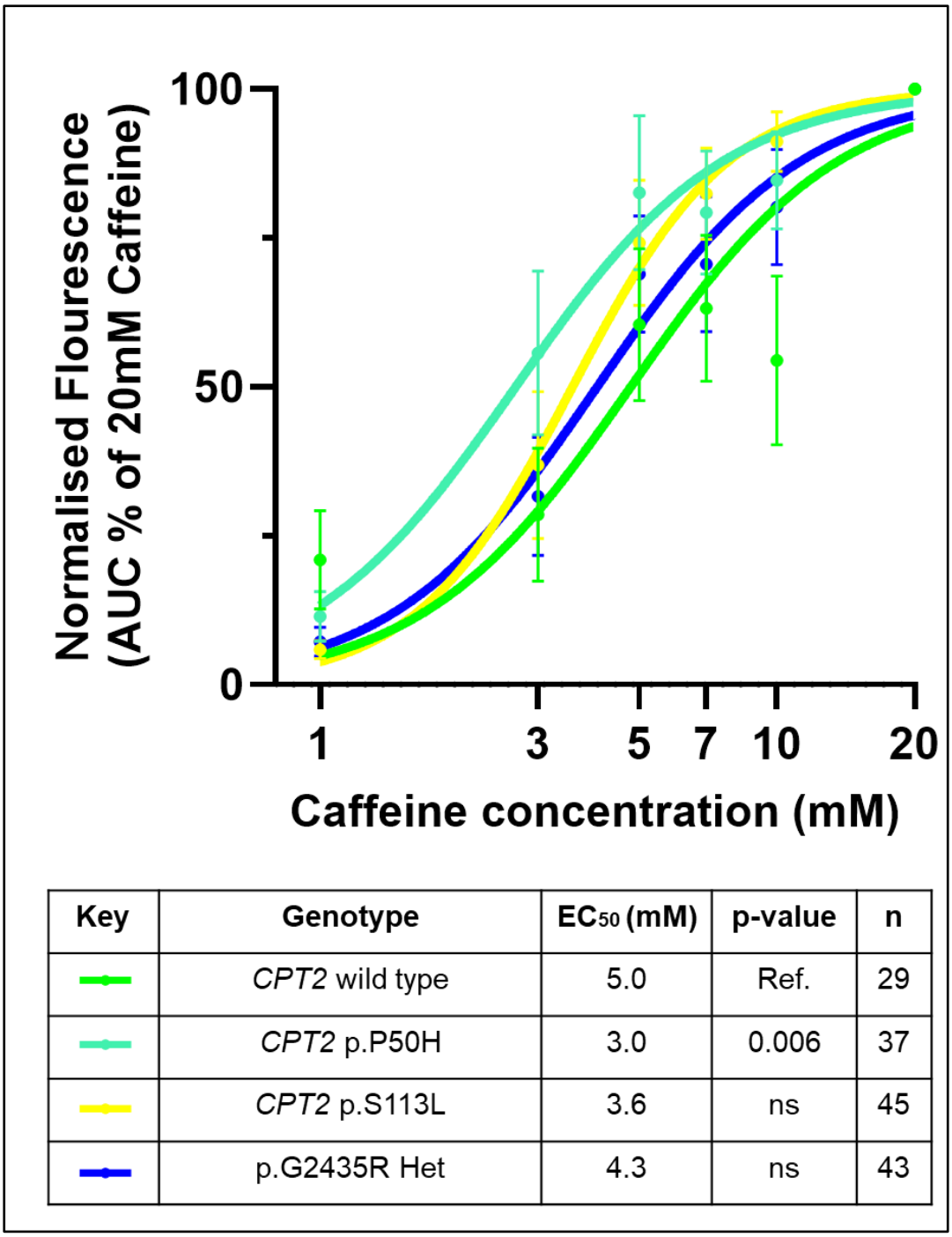

Key	Genotype	EC_{50} (mM)	p-value	n
	CPT2 wild type	5.0	Ref.	29
	CPT2 p.P50H	3.0	0.006	37
	CPT2 p.S113L	3.6	ns	45
	p.G2435R Het	4.3	ns	43

Figure 4.12: *CPT2* viral vector transduced clones Caffeine-dose response. Data points shown are mean with 95% confidence intervals of area under the curve for each concentration. Table below shows key for graph with corresponding EC_{50} (mM), p-value and n-number. P-values based on Brown-Forsythe and Welch's ANOVA with Tukey's correction for multiple comparisons.

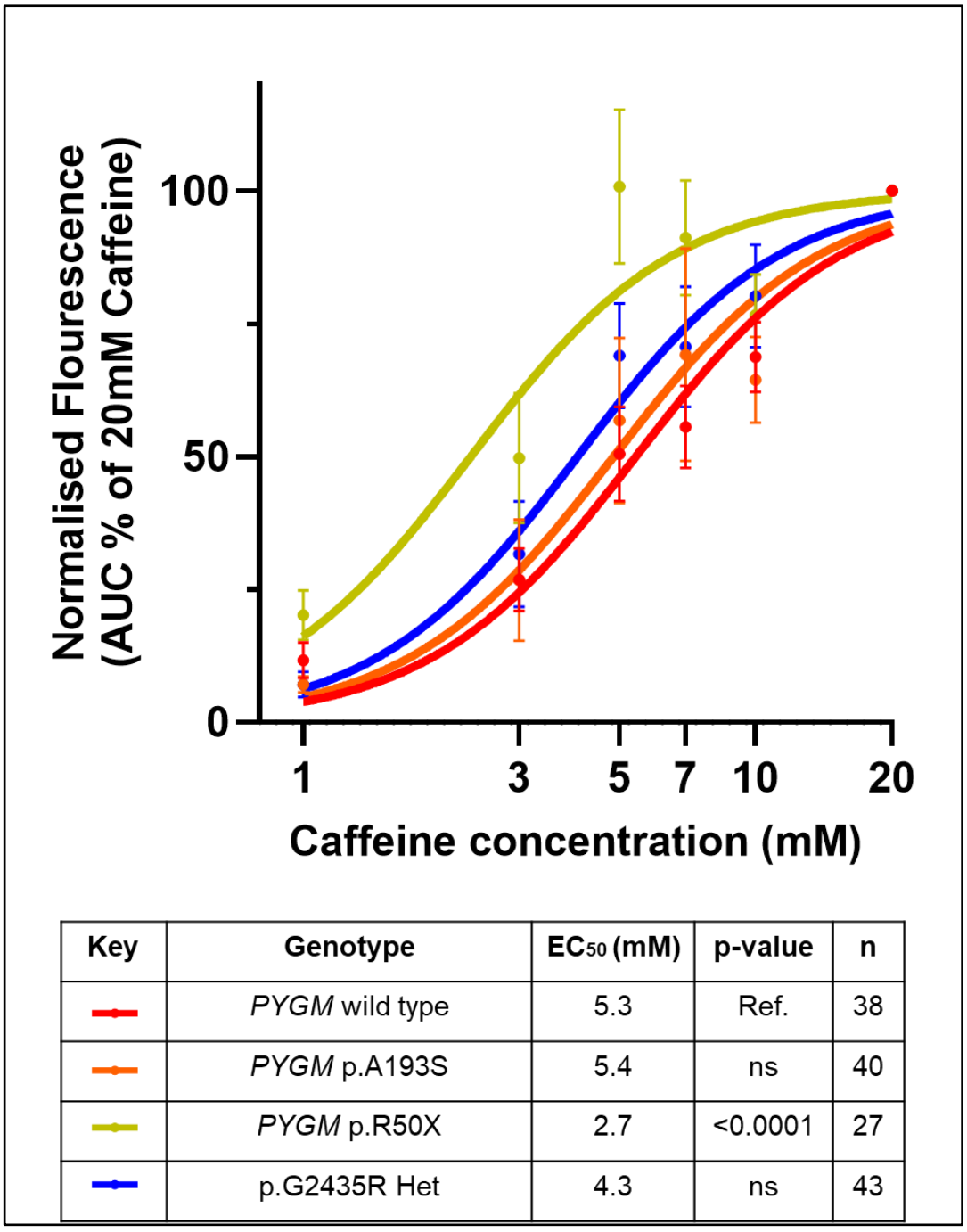

Key	Genotype	EC_{50} (mM)	p-value	n
	PYGM wild type	5.3	Ref.	38
	PYGM p.A193S	5.4	ns	40
	PYGM p.R50X	2.7	<0.0001	27
	p.G2435R Het	4.3	ns	43

Figure 4.13: *PYGM* viral vector transduced clones Caffeine-dose response. Data points shown are mean with 95% confidence intervals of area under the curve for each concentration. Table below shows key for graph with corresponding EC_{50} (mM), p-value and n-number. P-values based on Brown-Forsythe and Welch's ANOVA with Tukey's correction for multiple comparisons.

4.4 Discussion

The use of a lentiviral vector for transducing recombinant variants comes with certain considerations when interpreting the resulting data in this chapter. Firstly, the introduction of recombinant DNA is a fundamental difference to introducing changes into the native genome of the mouse model. Recombinant DNA does not have introns, or exon splicing for transcript variants. A specific coding sequence is instead introduced, alongside other lentiviral vector components, with it's own promoter. This may affect how the gene is expressed via transcription and translation. For example, the *PYGM* p.(R50X) variant would be expected to result in low transcript levels and no protein, were it introduced natively as seen in the knock-in p.(R50X) mouse (Nogales-Gadea et al., 2012). However, the expression of the recombinant variant in this chapter is relatively high compared to what would be expected. This is likely due to the use of recombinant DNA and the lack of exon splicing. The recombinant p.(R50X) variant transcript would not have exon junction complexes bound to it due the lack of exon boundaries in the continuous coding sequence, which would trigger nonsense mediated decay (Brogna & Wen, 2009). Furthermore, the constitutive CMV promoter in the lentiviral vector may mean the recombinant genes are not regulated in their expression as they would be natively. For example, *CPT2* expression is regulated by the binding of nuclear receptors, such as peroxisome proliferator-activated receptors binding to the 5' flanking region (Barrero et al., 2003), which may not occur in a transduce recombinant vector.

This is further compounded by the random nature of lentivirus integration. As the lentivirus is not directed to specific regions for insertion, there is a risk of insertion into regions that are difficult to access for transcription factors, or insertion into regions otherwise affecting cell functions. This risk is increased when considering the MOI of 50 used, to ensure suitable transduction efficiency, which may lead to multiple integration sites per cell. This would also affect the overall expression of the

recombinant genes as a product of the combination of expression conditions for each site of integration. The relative integration levels were assessed in this chapter to account for the possibility of variable integration between vectors. Specifically, this was observed in the case of the *CPT2* p.(P50H) and p.(S113L) vectors whereby normalising to integration levels showed that mRNA expression lower despite different copy numbers. Similarly, p.(R50X) in *PYGM* was seen to still have increased mRNA expression after normalisation, posited to be due to lack of triggering of NMD previously. Additionally, by using pools of cells, the variable number of integration sites between cells is averaged across the population and bypasses the need for clonal lines which may be difficult to achieve due to the limited lifespan of primary cells. Protein expression validation was also attempted, however a successful western blot was not achieved. An ELISA assay was subsequently attempted to fill this gap, however, was not successful. This would have been a useful step in confirming the gene expression of the variants at the protein level, as well evaluating whether some of the differences observed in the transcript and integration levels would follow through to protein.

However, the variation in integration numbers and sites between cells within the pooled population did also pose certain challenges. Gene expression and integration analysis mentioned previously provides an overview of the pool, such as the relative increase in copy number, on average, in the p.(R50X) pools compared to the reintroduced *PYGM* wild-type. However, variation between cells in the pool is more difficult to evaluate. This may also have implications in how the composition of the pool may change over passages based on which cells outgrow others/survive. To mitigate the inconsistency between assays this may result in, gene expression and integration assays were conducted on cells of a similar passage to those used in live-cell imaging assays. However, as the live-cell imaging assays look at individual myotubes formed from a handful of cells, the variability is considerably

increased as compared to the single cell colonies of chapter 3. This is especially noticeable in the *PYGM* p.(R50X) line, which tended to form myotubes from a lower number of myoblasts than other lines, where the variability in the live cell imaging assay is higher than other genotypes. This can be seen by the fewer nuclei per myotube in the p.(R50X) immunocytochemistry studies. Conversely this was not observed in the *Pygm* knock-out clone 13, suggesting this was an effect of the lentivirus transduction.

Finally, cytotoxicity is also a limitation of using viral vectors. A trade-off between transduction efficiency and cytotoxicity was considered in this chapter, however ultimately the use of lentiviral vectors will affect potential survivability of the clones derived from a transduced population (Hong et al., 2007). An additional consideration is the passage at which cells are transduced and prior conditions which may affect cell health. Transductions in this chapter took place in the knockout clones from chapter 3. These lines have already gone through a CRISPR editing process and as a result are also at relatively high passage of ~30. Observations from this chapter showed that whilst these cells did not reach senescence by passage 30, enabling the experiments in this chapter to take place, they did seem to be close. Anecdotally, the pools of cells seemed to reach senescence by around passage 40, with a notable increase in cell death and inability to differentiate into myotubes. This work could also help define the passage limit for primary mouse myoblasts, which has not previously been studied. Additionally, the background of these myoblasts may be different due to genetic drift over passages, as posited in the previous chapter, which may affect survivability and gene expression. This was considered by generating the pools of cells on the same knock-out clones, enabling more robust comparisons between variants in this chapter as they had the same genetic background.

With all that being said, the use of lentiviral vectors in a knock-out line enables the possibility of a two-step functional assessment of a candidate gene. Lentivirus vectors in particular allow the stable expression of candidate variants for the investigation of specific phenotypic consequences in malignant hyperthermia. By transducing in a knock-out line, the variants are also able to be studied in isolation without the interference of native genes confounding analyses. Additionally, this pipeline allows a deeper investigation of modifier loci than previously studied and presents novel techniques to be used to elucidate mechanisms in malignant hyperthermia susceptibility. The possibility of investigating multiple variants in one model proves to be a powerful tool for furthering the understanding of a threshold model and how multiple genes may interact and contribute to an MH event.

Table 4.1: Summary of assay results for each variant, relative to the relevant reintroduced wild-type control. Caffeine sensitivity, KCl sensitivity, and mRNA level changes indicated. Ns = non significance.

Gene	Variant	Caffeine Sensitivity	KCl Sensitivity	mRNA level
PYGM	**p.(R50X)**	Increased	Increased	Increased
PYGM	**p.(A193S)**	ns	Decreased	ns
CPT2	**p.(S113L)**	ns	Increased	Decreased
CPT2	**p.(P50H)**	Increased	ns	Decreased

CPT2 variant p.(P50H) resulted in increased sensitivity to caffeine in *Ryr1* p.(G2435R) heterozygous mouse myotubes, whilst *CPT2* p.(S113L) lead to increased sensitivity in KCl. These results would also inform the considerations of variability required in future work. Reintroduced *CPT2* wild type lines in both assays were also significantly different to *RYR1* p.(G2435R) heterozygous myotubes, suggesting lentiviral transduction may have modified the phenotype of the lines, possibly compounded by previous native *Cpt2* knock out. There is also a possibility that, despite the high homology, the discrepancy between the reintroduction of human orthologues in a mouse system may affect the functionality of the proteins as

seen in other studies (Gharib & Robinson-Rechavi, 2011). This was the primary reason for comparing variants against the reintroduced wild type as a control rather than the p.(G2435R) heterozygous myotubes. These results suggest that the *CPT2* p.(S113L) variant may affect excitation contraction coupling triggering. Furthermore, both variants may impact RYR1 function. RYR1 triggering is a part of excitation contraction coupling, and as such these results may suggest that pathogenic variants in *CPT2* may have multiple points of effect in the ECC function. It is important to note that although these variants cause a decrease in enzyme activity at 37ºC (Meinhardt et al., 2021), they do not completely knock-out the function of the gene, with p.(S113L) showing a 4x decrease in activity and p.(P50H) showing a 40x decrease in activity over 60 minutes. This is in contrast to the knockout clones generated in chapter 3. The reduced enzyme activity may result in increased production of reactive oxygen species due to disrupted mitochondrial lipid metabolism. The increased ROS would increase the sensitivity of RYR1 to agonists (Hamilton & Reid, 2000).

PYGM variant p.(A193S) resulted in decreased sensitivity to KCl, whilst variant p.(R50X) resulted in increased sensitivity to both KCl and caffeine, as compared to the reintroduced *PYGM* wild type. This may suggest that the p.(R50X) variant does contribute to malignant hyperthermia susceptibility. However, this variant results in a knockout, and so in theory should not differ significantly from the *PYGM* knock-out line where there is no significant difference in caffeine sensitivity as seen in section 3.3.6. This may mean that some other contributing factor is causing the differences in sensitivity to caffeine. It may be to do with the lentiviral vector integration sites, due to the random nature of integration. It would be useful to investigate integration loci amongst cells in this pool as a next step to elucidate the cause of this discrepancy. It is also unclear why the p.(A193S) variant would cause decreased sensitivity to KCl, and so investigating integration sites would also help here as well

as additional pools of cells for this variant. As before another point of difference is the transduction of human DNA in a mouse model, and so this may also account for certain differences observed between cell lines in this chapter compared to those in chapter 3 (Gharib & Robinson-Rechavi, 2011).

In conclusion, this chapter presents a novel gene editing pipeline in the research of MH pathogenesis. Specifically, the use of lentivirus vectors enables the stable transfection of candidate genes and variants of interest allowing deeper investigation into any potential effects they may have on the aetiology of malignant hyperthermia. Furthermore, this pipeline allows the generation of additional mutations in established models of MH, enabling the functional analysis of candidate modifier loci which is novel to MH research. Finally, this chapter also suggests the possible contribution of pathogenic variants in *CPT2* and *PYGM*, that have been observed in MHS patients, in increasing the sensitivity to triggering excitation contraction coupling and RYR1, which are the key dysfunctional components in MH. Although more data would be required to establish this.

5 Investigating candidate genes for association with malignant hyperthermia susceptibility.

5.1 Introduction

MH pathogenesis has been suggested to adhere to a threshold model rather than a strictly single gene disorder model. A quarter of families carrying a pathogenic *RYR1* variant exhibit phenotype-genotype discordance, where individuals may test IVCT negative despite carrying a pathogenic variant (Miller et al., 2018). Furthermore, there is a discrepancy in the incidence of MH susceptibility estimates based on clinical data (1:10000) (Halliday, 2003) as compared to the estimated prevalence of pathogenic variants associated with MH (1:1500) (Shaw & Hopkins, 2019). These observations support an oligogenic threshold model of inheritance rather than an autosomal dominant model, whereby individuals may require additional genetic contributions from 'modifier loci' alongside a MH associated pathogenic variant to reach a triggering threshold. MH pathogenesis is ultimately a result of calcium dysregulation upon exposure to triggering agents. Therefore, loci that may contribute to calcium dysregulation would be prime candidates for further investigation. In particular, three branches of exploration would be prudent.

Firstly, all diagnostic mutations currently used to identify malignant hyperthermia clinically are within genes involved in excitation-contraction coupling, of which the majority are in *RYR1* and two are in *CACNA1S*. Therefore, exploring components of this pathway would be a logical next step. *CACNA1S*, *CACNA2D1* and *STAC3* in particular are key components to the excitation contraction coupling pathway. The former 2 genes encode the alpha-1 and alpha-2/delta subunits, of DHPR respectively. The alpha-1 subunit in particular forms the pore for the voltage-gated calcium channel, whilst alpha-2/delta are involved in channel folding and transport of alpha-1 to cell membrane (Dolphin, 2016). Furthermore, loss of the II-III loop of

the alpha-1 subunit in particular results in loss of ECC (Grabner et al., 1999), whilst *CACNA2D1* has been previously suggested as a region of interest in association with MHS families (Iles et al., 1994), including those with a pathogenic *RYR1* mutation (ROBINSON et al., 2000). However, both studies utilise a single marker to tag for a large chromosomal region, thus limited by coverage and highlighting the need for more up to date linkage studies. Rare pathogenic variants in both genes have also been linked to disease. In particular, the *CACNA1S* p.(R528H), p.(R1239H) and p.(R1239G) variants have been reported in cases of hypokalaemic periodic paralysis, a skeletal muscle channelopathy (Matthews et al., 2009), whilst the *CACNA2D1* p.(D1045A) variant was reported in an MHSh patient (Gardner et al., 2020). STAC3 is suggested to be a key mediator of the interaction between the DHPR and RYR1 and loss of function was shown to disrupt ECC (Horstick et al., 2013). Furthermore, the p.(W284S) variant was identified in patients with *STAC3* myopathy that experienced an MH-like reaction (Zaharieva et al., 2018), as well as the p.(K288X) variant in another Russian patient with *STAC3* myopathy (Murtazina et al., 2022). *ATP2A1* is another gene of interest in this pathway encoding the Ca^{2+} ATPase in the sarcoplasmic reticulum which sequesters Ca^{2+} back into the SR after activation. Biallelic variation in this gene leads to Brody myopathy (Odermatt et al., 1996), a rare autosomal recessive myopathy with patients previously reported to be classified as MH susceptible after IVCT testing (Novelli et al., 2004). In particular the *ATP2A1* p.(C675X), p.(E982K), p.(P789K), p.(R198X) and p.(R560C) variants have been reported to be associated with Brody myopathy where patients exhibit reduced SERCA activity, of which the p.(E982K) variant in particular was identified in an individual that had previous episodes of MH (Molenaar et al., 2020). Variation in these four genes may lead to modification of the ECC pathway, and crucially its functional capabilities under exposure to volatile anaesthetics.

Secondly, given the dysregulation of calcium is central to pathogenesis, another potential avenue would be the investigation of genes involved in calcium homeostasis. *CASQ1* encodes calsequestrin 1, a SR luminal Ca^{2+} storage protein which binds to Ca^{2+} and regulates its release by RYR1 in skeletal muscle (Györke et al., 2004; Kawasaki & Kasai, 1994; Lamboley et al., 2013). *CASQ1*-null mice have shown to develop an MH phenotype upon exposure to volatile anaesthetics, specifically showing a deficiency to alter proper control of RYR1 function (Dainese et al., 2009). In particular the *CASQ1* p.(D244G) variant was reported in multiple patients exhibiting exercise intolerance, hyperCKaemia, myalgia and exertional rhabdomyolosis (Semplicini et al., 2018). TRPV1 encodes a non-cationic transient receptor potential channel that is expressed in skeletal muscle. Specifically, the channel is localised to the SR and acts as a reticular Ca2+ leak channel. Multiple variants have been previously suggested to be associated with MH and have been functionally characterized, showing increased sensitivity to volatile anaesthetics such as isoflurane (Vanden Abeele et al., 2019). The *TRPV1* rare variants p.(G684V) and p.(R772C) were reported in a heterozygous state in two exertional heat stroke patients, both of which were also confirmed to be MH susceptible upon conducting an IVCT (Bosson et al., 2020).

A final consideration should be made of the hypermetabolic nature of an MH episode, that occurs as a consequence of increased intracellular Ca^{2+} stimulating metabolism, and the lack of ability to keep up with the ATP demands resulting in rhabdomyolosis (Hopkins, 2000b). Previous studies have observed mitochondrial deficits observed in human MHS muscle fibres (Chang et al., 2019). Furthermore, the downregulation of genes associated with lipid metabolism, such as *ACADVL* and *CPT2* amongst others, was observed in knock-in mouse models of MH (Chang et al., 2020). *ACADVL* encodes the enzyme very-long-chain Acyl-CoA dehydrogenase (VLCAD), whilst *CPT2* encodes carnitine palmitoyl transferase II,

both involved in the beta oxidation pathway. Deficiencies in either enzyme can present in an adult onset myopathic form, amongst others, which presents with exercise induced myalgia and rhabdomyolysis. The most common pathogenic variants for CPT II deficiency amongst northern Europeans are the p.(P50H) and p.(S113L) variants (Wieser, 2004). The most recurring variants in patients screened for this VLCAD deficiency were p.(G441D), p.(R459Q) and p.(V283A) (Miller et al., 2015). Of these, the p.(V283A) variant was found in an exercise intolerant patient that was also classified as MHSh via IVCT (Gardner et al., 2020). The same study also identified the variants *PYGM* p.(R50X) and p.(A193S), and *AMPD1* p.(M343I) in exercise intolerant and MHSh individuals. *PYGM* encodes myophosphorylase, in which a deficiency causes McArdle's disease where patients may have symptoms of exercise intolerance, myalgia, exertional myoglobinuria and rhabdomyolysis (Nogales-Gadea et al., 2015a). This study also summarizes the common causative mutations observed in McArdle's patients, which include the aforementioned variants, as well as p.(G205S), p.(W798R) and p.(Y84X). McArdle's patients have also reportedly experienced rhabdomyolysis onset during surgery, and had positive IVCT results, although the risk for MH was stated to be inconclusive (Bollig et al., 2005). *AMPD1* encodes adenosine monophosphate deaminase, an enzyme involved in the purine cycle converting AMP to inosine monophosphate to produce conditions that are favourable for ATP production in skeletal muscle. A deficiency of this enzyme can lead to exercise intolerance, hyperCKemia and rhabdomyolysis. A common causative mutation is the p.(Q12X) variant (Teijeira et al., 2009). Furthermore, individuals with this disorder have also been reported to test positive for MH via IVCT (Fishbein et al., 1985; Fricker et al., 2002).

This chapter will present a case-control study, using DNA samples within the MH unit biobank in concert with high-throughput genotyping technologies to investigate the genes considered thus far and hope to elucidate further avenues for future

research into malignant hyperthermia within the context of the threshold model of susceptibility. Using linkage disequilibrium analysis and selecting tag-SNPs, the number of variants tested can be cut down whilst still shedding light on regions of interest.

5.1.1 Chapter aims

This chapter aims to use a case-control format to genotype ~1500 patient DNA samples, consisting of MHS, MHN and MHS relatives to identify regions of interest and discrepancies in incidence of pathogenic variants in 10 candidate genes (*ACADVL*, *AMPD1*, *ATP2A1*, *CACNA1S*, *CACNA2D1*, *CASQ1*, *CPT2*, *PYGM*, *STAC3*, *TRPV1)* between susceptible and negative populations. This will enable further investigation into candidate loci in a threshold model of MH, potentially even through the novel gene editing pipeline established in previous chapters. This will be achieved by identifying informative SNPs in linkage disequilibrium with surrounding regions to be used as tags in high-throughput genotyping. Additional pathogenic variants of interest will also be selected based on the literature, and genotyped to supplement the findings.

5.2 Methods

5.2.1 Samples

Our cohort consisted of patients that had been referred to the UK malignant hyperthermia unit in Leeds for *in vitro* contracture testing (IVCT). Patient DNA samples were selected from the MH Unit biobank to include 599 MHS probands that were IVCT positive and 535 MHN probands that were IVCT negative. A further 350 MHS individuals were chosen as each was a relative (counted as 0.5 'n' in statistical analyses based on approximate relatedness to the proband) of a different MHS proband and were IVCT positive. Individuals with known myopathies were excluded in this selection. Ethical approval was granted by the Leeds Healthcare St James's University Hospital NHS Trust Clinical Research (Ethics) Committee (10/H1306/70), with all patients providing written consent for peripheral blood and muscle samples to be stored for research purposes. DNA was quantified and quality checked on a nanodrop to ensure samples suitability downstream. DNA samples that had a concentration of less than 60ng/ul, a 260nm/280nm ratio outside of 1.6-2.0 and a 260nm/230nm ratio outside of 1.9-2.3 were not selected due to minimum requirements of the Fluidigm (Standard BioTools) and Taqman (Thermofisher) genotyping systems and DNA quality concerns.

5.2.2 Linkage disequilibrium analysis

GnomAD v3.1.2 was used to export single nucleotide variants for 10 genes, including their promoter/enhancer and/or up to 1000 bp up and downstream, for the non-Finnish European population. Promoter/enhancer regions were determined using their GeneHancer score on GeneCards, which predicts likely enhancer regions based on likelihood-scores (Fishilevich et al., 2017). In the case of there being no promoter/enhancer region on either side of the gene, the genomic region was increased by 1000bps either side of the gene to ensure potential SNPs for tagging were not missed. These variants were then filtered for single nucleotide

polymorphisms at minor allele frequency ≥ 0.01 for linkage disequilibrium analysis. Linkage disequilibrium heatmaps were produced for each gene using the LDmatrix tool in the online NIH application LDlink, specifying the non-Finnish European population in the tool parameters. LDlink is a web-based application that queries SNPs in a population to generate haplotype tables and interactive plots, using haplotypes from 26 different population groups in the 1000 genomes phase 3 call set as a reference for calculating pairwise metrics of LD (Machiela & Chanock, 2015). Tag-SNP's (table 5.1) were selected based on the R^2 value indicating the strength of LD for adjacent SNPs, as well as aiming for MAF as close to 0.5 as possible for each gene. Rare pathogenic variants were also chosen based on the literature surrounding related diseases for each gene (table 5.2). Variants and SNPs were selected specifically for downstream genotyping using Fluidigm® technology.

Table 5.1: Tag-SNPs selected for candidate genes. Starred rsID's represent SNP's that were later replaced by a TaqMan™ assay. MAFs exported from GnomAD v3.1.2.

Gene	rsID	Non-Finnish European MAF	Minor Allele	Allele 1	Allele 2
ACADVL	rs17671352	0.36	T	C	T
	rs2017365	0.36	G	A	G
	rs2521985	0.35	T	C	T
	rs35224044	0.4	C	C	T
	rs507506	0.4	A	A	G
AMPD1	rs2010899	0.47	G	G	T
	rs2268699	0.38	C	A	C
	rs55999139	0.07	G	C	G
	rs6679869	0.12	C	C	G
	rs6701427	0.14	C	C	T
	rs76710407	0.09	A	A	G
	rs77720559	0.09	G	C	G
ATP2A1	rs3888190	0.39	T	G	T
	rs6565261	0.29	A	A	C
	rs7498555	0.39	C	C	T
	rs8046545	0.35	G	A	G
	rs8056890	0.35	A	A	G
	rs8060365	0.35	C	A	C
	rs9931989	0.35	G	C	G
CACNA1S	rs10800757	0.47	T	C	T
	rs12409114*	0.41	T	A	T
	rs2296383	0.43	T	C	T
	rs3767499	0.47	C	C	T
	rs4498834	0.43	C	C	T
	rs734881	0.42	A	A	G
CACNA2D1	rs10237261	0.47	A	A	G

	rs12536871	0.44	T	G	T
	rs17247184	0.46	T	C	T
	rs2237505	0.44	T	C	T
	rs2237527	0.48	T	C	T
	rs258677	0.4	T	G	T
	rs258690	0.4	C	C	T
	rs35985094	0.4	T	C	T
	rs37134	0.41	G	C	G
	rs4732435	0.49	A	A	G
	rs6954596*	0.4	A	A	G
CASQ1	rs11265351	0.21	A	A	G
	rs11265352	0.38	A	A	G
	rs12070418	0.26	A	A	G
	rs3747623	0.38	T	C	T
	rs60043899	0.12	A	A	T
	rs617698	0.39	G	A	G
	rs686015	0.43	A	A	T
CPT2	rs1056425	0.32	T	C	T
	rs10888776	0.46	G	A	G
	rs1799821	0.46	G	A	G
	rs2062015	0.46	G	C	G
	rs6692897	0.44	A	A	G
	rs737464	0.46	T	C	T
	rs7539949	0.46	G	A	G
	rs78117157	0.11	T	C	T
PYGM	rs477549	0.1	A	A	G
	rs506354	0.09	C	C	T
	rs523200	0.11	C	A	C
	rs547066*	0.09	A	A	C
	rs555974	0.09	T	T	G
	rs569602	0.09	G	A	G
	rs589691*	0.11	C	C	T
	rs592521	0.09	C	C	T
STAC3	rs10876968	0.28	T	G	T
	rs11172134	0.19	A	T	A
	rs3204635	0.28	T	C	T
	rs7133915	0.48	C	T	C
TRPV1	rs12936340	0.36	G	A	G
	rs161366	0.49	C	C	T
	rs182637	0.45	A	A	G
	rs224534	0.36	A	A	G
	rs224537	0.36	A	A	G
	rs224546	0.43	C	C	T
	rs8078936	0.37	T	C	T

Table 5.2: Rare variants selected for genotyping based on the literature. MAF exported from GnomAD v3.1.2/v4.0.

Gene	rsID	Non – Finnish European MAF	Protein Change	Minor Allele	Allele 1	Allele 2
ACADVL	rs2309689	0.00004409	p.(G441D)	A	G	A
	rs751995154	0.00005881	p.(R459Q)	A	G	A
	rs113994167	0.001809	p.(V283A)	C	T	C

AMPD1	rs61752478	0.004586	p.(M343I)	A	C	A
	rs17602729	0.1323	p.(Q12X)	A	G	A
ATP2A1	rs121918114	0.00001709	p.(C675X)	A	C	A
	rs538702357	0	p.(E982K)	A	G	A
	rs121918115	0.00001471	p.(P789L)	T	C	T
	rs121918113	0.00001471	p.(R198X)	T	C	T
	rs761592113	0	p.(R560C)	T	C	T
CACNA1S	rs28930069	0	p.(R1239G)	C	G	C
	rs28930068	0	p.(R1239H)	T	C	T
	rs80338777	0.0000147	p.(R528H)	T	C	T
CACNA2D1	rs35131433	0.006797	p.(D1045A)	G	T	G
CASQ1	rs730882052	not reported	p.(D244G)	G	A	G
CPT2	rs28936375	0.0001912	p.(P50H)	A	C	A
	rs74315294	0.001999	p.(S113L)	T	C	T
PYGM	rs77656150	0.002984	p.(A193S)	A	C	A
	rs119103251	0.0003968	p.(G205S)	T	C	T
	rs116987552	0.003116	p.(R50X)	A	G	A
	rs119103258	0.00002945	p.(W798R)	G	A	G
	rs527236146	0.000004522	p.(Y85X)	T	G	T
STAC3	rs371720347	0.0002352	p.(K288X)	A	T	A
	rs140291094	0.00005879	p.(W284S)	G	C	G
TRPV1	rs759094783	0.000002856	p.(G684V)	A	C	A
	rs1217651219	0.0000294	p.(R772C)	A	G	A

5.2.3 Fluidigm® high throughput genotyping

Custom allele-specific primers for each variant were designed using Standard BioTools D3 design portal for use with their Fluidigm® SNP Type™ genotyping technology (Standard BioTools) (figure 5.1). Genotyping of patient samples were done according to the manufacturers protocol. Briefly, the SNP Type™ allele specific primers (7.5μM) were combined with SNP Type™ locus specific primers (20μM), TE DNA suspension buffer, 2X assay loading reagent and nuclease-free water (Ambion) to produce a final 10X assay mix at a final volume of 6μl per assay. Sample mixes were also prepared to a final volume of 6μl per sample by combining 2X fast probe master mix (Biotium), 20X SNP Type™ sample loading reagent, 60X SNP Type™ reagent, ROX (Thermofisher), nuclease-free water (Ambion) and gDNA. All reagents were from Standard BioTools, unless stated otherwise. Subsequently, 5μl of each mix was loaded onto a primed 96x96 Dynamic Array integrated fluidics circuit (IFC) (Standard BioTools) using the IFC controller HX and

then run on BioMark™ HD system using an altered version of the SNP Type™ 96x96 v1 thermal cycling program which included additional capture steps at the end of each cycle for 40 cycles. Universal fluorescent probes containing flourophores SNP Type™-FAM and SNP Type™-HEX were used to distinguish alleles. For rare variants, a mixed pool of positive control ssDNA oligos (90nt, GenScript) harbouring the pathogenic variant were included on each IFC. Data was analysed using the SNP genotyping software by Standard Biotools. Hardy-Weinberg equilibrium for each SNP within each sub-group and genotype differences between sub-groups for each SNP were tested using a right-tailed Chi-squared test.

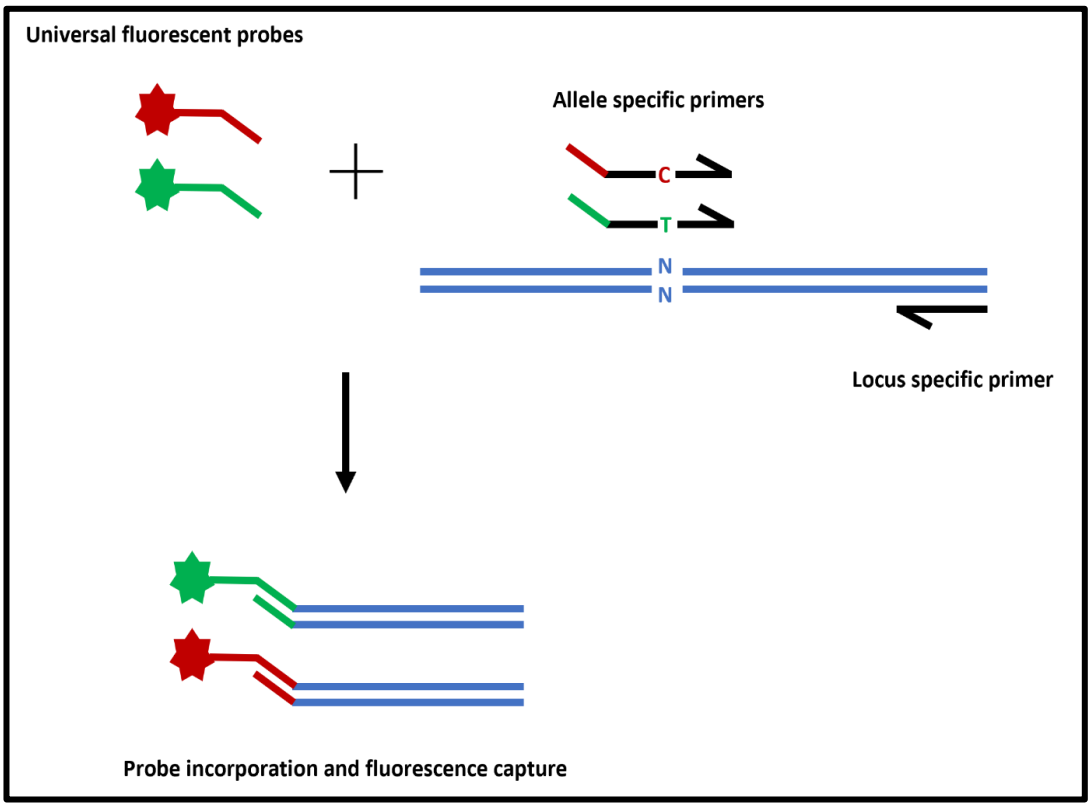

Figure 5.1: Diagrammatic representation of Fluidigm® SNPType™ genotyping chemistry. Probes colour-coded to represent different allele-specific markers. Allele specific primers enable detection of either variant and contain hybridisation region for relevant fluorescent probe. After probe is incorporated into relevant amplicons, fluorescence is captured and quantified against background ROX to enable genotype calling.

5.2.4 Specific target amplification

Any samples that failed to be called for a genotype were then pre-amplified according to the manufacturers protocol prior to repeating the fluidigm workflow above. Briefly, SNP Type™ specific target amplification primers (500nM) were combined with SNP Type™ locus specific primers (500nM) to produce a 10X STA primer pool. This was subsequently combined with 2X multiplex PCR master mix (Qiagen), nuclease-free water (Ambion) and gDNA for amplification. The reaction was run for 15 minutes at 95ºC followed by 20 cycles of: 95ºC/15s, 60ºC/4mins. The STA products were then diluted 1:20 in TE DNA suspension buffer and stored at -20ºC. Final dilution of STA products was determined by performing a dilution series ranging from 1:10 to 1:100 and examining call rates for each dilution across 5 independent patient DNA samples (figure 5.2). Dilution was chosen based on a trade-off between average call rate of each sample and avoiding STA reagents being too concentrated for downstream genotyping.

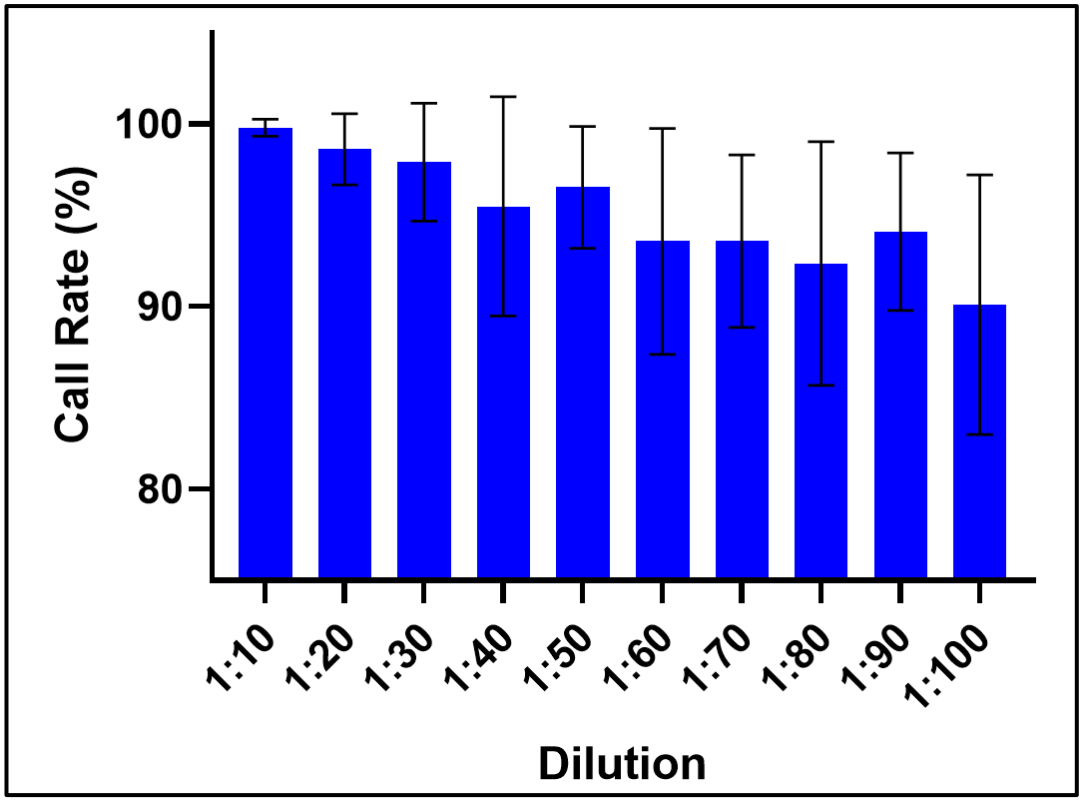

Figure 5.2: Call rate average for STA product dilution series. N=5, Mean ± SD of call rate (%) plotted for each dilution, ranging from 1:10 to 1:100. Y axis scale = 75% - 105% to enable clearer visualisation of differences between dilutions. Call rate denotes the percentage of variants each sample was successfully and accurately genotype-called for. Accuracy was determined by examining fluorescent signal across PCR cycles to QC genotypes called by SNP genotyping software from Standard Biotools. Graph was made in GraphPad Prism 10.

5.2.5 TaqMan™ Genotyping

Select probes (table 5.3) that were either not in Hardy-Weinberg equilibrium (HWE) or were inefficient resulting in low sample numbers were re-tested using pre-designed TaqMan™ probes (Applied Biosystems). Genotyping was conducted according to manufacturer's protocol. Briefly, 2X TaqMan™ Genotyping mastermix (Applied Biosystems) was combined with 20X working stock of the assay, nuclease free water (Ambion) and gDNA. The reaction was run for 10 minutes at 95ºC followed by 40 cycles of: 95ºC/15s, 60ºC/1min. Capture was performed at the end of each cycle, alongside a pre- and post-PCR read. Probes contained fluorophores VIC and FAM. Data was analysed on the TaqMan™ Genotyper (Applied Biosystems) software for genotype calls. Genotype calls by software were quality checked by assessing fluorescent signal at each PCR cycle.

Table 5.3: Tag-SNPs conducted using TaqMan™ assays. MAF exported from GnomAD v3.1.2.

Gene	rsID	Non – Finnish European MAF	Minor Allele	Allele 1	Allele 2
CACNA1S	rs12409114	0.41	T	A	T
CACNA2D1	rs2190232	0.41	T	T	C
PYGM	rs547066	0.09	A	A	C
	rs630966	0.09	C	C	G

5.2.6 Data analysis and statistics

Chi-squared tests were used to calculate whether Hardy-Weinberg equilibrium was met within MHS, MHN and MHS(R) subgroups, as well as to assess significant differences in observed genotypes between groups. When combining MHS(R) subgroup into the analysis, each related individual added 0.5 to the total N number to account for relatedness to MHS probands. If conditions for Chi-squared test were not met, Fisher's exact test was used. P-values are presented as uncorrected, with those in bold indicating significance after Bonferroni correction (total SNPs – 1). Correction was applied independently to SNPs and rare variants. Genomic co-ordinates used in identifying regions of interest are in build Grch38.

5.3 Results

Out of 599 MHS probands only 330 (~55%) had one or more diagnostic variants, of which the vast majority were in *RYR1* (327, ~54.5%) as compared to *CACNA1S* (3, ~0.5%). Two individuals had more than one diagnostic *RYR1* variant which accounted for around 0.3% of total MHS probands and around 0.6% of probands with one or more *RYR1* variant. Both individuals also had IVCT responses to halothane, with only one also reacting to caffeine. Typically, a reaction to both agonists may suggest a more 'severe' IVCT phenotype, which has been previously shown to also correlate with markers of clinical severity (Carpenter et al., 2009). The findings in this dataset further emphasise the rarity of individuals with multiple pathogenic *RYR1* variants, and thus making further conclusive comparisons of clinical severity due to multiple variants in the gene difficult to establish. Furthermore, of those with a diagnostic variant the majority had IVCT responses to both halothane and caffeine (267, ~81%) (table 5.4). Of those with one or more diagnostic *RYR1* variant, 60 had an MHSh classification (~18%) and only one individual had an MHSc classification. The spread of IVCT phenotypes was slightly different, however, amongst individuals with no diagnostic variant. Both MHShc (~41%) and MHSh (~50%) classifications had a similar number of individuals, with only 3 individuals classified as MHSc (~0.01%).

Table 5.4: Diagnostic variant spread within MHS probands selected for high-throughput genotyping.

Gene	Total	MHShc	MHSh	MHSc
RYR1	327	264	60	1
CACNA1S	3	3	0	0
none	269	110	135	3

Genotyping was successfully conducted using a combination of Fluidigm® SNP Type™ and TaqMan™ chemistries for 67 out of 70 tag-SNPs and for 24 out of 26

rare variants. Out of the 91 successful assays in total, 78 had a sample call rate of 80% or more (with 64 of those exceeding 95%) and only 10 had a sample call rate below 70% (table 5.5). An example of allelic plots is also shown in figure 5.3 for the tag-SNPs rs258677 (*CACNA2D1*, Fluidigm® SNP Type™), rs630966 (*PYGM*, TaqMan™) and the *PYGM* p.(R50X) rare variant (Fluidigm® SNP Type™).

Table 5.5: Breakdown of successful assays and their respective sample call rates.

Assay type	Number of assays				
	Total	≥95% call rate	≥90% call rate	≥80% call rate	≤70% call rate
Fluidigm® tag-SNPs	63	49	53	55	5
TaqMan™ tag-SNPs	4	0	0	3	1
Rare variants	24	15	17	20	4

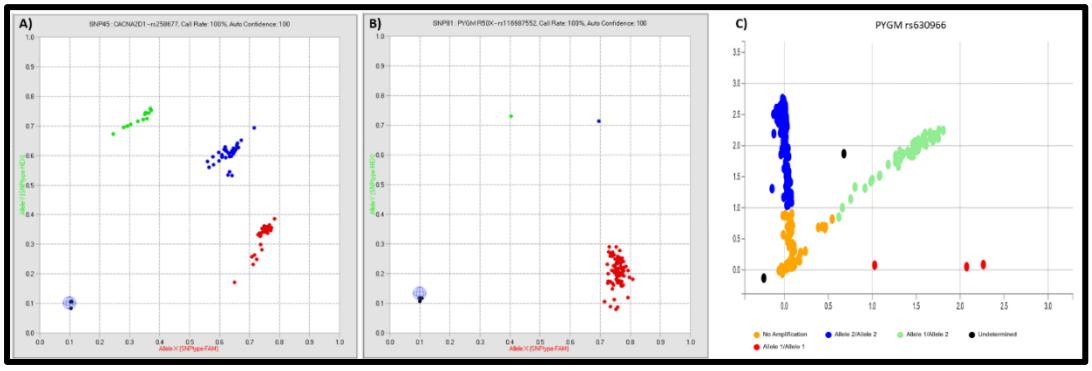

Figure 5.3: Example allelic plots. A and B show Fluidigm® plots where red indicates homozygous for allele 1, green indicates homozygous for allele 2, blue indicates heterozygous samples, and black indicates no template controls with A showing genotype calls for rs258677 and B showing calls for *PYGM* p.(R50X). C shows a TaqMan™ plot for rs630966 with red indicating homozygous for allele 1, blue indicating homozygous for allele 2, green indicating heterozygous samples, and yellow and black indicating either unamplified or undetermined calls respectively.

5.3.1 Genes involved in excitation contraction coupling

Amongst tag-SNPs tested in the genes involved in ECC (figure 5.4), a total of 10 were identified as having either significantly different genotypes or allele counts between MH susceptible and negative populations after correcting for multiple comparisons (table 5.6). Two showed over-representation of both homozygote genotypes relative to MHN in *ATP2A1*. Rs8046545 has partial coverage for the chromosomal region 16: 28902466 – 28904206, which spans exon 18 to 23, and harbours the p.(E982K) pathogenic variant. Rs8056890 tags for the chromosomal region 16:28884694 – 28887472, which spans exons 7 to 8, and harbours the p.(R198X) pathogenic variant. When including MHS relatives, as an addition of 0.5 to the total N numbers during analysis, rs8046545 was no longer significantly different for genotypes between groups.

Three were significant in *CACNA1S*. Rs3767499 showed an increase in heterozygotes amongst the MHS group and tags for the region 1:201039454 – 201063145, spanning exons 23 to 44. This region also harbours the pathogenic variants p.(R1239G) and p.(R1239H). Rs734881 showed a decreased ‘11’ genotype in the MHS group and tags for the regions 1: 201080731 – 201081904, spanning the intron between exons 10 and 11. Rs10800757, showed a significant increase in the ‘11’ genotype between susceptible and negative groups when adding relatives to the analysis and tags for the region 1: 201073490 – 201075216, spanning exons 14 and 15.

Four SNPs were significant in *CACNA2D1*. Rs2237505 had an increase of heterozygotes amongst MHS probands and tags for the region 7: 82061610 – 82082657, spanning the entirety of exon 16 and neighbouring introns. Rs258690 had an increase of heterozygotes amongst the MHS group and tags for the region 7: 82119966 – 82126997, spanning the entirety of exon 15 and neighbouring introns. Rs4732435 had an increase of heterozygotes alongside a decrease of ’11’

homozygotes and tags for the region 7: 82197831 – 82219010, located in the intronic region between exons 3 and 4. Rs2237527 had a significant increase of allele ‘2’ count in MHS probands relative to the MHN group and tags for the region 7: 82382794 – 82384018, spanning the intronic region between exons 1 and 2.

Rs7133915 was the only SNP in *STAC3* identified as showing significant difference between susceptible and negative groups, with an increase of heterozygotes alongside increased allele ‘1’ count amongst MHS probands and was not in strong LD with surrounding SNPs.

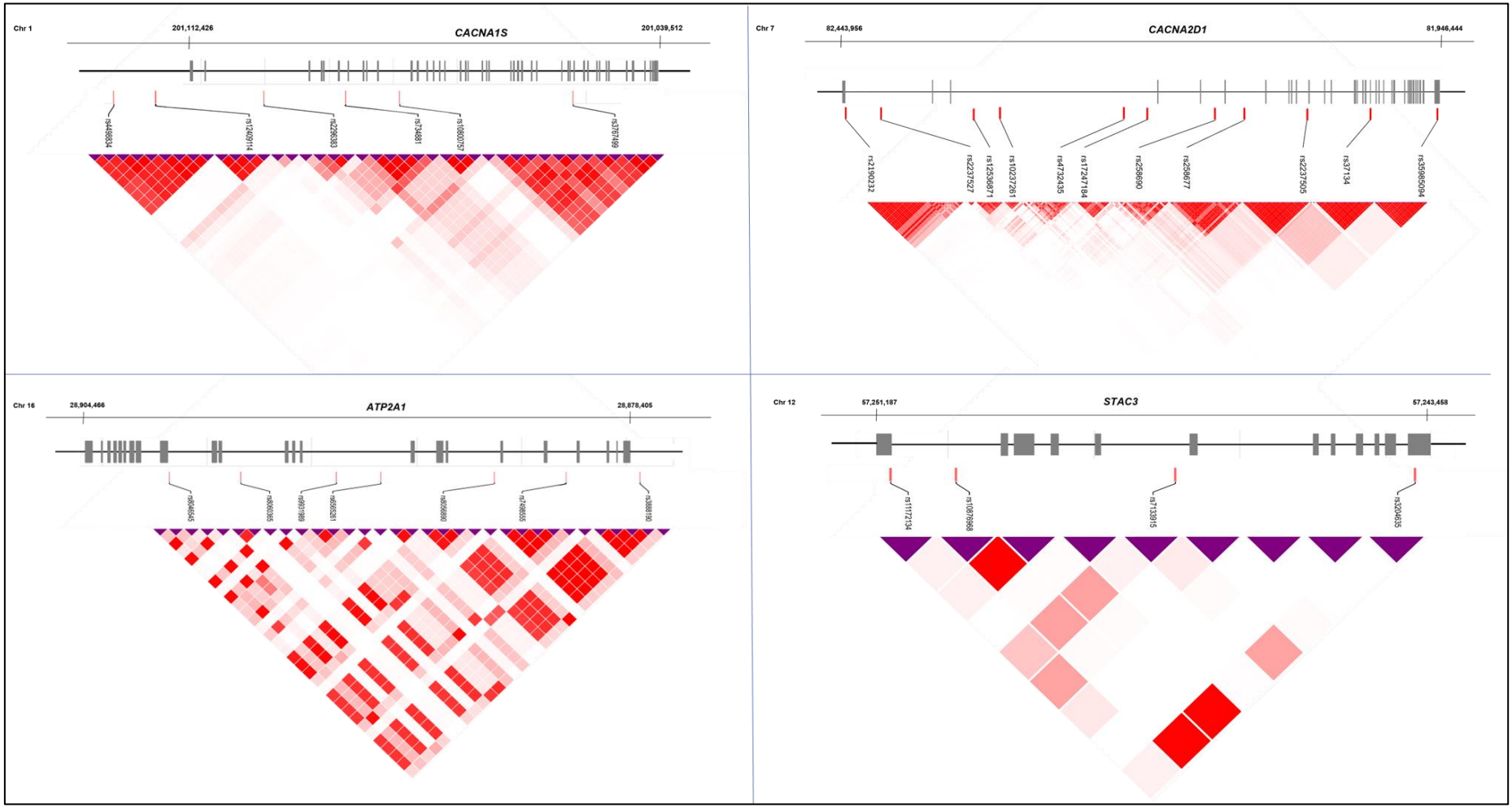

Figure 5.4: LD heatmaps for genes involved in ECC generated via LDlink. Only tag-SNPs shown for simplicity, alongside schematic of loci with genomic coordinates and grey squares indicating exons. Red squares indicate R^2 values, with deeper shades indicating higher values.

Table 5.6: Successfully genotyped tag-SNPs in genes involved in ECC, with observed genotype numbers for each sub-group.
Uncorrected p-values, with bold indicting significance (p<0.05) after Bonferroni correction, calculated using Chi-Squared test, or Fisher's exact test where conditions for Chi-Squared were not met. †=TaqMan™ assays. *=not in Hardy-Weinberg equilibrium in the control (MHN) sub-group.

Gene	rsID	MHS			MHN			MHS(R)			MH (S) vs (N) p-value		MH (S+R) vs (N) p-value	
		11	12	22	11	12	22	11	12	22	Genotype	Allele count	Genotype	Allele count
ATP2A1	Rs3888190	228	247	114	209	242	74	123	163	62	0.047	ns	0.049	ns
	Rs6565261	48	169	233	33	141	188	10	33	30	0.049	ns	0.039	ns
	Rs8046545	213	123	104	181	139	39	137	142	40	**<0.001**	0.002	0.003	0.003
	Rs8056890	96	242	256	62	243	227	40	156	139	**<0.001**	ns	**<0.001**	ns
	Rs8060365	249	244	90	230	225	70	146	151	49	ns	ns	ns	ns
	Rs9931989	257	238	96	227	241	63	145	159	44	0.049	ns	ns	ns
CACNA1S	Rs10800757	208	276	109	188	241	101	210	86	41	0.005	ns	**<0.001**	0.050
	Rs12409114†	203	228	77	195	190	86	120	88	50	0.003	ns	0.011	ns
	Rs2296383	191	293	110	183	245	104	113	166	59	0.002	ns	0.003	ns
	Rs3767499	132	299	154	105	251	169	70	173	95	**<0.001**	0.047	**<0.001**	ns
	Rs4498834	122	263	202	111	253	168	61	160	127	0.001	ns	0.002	ns
	Rs734881	85	270	235	97	229	205	65	82	190	**<0.001**	ns	**<0.001**	0.048
CACNA2D1	Rs10237261	153	280	163	134	259	138	91	158	98	0.003	ns	0.004	ns
	Rs12536871	160	252	180	147	251	134	72	124	95	0.005	ns	0.005	ns
	Rs17247184	183	290	120	190	238	103	118	150	70	0.003	ns	0.006	ns
	Rs2237505	202	276	116	182	230	117	114	175	59	**<0.001**	ns	**<0.001**	ns
	Rs2237527	147	273	173	170	244	117	101	167	74	0.002	**<0.001**	0.003	0.004
	Rs258677	227	280	83	196	255	78	138	159	41	0.015	ns	0.013	ns
	Rs258690	121	300	163	124	253	150	71	176	100	**<0.001**	ns	**<0.001**	ns
	Rs35985094	205	275	97	182	259	87	123	163	54	0.018	ns	0.021	ns
	Rs37134	200	278	113	177	258	95	118	166	64	0.019	ns	0.023	ns
	Rs4732435	113	358	115	167	253	110	115	150	73	**<0.001**	0.009	**<0.001**	0.039
	Rs2190232†	87	46	3	131	65	0	46	26	0	ns	ns	ns	ns
STAC3	Rs10876968	294	240	60	280	212	36	175	127	37	ns	ns	ns	ns
	Rs11172134	396	167	28	350	160	18	230	95	17	ns	ns	ns	ns
	Rs3204635*	114	400	72	103	369	50	100	191	55	ns	ns	ns	ns
	Rs7133915	0	80	458	1	0	447	0	0	173	**<0.001**	**<0.001**	**<0.001**	**<0.001**

5.3.2 Genes involved in calcium homeostasis

Amongst tag-SNPs tested in genes involved in calcium homeostasis (figure 5.5), a total of 8 were identified as having either significantly different genotypes or allele counts between MH susceptible and negative populations after correcting for multiple comparisons (Table 5.7). Five of these SNPs were in *CASQ1*. Rs11265351 had an increase in '11' homozygotes alongside a decrease in '22' homozygotes amongst the susceptible group and has strong association with rs12070418, which shows the same differences between susceptible and negative genotypes. Both are located within the promoter/enhancer region for *CASQ1*, of which rs12070418 is weakly associated with the region 1:160187452 – 160187575. Rs3747623 had an increase in heterozygotes and a decrease in '22' homozygotes between susceptible and negative groups. Specifically, when combining susceptible relatives into the analysis, a significant increase in allele '1' count was also noted. This SNP tags for the genomic region 1:160195305 – 160193719, spanning the entirety of exons 3 to 4. Rs60043899 had an increase in heterozygotes amongst the susceptible group and is weakly associated with the region 1: 160195782 – 160196445, spanning the entirety of exon 6, with further weaker associations upstream. Rs686015 had an increase in heterozygotes and has no strong associations within the gene.

Three SNPs in *TRPV1* were significantly different between groups. Rs12936340 had an increase in heterozygotes amongst the susceptible group and tags for the region 17: 3585283 – 3590694, spanning exons 6 to 9. Rs224534 is in strong association with rs12936340 and similarly had increased heterozygotes amongst the susceptible group. This SNP tags for the region 17: 3583408 – 3583673, spanning exon 10 partially. Rs161366 had an increase of heterozygotes alongside increased allele '2' count amongst MHS probands and tags for the region 17: 3580806 – 3581516, spanning the intronic region between exons 10 and 11.

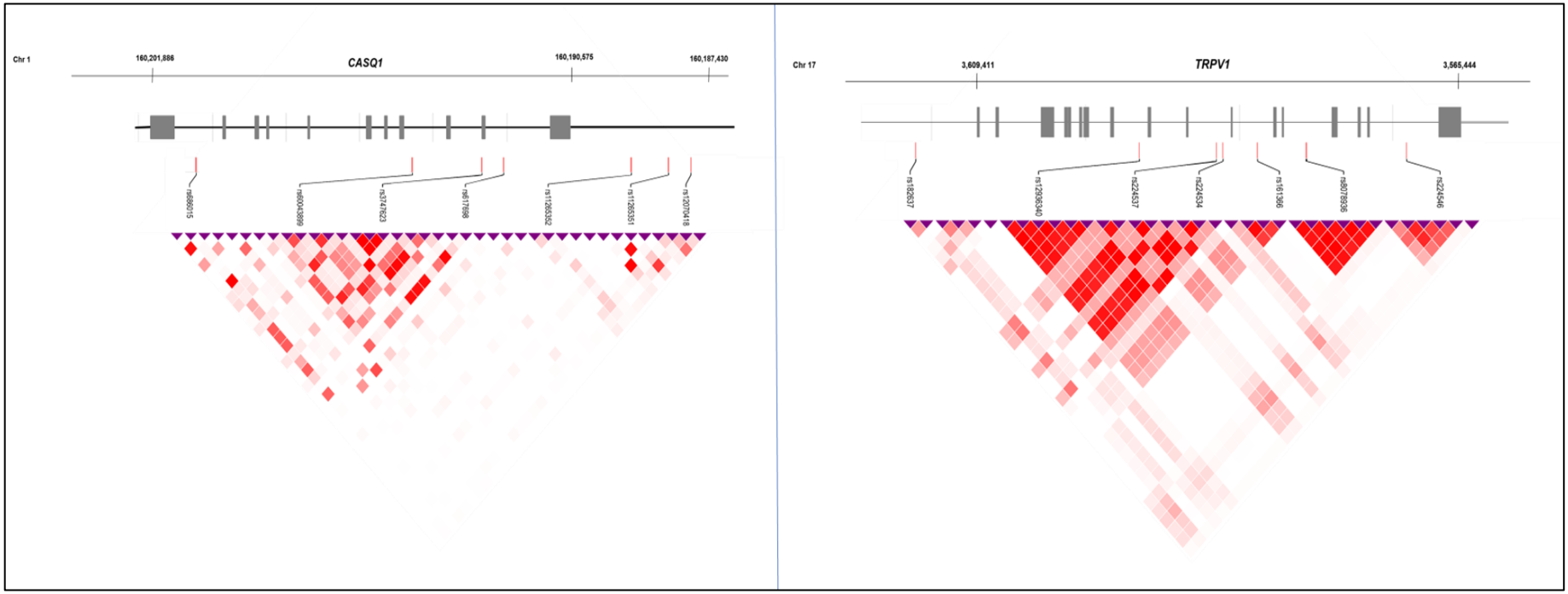

Figure 5.5: LD heatmaps for genes involved in calcium homeostasis generated via LDlink. Only tag-SNPs shown for simplicity, alongside schematic of loci with genomic coordinates and grey squares indicating exons.. Red squares indicate R^2 values, with deeper shades indicating higher values.

Table 5.7: Successfully genotyped tag-SNPs in genes involved in calcium homeostasis, with observed genotype numbers for each sub-group. Uncorrected p-values, with bold indicting significance (p<0.05) after Bonferroni correction, calculated using Chi-Squared test, or Fisher's exact test where conditions for Chi-Squared were not met. *=not in Hardy-Weinberg equilibrium in the control (MHN) sub-group.

Gene	rsID	MHS			MHN			MHS(R)			MH (S) vs (N) p-value		MH (S+R) vs (N) p-value	
		11	12	22	11	12	22	11	12	22	Genotype	Allele count	Genotype	Allele count
CASQ1	Rs11265351*	27	93	469	15	83	432	14	23	301	**<0.001**	ns	**<0.001**	ns
	Rs11265352	86	275	233	85	267	179	48	161	129	0.001	ns	0.001	ns
	Rs12070418	50	235	308	26	210	295	31	146	171	**<0.001**	ns	**<0.001**	0.026
	Rs3747623*	230	293	62	205	198	124	164	132	42	**<0.001**	0.001	**<0.001**	**<0.001**
	Rs60043899	10	127	455	11	106	414	7	69	263	**<0.001**	ns	**<0.001**	ns
	Rs617698	170	224	56	160	151	49	22	35	13	0.031	ns	0.029	ns
	Rs686015	192	308	88	189	229	111	135	153	48	**<0.001**	ns	**<0.001**	ns
TRPV1	Rs12936340	203	315	72	210	251	72	146	148	45	**<0.001**	ns	0.008	ns
	Rs161366	580	16	0	532	0	0	349	0	0	**<0.001**	**<0.001**	**<0.001**	0.001
	Rs182637	73	162	121	113	258	156	47	125	95	0.002	ns	0.003	ns
	Rs224534	62	283	248	64	239	227	43	151	145	**<0.001**	ns	**<0.001**	ns
	Rs224537	41	219	185	41	160	153	8	35	27	0.038	ns	0.038	ns
	Rs224546	105	268	193	97	243	168	69	164	112	0.001	ns	0.002	ns
	Rs8078936	226	226	80	191	203	65	128	140	47	ns	ns	ns	ns

5.3.3 Genes involved in metabolism

Amongst tag-SNPs tested in genes involved in calcium homeostasis (figure 5.6), 9 were identified as having either significantly different genotypes or allele counts between MH susceptible and negative populations after correcting for multiple comparisons (table 5.8). Rs507506, downstream of *ACADVL*, had a significant increase in heterozygotes and '22' homozygotes amongst susceptible probands and tags for the region 17:7213534 – 7215003, located within the promoter/enhancer region. This SNP is also in strong association with several other SNP's that tag for the region 17:7219058 – 7219305, spanning the 5' UTR. Rs507506 was no longer significant when introducing susceptible relatives into the analysis. However, rs35224044 did exhibit a significant increase in heterozygotes alongside increased allele '2' count amongst the susceptible group, when relatives were included. Rs35224044 has strong associations with multiple SNPs across the promoter/enhancer and 5' regions of the *ACADVL*, providing partial coverage up to exon 2.

Three SNPs were significant in *AMPD1*. Rs2010899 has an increase of heterozygotes amongst susceptible groups and has coverage across the region 1:114692389 – 114693164, which spans the intronic region between exons 2 and 3. Rs55999139 has an increase of heterozygotes, '22' homozygotes and allele '2' count amongst the susceptible group. The SNP tags for the region 1:114682595 – 114682617, spanning the intronic region between exons 5 and 6. Rs6701427 has an increase of both homozygote genotypes amongst the susceptible group and exhibits weak associations with other SNPs within the gene.

Four SNPs were significant in *CPT2*. Rs10888776 and rs737464 have an increase in heterozygotes amongst the susceptible group, whilst rs2062015 and rs7539949 have an increase in '22' homozygotes amongst the susceptible group. Rs2062015 tags for the region 1:53199479 – 53199940, located within the intronic region

between exons 1 and 2. All four SNPs have strong associations with each other alongside weaker associations with several other SNPs along the gene, providing partial coverage.

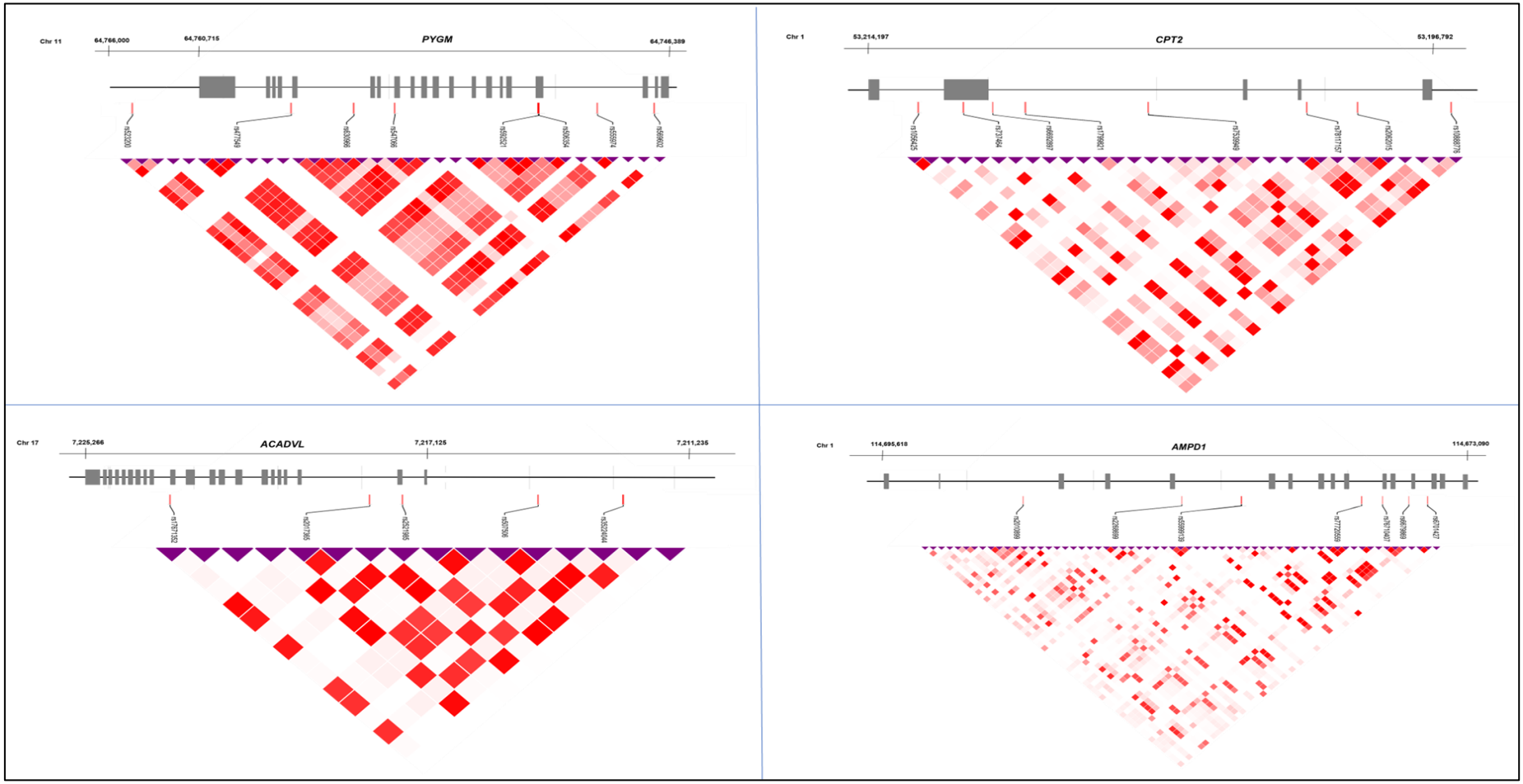

Figure 5.6: LD heatmaps for genes involved in metabolic pathways generated via LDlink. Only tag-SNPs shown for simplicity, alongside schematic of loci with genomic coordinates and grey squares indicating exons. Red squares indicate R^2 values, with deeper shades indicating higher values.

Table 5.8: Successfully genotyped tag-SNPs in genes involved in metabolic pathways, with observed genotype numbers for each sub-group. Uncorrected p-values, with bold indicting significance (p<0.05) after Bonferroni correction, calculated using Chi-Squared test, or Fisher's exact test where conditions for Chi-Squared were not met. †=TaqMan™ assays. *=not in Hardy-Weinberg equilibrium in the control (MHN) sub-group.

Gene	rsID	MHS			MHN			MHS(R)			MH (S) vs (N) p-value		MH (S +R) vs (N) p-value	
		11	12	22	11	12	22	11	12	22	Genotype	Allele count	Genotype	Allele count
ACADVL	Rs17671352	97	96	28	103	116	29	143	129	40	ns	ns	ns	ns
	Rs2017365	211	220	63	197	250	72	154	137	45	0.006	ns	0.004	ns
	Rs2521985	229	223	69	216	260	55	165	138	42	0.040	ns	0.018	ns
	Rs35224044	497	95	0	476	55	0	239	109	0	0.009	0.007	**<0.001**	**<0.001**
	Rs507506	92	274	228	93	255	183	48	146	144	**<0.001**	ns	0.001	ns
AMPD1	Rs2010899	127	272	192	139	228	162	72	170	106	**<0.001**	ns	**<0.001**	ns
	Rs2268699	205	287	99	217	229	87	114	172	54	0.002	ns	0.001	ns
	Rs55999139	479	76	9	421	5	3	293	17	3	**<0.001**	**<0.001**	**<0.001**	**<0.001**
	Rs6679869	5	91	345	6	73	287	0	12	68	ns	ns	ns	ns
	Rs6701427	17	123	453	12	131	388	7	87	244	**<0.001**	ns	**<0.001**	ns
	Rs76710407	4	96	491	2	83	445	2	42	294	ns	ns	ns	ns
	Rs77720559	452	115	18	444	81	6	295	45	2	0.028	0.002	ns	0.020
CPT2	Rs1056425	280	248	67	242	235	54	162	130	47	ns	ns	ns	ns
	Rs10888776	181	287	123	161	242	128	113	166	59	**<0.001**	ns	**<0.001**	ns
	Rs1799821*	181	333	77	152	312	65	113	181	44	0.049	ns	0.044	ns
	Rs2062015	120	264	213	129	228	175	60	174	115	**<0.001**	ns	**<0.001**	ns
	Rs737464	180	292	120	155	253	122	113	168	57	**<0.001**	ns	**<0.001**	ns
	Rs7539949*	13	71	507	16	83	433	56	124	167	**<0.001**	0.035	**<0.001**	0.014
	Rs78117157	454	131	6	415	105	11	241	87	13	ns	ns	ns	ns
PYGM	Rs477549	456	87	6	411	106	5	261	53	3	ns	ns	ns	ns
	Rs506354	594	0	1	525	5	0	285	58	0	0.023	ns	0.002	0.001
	Rs523200*	468	89	20	399	88	31	282	57	7	0.007	0.021	0.003	0.008
	Rs547066†	4	74	456	3	78	386	2	42	226	ns	ns	ns	ns
	Rs555974	596	0	1	534	0	0	273	0	0	ns	ns	ns	ns
	Rs569602	485	76	4	433	85	5	282	49	3	ns	ns	ns	ns
	Rs630966†	4	80	452	4	91	378	4	50	242	ns	ns	ns	ns

5.3.4 Pathogenic variants

Eight pathogenic variants were identified as having either significantly different genotypes or allele counts between MH susceptible and negative populations after correcting for multiple comparisons (table 5.9). The *ACADVL* variants p.(R459Q) and p.(V283A) have an increase in heterozygotes, along with a few homozygotes in the MHS proband group. Despite both of these variants being two of the most common that are causative for VLCAD deficiency, the scale at which heterozygous individuals are observed within the MH susceptible population is surprising, especially given the identification of only one MHSh patient carrying this the p.(V283A) variant previously (Gardner et al., 2020). In contrast, only one heterozygous p.(V283A) individual was noted within the MHN group. The presence of pathogenic variants in this gene within the MHS population coincides with previous studies implicating the downregulation of fatty acid oxidation pathways in MHS mouse models (Chang et al., 2020). Additionally, the frequency at which pathogenic variants occur, as well as the identification of homozygote individuals, presents a strong case for further characterisation of these variants within the context of MH susceptibility. Finally, although not statistically significant, 2 homozygote individuals for the p.(G441D) variant were also noted amongst the MHS relatives, as compared to lack of MHN individuals that carry the allele.

In *PYGM*, the p.(G205S) and p.(W798R) variants show a significant increase in heterozygotes within the MHS group, as well as 2 homozygotes for p.(W798R). This was particularly interesting due to the prevalence of these variants as compared to p.(R50X), which is the most common causative variant for McArdle's disease within the UK and has also been previously identified in MHS patients (Gardner et al., 2020). These variants are common in Spanish populations in particular, possibly indicating increased prevalence of individuals from this background within our cohort(Nogales-Gadea et al., 2015b). Furthermore, the prevalence of homozygote

individuals for the p.(W798R) variant is equal to that of p.(R50X), with many more heterozygote carriers. Finally, although not statistically significant, the identification of homozygote individuals for both p.(R50X) and p.(Y85X) variants is an interesting observation, given the lack of homozygote individuals for either variant amongst the MHN group.

In *AMPD1*, both p.(M343I) and p.(Q12X) are relatively underrepresented within the susceptible group. Additionally, in *ATP2A1*, both p.(C675X) and p.(R198X) are also relatively underrepresented within the MHS group. All showed a significant decrease in heterozygotes and homozygotes for the pathogenic variant within the MHS groups. However, the p.(R198X) variant did have a few homozygous individuals within the MHS probands, which were not observed in the MHN group. It is important to note that in the case of pathogenic variants, the identification of these in MHS individuals is important in the context of a threshold model of MH, as they could of course still contribute to a MHS phenotype in MHS individuals. Here, it is also interesting to note, although not statistically significant, the identification of several individuals homozygous for pathogenic variants in *ATP2A1* (p.(E982K), p.(P789L), p.(R560C)), where none were found in the MHN group. Furthermore, all 5 *ATP2A1* variants discussed were more frequent in the control MHN group as compared to the reported non-Finnish European allele frequencies in GnomAD v3.1.2. When compared to the reported frequencies, the variants discussed are significantly over-represented within the MHS subgroups.

Similarly, the *CPT2* variants p.(P50H) and p.(S113L) were identified in several individuals, with many homozygous for the pathogenic variants, in contrast to no homozygous individuals identified in the MHN group. Additionally, the *CACNA1S* variants p.(R1239H) and p.(R1239G) were identified in individuals homozygous for the variant, in contrast to none identified in the MHN group. These variants are also at a higher observed frequency within the control MHN group as compared to the

reported frequency for the non-Finnish European population in GnomAD v.3.1.2. When compared to the reported frequencies, the discussed *CPT2* and *CACNA1S* variants are over-represented within the MHS proband population.

Table 5.9: Successfully genotyped rare variants, with observed genotype numbers for each sub-group. Uncorrected p-values shown, with bold indicting significance (p<0.05) after Bonferroni correction (total number of variants – 1). P-values calculated using Chi-Squared test, or Fisher's exact test where conditions for Chi-Squared were not met. Starred variants (DNA change) indicate those not in Hardy-Weinberg equilibrium in the control (MHN) subgroup. Underlined variants (protein change) indicate those that had different minor allele frequencies in the control (MHN) group compared to those for the non-Finnish European population in GnomAD v3.1.2.

Gene	DNA change	Protein change	MHS			MHN			MHS(R)			MH (S) vs (N) p-value		MH (S+R) vs (N) p-value	
			11	12	22	11	12	22	11	12	22	Genotype	Allele count	Genotype	Allele count
ACADVL	c.1322G>A	p.(G441D)	430	0	0	356	0	0	67	0	2	ns	ns	ns	ns
	c.1376G>A	p.(R459Q)	542	50	2	529	0	0	337	7	4	**<0.001**	**<0.001**	**<0.001**	**<0.001**
	c.848T>C	p.(V283A)	547	31	1	530	1	0	345	1	0	**<0.001**	**<0.001**	**<0.001**	**<0.001**
AMPD1	c.1029G>T	p.(M343I)	508	3	1	492	38	1	314	27	0	**<0.001**	**<0.001**	**<0.001**	**<0.001**
	c.34C>T	p.(Q12X)	412	87	10	388	131	12	279	55	4	0.004	0.005	**0.001**	**0.001**
ATP2A1	c.2025C>A*	p.(C675X)	439	1	0	338	1	12	69	0	1	**<0.001**	**<0.001**	**<0.001**	**<0.001**
	c.2944G>A	p.(E982K)	588	0	1	525	6	0	302	31	0	0.011	ns	ns	ns
	c.2366C>T	p.(P789L)	540	53	2	497	32	0	344	0	0	ns	0.032	ns	ns
	c.592C>T	p.(R198X)	594	0	2	495	35	0	305	32	0	**<0.001**	**<0.001**	**<0.001**	**<0.001**
	c.1678C>T	p.(R560C)	588	1	3	530	0	0	326	11	0	ns	0.016	0.014	0.003
CACNA1S	c.3715C>G	p.(R1239G)	593	0	1	529	1	0	347	0	1	ns	ns	ns	ns
	c.3716G>A	p.(R1239H)	467	127	1	447	84	0	348	0	0	0.020	0.018	ns	ns
	c.1583G>A	p.(R528H)	589	1	0	531	0	0	348	0	0	ns	ns	ns	ns
CACNA2D1	c.3134A>C	p.(D1045A)	581	6	1	514	4	1	321	1	0	ns	ns	ns	ns
CASQ1	c.731A>G	p.(D244G)	589	0	1	533	0	0	338	0	0	ns	ns	ns	ns
CPT2	c.149C>A	p.(P50H)	544	0	5	419	3	0	270	7	1	0.009	ns	ns	ns
	c.338C>T	p.(S113L)	579	6	1	526	4	0	335	3	1	ns	ns	ns	ns
PYGM	c.613G>A	p.(G205S)	419	20	0	359	0	0	69	0	0	**<0.001**	**<0.001**	**<0.001**	**<0.001**
	c.148C>T	p.(R50X)	588	3	2	391	2	0	293	3	0	ns	ns	ns	ns
	c.2392T>C	p.(W798R)	482	102	2	525	5	0	338	0	0	**<0.001**	**<0.001**	**<0.001**	**<0.001**
	c.255C>A	p.(Y85X)	556	1	2	520	0	0	342	0	0	ns	ns	ns	ns
STAC3	c.862A>T	p.(K288X)	589	0	0	530	0	0	347	0	0	ns	ns	ns	ns
	c.851G>C	p.(W284S)	445	0	0	358	0	0	69	0	0	ns	ns	ns	ns
TRPV1	c.2051G>T	p.(G684V)	579	0	0	433	0	0	265	0	0	ns	ns	ns	ns

5.4 Discussion

This study aimed to utilise high-throughput genotyping techniques to assess whether there were any differences between MH susceptible and negative populations in defined regions of candidate genes as well as the presence of rare pathogenic variants. To achieve this, linkage disequilibrium was assessed across genes involved in ECC, calcium homeostasis and metabolism. SNPs were then selected based on their degrees of association and minor allele frequency. Testing these SNPs across our samples, regions of interest could be identified using a case-control comparison. The study does have certain limitations, which must be considered prior to discussing the significance of the results and may provide additional context within which they may be discussed.

Assay efficiency was a limiting factor in some cases with certain assays resulting in no amplification, reduced amplification, or erroneous genotyping where all samples were genotype-called as heterozygous. Although, this did not impede the study significantly with a loss of only 5 variants. Furthermore, the majority of successfully genotyped variants had a good call rate of more than 80%. The PCR based chemistries of the Fluidigm® SNPType™ and Taqman™ genotyping technologies means that there is a potential for preferential amplification of one allele over another which may skew the final numbers. Furthermore, if the sample was amplified according to the STA protocol, this would provide another opportunity for preferential amplification. The extent of this can be considered via the HWE calculations showing issues with assay efficacy as well as comparing the sample allele frequencies for the control group with that of the non-Finnish European population estimates in GnomAD v3.1.2.

Ultimately, only 7 assays were not in HWE for the control MHN group, and rather still had some degree of interpretations that could be made, although with caution. Assays not in HWE within the control MHN group were flagged in the results. MHS

and MHS(R) sub-group HWE values were not indicated in the main results, although are available in the appendices, due to the possible effect of allele associations with MH skewing the HWE values. Therefore, the control group HWE calculations were considered more reliable in indicating possible issues with assay efficacy. Of the pathogenic variants, 9 assays had an increased minor allele frequency in the MHN group as compared to that reported for the non-Finnish European population in GnomAD. Aside from preferential amplification, this observation may also be due to the reporting criteria for IVCT testing that all patients in this study would have undergone. The MHN group also consisted of probands referred for susceptibility testing, and therefore would have had some indicative clinical traits as a prerequisite. Therefore, there may be a higher incidence of disorders that have overlapping symptoms amongst the MHN group, which could have led to the referral. As such, a higher incidence of the pathogenic variants in candidate genes for MH susceptibility within the MHN group would not be surprising. That said, this can only be speculated, and so non-significant results should not be discounted in the case of the pathogenic variants. Interpretations should be made with this context in mind and proceeding with caution may still lead to meaningful conclusions. Additionally, it may be important to confirm findings of interest within the pathogenic variants panel with a second technology to ensure that genotype calls are not false positives, such as Sanger or next-generation sequencing.

Another consideration is the selection of tag-SNPs and the coverage that they provide. As seen in linkage disequilibrium heatmaps, not all the candidate genes had well defined linkage disequilibrium that would enable the use of a single SNP to cover an entire region. In fact, in many cases only partial or low coverage was possible. This, ultimately, makes it difficult in some case to implicate defined regions for further investigation in MH susceptibility. This is particularly apparent in the

candidate genes that have a relatively smaller size, and consequently less SNPs and, perhaps surprisingly, less linkage. In these cases it is possible to conclude whether there are differences in these genes between susceptible and negative groups, which may still mark them for further investigation, but unable to isolate specific regions that could be explored. Another compounding factor in the selection of SNPs for genotyping is the minor allele frequency. SNPs were chosen based on the information they could provide and, based on this, would ideally have minor allele frequencies approaching 0.5. However, there was a degree of variability between candidate genes, and several had chosen SNPs with a minor allele frequency that was closer to 0.1, or sometimes lower. This, ultimately, increased the required power to detect the smaller observed differences in genotype and allele count between susceptible and negative groups, sometimes beyond the scope of this study. This is particularly relevant when considering the pathogenic variants panel, most of which are rare.

Finally, with the large number of SNPs and rare variants tested, there is an increased chance of type 1 errors and therefore, false associations. This was accounted for by applying a Bonferroni correction for multiple testing, and both p-values were represented in the results for interpretation. The inclusion of susceptible relatives in analysis also posed design considerations, as they must be counted in the context of how closely related they are to a proband. This inclusion may also slightly skew the results in this analysis if variants co-segregate within the families, therefore increasing the likelihood of a significant difference between susceptible and nulls. This was tackled by considering each relative as 0.5 when consolidating the N number, decreasing the likelihood and magnitude of this effect.

Table 5.10: Summary of findings for each candidate gene. Tick marks indicate features identified to be significantly different between MH susceptible and normal populations, after Bonferroni correction.

Gene	Pathogenic variants	Intronic regions	Coding regions
ACADVL	✓		✓
AMPD1	✓	✓	
ATP2A1	✓		✓
CACNA1S		✓	✓
CACNA2D1		✓	✓
CASQ1			✓
CPT2		✓	✓
PYGM	✓		
STAC3		✓	
TRPV1		✓	✓

Table 5.10 serves as an indicative summary to aid discussion of the results, with results summarised into whether candidate genes showed significant differences between susceptible and normal individuals for coding and intronic regions, as determined by linkage disequilibrium blocks surrounding chosen SNPs, as well pathogenic variants.

ATP2A1 had two regions of interest amongst the MHS probands, relative to the MHN group. Exons 18 to 23, although partially covered, were of interest amongst susceptibles. This region covered the p.(E982K) variant, which was also identified as homozygous in one MHS individual and heterozygous in many MHS relatives. When comparing this rare variant to the reported MAF in GnomAD, it is notably over-represented within the MHS group, which coincides with the significance of the surrounding region. Exons 7 to 8 were also of interest amongst susceptible individuals, which coincides with the significant over-representation of the p.(R198X) variant in the MHS group, that is located within this region. The p.(R198X) variant was also identified as heterozygous in several and homozygous in two susceptible individuals. Additionally, the p.(P789K) and p.(R560C) variants were also observed in several MHS individuals, and when compared to the reported MAF in GnomAD p.(P789K) was notably over-represented in the MHS population. All four pathogenic

variants were in HWE in all subgroups, although had increased observed MAF within the control MHN group (except for p.(R560C)). All four pathogenic variants, alongside the regions of interest, are located around calcium and ATP binding motifs in the protein and are also causative of Brody myopathy in an autosomal recessive fashion, leading to decreased SERCA1 expression (Molenaar et al., 2020). Inhibition of SERCA activity has been identified to disproportionately increase the sensitivity to halothane and caffeine in MHS muscle, relative to MHN (Schuster et al., 2005). Thus, it could be possible that decreased SERCA expression could result in reduced activity, and therefore may also result in increased sensitivity to triggering agents. In fact, it has also been previously observed that MHS muscle have deficient SR Ca^{2+} uptake (Condrescu et al., 1987).

CACNA1S exons 14-15 and 23-44 were identified as regions of interest in the MHS population. Exons 23 to 44 also harbour the pathogenic variants p.(R1239G) and p.(R1239H), as well as the p.(R1086H) variant diagnostic for MH. Furthermore, the regions of interest span a large section of the gene, encoding the repeat III and IV regions of the protein, including both pore forming and voltage sensor domains, and therefore wide-spread implications for candidate modifier variants. The pathogenic variants p.(R1239G) and p.(R1239H) were notably over-represented in the susceptible groups when compared to reported MAF in GnomAD, of which the former was identified as homozygous in two susceptible individuals and the latter was observed as heterozygous in several and homozygous in one susceptible individual(s). Both variants were in HWE in all subgroups but had increased MAF in the MHN population. Both variants are also located within S4 of the transmembrane voltage sensor domain and causative for hypokalaemic periodic paralysis (HypoPP) in an autosomal dominant fashion (Fouad et al., 1997). These findings would suggest a high incidence of HypoPP in the MHS population, as well as those referred to testing regardless of MH status. Additionally, the p.(R1086H) variant has

been shown to enhance RYR1 sensitivity to both endogenous and exogenous activators (Weiss et al., 2004, p. 20), indicating the relevance of the voltage sensing domain to MH pathogenesis. Thus, it may be plausible that other pathogenic variants in this region, such as the p.(R1239G) and p.(R1239H) may lead to similar enhanced sensitivity of RYR1.

CACNA2D1 exons 15 and 16 were identified as regions of interest in the susceptible group. The p.(D1045A) pathogenic variant was also identified as homozygous in one and heterozygous in seven MHS individuals, although not statistically significant as it was also observed in the MHN group in the pathogenic variant panel (section 5.3.4). The pathogenic variant was also in HWE in all subgroups, and the MAF also coincided with the reported MAF in GnomAD for all subgroups. *CACNA2D1* has previously been identified as a gene of interest in MH association studies (Iles et al., 1994; ROBINSON et al., 2000), which these results corroborate, especially in the context of a threshold model. However, previous studies regarding the involvement of *CACNA2D1* are scarce, and so these results provide additional and novel insights into the potential involvement of this gene in MH pathogenesis. The role of the alpha-2/delta subunits in channel folding of the DHPR (Dolphin, 2016) may indicate that pathogenic variants in this gene could affect the quaternary structure the L-type channel, with wide ranging consequences from voltage sensing to RYR1 signalling by the alpha-1s subunit. Further investigations into the pathogenic variants, possibly by insertion into the gene editing pipeline developed in this thesis, would enable the elucidation of their potential effects on RYR1 sensitivity to triggering agents and therefore MH pathogenesis.

The promoter/enhancer region of *CASQ1*, alongside exons 3-4 and exon 6 were identified as regions of interest in the MHS group. Although not statistically significant, the p.(D244G) pathogenic variant was also identified as homozygous in

one MHS individual, which is in exon 6 of the gene, and was in HWE amongst all subgroups. Although associations in this gene were weaker, with less defined LD blocks, the significance of multiple variants still indicate its potential as a candidate gene for modifier loci and regions of interest should still be explored for candidate variants. *CASQ1* pathogenic variants have also previously been identified within the unit in MHS individuals, such as the p.(F186Y) and p.(I138T) which are located in exons 4 and 3 respectively. Furthermore, previous work within the unit has also shown that *CASQ1* null C2C12 myotubes show an increased sensitivity to caffeine as compared to wild type (Personal communications, Rachel Dodds, UK MH unit). Finally, the exons identified as regions of interest are involved in calcium binding by Calsequestrin 1 (Kumar et al., 2013), therefore it may be speculated that loss-of-function mutations in these regions, alongside the promoter/enhancer region identified, may lead to reduced calcium sequestration in the context of MH susceptibility.

TRPV1 exons 6 to 10 were identified as a region of interest, resulting from a combination of three SNPs. The defined LD structure of this gene allowed for a more specific and distinct region of interest. The region of interest contains ATP binding sites, which are a sensitiser of the calcium channel (Shimizu et al., 2022). It could be speculated that gain-of-function mutations in this region could lead to an increase in intracellular calcium at rest, which is seen in models of malignant hyperthermia (Lopez et al., 2018).

CPT2 had less coverage due to less defined LD structure, however had several SNPs that were significantly different between MHS and MHN groups. Six MHS individuals homozygous for the p.(P50H) and two MHS individuals homozygous for the p.(S113L) variants were also identified, in contrast to none in the MHN group. Additionally, the p.(P50H) variant was not in HWE for the MHS probands, indicating a greater number of homozygous individuals in this group than would be expected.

Both variants were also notably over-represented amongst the MHS group as compared to reported MAF in GnomAD. The identification of multiple loci that differ between susceptible and negative populations, alongside the presence of several susceptible individuals homozygous for causative pathogenic variants in this gene also supplement the previous findings in chapters 3 and 4 in elucidating the potential role of CPT II in MH pathogenesis. Pathogenic variants in this gene typically result in reduced enzyme activity (Meinhardt et al., 2021; Motlagh et al., 2016), and the identification of these in MHS individuals would tie in with the observations of downregulated fatty acid oxidation in models of MH (Chang et al., 2020).

The 5' region for *ACADVL*, spanning from the promoter/enhancer region upstream down to exon 2, was identified as a region of interest, although only had partial coverage. Additionally, all three pathogenic variants were identified as homozygous in several MHS individuals, with a notable amount heterozygous for p.(R459Q) and p.(V283A) in particular. All three variants were in HWE amongst all subgroups with MHN MAFs resembling those reported in GnomAD. Pathogenic variants in this gene typically lead to loss of function, and the identification of the promoter/enhancer region as one of interest would tie into this, as well as the findings that fatty acid oxidation is downregulated in MHS models (Chang et al., 2020) and that the p.(V283A) variant co-segregated with the IVCT phenotype in an MHS individual (Gardner et al., 2020).

Several of the pathogenic variants in *PYGM* were identified in MHS individuals. Six MHS individuals carried homozygous mutations in *PYGM,* with 2 in p.(R50X), 2 in p.(W798R), and 2 in p.(Y85X), with the p.(W798R) variant heterozygous in many MHS individuals. Additionally, the p.(G205S) was observed as heterozygous in several MHS individuals, with no incidence in the MHN group. All four variants were in HWE for all subgroups and MAFs for the MHN subgroup resembled those

reported in GnomAD, except for p.(W798R) that occurred at a higher frequency. Of all the pathogenic variants tested, those in *PYGM* had the most notable contrast between susceptible and negative groups. Although there is no defined link between McArdle's disease and MH, the relatively high presence of causative pathogenic variants for McArdle's in MHS individuals lends to the idea that there may be genetic contributors to MH in *PYGM*.

A final note should also be made of the over-representation of intronic regions amongst several genes spanning all three functional subgroups (ECC, calcium homeostasis, metabolism) in the MHS population (*CACNA1S*, *CACNA2D1*, *STAC3*, *TRPV1*, *AMPD1*, *CPT2*), although the role of these regions is less certain. Introns have been shown to have a variety of functions, which may play an important role in MH pathogenesis. Introns play a role in regulating alternative splicing of genes (Pan et al., 2008; Roy et al., 2008; Sorek & Ast, 2003), which may be important in genes such as *CACNA2D1* that encodes two different subunits of the DHPR. Introns have also been shown to enhance gene expression (Beaulieu et al., 2011; Callis et al., 1987; Gruss et al., 1979), which may lead to the possibility that variations in these regions could lead to the downregulation of affected genes. Similarly, introns have also been shown to encode non-coding RNAs that may also affect gene expression and function (BASKERVILLE & BARTEL, 2005; Dieci et al., 2009; Rearick et al., 2011). The intronic associations identified in this chapter cannot be dismissed, especially given the high incidence of trait-associated SNPs in intronic regions as opposed to exons in GWAS studies, indicating their significance (Jo & Choi, 2015; Li et al., 2012; Welter et al., 2014).

To emphasize the importance and context of these findings, it is crucial to revisit the genetic epidemiology of MH, specifically in the United Kingdom. As stated previously, around a quarter of MH Susceptible families have no known major gene effect, when accounting for known pathogenic variants, and families with a

pathogenic *RYR1* variant frequently exhibit genotype-phenotype discordance (Miller et al., 2018). When constraining this further to diagnostic variants specifically, half of MHS individuals do not have a pathogenic variant sufficiently functionally characterised to be stated as causative for the disorder. This is a substantial gap in the understanding of the genetic basis of MH. Thus, the identification of contributory loci for malignant hyperthermia susceptibility is key in providing more comprehensive screening measures for patients, to ultimately avoid preventable MH events and maximise patient safety. In the context of a threshold model of MH, the identification of modifier loci in particular is crucial to closing the aforementioned gap. Indeed, MHS individuals may have multiple contributory loci, with each individual presenting with a different combination of variants. Therefore, in order to provide comprehensive screening measures, all avenues for candidate modifier loci must be pursued.

This study adds to previous findings, sometimes building on the understanding of the contributions of candidate genes previously identified. By identifying regions of interest in candidate genes through this trait-association method, this study aims to provide direction to understanding how candidate genes may contribute to malignant hyperthermia pathogenesis. Furthermore, by examining a pathogenic variant panel, this study identifies candidate variants for functional characterisation, possibly via pipelines explored in previous chapters, with particular emphasis on those that align with the regions of interest identified.

6 General discussion

6.1 Importance of investigating candidate modifier loci

It is estimated that up to 25% of MH families do not have a potentially pathogenic variant in *RYR1*, *CACNA1S* or *STAC3* (Miller et al., 2018). This proportion further increases to around 45% when considering only variants used diagnostically, as seen in this thesis. This data emphasises the gap in known causative variants for MH that can be used to screen individuals prior to the use of volatile anaesthetics which may trigger a reaction, ultimately leading to patients being at risk of an MH crisis. The prevalence of discordance further complicates the issue, with a further ~25% of families with a pathogenic *RYR1* variant exhibiting genotype-phenotype discordance (Miller et al., 2018). With malignant hyperthermia increasingly seemingly adhering to a threshold model (Carpenter, et al., 2009; Miller et al., 2018; ROBINSON et al., 2000) rather than the previously thought autosomal dominant model, the investigation of modifier loci becomes all the more important. The gap in knowledge of causative or pathogenic variants for MH poses a challenge to the use of genetic diagnosis, and thus necessitates the use of more invasive testing in a large proportion of referrals (personal communications Phil Hopkins, UK MH unit).

Both the exploration of additional genetic contributors followed by their functional characterisation is key in closing the gap between genetic and IVCT diagnosis. This work would enable the confirmation of additional diagnostic variants and/or variant combinations that could also be used to screen individuals prior to exposure to triggering agents, with the ultimate goal of decreasing patient risk. Furthermore, an increase in confirmed variants could enable less invasive testing with more individuals diagnosed through genetic means rather than the IVCT.

6.2 The suitability of gene editing techniques in the characterisation of modifier loci

The combination of CRISPR-mediated knockout with lentiviral reintroduction provides a useful two step investigation into the contribution of candidate genes towards MH susceptibility, in the context of a threshold model. It allows both a broader investigation into the contributory potential of a gene, due to complete knockout, as well as the specific inquiry into candidate variants. As the pipeline enables these perturbations to be produced on established *in vitro* models of MH, the specific investigation of modifier loci is made possible. This body of work provides a proof of principle for the introduction of candidate variants into established *in vitro* models of MH. However, the pipeline is not without limitations and insights gleaned from the results may inform the next steps in further optimisation of the introduction of candidate modifier variants.

The established *RYR1* p.(G2435R) primary mouse model of MH was chosen as the background against which candidate variants would be introduced (Lopez et al., 2018). Whilst this provided a controlled genetic background to investigate against, it also provided limitations in the form of cell lifespan. The robustness of the primary myoblasts meant that the cytotoxicity of both the CRISPR pipeline and the introduction of lentiviral vectors limited the number of clones that could be produced and also pushed them to their passage limits. Based on this, whilst the two-step procedure was useful, it may be worth conducting knockouts and the specific introduction of variants in separate cell populations in tandem. Developments in CRISPR applications make this possible.

A pooled CRISPR screening strategy would allow for a high-throughput method of screening candidate genes (Bock et al., 2022). By designing multiple guides for target genes and introducing the gRNA and Cas9 in a pooled cell population, several genetic perturbations could be studied at once. This could then be

combined with current work in the MH unit that is establishing a caffeine dose-dependent kill assay to identify variants with enhanced sensitivity. Caffeine could be used as a biological challenge against the pool of cells. By identifying those that survive and those that die after exposure, candidate genes or variants could be screened for potential contribution to MH. Once identified, they could be further functionally characterised.

Another development in CRISPR techniques is base editing and prime editing. Base editing utilises a fusion protein consisting of Cas9 and a cytidine or adenine base editor which enable C-G to T-A or A-T to G-C base pair conversions respectively in a programmable manner (Gaudelli et al., 2017; Komor et al., 2016). Between the use of the two types of fusion proteins, base editing can mediate all possible transition mutations at specific target sites. Prime editing utilises a Cas9 nickase variant fused with a reverse transcriptase and a specific guide RNA (pegRNA) which allow for the introduction of new DNA sequences up to ~20bp in length without the need for a double strand break or donor template (Anzalone et al., 2019). Instead, the pegRNA includes the change that the user wants to introduce. This method also shows similar or higher efficiency than HDR mediated CRISPR methodologies. This could be used to introduce specific SNVs in one step rather than two, potentially reducing the overall cytotoxicity, at a trade-off of lower efficiency as compared to CRISPR mediated knockout.

6.3 Functional assessment of modifier loci

The use of caffeine as to assess the contribution of candidate modifier loci to MH pathogenesis focuses specifically on a potential effect on RYR1 activation (des Georges et al., 2016). As the vast majority of MH cases are caused by RYR1 dysfunction (Miller et al., 2018; Robinson et al., 2006), this is a logical avenue for functional characterisation. However, MH is characterised by dysfunction in calcium homeostasis and ECC broadly, not just RYR1 (Hopkins et al., 2015). Therefore,

there is potential that modifier loci may have various routes of affecting the MH phenotype. Furthermore, each locus may have a different effect, and so a bespoke and considered approach to the most likely mechanism of action would be necessary when testing each candidate locus, alongside the assessment of ECC and RYR1 function as conducted in this thesis. For example, for loci involved in metabolism it may be worth considering more active processes in ECC that utilise ATP. An important step in ECC is the active sequestration of calcium by SERCA into the SR lumen (Zhang et al., 1995). A lack of ATP, due to the effects of a modifier locus, may affect SERCA activity and could be characterised as diminished sequestration leading to higher intracellular calcium and slower rates of Ca^{2+} uptake. These would be useful inquires to make next in the genetically modified myoblast populations generated in this thesis.

6.4 Findings and next steps

The sensitivity of the *Cpt2* KO cell line to KCl and caffeine requires further investigation. The decrease in sensitivity to caffeine, an RYR1 agonist, was unexpected and may possibly be explained by genetic compensation. This seems even more likely when considering the results of the reintroduction of specific variants and the wild-type gene, where we see an expected increase in sensitivity to caffeine in the p.(P50H) variant, as well as an increase in sensitivity to KCl in the p.(S113L) variant, relative to the reintroduced wild-type. This would suggest that there are alternate mechanisms between knock-out and knock-down affecting excitation-contraction coupling and RYR1 sensitivity between CPT II variants. Based on the sensitivity to agonists in the two reintroduced pathogenic variants, it would seem likely that the p.(S113L) and p.(P50H) variants in CPT II modify the heterozygous p.(G2435R) RYR1 phenotype and may contribute to MH susceptibility. Additionally, the identification of both variants in multiple MHS individuals provides genetic epidemiological data that supplements the functional work in chapters 3 and

4. The over-representation of several SNPs spanning *CPT2* amongst the susceptible population also indicates the relevance of this gene to MH pathogenesis and may suggest that additional known pathogenic variants would be worth investigating in similar manners to this thesis. Ultimately the results described in this thesis suggest that CPT2 variants may act as modifier alleles, contributing to MH phenotypes and to pathogenesis in a threshold context.

The *Pygm* KO cell line had increased sensitivity to KCl suggesting increased sensitivity to triggering excitation-contraction coupling. Furthermore, the p.(R50X) variant also showed increased sensitivity to both KCl and caffeine. This would very likely suggest the contribution of this pathogenic variant to MH susceptibility and the modification of MH phenotypes. The p.(A193S) variant, however, exhibited a decreased sensitivity to KCl and no significant difference to caffeine. The decreased sensitivity to KCl would require further investigation as to the underlying mechanism. However, p.(A193S) cannot be confidently stated to contribute toward MH susceptibility. The identification of the pathogenic variants p.(R50X), p.(Y85X), p.(G205S) and p.(W789R) in several MHS individuals would also indicate their candidacy as contributory factors to MH and would make ideal candidates for investigation using the gene editing pipeline established in this thesis. The majority of these variants are novel to associations with MH and grow the body of work towards identifying candidate modifier loci. Overall, this thesis suggests that *PYGM* may contain modifier variants of MH phenotypes and contributes to pathogenesis in a threshold context, however further work is required, such as additional KO clones to verify the results as well as the use of another gene editing mechanism that bypasses the limitations of lentiviral transduction.

The development of this gene editing pipeline enables the future investigation of additional candidate modifier loci, such as the pathogenic variants identified in MHS individuals in chapter 5. Specifically, the p.(R549Q) and p.(V283A) variants in

ACADVL would be excellent candidates to introduce into an MH mouse model for investigation, due to their significant over-representation in the MHS populations. However, even the mere identification of these variants in susceptible individuals is sufficient basis to warrant further exploration. Additionally, this pipeline exhibits flexibility in the form of which mouse model is chosen. The characterisation of candidate modifier loci introduced to a variety of the mouse models of MH would add further weight to solidify their contributions to a threshold model and may elucidate additional phenotypic changes not seen in this model. Ultimately, the combination of techniques utilised in this thesis provide a solid foundation to build off of for the future investigation of candidate modifier loci in a threshold model.

NGS sequencing of the regions of interest identified in chapter 5, with annotation of pathogenic variants identified, would also provide more depth to the findings of the case-control study. This would enable further characterisation of the genetic epidemiology of the UK MH cohort, and, crucially, provide additional candidate modifier variants identified in susceptible individuals for functional characterisation. Specifically, the genes *CACNA1S*, *CACNA2D1*, and *TRPV1* had multiple regions of interest identified and are involved in excitation contraction coupling and calcium homeostasis, which are key areas that are disrupted in MH. These would be ideal candidates for further investigation. Identified pathogenic variants in these genes in susceptible individuals could then be investigated using the gene editing pipeline this thesis for characterisation in the context of a threshold model.

Additional inquiries into how metabolism may be affected, such as using a Seahorse assay, could also be useful in identifying other phenotypes that may be affected. Differences in the metabolic profile between diagnostic MH variants have been observed using the Seahorse analyser within the unit (Personal communications, Vikas Kaura), as well as metabolic deficiencies between MHS and MHN muscle (Chang et al., 2020), identifying disrupted metabolic profiles as an MH phenotype.

Investigating whether there is an additive effect of introducing a second mutation would be useful in furthering the understanding of a threshold model.

Finally, the results for this thesis warrant clinical research into whether phenotypic changes are present in the individuals identified in chapter 5 with pathogenic alleles. Specifically, a comparison of serum CK, MH crisis onset time, and IVCT traces between MHS individuals with identified pathogenic alleles and MHN individuals/MHS individuals without additional pathogenic variants would enable a clinical measure of the possible contribution of the candidate modifier mutations discussed. However, the frequency of these variants may not provide the statistical power on an individual variant basis to draw conclusions from. Instead this may rather inform more broadly on the prospect of a threshold model in the context of MH and how well this may translate into the clinical domain for pre-emptive variant testing.

6.5 Conclusion

To summarise, a novel gene editing pipeline in primary mouse myoblasts to enable a multi-faceted approach to the characterisation of candidate modifier loci in a threshold model of MH has been developed in this thesis. Further optimisation of this pipeline to limit cytotoxicity and passage effects would remove current limitations and facilitate more powerful analyses of candidate loci. The characterisation of the p.(S113L), p.(P50H) and p.(R50X) variants suggest a possible contribution to MH susceptibility. Furthermore, the identification of additional pathogenic variants and loci in other candidate genes involved in ECC, calcium homeostasis and metabolism present the opportunity for characterisation, using the gene editing pipeline in this thesis, of novel variants that may contribute to MH susceptibility.

References

Allen, G. C., Larach, M. G., & Kunselman, A. R. (1998). The Sensitivity and Specificity of the Caffeine-Halothane Contracture Test: A Report from the North American Malignant Hyperthermia Registry. *Anesthesiology*, *88*(3), 579–588. https://doi.org/10.1097/00000542-199803000-00006

Almagor, L., Chomsky-Hecht, O., Ben-Mocha, A., Hendin-Barak, D., Dascal, N., & Hirsch, J. A. (2012). The role of a voltage-dependent Ca2+ channel intracellular linker: A structure-function analysis. *The Journal of Neuroscience: The Official Journal of the Society for Neuroscience*, *32*(22), 7602–7613. https://doi.org/10.1523/JNEUROSCI.5727-11.2012

Andronache, Z., Ursu, D., Lehnert, S., Freichel, M., Flockerzi, V., & Melzer, W. (2007). The auxiliary subunit gamma 1 of the skeletal muscle L-type Ca2+ channel is an endogenous Ca2+ antagonist. *Proceedings of the National Academy of Sciences of the United States of America*, *104*(45), 17885–17890. https://doi.org/10.1073/pnas.0704340104

Anichini, A., Fanin, M., Vianey-Saban, C., Cassandrini, D., Fiorillo, C., Bruno, C., & Angelini, C. (2011). Genotype-phenotype correlations in a large series of patients with muscle type CPT II deficiency. *Neurological Research*, *33*(1), 24–32. https://doi.org/10.1179/016164110X12767786356390

Anzalone, A. V., Randolph, P. B., Davis, J. R., Sousa, A. A., Koblan, L. W., Levy, J. M., Chen, P. J., Wilson, C., Newby, G. A., Raguram, A., & Liu, D. R. (2019). Search-and-replace genome editing without double-strand breaks or donor DNA. *Nature*, *576*(7785), 149–157. https://doi.org/10.1038/s41586-019-1711-4

Armstrong, L. E., Casa, D. J., Millard-Stafford, M., Moran, D. S., Pyne, S. W., & Roberts, W. O. (2007). Exertional Heat Illness during Training and Competition. *Medicine & Science in Sports & Exercise*, *39*(3), 556. https://doi.org/10.1249/MSS.0b013e31802fa199

Avila, G., & Dirksen, R. T. (2001). Functional Effects of Central Core Disease Mutations in the Cytoplasmic Region of the Skeletal Muscle Ryanodine Receptor. *The Journal of General Physiology*, *118*(3), 277–290.

Bailey, A. G., & Bloch, E. C. (1987). Malignant Hyperthermia in a Three-Month-Old American Indian Infant. *Anesthesia & Analgesia*, *66*(10), 1043.

Bannister, R. A. (2013). Dantrolene-Induced Inhibition of Skeletal L-Type Ca2+ Current Requires RyR1 Expression. *BioMed Research International*, *2013*, 390493. https://doi.org/10.1155/2013/390493

Barrero, M. J., Camarero, N., Marrero, P. F., & Haro, D. (2003). Control of human carnitine palmitoyltransferase II gene transcription by peroxisome proliferator-activated receptor through a partially conserved peroxisome proliferator-responsive element. *The Biochemical Journal*, *369*(Pt 3), 721–729. https://doi.org/10.1042/BJ20020851

BASKERVILLE, S., & BARTEL, D. P. (2005). Microarray profiling of microRNAs reveals frequent coexpression with neighboring miRNAs and host genes. *RNA*, *11*(3), 241–247. https://doi.org/10.1261/rna.7240905

Beaufils, M., Tourel, A., Petiot, A., Halmai, N. B., Segal, D. J., Rendu, J., & Marty, I. (2022). Development of Knock-Out Muscle Cell Lines using Lentivirus-Mediated CRISPR/Cas9 Gene Editing. *Journal of Visualized Experiments: JoVE*, *184*. https://doi.org/10.3791/64114

Beaulieu, E., Green, L., Elsby, L., Alourfi, Z., Morand, E. F., Ray, D. W., & Donn, R. (2011). Identification of a novel cell type-specific intronic enhancer of macrophage migration inhibitory factor (MIF) and its regulation by mithramycin. *Clinical and Experimental Immunology*, *163*(2), 178–188. https://doi.org/10.1111/j.1365-2249.2010.04289.x

Bock, C., Datlinger, P., Chardon, F., Coelho, M. A., Dong, M. B., Lawson, K. A., Lu, T., Maroc, L., Norman, T. M., Song, B., Stanley, G., Chen, S., Garnett, M., Li, W., Moffat, J., Qi, L.

S., Shapiro, R. S., Shendure, J., Weissman, J. S., & Zhuang, X. (2022). High-content CRISPR screening. *Nature Reviews. Methods Primers*, *2*(1), 9. https://doi.org/10.1038/s43586-022-00098-7

Bojko, B., Vasiljevic, T., Boyaci, E., Roszkowska, A., Kraeva, N., Ibarra Moreno, C. A., Koivu, A., Wąsowicz, M., Hanna, A., Hamilton, S., Riazi, S., & Pawliszyn, J. (2021). Untargeted metabolomics profiling of skeletal muscle samples from malignant hyperthermia susceptible patients. *Canadian Journal of Anesthesia*, *68*(6), 761–772. https://doi.org/10.1007/S12630-020-01895-Y/TABLES/3

Bollig, G. (2013). McArdle's disease (glycogen storage disease type V) and anesthesia – a case report and review of the literature. *Pediatric Anesthesia*, *23*(9), 817–823. https://doi.org/10.1111/pan.12164

Bollig, G., Mohr, S., & Ræder, J. (2005). McArdle's disease and anaesthesia: Case reports. Review of potential problems and association with malignant hyperthermia. *Acta Anaesthesiologica Scandinavica*, *49*(8), 1077–1083. https://doi.org/10.1111/j.1399-6576.2005.00755.x

Bosson, C., Rendu, J., Pelletier, L., Abriat, A., Chatagnon, A., Brocard, J., Brocard, J., Figarella-Branger, D., Ducreux, S., van Coppenolle, F., Sagui, E., Marty, I., Roux-Buisson, N., & Faure, J. (2020). Variations in the TRPV1 gene are associated to exertional heat stroke. *Journal of Science and Medicine in Sport*, *23*(11), 1021–1027. https://doi.org/10.1016/j.jsams.2020.04.018

Bothmer, A., Phadke, T., Barrera, L. A., Margulies, C. M., Lee, C. S., Buquicchio, F., Moss, S., Abdulkerim, H. S., Selleck, W., Jayaram, H., Myer, V. E., & Cotta-Ramusino, C. (2017). Characterization of the interplay between DNA repair and CRISPR/Cas9-induced DNA lesions at an endogenous locus. *Nature Communications*, *8*(1), Article 1. https://doi.org/10.1038/ncomms13905

Brinkman, E. K., Chen, T., Amendola, M., & Van Steensel, B. (2014). Easy quantitative assessment of genome editing by sequence trace decomposition. *Nucleic Acids Research*, *42*(22), e168–e168. https://doi.org/10.1093/nar/gku936

Brinkmeier, H., Krämer, J., Krämer, R., Iaizzo, P. A., Baur, C., Lehmann-Horn, F., & Rüdel, R. (1999). Malignant hyperthermia causing Gly2435Arg mutation of the ryanodine receptor facilitates ryanodine-induced calcium release in myotubes. *British Journal of Anaesthesia*, *83*(6), 855–861. https://doi.org/10.1093/bja/83.6.855

Brogna, S., & Wen, J. (2009). Nonsense-mediated mRNA decay (NMD) mechanisms. *Nature Structural & Molecular Biology*, *16*(2), Article 2. https://doi.org/10.1038/nsmb.1550

Buchbinder, J. L., & Fletterick, R. J. (1996). Role of the active site gate of glycogen phosphorylase in allosteric inhibition and substrate binding. *The Journal of Biological Chemistry*, *271*(37), 22305–22309. https://doi.org/10.1074/jbc.271.37.22305

Calderón, J. C., Bolaños, P., & Caputo, C. (2014). The excitation-contraction coupling mechanism in skeletal muscle. *Biophysical Reviews*, *6*(1), 133–160. https://doi.org/10.1007/s12551-013-0135-x

Callis, J., Fromm, M., & Walbot, V. (1987). Introns increase gene expression in cultured maize cells. *Genes & Development*, *1*(10), 1183–1200. https://doi.org/10.1101/gad.1.10.1183

Capacchione, J. F., & Muldoon, S. M. (2009). The Relationship Between Exertional Heat Illness, Exertional Rhabdomyolysis, and Malignant Hyperthermia. *Anesthesia & Analgesia*, *109*(4), 1065. https://doi.org/10.1213/ane.0b013e3181a9d8d9

Carpenter, D., Ringrose, C., Leo, V., Morris, A., Robinson, R. L., Halsall, P. J., Hopkins, P. M., & Shaw, M.-A. (2009). The role of CACNA1S in predisposition to malignant hyperthermia. *BMC Medical Genetics*, *10*, 104. https://doi.org/10.1186/1471-2350-10-104

Carpenter, D., Robinson, R. L., Quinnell, R. J., Ringrose, C., Hogg, M., Casson, F., Booms, P., Iles, D. E., Halsall, P. J., Steele, D. S., Shaw, M. A., & Hopkins, P. M. (2009). Genetic variation in RYR1 and malignant hyperthermia phenotypes. *British Journal of Anaesthesia*, *103*(4), 538–548. https://doi.org/10.1093/bja/aep204

Catterall, W. A. (2011). Voltage-Gated Calcium Channels. *Cold Spring Harbor Perspectives in Biology*, *3*(8), a003947. https://doi.org/10.1101/cshperspect.a003947

Censier, K., Urwyler, A., Zorzato, F., & Treves, S. (1998). Intracellular calcium homeostasis in human primary muscle cells from malignant hyperthermia-susceptible and normal individuals. Effect Of overexpression of recombinant wild-type and Arg163Cys mutated ryanodine receptors. *Journal of Clinical Investigation*, *101*(6), 1233–1242.

Chang, L., Daly, C., Miller, D. M., Allen, P. D., Boyle, J. P., Hopkins, P. M., & Shaw, M. A. (2019). Permeabilised skeletal muscle reveals mitochondrial deficiency in malignant hyperthermia-susceptible individuals. *British Journal of Anaesthesia*, *122*(5), 613–621. https://doi.org/10.1016/j.bja.2019.02.010

Chang, L., Liu, X., Diggle, C. P., Boyle, J. P., Hopkins, P. M., Shaw, M. A., & Allen, P. D. (2020). Bioenergetic defects in muscle fibers of RYR1 mutant knock-in mice associated with malignant hyperthermia. *The Journal of Biological Chemistry*, *295*(45), 15226. https://doi.org/10.1074/JBC.RA120.013537

Chang, L., Motley, R., Daly, C. L., Diggle, C. P., Hopkins, P. M., & Shaw, M.-A. (2024). An Association between OXPHOS-Related Gene Expression and Malignant Hyperthermia Susceptibility in Human Skeletal Muscle Biopsies. *International Journal of Molecular Sciences*, *25*(6), Article 6. https://doi.org/10.3390/ijms25063489

Chaube, R., Hess, D. T., Wang, Y.-J., Plummer, B., Sun, Q.-A., Laurita, K., & Stamler, J. S. (2014). Regulation of the Skeletal Muscle Ryanodine Receptor/Ca2+-release

Channel RyR1 by S-Palmitoylation. *The Journal of Biological Chemistry*, *289*(12), 8612–8619. https://doi.org/10.1074/jbc.M114.548925

Chelu, M. G., Goonasekera, S. A., Durham, W. J., Tang, W., Lueck, J. D., Riehl, J., Pessah, I. N., Zhang, P., Bhattacharjee, M. B., Dirksen, R. T., & Hamilton, S. L. (2006). Heat- and anesthesia-induced malignant hyperthermia in an RyR1 knock-in mouse. *The FASEB Journal*, *20*(2), 329–330. https://doi.org/10.1096/fj.05-4497fje

Cherednichenko, G., Hurne, A. M., Fessenden, J. D., Lee, E. H., Allen, P. D., Beam, K. G., & Pessah, I. N. (2004). Conformational activation of Ca2+ entry by depolarization of skeletal myotubes. *Proceedings of the National Academy of Sciences of the United States of America*, *101*(44), 15793–15798. https://doi.org/10.1073/pnas.0403485101

Condrescu, M., López, J. R., Medina, P., & Alamo, L. (1987). Deficient function of the sarcoplasmic reticulum in patients susceptible to malignant hyperthermia. *Muscle & Nerve*, *10*(3), 238–241. https://doi.org/10.1002/mus.880100307

Cong, L., Ran, F. A., Cox, D., Lin, S., Barretto, R., Habib, N., Hsu, P. D., Wu, X., Jiang, W., Marraffini, L. A., & Zhang, F. (2013). Multiplex Genome Engineering Using CRISPR/Cas Systems. *Science (New York, N.Y.)*, *339*(6121), 819–823. https://doi.org/10.1126/science.1231143

Dainese, M., Quarta, M., Lyfenko, A. D., Paolini, C., Canato, M., Reggiani, C., Dirksen, R. T., & Protasi, F. (2009). Anesthetic- and heat-induced sudden death in calsequestrin-1-knockout mice. *The FASEB Journal*, *23*(6), 1710–1720. https://doi.org/10.1096/fj.08-121335

Davidson, E., & Levin, M. (2005). Gene regulatory networks. *Proceedings of the National Academy of Sciences of the United States of America*, *102*(14), 4935. https://doi.org/10.1073/pnas.0502024102

Delenda, C. (2004). Lentiviral vectors: Optimization of packaging, transduction and gene expression. *The Journal of Gene Medicine*, *6*(S1), S125–S138. https://doi.org/10.1002/jgm.501

des Georges, A., Clarke, O. B., Zalk, R., Yuan, Q., Condon, K. J., Grassucci, R. A., Hendrickson, W. A., Marks, A. R., & Frank, J. (2016). Structural Basis for Gating and Activation of RyR1. *Cell*, *167*(1), 145-157.e17. https://doi.org/10.1016/j.cell.2016.08.075

Deschauer, M., Wieser, T., & Zierz, S. (2005). Muscle carnitine palmitoyltransferase II deficiency: Clinical and molecular genetic features and diagnostic aspects. *Archives of Neurology*, *62*(1), 37–41. https://doi.org/10.1001/archneur.62.1.37

Di Mauro, S. (2007). Muscle glycogenoses: An overview. *Acta Myologica*, *26*(1), 35–41.

Dieci, G., Preti, M., & Montanini, B. (2009). Eukaryotic snoRNAs: A paradigm for gene expression flexibility. *Genomics*, *94*(2), 83–88. https://doi.org/10.1016/j.ygeno.2009.05.002

Dlamini, N., Voermans, N. C., Lillis, S., Stewart, K., Kamsteeg, E.-J., Drost, G., Quinlivan, R., Snoeck, M., Norwood, F., Radunovic, A., Straub, V., Roberts, M., Vrancken, A. F. J. E., van der Pol, W. L., de Coo, R. I. F. M., Manzur, A. Y., Yau, S., Abbs, S., King, A., … Jungbluth, H. (2013). Mutations in RYR1 are a common cause of exertional myalgia and rhabdomyolysis. *Neuromuscular Disorders: NMD*, *23*(7), 540–548. https://doi.org/10.1016/j.nmd.2013.03.008

Dolphin, A. C. (2012). Calcium channel auxiliary α2δ and β subunits: Trafficking and one step beyond. *Nature Reviews Neuroscience*, *13*(8), 542–555. https://doi.org/10.1038/nrn3311

Dolphin, A. C. (2013). The α2δ subunits of voltage-gated calcium channels. *Biochimica et Biophysica Acta (BBA) - Biomembranes*, *1828*(7), 1541–1549. https://doi.org/10.1016/j.bbamem.2012.11.019

Dolphin, A. C. (2016). Voltage-gated calcium channels and their auxiliary subunits: Physiology and pathophysiology and pharmacology. *The Journal of Physiology*, *594*(19), 5369–5390. https://doi.org/10.1113/JP272262

Dull, T., Zufferey, R., Kelly, M., Mandel, R. J., Nguyen, M., Trono, D., & Naldini, L. (1998). A Third-Generation Lentivirus Vector with a Conditional Packaging System. *Journal of Virology*, *72*(11), 8463–8471.

El-Brolosy, M. A., & Stainier, D. Y. R. (2017). Genetic compensation: A phenomenon in search of mechanisms. *PLOS Genetics*, *13*(7), e1006780. https://doi.org/10.1371/journal.pgen.1006780

Ellis, K. O., & Bryant, S. H. (1972). Excitation-contraction uncoupling in skeletal muscle by dantrolene sodium. *Naunyn-Schmiedeberg's Archives of Pharmacology*, *274*(1), 107–109. https://doi.org/10.1007/BF00501011

Elsea, S. H., & Lucas, R. E. (2002). The mousetrap: What we can learn when the mouse model does not mimic the human disease. *ILAR Journal*, *43*(2), 66–79. https://doi.org/10.1093/ilar.43.2.66

Eltit, J. M., Bannister, R. A., Moua, O., Altamirano, F., Hopkins, P. M., Pessah, I. N., Molinski, T. F., López, J. R., Beam, K. G., & Allen, P. D. (2012). Malignant hyperthermia susceptibility arising from altered resting coupling between the skeletal muscle L-type Ca2+ channel and the type 1 ryanodine receptor. *Proceedings of the National Academy of Sciences*, *109*(20), 7923–7928. https://doi.org/10.1073/pnas.1119207109

Endo, M. (2009). Calcium-induced calcium release in skeletal muscle. *Physiological Reviews*, *89*(4), 1153–1176. https://doi.org/10.1152/physrev.00040.2008

European Malignant Hyperpyrexia Group, T. (1984). *A PROTOCOL FOR THE INVESTIGATION OF MALIGNANT HYPERPYREXIA (MH) SUSCEPTIBILITY THE EUROPEAN MALIGNANT HYPERPYREXIA GROUP SUMMARY*. https://doi.org/10.1093/bja/56.11.1267

Farboud, B., Jarvis, E., Roth, T. L., Shin, J., Corn, J. E., Marson, A., Meyer, B. J., Patel, N. H., & Hochstrasser, M. L. (2018). Enhanced Genome Editing with Cas9 Ribonucleoprotein in Diverse Cells and Organisms. *Journal of Visualized Experiments : JoVE*, *135*, 57350. https://doi.org/10.3791/57350

Feng, W., Lopez, J. R., Antrobus, S., Zheng, J., Uryash, A., Dong, Y., Beqollari, D., Bannister, R. A., Hopkins, P. M., Beam, K. G., Allen, P. D., & Pessah, Isaac. N. (2023). Putative malignant hyperthermia mutation CaV1.1-R174W is insufficient to trigger a fulminant response to halothane or confer heat stress intolerance. *The Journal of Biological Chemistry*, *299*(8), 104992. https://doi.org/10.1016/j.jbc.2023.104992

Feuerman, T., Gade, G. F., & Reynolds, R. (1988). *Stress-induced malignant hyperthermia in a head-injured patient*. https://doi.org/10.3171/jns.1988.68.2.0297

Finsterer, J., Michalek-Sauberer, A., & Höftberger, R. (2009). Malignant hyperthermia susceptibility in a patient with mitochondrial disorder. *Metabolic Brain Disease*, *24*(3), 501–506. https://doi.org/bann

Fishbein, W. N., Muldoon, S. M., Deuster, P. A., & Armbrustmacher, V. W. (1985). Myoadenylate deaminase deficiency and malignant hyperthermia susceptibility: Is there a relationship? *Biochemical Medicine*, *34*(3), 344–354. https://doi.org/10.1016/0006-2944(85)90097-3

Fishilevich, S., Nudel, R., Rappaport, N., Hadar, R., Plaschkes, I., Iny Stein, T., Rosen, N., Kohn, A., Twik, M., Safran, M., Lancet, D., & Cohen, D. (2017). GeneHancer: Genome-wide integration of enhancers and target genes in GeneCards. *Database*, *2017*, bax028. https://doi.org/10.1093/database/bax028

Fouad, G., Dalakas, M., Servidei, S., Mendell, J. R., Bergh, P. V. den, Angelini, C., Alderson, K., Griggs, R. C., Tawil, R., Gregg, R., Hogan, K., Powers, P. A., Weinberg, N., Malonee, W., & Ptáček, L. J. (1997). Genotype-phenotype correlations of DHP receptor α1-

subunit gene mutations causing hypokalemic periodic paralysis. *Neuromuscular Disorders*, *7*(1), 33–38. https://doi.org/10.1016/S0960-8966(96)00401-4

Fricker, R. M., Raffelsberger, T., Rauch-Shorny, S., Finsterer, J., Müller-Reible, C., Gilly, H., & Bittner, R. E. (2002). Positive Malignant Hyperthermia Susceptibility In Vitro Test in a Patient with Mitochondrial Myopathy and Myoadenylate Deaminase Deficiency. *Anesthesiology*, *97*(6), 1635–1637. https://doi.org/10.1097/00000542-200212000-00044

Frontera, W. R., & Ochala, J. (2015). Skeletal Muscle: A Brief Review of Structure and Function. *Behavior Genetics*, *45*(2), 183–195. https://doi.org/10.1007/s00223-014-9915-y

Fujii, J., Otsu, K., Zorzato, F., de Leon, S., Khanna, V. K., Weiler, J. E., O'Brien, P. J., & MacLennan, D. H. (1991). Identification of a mutation in porcine ryanodine receptor associated with malignant hyperthermia. *Science (New York, N.Y.)*, *253*(5018), 448–451. https://doi.org/10.1126/science.1862346

Gama-Norton, L., Botezatu, L., Herrmann, S., Schweizer, M., Alves, P. M., Hauser, H., & Wirth, D. (2011). Lentivirus production is influenced by SV40 large T-antigen and chromosomal integration of the vector in HEK293 cells. *Human Gene Therapy*, *22*(10), 1269–1279. https://doi.org/10.1089/hum.2010.143

Gardner, L., Miller, D. M., Daly, C., Gupta, P. K., House, C., Roiz De Sa, D., Shaw, M. A., & Hopkins, P. M. (2020). Investigating the genetic susceptibility to exertional heat illness. *Journal of Medical Genetics*, *57*(8), 531–541. https://doi.org/10.1136/JMEDGENET-2019-106461

Gaudelli, N. M., Komor, A. C., Rees, H. A., Packer, M. S., Badran, A. H., Bryson, D. I., & Liu, D. R. (2017). Programmable base editing of A•T to G•C in genomic DNA without DNA cleavage. *Nature*, *551*(7681), 464–471. https://doi.org/10.1038/nature24644

Gempel, K., Kiechl, S., Hofmann, S., Lochmüller, H., Kiechl-Kohlendorfer, U., Willeit, J., Sperl, W., Rettinger, A., Bieger, I., Pongratz, D., Gerbitz, K. D., & Bauer, M. F. (2002). Screening for carnitine palmitoyltransferase II deficiency by tandem mass spectrometry. *Journal of Inherited Metabolic Disease*, *25*(1), 17–27. https://doi.org/10.1023/a:1015109127986

Gharib, W. H., & Robinson-Rechavi, M. (2011). When orthologs diverge between human and mouse. *Briefings in Bioinformatics*, *12*(5), 436–441. https://doi.org/10.1093/bib/bbr031

Gibbs, I. C., Fadahunsi, O., Reid, N., & Bonnick, A. M. (2019). Malignant Hyperthermia: A Case Report in a Trauma Patient. *Journal of Oral and Maxillofacial Surgery: Official Journal of the American Association of Oral and Maxillofacial Surgeons*, *77*(1), 54–58. https://doi.org/10.1016/j.joms.2018.07.009

Glahn, K. P. E., Bendixen, D., Girard, T., Hopkins, P. M., Johannsen, S., Rüffert, H., Snoeck, M. M., & Urwyler, A. (2020). Availability of dantrolene for the management of malignant hyperthermia crises: European Malignant Hyperthermia Group guidelines. *British Journal of Anaesthesia*, *125*(2), 133–140. https://doi.org/10.1016/j.bja.2020.04.089

Grabner, M., Dirksen, R. T., Suda, N., & Beam, K. G. (1999). The II-III Loop of the Skeletal Muscle Dihydropyridine Receptor Is Responsible for the Bi-directional Coupling with the Ryanodine Receptor *. *Journal of Biological Chemistry*, *274*(31), 21913–21919. https://doi.org/10.1074/jbc.274.31.21913

Gronert, G. A., Tobin, J. R., & Muldoon, S. (2011). Malignant hyperthermia—Human stress triggering. *Biochimica et Biophysica Acta (BBA) - Molecular Cell Research*, *1813*(12), 2191–2192. https://doi.org/10.1016/j.bbamcr.2011.08.001

Gruss, P., Lai, C. J., Dhar, R., & Khoury, G. (1979). Splicing as a requirement for biogenesis of functional 16S mRNA of simian virus 40. *Proceedings of the National Academy of Sciences of the United States of America*, *76*(9), 4317–4321.

Gupta, P. K., & Hopkins, P. M. (2017). Diagnosis and management of malignant hyperthermia. *BJA Education*, *17*(7), 249–254. https://doi.org/10.1093/bjaed/mkw079

Györke, I., Hester, N., Jones, L. R., & Györke, S. (2004). The role of calsequestrin, triadin, and junctin in conferring cardiac ryanodine receptor responsiveness to luminal calcium. *Biophysical Journal*, *86*(4), 2121–2128. https://doi.org/10.1016/S0006-3495(04)74271-X

Halliday, N. J. (2003). Malignant hyperthermia. *The Journal of Craniofacial Surgery*, *14*(5), 800–802. https://doi.org/10.1097/00001665-200309000-00039

Hamilton, S. L., & Reid, M. B. (2000). RyR1 modulation by oxidation and calmodulin. *Antioxidants & Redox Signaling*, *2*(1), 41–45. https://doi.org/10.1089/ARS.2000.2.1-41

Hildyard, J. C. W., & Wells, D. J. (2014). Identification and Validation of Quantitative PCR Reference Genes Suitable for Normalizing Expression in Normal and Dystrophic Cell Culture Models of Myogenesis. *PLoS Currents*, *6*(MAR). https://doi.org/10.1371/currents.md.faafdde4bea8df4aa7d06cd5553119a6

Hogan, K. J., & Vladutiu, G. D. (2009). Malignant Hyperthermia-Like Syndrome and Carnitine Palmitoyltransferase II Deficiency with Heterozygous R503C Mutation. *Anesthesia & Analgesia*, *109*(4), 1070–1072. https://doi.org/10.1213/ane.0b013e3181ad63b4

Hong, S., Hwang, D.-Y., Yoon, S., Isacson, O., Ramezani, A., Hawley, R. G., & Kim, K.-S. (2007). Functional Analysis of Various Promoters in Lentiviral Vectors at Different Stages of In Vitro Differentiation of Mouse Embryonic Stem Cells. *Molecular Therapy*, *15*(9), 1630–1639. https://doi.org/10.1038/sj.mt.6300251

Hopkins, P. M. (2000a). Malignant hyperthermia: Advances in clinical management and diagnosis. *British Journal of Anaesthesia*, *85*(1), 118–128. https://doi.org/10.1093/bja/85.1.118

Hopkins, P. M. (2000b). Malignant hyperthermia: Advances in clinical management and diagnosis. *British Journal of Anaesthesia*, *85*(1), 118–128. https://doi.org/10.1093/bja/85.1.118

Hopkins, P. M. (2011). Malignant hyperthermia: Pharmacology of triggering. *British Journal of Anaesthesia*, *107*(1), 48–56. https://doi.org/10.1093/bja/aer132

Hopkins, P. M., Ellis, F. R., & Halsall, P. J. (1991). Evidence for related myopathies in exertional heat stroke and malignant hyperthermia. *The Lancet*, *338*(8781), 1491–1492. https://doi.org/10.1016/0140-6736(91)92304-K

Hopkins, P. M., Rüffert, H., Snoeck, M. M., Girard, T., Glahn, K. P. E., Ellis, F. R., Müller, C. R., Urwyler, A., Bandschapp, O., Gillies, R., Glauber, V., Heytens, L., Islander, G., Klingler, W., Kraft, B., Krivosic-Horber, R., Pollock, N., Schuster, F., Silva, H., … Tzanova, I. (2015). European Malignant Hyperthermia Group guidelines for investigation of malignant hyperthermia susceptibility. *British Journal of Anaesthesia*, *115*(4), 531–539. https://doi.org/10.1093/bja/aev225

Horstick, E. J., Linsley, J. W., Dowling, J. J., Hauser, M. A., McDonald, K. K., Ashley-Koch, A., Saint-Amant, L., Satish, A., Cui, W. W., Zhou, W., Sprague, S. M., Stamm, D. S., Powell, C. M., Speer, M. C., Franzini-Armstrong, C., Hirata, H., & Kuwada, J. Y. (2013). Stac3 is a component of the excitation-contraction coupling machinery and mutated in Native American myopathy. *Nature Communications*, *4*, 1952. https://doi.org/10.1038/ncomms2952

Hsu, P. D., Scott, D. A., Weinstein, J. A., Ran, F. A., Konermann, S., Agarwala, V., Li, Y., Fine, E. J., Wu, X., Shalem, O., Cradick, T. J., Marraffini, L. A., Bao, G., & Zhang, F. (2013).

DNA targeting specificity of RNA-guided Cas9 nucleases. *Nature Biotechnology*, *31*(9), 827–832. https://doi.org/10.1038/nbt.2647

Hu, H., Wang, Z., Wei, R., Fan, G., Wang, Q., Zhang, K., & Yin, C.-C. (2015). The molecular architecture of dihydropyrindine receptor/L-type Ca2+ channel complex. *Scientific Reports*, *5*(1), 8370. https://doi.org/10.1038/srep08370

Huxley, A. F., & Niedergerke, R. (1954). Structural changes in muscle during contraction: Interference microscopy of living muscle fibres. *Nature*, *173*(4412), 971–973. https://doi.org/10.1038/173971a0

Huxley, H., & Hanson, J. (1954). Changes in the Cross-striations of muscle during contraction and stretch and their structural interpretation. *Nature*, *173*(4412), 973–976. https://doi.org/10.1038/173973a0

Ibarra Moreno, C. A., Hu, S., Kraeva, N., Schuster, F., Johannsen, S., Rueffert, H., Klingler, W., Heytens, L., & Riazi, S. (2019). An assessment of penetrance and clinical expression of malignant hyperthermia in individuals carrying diagnostic ryanodine receptor 1 gene mutations. *Anesthesiology*, *131*(5), 983–991. https://doi.org/10.1097/ALN.0000000000002813

Iles, D. E., Lehmann-Horn, F., Scherer, S. W., Tsui, L. C., Olde Weghuis, D., Suijkerbuijk, R. F., Heytens, L., Mikala, G., Schwartz, A., & Ellis, F. R. (1994). Localization of the gene encoding the alpha 2/delta-subunits of the L-type voltage-dependent calcium channel to chromosome 7q and analysis of the segregation of flanking markers in malignant hyperthermia susceptible families. *Human Molecular Genetics*, *3*(6), 969–975. https://doi.org/10.1093/hmg/3.6.969

Inui, M., Saito, A., & Fleischer, S. (1987). Purification of the ryanodine receptor and identity with feet structures of junctional terminal cisternae of sarcoplasmic reticulum from fast skeletal muscle. *The Journal of Biological Chemistry*, *262*(4), 1740–1747.

Isaacs, H., Badenhorst, M. E., & Sautoy, C. D. (1989). Myophosphorylase B deficiency and malignant hyperthermia. *Muscle & Nerve*, *12*(3), 203–205. https://doi.org/10.1002/mus.880120307

Isackson, P. J., Bennett, M. J., Lichter-Konecki, U., Willis, M., Nyhan, W. L., Sutton, V. R., Tein, I., & Vladutiu, G. D. (2008). CPT2 gene mutations resulting in lethal neonatal or severe infantile carnitine palmitoyltransferase II deficiency. *Molecular Genetics and Metabolism*, *94*(4), 422–427. https://doi.org/10.1016/j.ymgme.2008.05.002

Jinek, M., Chylinski, K., Fonfara, I., Hauer, M., Doudna, J. A., & Charpentier, E. (2012). A programmable dual RNA-guided DNA endonuclease in adaptive bacterial immunity. *Science (New York, N.Y.)*, *337*(6096), 816–821. https://doi.org/10.1126/science.1225829

Jo, B.-S., & Choi, S. S. (2015). Introns: The Functional Benefits of Introns in Genomes. *Genomics & Informatics*, *13*(4), 112–118. https://doi.org/10.5808/GI.2015.13.4.112

Johnson, L. N. (1992). Glycogen phosphorylase: Control by phosphorylation and allosteric effectors. *FASEB Journal: Official Publication of the Federation of American Societies for Experimental Biology*, *6*(6), 2274–2282. https://doi.org/10.1096/fasebj.6.6.1544539

Jumper, J., Evans, R., Pritzel, A., Green, T., Figurnov, M., Ronneberger, O., Tunyasuvunakool, K., Bates, R., Žídek, A., Potapenko, A., Bridgland, A., Meyer, C., Kohl, S. A. A., Ballard, A. J., Cowie, A., Romera-Paredes, B., Nikolov, S., Jain, R., Adler, J., … Hassabis, D. (2021). Highly accurate protein structure prediction with AlphaFold. *Nature*, *596*(7873), 583–589. https://doi.org/10.1038/s41586-021-03819-2

Jungbluth, H. (2007a). Central core disease. *Orphanet Journal of Rare Diseases*, *2*, 25. https://doi.org/10.1186/1750-1172-2-25

Jungbluth, H. (2007b). Multi-minicore Disease. *Orphanet Journal of Rare Diseases*, *2*(1), 31. https://doi.org/10.1186/1750-1172-2-31

Kaczor, J. J., Robertshaw, H. A., & Tarnopolsky, M. A. (2017). Higher oxidative stress in skeletal muscle of McArdle disease patients. *Molecular Genetics and Metabolism Reports*, *12*, 69–75. https://doi.org/10.1016/j.ymgmr.2017.05.009

Kaura, V., Liu, X., Diggle, C., Allen, P. D., & Hopkins, P. M. (2022). The Cav1.1 p.T1009K variant is a novel pathogenic variant for malignant hyperthermia. *British Journal of Anaesthesia*, *128*(2), e60. https://doi.org/10.1016/j.bja.2021.11.002

Kawasaki, T., & Kasai, M. (1994). Regulation of calcium channel in sarcoplasmic reticulum by calsequestrin. *Biochemical and Biophysical Research Communications*, *199*(3), 1120–1127. https://doi.org/10.1006/bbrc.1994.1347

Kok, F. O., Shin, M., Ni, C.-W., Gupta, A., Grosse, A. S., van Impel, A., Kirchmaier, B. C., Peterson-Maduro, J., Kourkoulis, G., Male, I., DeSantis, D. F., Sheppard-Tindell, S., Ebarasi, L., Betsholtz, C., Schulte-Merker, S., Wolfe, S. A., & Lawson, N. D. (2015). Reverse genetic screening reveals poor correlation between morpholino-induced and mutant phenotypes in zebrafish. *Developmental Cell*, *32*(1), 97–108. https://doi.org/10.1016/j.devcel.2014.11.018

Komor, A. C., Kim, Y. B., Packer, M. S., Zuris, J. A., & Liu, D. R. (2016). Programmable editing of a target base in genomic DNA without double-stranded DNA cleavage. *Nature*, *533*(7603), 420–424. https://doi.org/10.1038/nature17946

Kotha, R., Jones, A., Girgenti, G. T., & Nahrwold, D. A. (n.d.). Anesthetic Management of a Patient With McArdle Disease: A Case Report and Review of the Literature. *Cureus*, *15*(6), e40092. https://doi.org/10.7759/cureus.40092

Kumar, A., Chakravarty, H., Bal, N. C., Balaraju, T., Jena, N., Misra, G., Bal, C., Pieroni, E., Periasamy, M., & Sharon, A. (2013). Identification of Calcium binding sites on calsequestrin 1 and its implications to polymerization. *Molecular bioSystems*, *9*(7), 1949–1957. https://doi.org/10.1039/c3mb25588c

Lamboley, C. R., Murphy, R. M., McKenna, M. J., & Lamb, G. D. (2013). Endogenous and maximal sarcoplasmic reticulum calcium content and calsequestrin expression in type I and type II human skeletal muscle fibres. *The Journal of Physiology*, *591*(Pt 23), 6053–6068. https://doi.org/10.1113/jphysiol.2013.265900

Lanner, J. T., Georgiou, D. K., Joshi, A. D., & Hamilton, S. L. (2010). Ryanodine receptors: Structure, expression, molecular details, and function in calcium release. *Cold Spring Harbor Perspectives in Biology*, *2*(11). https://doi.org/10.1101/cshperspect.a003996

Laver, D. R., Baynes, T. M., & Dulhunty, A. F. (1997). Magnesium inhibition of ryanodine-receptor calcium channels: Evidence for two independent mechanisms. *The Journal of Membrane Biology*, *156*(3), 213–229. https://doi.org/10.1007/s002329900202

Lebo, R. V., Gorin, F., Fletterick, R. J., Kao, F. T., Cheung, M. C., Bruce, B. D., & Kan, Y. W. (1984). High-resolution chromosome sorting and DNA spot-blot analysis assign McArdle's syndrome to chromosome 11. *Science (New York, N.Y.)*, *225*(4657), 57–59. https://doi.org/10.1126/science.6587566

Li, M. J., Wang, P., Liu, X., Lim, E. L., Wang, Z., Yeager, M., Wong, M. P., Sham, P. C., Chanock, S. J., & Wang, J. (2012). GWASdb: A database for human genetic variants identified by genome-wide association studies. *Nucleic Acids Research*, *40*(Database issue), D1047–D1054. https://doi.org/10.1093/nar/gkr1182

Litman, R. S., Flood, C. D., Kaplan, R. F., Kim, Y. L., & Tobin, J. R. (2008). Postoperative malignant hyperthermia: An analysis of cases from the North American Malignant Hyperthermia Registry. *Anesthesiology*, *109*(5), 825–829. https://doi.org/10.1097/ALN.0b013e31818958e5

Litman, R. S., Griggs, S. M., Dowling, J. J., & Riazi, S. (2018). Malignant Hyperthermia Susceptibility and Related Diseases. *Anesthesiology*, *128*(1), 159–167. https://doi.org/10.1097/ALN.0000000000001877

Livak, K. J., & Schmittgen, T. D. (2001). Analysis of relative gene expression data using real-time quantitative PCR and the 2-ΔΔCT method. *Methods*, *25*(4), 402–408. https://doi.org/10.1006/meth.2001.1262

Lobato, E. B., Janelle, G. M., Urdaneta, F., & Malias, M. A. (1999). Noncardiogenic Pulmonary Edema and Rhabdomyolysis after Protamine Administration in a Patient with Unrecognized McArdle's Disease. *Anesthesiology*, *91*(1), 303–305. https://doi.org/10.1097/00000542-199907000-00039

Lopez, J. R., Kaura, V., Diggle, C. P., Hopkins, P. M., & Allen, P. D. (2018). Malignant hyperthermia, environmental heat stress, and intracellular calcium dysregulation in a mouse model expressing the p.G2435R variant of RYR1. *British Journal of Anaesthesia*, *121*(4), 953–961. https://doi.org/10.1016/j.bja.2018.07.008

Lotteau, S., Ducreux, S., Romestaing, C., Legrand, C., & Van Coppenolle, F. (2013). Characterization of Functional TRPV1 Channels in the Sarcoplasmic Reticulum of Mouse Skeletal Muscle. *PLoS ONE*, *8*(3), e58673. https://doi.org/10.1371/journal.pone.0058673

Lucia, A., Nogales-Gadea, G., Pérez, M., Martín, M. A., Andreu, A. L., & Arenas, J. (2008). McArdle disease: What do neurologists need to know? *Nature Clinical Practice Neurology*, *4*(10), 568–577. https://doi.org/10.1038/ncpneuro0913

Lukacs, C. M., Oikonomakos, N. G., Crowther, R. L., Hong, L.-N., Kammlott, R. U., Levin, W., Li, S., Liu, C.-M., Lucas-McGady, D., Pietranico, S., & Reik, L. (2006). The crystal structure of human muscle glycogen phosphorylase a with bound glucose and AMP: An intermediate conformation with T-state and R-state features. *Proteins: Structure, Function, and Bioinformatics*, *63*(4), 1123–1126. https://doi.org/10.1002/prot.20939

Machiela, M. J., & Chanock, S. J. (2015). LDlink: A web-based application for exploring population-specific haplotype structure and linking correlated alleles of possible

functional variants. *Bioinformatics*, *31*(21), 3555–3557. https://doi.org/10.1093/bioinformatics/btv402

MacLennan, D. H., Duff, C., Zorzato, F., Fujii, J., Phillips, M., Korneluk, R. G., Frodis, W., Britt, B. A., & Wortont, R. G. (1990). Ryanodine receptor gene is a candidate for predisposition to malignant hyperthermia. *Nature*, *343*(6258), 559–561. https://doi.org/10.1038/343559a0

Madsen, N. B., Avramovic-Zikic, O., & Honikel, K. O. (1973). Structure-function relationships in glycogen phosphorylase with respect to its control characteristics. *Annals of the New York Academy of Sciences*, *210*, 222–237. https://doi.org/10.1111/j.1749-6632.1973.tb47575.x

Matthews, E., Labrum, R., Sweeney, M. G., Sud, R., Haworth, A., Chinnery, P. F., Meola, G., Schorge, S., Kullmann, D. M., Davis, M. B., & Hanna, M. G. (2009). Voltage sensor charge loss accounts for most cases of hypokalemic periodic paralysis. *Neurology*, *72*(18), 1544–1547. https://doi.org/10.1212/01.wnl.0000342387.65477.46

Meinhardt, B., Motlagh Scholle, L., Seifert, F., Anwand, M., Pietzsch, M., & Zierz, S. (2021). Cardiolipin Stabilizes and Increases Catalytic Efficiency of Carnitine Palmitoyltransferase II and Its Variants S113L, P50H, and Y479F. *International Journal of Molecular Sciences*, *22*(9), 4831. https://doi.org/10.3390/ijms22094831

Miller, D. M., Daly, C., Aboelsaod, E. M., Gardner, L., Hobson, S. J., Riasat, K., Shepherd, S., Robinson, R. L., Bilmen, J. G., Gupta, P. K., Shaw, M. A., & Hopkins, P. M. (2018). Genetic epidemiology of malignant hyperthermia in the UK. *British Journal of Anaesthesia*, *121*(4), 944–952. https://doi.org/10.1016/j.bja.2018.06.028

Miller, M. J., Burrage, L. C., Gibson, J. B., Strenk, M. E., Lose, E. J., Bick, D. P., Elsea, S. H., Sutton, V. R., Sun, Q., Graham, B. H., Craigen, W. J., Zhang, V. W., & Wong, L.-J. C. (2015). Recurrent ACADVL molecular findings in individuals with a positive newborn screen for very long chain acyl-coA dehydrogenase (VLCAD) deficiency in the United

States. *Molecular Genetics and Metabolism*, *116*(3), 139–145. https://doi.org/10.1016/j.ymgme.2015.08.011

Mitchell, G., & Heffron, J. J. A. (1982). Porcine Stress Syndromes. In C. O. Chichester, E. M. Mrak, & G. F. Stewart (Eds.), *Advances in Food Research* (Vol. 28, pp. 167–230). Academic Press. https://doi.org/10.1016/S0065-2628(08)60112-3

Molenaar, J. P., Verhoeven, J. I., Rodenburg, R. J., Kamsteeg, E. J., Erasmus, C. E., Vicart, S., Behin, A., Bassez, G., Magot, A., Péréon, Y., Brandom, B. W., Guglielmi, V., Vattemi, G., Chevessier, F., Mathieu, J., Franques, J., Suetterlin, K., Hanna, M. G., Guyant-Marechal, L., … Sternberg, D. (2020). Clinical, morphological and genetic characterization of Brody disease: An international study of 40 patients. *Brain*, *143*(2), 452–466. https://doi.org/10.1093/brain/awz410

Monnier, N., Procaccio, V., Stieglitz, P., & Lunardi, J. (1997). Malignant-hyperthermia susceptibility is associated with a mutation of the α1-subunit of the human dihydropyridine-sensitive L-type voltage- dependent calcium-channel receptor in skeletal muscle. *American Journal of Human Genetics*, *60*(6), 1316–1325. https://doi.org/10.1086/515454

Montini, E., Cesana, D., Schmidt, M., Sanvito, F., Bartholomae, C. C., Ranzani, M., Benedicenti, F., Sergi, L. S., Ambrosi, A., Ponzoni, M., Doglioni, C., Di Serio, C., von Kalle, C., & Naldini, L. (2009). The genotoxic potential of retroviral vectors is strongly modulated by vector design and integration site selection in a mouse model of HSC gene therapy. *The Journal of Clinical Investigation*, *119*(4), 964–975. https://doi.org/10.1172/JCI37630

Motlagh, L., Golbik, R., Sippl, W., & Zierz, S. (2016). Stabilization of the thermolabile variant S113L of carnitine palmitoyltransferase II. *Neurology: Genetics*, *2*(2), e53. https://doi.org/10.1212/NXG.0000000000000053

Mouse Genome Sequencing Consortium, Waterston, R. H., Lindblad-Toh, K., Birney, E., Rogers, J., Abril, J. F., Agarwal, P., Agarwala, R., Ainscough, R., Alexandersson, M., An, P., Antonarakis, S. E., Attwood, J., Baertsch, R., Bailey, J., Barlow, K., Beck, S., Berry, E., Birren, B., … Lander, E. S. (2002). Initial sequencing and comparative analysis of the mouse genome. *Nature*, *420*(6915), 520–562. https://doi.org/10.1038/nature01262

Murtazina, A., Demina, N., Chausova, P., Shchagina, O., Borovikov, A., & Dadali, E. (2022). The First Russian Patient with Native American Myopathy. *Genes*, *13*(2), Article 2. https://doi.org/10.3390/genes13020341

Naldini, L., Blömer, U., Gallay, P., Ory, D., Mulligan, R., Gage, F. H., Verma, I. M., & Trono, D. (1996). In vivo gene delivery and stable transduction of nondividing cells by a lentiviral vector. *Science (New York, N.Y.)*, *272*(5259), 263–267. https://doi.org/10.1126/science.272.5259.263

Nogales-Gadea, G., Brull, A., Santalla, A., Andreu, A. L., Arenas, J., Martín, M. A., Lucia, A., de Luna, N., & Pinós, T. (2015a). McArdle Disease: Update of Reported Mutations and Polymorphisms in the *PYGM* Gene. *Human Mutation*, *36*(7), 669–678. https://doi.org/10.1002/humu.22806

Nogales-Gadea, G., Brull, A., Santalla, A., Andreu, A. L., Arenas, J., Martín, M. A., Lucia, A., de Luna, N., & Pinós, T. (2015b). McArdle Disease: Update of Reported Mutations and Polymorphisms in the *PYGM* Gene. *Human Mutation*, *36*(7), 669–678. https://doi.org/10.1002/humu.22806

Nogales-Gadea, G., Pinós, T., Lucia, A., Arenas, J., Camara, Y., Brull, A., de Luna, N., Martín, M. A., Garcia-Arumí, E., Martí, R., & Andreu, A. L. (2012). Knock-in mice for the R50X mutation in the PYGM gene present with McArdle disease. *Brain*, *135*(7), 2048–2057. https://doi.org/10.1093/brain/aws141

Nogales-Gadea, G., Rubio, J. C., Fernandez-Cadenas, I., Garcia-Consuegra, I., Lucia, A., Cabello, A., Garcia-Arumi, E., Arenas, J., Andreu, A. L., & Martín, M. A. (2008). Expression of the muscle glycogen phosphorylase gene in patients with McArdle disease: The role of nonsense-mediated mRNA decay. *Human Mutation*, *29*(2), 277–283. https://doi.org/10.1002/humu.20649

Novelli, A., Valente, E. M., Bernardini, L., Ceccarini, C., Sinibaldi, L., Caputo, V., Cavalli, P., & Dallapiccola, B. (2004). Autosomal dominant Brody disease cosegregates with a chromosomal (2;7)(p11.2;p12.1) translocation in an Italian family. *European Journal of Human Genetics*, *12*(7), Article 7. https://doi.org/10.1038/sj.ejhg.5201200

Odermatt, A., Taschner, P. E., Khanna, V. K., Busch, H. F., Karpati, G., Jablecki, C. K., Breuning, M. H., & MacLennan, D. H. (1996). Mutations in the gene-encoding SERCA1, the fast-twitch skeletal muscle sarcoplasmic reticulum Ca2+ ATPase, are associated with Brody disease. *Nature Genetics*, *14*(2), 191–194. https://doi.org/10.1038/ng1096-191

Olpin, S. E., Afifi, A., Clark, S., Manning, N. J., Bonham, J. R., Dalton, A., Leonard, J. V., Land, J. M., Andresen, B. S., Morris, A. A., Muntoni, F., Turnbull, D., Pourfarzam, M., Rahman, S., & Pollitt, R. J. (2003). Mutation and biochemical analysis in carnitine palmitoyltransferase type II (CPT II) deficiency. *Journal of Inherited Metabolic Disease*, *26*(6), 543–557. https://doi.org/10.1023/A:1025947930752

Ording, H., Brancadoro, V., Cozzolino, S., Ellis, F. R., Glauber, V., Gonano, E. F., Halsall, P. J., Hartung, E., Heffron, J. J., Heytens, L., Kozak-Ribbens, G., Kress, H., Krivosic-Horber, R., Lehmann-Horn, F., Mortier, W., Nivoche, Y., Ranklev-Twetman, E., Sigurdsson, S., Snoeck, M., … Wappler, F. (1997). In vitro contracture test for diagnosis of malignant hyperthermia following the protocol of the European MH Group: Results of testing patients surviving fulminant MH and unrelated low-risk subjects. The European

Malignant Hyperthermia Group. *Acta Anaesthesiologica Scandinavica*, *41*(8), 955–966. https://doi.org/10.1111/j.1399-6576.1997.tb04820.x

Pan, Q., Shai, O., Lee, L. J., Frey, B. J., & Blencowe, B. J. (2008). Deep surveying of alternative splicing complexity in the human transcriptome by high-throughput sequencing. *Nature Genetics*, *40*(12), 1413–1415. https://doi.org/10.1038/ng.259

Paul-Pletzer, K., Yamamoto, T., Bhat, M. B., Ma, J., Ikemoto, N., Jimenez, L. S., Morimoto, H., Williams, P. G., & Parness, J. (2002). Identification of a dantrolene-binding sequence on the skeletal muscle ryanodine receptor. *The Journal of Biological Chemistry*, *277*(38), 34918–34923. https://doi.org/10.1074/jbc.M205487200

Perlman, R. L. (2016). Mouse models of human disease. *Evolution, Medicine, and Public Health*, *2016*(1), 170–176. https://doi.org/10.1093/emph/eow014

Pirone, A., Schredelseker, J., Tuluc, P., Gravino, E., Fortunato, G., Flucher, B. E., Carsana, A., Salvatore, F., & Grabner, M. (2010). Identification and functional characterization of malignant hyperthermia mutation T1354S in the outer pore of the Cavα1S-subunit. *American Journal of Physiology - Cell Physiology*, *299*(6), C1345–C1354. https://doi.org/10.1152/ajpcell.00008.2010

Pizzamiglio, C., Mahroo, O. A., Khan, K. N., Patasin, M., & Quinlivan, R. (2021). Phenotype and genotype of 197 British patients with McArdle disease: An observational single-centre study. *Journal of Inherited Metabolic Disease*, *44*(6), 1409–1418. https://doi.org/10.1002/jimd.12438

Poletti, V., & Mavilio, F. (2021). Designing Lentiviral Vectors for Gene Therapy of Genetic Diseases. *Viruses*, *13*(8), 1526. https://doi.org/10.3390/v13081526

Polster, A., Nelson, B. R., Olson, E. N., & Beam, K. G. (2016). Stac3 has a direct role in skeletal muscle-type excitation–contraction coupling that is disrupted by a myopathy-causing mutation. *Proceedings of the National Academy of Sciences of*

the United States of America, *113*(39), 10986–10991. https://doi.org/10.1073/pnas.1612441113

Polster, A., Nelson, B. R., Papadopoulos, S., Olson, E. N., & Beam, K. G. (2018). Stac proteins associate with the critical domain for excitation-contraction coupling in the II-III loop of CaV1.1. *The Journal of General Physiology*, *150*(4), 613–624. https://doi.org/10.1085/jgp.201711917

Protasi, F., Paolini, C., & Dainese, M. (2009). Calsequestrin-1: A new candidate gene for malignant hyperthermia and exertional/environmental heat stroke. *The Journal of Physiology*, *587*(Pt 13), 3095–3100. https://doi.org/10.1113/jphysiol.2009.171967

Quinlivan, R., Buckley, J., James, M., Twist, A., Ball, S., Duno, M., Vissing, J., Bruno, C., Cassandrini, D., Roberts, M., Winer, J., Rose, M., & Sewry, C. (2010). McArdle disease: A clinical review. *Journal of Neurology, Neurosurgery and Psychiatry*, *81*(11), 1182–1188. https://doi.org/10.1136/jnnp.2009.195040

Ran, F. A., Hsu, P. D., Lin, C. Y., Gootenberg, J. S., Konermann, S., Trevino, A. E., Scott, D. A., Inoue, A., Matoba, S., Zhang, Y., & Zhang, F. (2013). Double nicking by RNA-guided CRISPR cas9 for enhanced genome editing specificity. *Cell*, *154*(6), 1380–1389. https://doi.org/10.1016/j.cell.2013.08.021

Ran, F. A., Hsu, P. D., Wright, J., Agarwala, V., Scott, D. A., & Zhang, F. (2013). Genome engineering using the CRISPR-Cas9 system. *Nature Protocols*, *8*(11), Article 11. https://doi.org/10.1038/nprot.2013.143

Rearick, D., Prakash, A., McSweeny, A., Shepard, S. S., Fedorova, L., & Fedorov, A. (2011). Critical association of ncRNA with introns. *Nucleic Acids Research*, *39*(6), 2357–2366. https://doi.org/10.1093/nar/gkq1080

Rios, E., & Brum, G. (1987). Involvement of dihydropyridine receptors in excitation-contraction coupling in skeletal muscle. *Nature*, *325*(6106), 717–720. https://doi.org/10.1038/325717a0

Robinson, R., Carpenter, D., Shaw, M. A., Halsall, J., & Hopkins, P. (2006). Mutations in RYR1 in malignant hypertheraiia and central core disease. *Human Mutation*, *27*(10), 977–989. https://doi.org/10.1002/humu.20356

ROBINSON, R. L., CURRAN, J. L., ELLIS, F. R., HALSALL, P. J., HALL, W. J., HOPKINS, P. M., ILES, D. E., WEST, S. P., & SHAW, M.-A. (2000). Multiple interacting gene products may influence susceptibility to malignant hyperthermia. *Annals of Human Genetics*, *64*(4), 307–320. https://doi.org/10.1046/j.1469-1809.2000.6440307.x

Roos, J., DiGregorio, P. J., Yeromin, A. V., Ohlsen, K., Lioudyno, M., Zhang, S., Safrina, O., Kozak, J. A., Wagner, S. L., Cahalan, M. D., Veliçelebi, G., & Stauderman, K. A. (2005). STIM1, an essential and conserved component of store-operated Ca2+ channel function. *Journal of Cell Biology*, *169*(3), 435–445. https://doi.org/10.1083/jcb.200502019

Rosenberg, H., Pollock, N., Schiemann, A., Bulger, T., & Stowell, K. (2015). Malignant hyperthermia: A review. *Orphanet Journal of Rare Diseases*, *10*(1), 1–19. https://doi.org/10.1186/S13023-015-0310-1/TABLES/2

Roy, M., Kim, N., Xing, Y., & Lee, C. (2008). The effect of intron length on exon creation ratios during the evolution of mammalian genomes. *RNA*, *14*(11), 2261–2273. https://doi.org/10.1261/rna.1024908

Rufer, A. C., Thoma, R., Benz, J., Stihle, M., Gsell, B., De Roo, E., Banner, D. W., Mueller, F., Chomienne, O., & Hennig, M. (2006). The Crystal Structure of Carnitine Palmitoyltransferase 2 and Implications for Diabetes Treatment. *Structure*, *14*(4), 713–723. https://doi.org/10.1016/j.str.2006.01.008

S. Makarova, K., H. Haft, D., Barrangou, R., J. J. Brouns, S., Charpentier, E., Horvath, P., Moineau, S., J. M. Mojica, F., I. Wolf, Y., Yakunin, A. F., van der Oost, J., & V. Koonin, E. (2011). Evolution and classification of the CRISPR-Cas systems. *Nature Reviews. Microbiology*, *9*(6), 467–477. https://doi.org/10.1038/nrmicro2577

Sandow, A. (1952). Excitation-Contraction Coupling in Muscular Response. *The Yale Journal of Biology and Medicine*, *25*(3), 176–201.

Schiaffino, S., & Reggiani, C. (2011). Fiber Types in Mammalian Skeletal Muscles. *Physiological Reviews*, *91*(4), 1447–1531. https://doi.org/10.1152/physrev.00031.2010

Schneider, C. A., Rasband, W. S., & Eliceiri, K. W. (2012). NIH Image to ImageJ: 25 years of image analysis. *Nature Methods*, *9*(7), Article 7. https://doi.org/10.1038/nmeth.2089

Schuster, F., Müller, R., Hartung, E., Roewer, N., & Anetseder, M. (2005). Inhibition of sarcoplasmic Ca2+-ATPase increases caffeine- and halothane-induced contractures in muscle bundles of malignant hyperthermia susceptible and healthy individuals. *BMC Anesthesiology*, *5*, 8. https://doi.org/10.1186/1471-2253-5-8

Scriver, C. R., & Waters, P. J. (1999). Monogenic traits are not simple: Lessons from phenylketonuria. *Trends in Genetics: TIG*, *15*(7), 267–272. https://doi.org/10.1016/s0168-9525(99)01761-8

Seki, A., & Rutz, S. (2018). Optimized RNP transfection for highly efficient CRISPR/Cas9-mediated gene knockout in primary T cells. *The Journal of Experimental Medicine*, *215*(3), 985. https://doi.org/10.1084/JEM.20171626

Semplicini, C., Bertolin, C., Bello, L., Pantic, B., Guidolin, F., Vianello, S., Catapano, F., Colombo, I., Moggio, M., Gavassini, B. F., Cenacchi, G., Papa, V., Previtero, M., Calore, C., Sorarù, G., Minervini, G., Tosatto, S. C. E., Stramare, R., & Pegoraro, E. (2018). The clinical spectrum of CASQ1-related myopathy. *Neurology*, *91*(17), e1629–e1641. https://doi.org/10.1212/WNL.0000000000006387

Shaw, M. A., & Hopkins, P. M. (2019). Mission impossible or mission futile?: Estimating penetrance for malignant hyperthermia. *Anesthesiology*, *131*(5), 957–959. https://doi.org/10.1097/ALN.0000000000002884

Shimizu, T., Yanase, N., Fujii, T., Sakakibara, H., & Sakai, H. (2022). Regulation of TRPV1 channel activities by intracellular ATP in the absence of capsaicin. *Biochimica et Biophysica Acta (BBA) - Biomembranes*, *1864*(1), 183782. https://doi.org/10.1016/j.bbamem.2021.183782

Shishmarev, D. (2020). Excitation-contraction coupling in skeletal muscle: Recent progress and unanswered questions. *Biophysical Reviews 2020 12:1*, *12*(1), 143–153. https://doi.org/10.1007/S12551-020-00610-X

Slaymaker, I. M., Gao, L., Zetsche, B., Scott, D. A., Yan, W. X., & Zhang, F. (2016). Rationally engineered Cas9 nucleases with improved specificity. *Science*, *351*(6268), 84–88. https://doi.org/10.1126/science.aad5227

Snoeck, M., Treves, S., Molenaar, J. P., Kamsteeg, E. J., Jungbluth, H., & Voermans, N. C. (2016). "Human Stress Syndrome" and the Expanding Spectrum of RYR1-Related Myopathies. *Cell Biochemistry and Biophysics*, *74*(1), 85–87. https://doi.org/10.1007/s12013-015-0704-7

Sorek, R., & Ast, G. (2003). Intronic Sequences Flanking Alternatively Spliced Exons Are Conserved Between Human and Mouse. *Genome Research*, *13*(7), 1631–1637. https://doi.org/10.1101/gr.1208803

Stamm, D. S., Aylsworth, A. S., Stajich, J. M., Kahler, S. G., Thorne, L. B., Speer, M. C., & Powell, C. M. (2008). Native American myopathy: Congenital myopathy with cleft palate, skeletal anomalies, and susceptibility to malignant hyperthermia. *American Journal of Medical Genetics Part A*, *146A*(14), 1832–1841. https://doi.org/10.1002/ajmg.a.32370

Staron, R. S., Hagerman, F. C., Hikida, R. S., Murray, T. F., Hostler, D. P., Crill, M. T., Ragg, K. E., & Toma, K. (2000). Fiber type composition of the vastus lateralis muscle of young men and women. *The Journal of Histochemistry and Cytochemistry: Official Journal*

of the Histochemistry Society, *48*(5), 623–629. https://doi.org/10.1177/002215540004800506

Stockmar, C., Lill, H., Trapp, A., Josten, C., & Punkt, K. (2006). Fibre type related changes in the metabolic profile and fibre diameter of human vastus medialis muscle after anterior cruciate ligament rupture. *Acta Histochemica*, *108*(5), 335–342. https://doi.org/10.1016/j.acthis.2006.05.005

Takeshima, H., Komazaki, S., Nishi, M., Iino, M., & Kangawa, K. (2000). Junctophilins: A novel family of junctional membrane complex proteins. *Molecular Cell*, *6*(1), 11–22. https://doi.org/10.1016/s1097-2765(00)00003-4

Takeshima, H., Lino, M., Takekura, H., Nishi, M., Kuno, J., Minowa, O., Takano, H., & Noda, T. (1994). Excitation-contraction uncoupling and muscular degeneration in mice lacking functional skeletal muscle ryanodine-receptor gene. *Nature*, *369*(6481), 556–559. https://doi.org/10.1038/369556a0

Tanabe, T., Beam, K. G., Adams, B. A., Niidome, T., & Numa, S. (1990). Regions of the skeletal muscle dihydropyridine receptor critical for excitation-contraction coupling. *Nature*, *346*(6284), 567–569. https://doi.org/10.1038/346567a0

Teijeira, S., San Millán, B., Fernández, J. M., Rivas, E., Viéitez, I., Miranda, S., González, F., & Navarro, C. (2009). Myoadenylate deaminase deficiency: Clinico-pathological and molecular study of a series of 27 Spanish cases. *Clinical Neuropathology*, *28*(2), 136–142. https://doi.org/10.5414/npp28136

Thomas, J., & Crowhurst, T. (2013). Exertional heat stroke, rhabdomyolysis and susceptibility to malignant hyperthermia. *Internal Medicine Journal*, *43*(9), 1035–1038. https://doi.org/10.1111/imj.12232

Tong, J., Oyamada, H., Demaurex, N., Grinstein, S., McCarthy, T. V., & MacLennan, D. H. (1997). Caffeine and halothane sensitivity of intracellular Ca2+ release is altered by 15 calcium release channel (ryanodine receptor) mutations associated with

malignant hyperthermia and/or central core disease. *The Journal of Biological Chemistry*, *272*(42), 26332–26339. https://doi.org/10.1074/jbc.272.42.26332

Van Petegem, F. (2012). Ryanodine receptors: Structure and function. *Journal of Biological Chemistry*, *287*(38), 31624–31632. https://doi.org/10.1074/jbc.R112.349068

Vanden Abeele, F., Lotteau, S., Ducreux, S., Dubois, C., Monnier, N., Hanna, A., Gkika, D., Romestaing, C., Noyer, L., Flourakis, M., Tessier, N., Al-Mawla, R., Chouabe, C., Lefai, E., Lunardi, J., Hamilton, S., Fauré, J., Van Coppenolle, F., & Prevarskaya, N. (2019). TRPV1 variants impair intracellular Ca2+ signaling and may confer susceptibility to malignant hyperthermia. *Genetics in Medicine*, *21*(2), 441–450. https://doi.org/10.1038/s41436-018-0066-9

Vandesompele, J., De Preter, K., Pattyn, F., Poppe, B., Van Roy, N., De Paepe, A., & Speleman, F. (2002). Accurate normalization of real-time quantitative RT-PCR data by geometric averaging of multiple internal control genes. *Genome Biology*, *3*(7), 1–12. https://doi.org/10.1186/gb-2002-3-7-research0034

Violante, S., IJlst, L., van Lenthe, H., de Almeida, I. T., Wanders, R. J., & Ventura, F. V. (2010). Carnitine palmitoyltransferase 2: New insights on the substrate specificity and implications for acylcarnitine profiling. *Biochimica et Biophysica Acta (BBA) - Molecular Basis of Disease*, *1802*(9), 728–732. https://doi.org/10.1016/j.bbadis.2010.06.002

Wang, Y., Schnegelsberg, P. N., Dausman, J., & Jaenisch, R. (1996). Functional redundancy of the muscle-specific transcription factors Myf5 and myogenin. *Nature*, *379*(6568), 823–825. https://doi.org/10.1038/379823a0

Weiss, R. G., O'Connell, K. M. S., Flucher, B. E., Allen, P. D., Grabner, M., & Dirksen, R. T. (2004). Functional analysis of the R1086H malignant hyperthermia mutation in the DHPR reveals an unexpected influence of the III-IV loop on skeletal muscle EC

coupling. *American Journal of Physiology-Cell Physiology*, *287*(4), C1094–C1102. https://doi.org/10.1152/ajpcell.00173.2004

Welter, D., MacArthur, J., Morales, J., Burdett, T., Hall, P., Junkins, H., Klemm, A., Flicek, P., Manolio, T., Hindorff, L., & Parkinson, H. (2014). The NHGRI GWAS Catalog, a curated resource of SNP-trait associations. *Nucleic Acids Research*, *42*(Database issue), D1001–D1006. https://doi.org/10.1093/nar/gkt1229

White, J. K., Gerdin, A.-K., Karp, N. A., Ryder, E., Buljan, M., Bussell, J. N., Salisbury, J., Clare, S., Ingham, N. J., Podrini, C., Houghton, R., Estabel, J., Bottomley, J. R., Melvin, D. G., Sunter, D., Adams, N. C., Sanger Institute Mouse Genetics Project, Tannahill, D., Logan, D. W., … Steel, K. P. (2013). Genome-wide generation and systematic phenotyping of knockout mice reveals new roles for many genes. *Cell*, *154*(2), 452–464. https://doi.org/10.1016/j.cell.2013.06.022

White, R., Schiemann, A. H., Burling, S. M., Bjorksten, A., Bulger, T., Gillies, R., Hopkins, P. M., Kamsteeg, E.-J., Machon, R. G., Massey, S., Miller, D., Perry, M., Snoeck, M. M. J., Stephens, J., Street, N., van den Bersselaar, L. R., & Stowell, K. M. (2022). Functional analysis of RYR1 variants in patients with confirmed susceptibility to malignant hyperthermia. *British Journal of Anaesthesia*, *129*(6), 879–888. https://doi.org/10.1016/j.bja.2022.08.029

Wieser, T. (1993). Carnitine Palmitoyltransferase II Deficiency. In *GeneReviews®*. University of Washington, Seattle. http://www.ncbi.nlm.nih.gov/pubmed/20301431

Wieser, T. (2004). Carnitine Palmitoyltransferase II Deficiency. In *GeneReviews®*. University of Washington, Seattle. http://www.ncbi.nlm.nih.gov/pubmed/20301431

Wieser, T., Deschauer, ; M, Olek, ; K, Hermann, ; T, & Zierz, S. (2003). *Carnitine palmitoyltransferase II deficiency Molecular and biochemical analysis of 32 patients*. www.neurology.org

Withers, S. G., Madsen, N. B., Sykes, B. D., Takagi, M., Shimomura, S., & Fukui, T. (1981). Evidence for direct phosphate-phosphate interaction between pyridoxal phosphate and substrate in the glycogen phosphorylase catalytic mechanism. *The Journal of Biological Chemistry*, *256*(21), 10759–10762.

Yan, Z., Bai, X., Yan, C., Wu, J., Li, Z., Xie, T., Peng, W., Yin, C., Li, X., Scheres, S. H. W., Shi, Y., & Yan, N. (2015). Structure of the rabbit ryanodine receptor RyR1 at near-atomic resolution. *Nature*, *517*(7532), 50–55. https://doi.org/10.1038/nature14063

Yang, T., Riehl, J., Esteve, E., Matthaei, K. I., Goth, S., Allen, P. D., Pessah, I. N., & Lopez, J. R. (2006). Pharmacologic and functional characterization of malignant hyperthermia in the R163C RyR1 knock-in mouse. *Anesthesiology*, *105*(6), 1164–1175. https://doi.org/10.1097/00000542-200612000-00016

Yang, T., Ta, T. A., Pessah, I. N., & Allen, P. D. (2003). Functional defects in six ryanodine receptor isoform-1 (RyR1) mutations associated with malignant hyperthermia and their impact on skeletal excitation-contraction coupling. *The Journal of Biological Chemistry*, *278*(28), 25722–25730. https://doi.org/10.1074/jbc.M302165200

Yin, H., Price, F., & Rudnicki, M. A. (2013). Satellite cells and the muscle stem cell niche. *Physiological Reviews*, *93*(1), 23–67. https://doi.org/10.1152/physrev.00043.2011

Yuen, B., Boncompagni, S., Feng, W., Yang, T., Lopez, J. R., Matthaei, K. I., Goth, S. R., Protasi, F., Franzini-Armstrong, C., Allen, P. D., & Pessah, I. N. (2012). Mice expressing T4826I-RYR1 are viable but exhibit sex- and genotype-dependent susceptibility to malignant hyperthermia and muscle damage. *The FASEB Journal*, *26*(3), 1311–1322. https://doi.org/10.1096/fj.11-197582

Zaharieva, I. T., Sarkozy, A., Munot, P., Manzur, A., O'Grady, G., Rendu, J., Malfatti, E., Amthor, H., Servais, L., Urtizberea, J. A., Neto, O. A., Zanoteli, E., Donkervoort, S., Taylor, J., Dixon, J., Poke, G., Foley, A. R., Holmes, C., Williams, G., … Muntoni, F. (2018). STAC3 variants cause a congenital myopathy with distinctive dysmorphic

features and malignant hyperthermia susceptibility. *Human Mutation*, *39*(12), 1980–1994. https://doi.org/10.1002/humu.23635

Zhang, Y., Fujii, J., Phillips, M. S., Chen, H. S., Karpati, G., Yee, W. C., Schrank, B., Cornblath, D. R., Boylan, K. B., & MacLennan, D. H. (1995). Characterization of cDNA and genomic DNA encoding SERCA1, the Ca(2+)-ATPase of human fast-twitch skeletal muscle sarcoplasmic reticulum, and its elimination as a candidate gene for Brody disease. *Genomics*, *30*(3), 415–424. https://doi.org/10.1006/geno.1995.1259

Zhao, X., Song, Q., & Gao, Y. (2014). Hypothesis: Exertional Heat Stroke-Induced Myopathy and Genetically Inherited Malignant Hyperthermia Represent the Same Disorder, the Human Stress Syndrome. *Cell Biochemistry and Biophysics*, *70*(2), 1325–1329. https://doi.org/10.1007/s12013-014-0059-5

Appendices

Appendix 1

Table A.1: Primer sequences for each sample type and purpose.

Sample	Forward	Reverse	Purpose
Pygm KO	ACAGGCATCAAAAGGGAGCC	CTGACCACAGGCCAGGAAAA	PCR/Sanger sequencing
Cpt2 KO	AGAAACTCTCGGGCATTGCG	TAGTAAGCTGGAGGCGTGCG	PCR/Sanger sequencing
Pygm KO + *Cpt2* KO	GTAAAACGACGGCCAG	CAGGAAACAGCTATGAC	TA Cloning (M13 primers)
PYGM Lentivirus transduced cells	GGAGAACGTGACTGAGCTGAA	CAGTACCACCTGTGTGTCCA	PCR/Sanger sequencing
CPT2 Lentivirus transduced cells	GGCCCCGCGGTTGGT	CAGAAACCGGATGGCAGAAAC	PCR/Sanger sequencing

Appendix 2

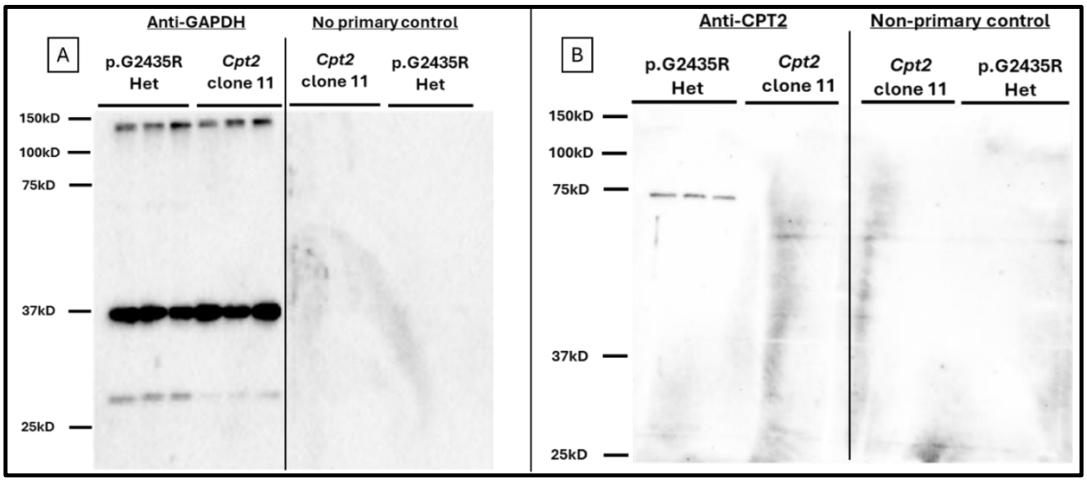

Figure A.1: Full blots for *Cpt2* clone 11. A) Anti-GAPH loading control blot with no primary control. B) Anti-CPT2 blot with no primary control.

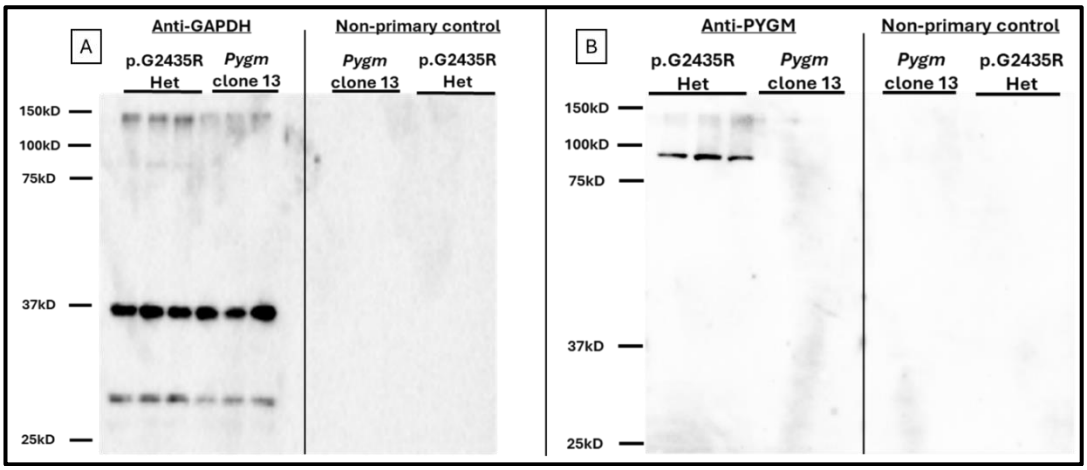

Figure A.2: Full blots for *Pygm* clone 13. A) Anti-GAPH loading control blot with no primary control. B) Anti-PYGM blot with no primary control.

Appendix 3

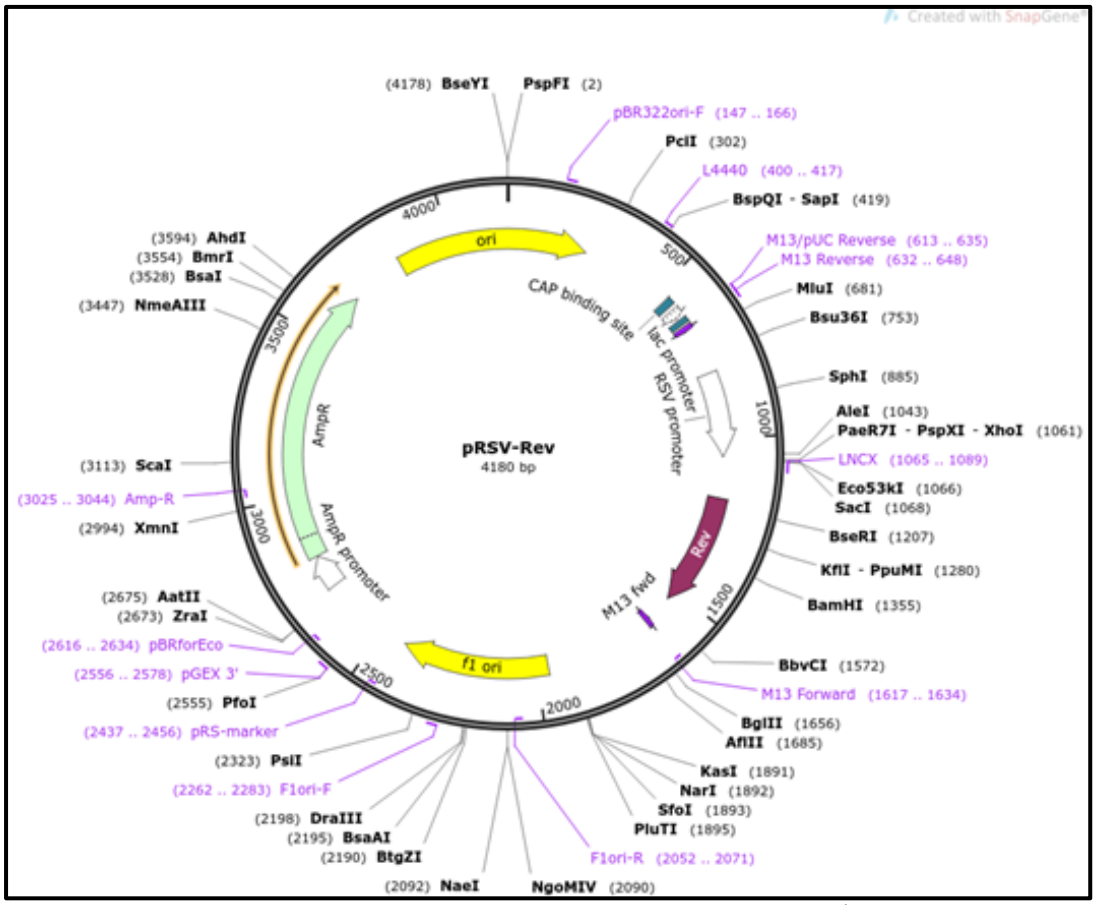

Figure A.3: pRSV-Rev plasmid vector map, from addgene. 3rd generation lentivirus vector packaging plasmid, encoding Rev, to facilitate nuclear transport, under transcriptional control of RSV U3 promoter. Vector also contains ampicillin resistance cassette (AmpR) for bacterial selection during plasmid purification, alongside details of cut sites for restriction enzymes. pRSV-Rev was a gift from Didier Trono (Addgene plasmid # 12253 ; http://n2t.net/addgene:12253 ; RRID:Addgene_12253).

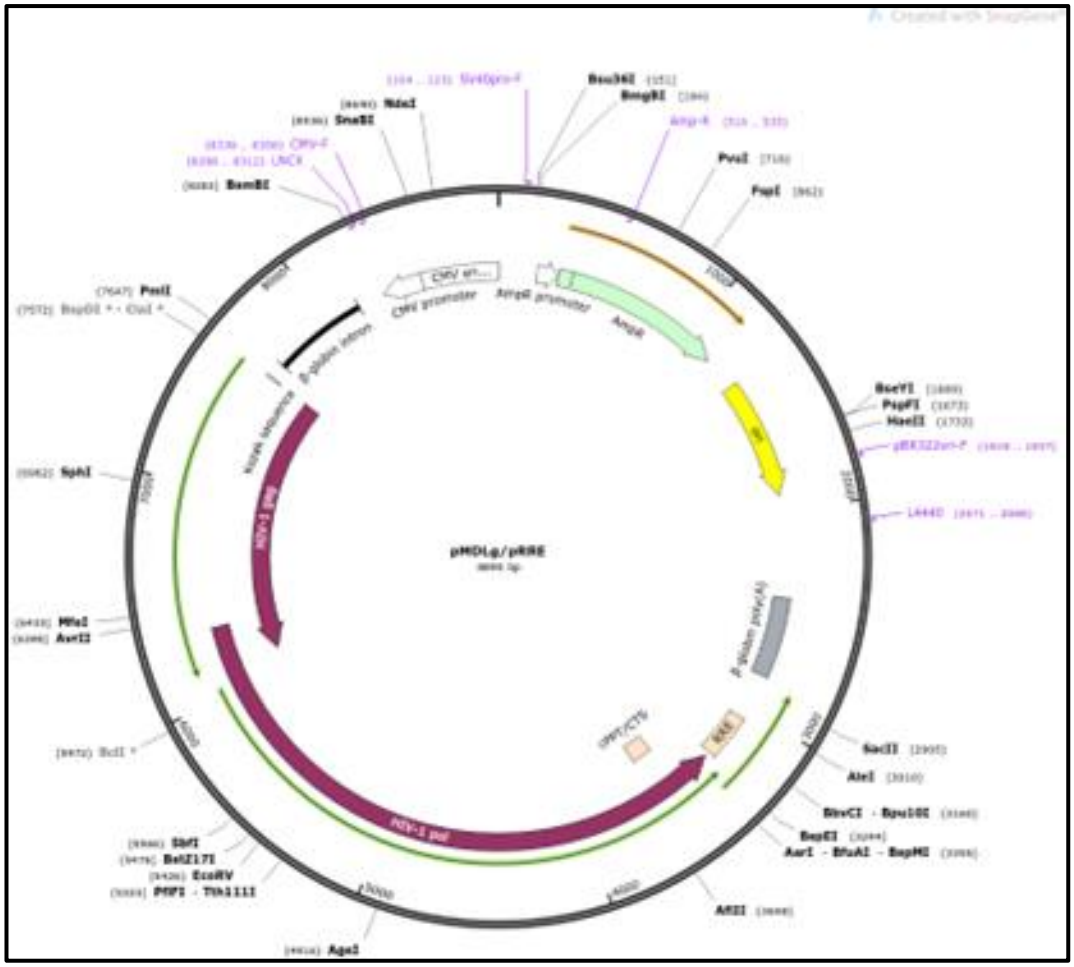

Figure A.4: pMDLg/pRRE plasmid vector map, from addgene. 3rd generation lentivirus vector packaging plasmid, encoding gag, responsible for the virion main structural proteins; pol, responsible for the retrovirus-specific enzymes; and RRE, a binding site for the Rev protein. Vector also contains ampicillin resistance cassette (AmpR) for bacterial selection during plasmid purification, alongside details of cut sites for restriction enzymes. pMDLg/pRRE was a gift from Didier Trono (Addgene plasmid # 12251 ; http://n2t.net/addgene:12251 ; RRID:Addgene_12251).

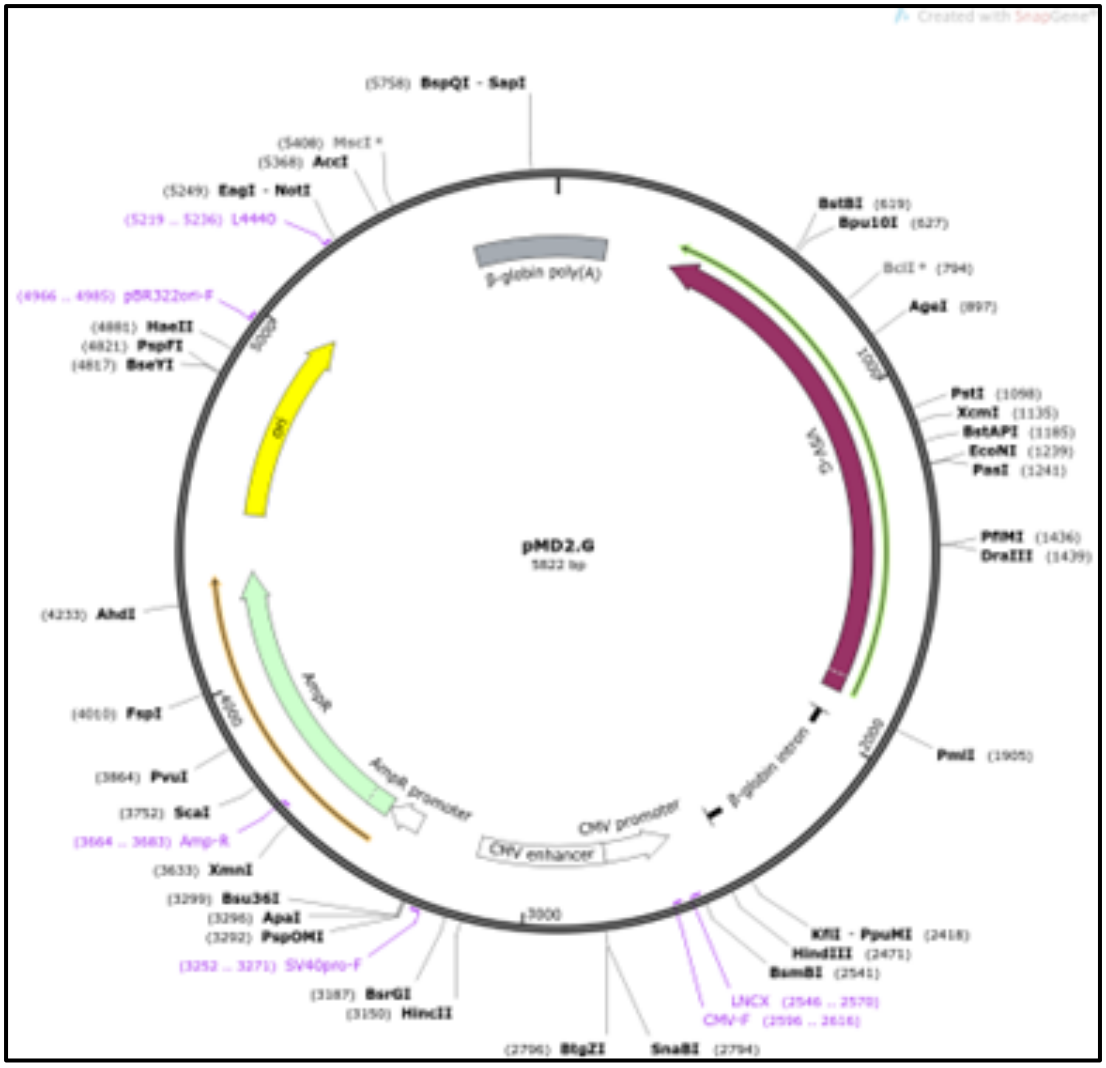

Figure A.5: pMD2.G plasmid vector map, from addgene. 3rd generation lentivirus vector packaging plasmid, encoding VSV-G viral envelope. Vector also contains ampicillin resistance cassette (AmpR) for bacterial selection during plasmid purification, alongside details of cut sites for restriction enzymes. pMD2.G was a gift from Didier Trono (Addgene plasmid # 12259 ; http://n2t.net/addgene:12259 ; RRID:Addgene_12259).

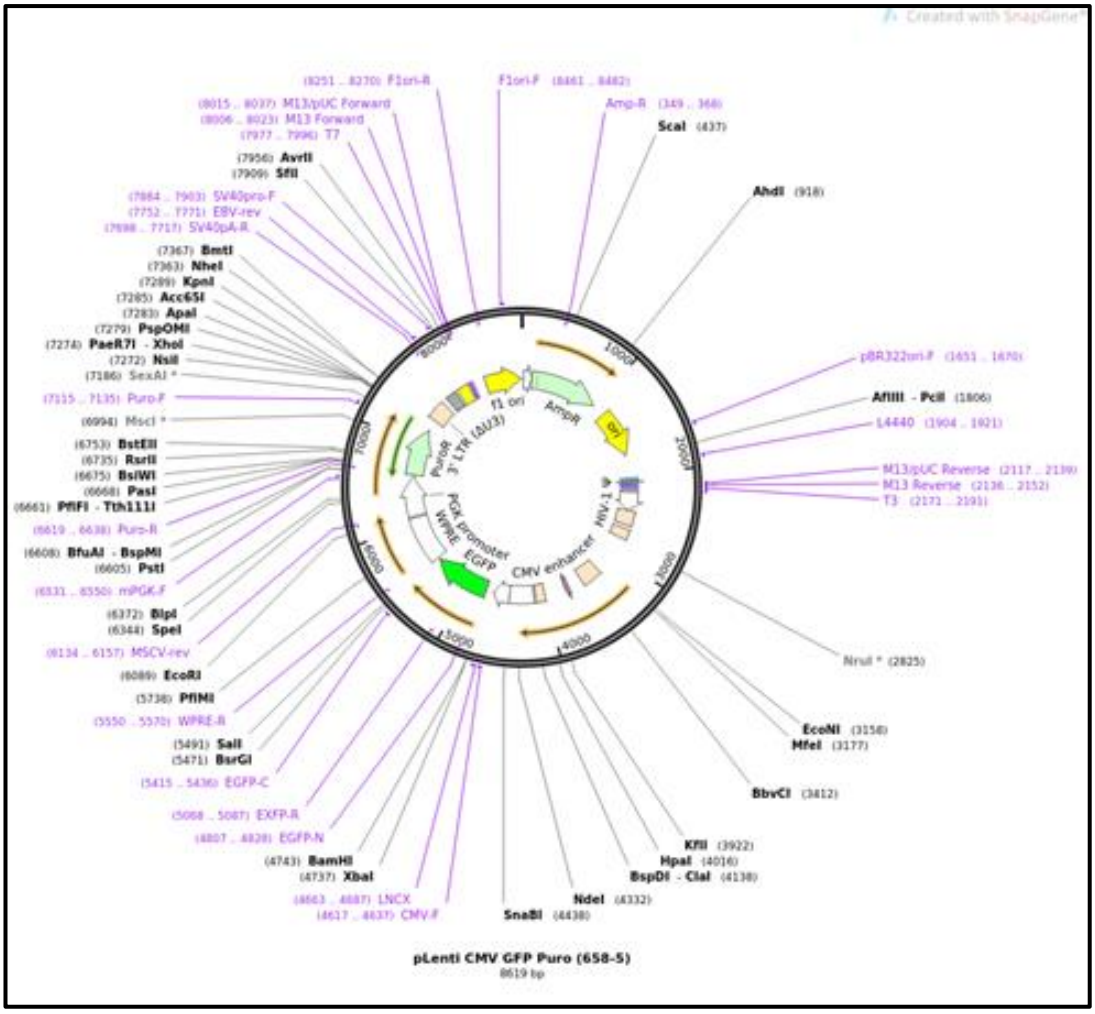

Figure A.6: pLenti CMV GFP Puro (658-5) plasmid vector map, from addgene. 3rd generation lentivirus vector transfer plasmid, encoding eGFP under transcriptional control of CMV promoter, with puromycin selection cassette (PuroR) for mammalian cells. Vector also contains ampicillin resistance cassette (AmpR) for bacterial selection during plasmid purification, alongside details of cut sites for restriction enzymes. pLenti CMV GFP Puro (658-5) was a gift from Eric Campeau & Paul Kaufman (Addgene plasmid # 17448 ; http://n2t.net/addgene:17448 ; RRID:Addgene_17448).

Appendix 4

Table A.2: Hardy-Weinberg equilibrium significance values and allele frequencies for SNPs. Bonferroni Corrected HWE values presented, alongside allele frequencies (AF) and total N numbers for successfully genotype-called samples in each subgroup. Minor allele frequency (MAF) presented for non-Finnish European population as reported in GnomAD v3.1.2.

Gene	rsID	MAF	Minor Allele	Allele 1	Allele 2	Total MHS	MHS 1 AF	MHS 2 AF	MHS HWE	Total MHN	MHN 1 AF	MHN 2 AF	MHN HWE	Total MHSR	MHSR 1 AF	MHSR 2 AF	MHSR HWE
ACADVL	rs17671352	0.36	T	C	T	221	0.66	0.34	ns	248	0.65	0.35	ns	312	0.67	0.33	ns
ACADVL	rs2017365	0.36	G	A	G	494	0.65	0.35	ns	519	0.62	0.38	ns	336	0.66	0.34	ns
ACADVL	rs2521985	0.35	T	C	T	521	0.65	0.35	ns	531	0.65	0.35	ns	345	0.68	0.32	ns
ACADVL	rs35224044	0.4	C	C	T	592	0.92	0.08	ns	531	0.95	0.05	ns	348	0.84	0.16	ns
ACADVL	rs507506	0.4	A	A	G	594	0.39	0.61	ns	531	0.42	0.58	ns	338	0.36	0.64	ns
AMPD1	rs2010899	0.47	G	G	T	591	0.45	0.55	ns	529	0.48	0.52	ns	348	0.45	0.55	ns
AMPD1	rs2268699	0.38	C	A	C	591	0.59	0.41	ns	533	0.62	0.38	ns	340	0.59	0.41	ns
AMPD1	rs55999139	0.07	G	C	G	564	0.92	0.08	ns	429	0.99	0.01	ns	313	0.96	0.04	ns
AMPD1	rs6679869	0.12	C	C	G	441	0.11	0.89	ns	366	0.12	0.88	ns	80	0.08	0.93	ns
AMPD1	rs6701427	0.14	C	C	T	593	0.13	0.87	ns	531	0.15	0.85	ns	338	0.15	0.85	ns
AMPD1	rs76710407	0.09	A	A	G	591	0.09	0.91	ns	530	0.08	0.92	ns	338	0.07	0.93	ns
AMPD1	rs77720559	0.09	G	C	G	585	0.87	0.13	ns	531	0.91	0.09	ns	342	0.93	0.07	ns
ATP2A1	rs3888190	0.39	T	G	T	589	0.60	0.40	ns	525	0.63	0.37	ns	348	0.59	0.41	ns
ATP2A1	rs6565261	0.29	A	A	C	450	0.29	0.71	ns	362	0.29	0.71	ns	73	0.36	0.64	ns
ATP2A1	rs7498555	0.39	C	C	T	586	0.50	0.50	<0.0001	526	0.50	0.50	<0.0001	349	0.48	0.52	<0.0001
ATP2A1	rs8046545	0.35	G	A	G	440	0.62	0.38	<0.0001	359	0.70	0.30	ns	319	0.65	0.35	ns
ATP2A1	rs8056890	0.35	A	A	G	594	0.37	0.63	ns	532	0.34	0.66	ns	335	0.35	0.65	ns
ATP2A1	rs8060365	0.35	C	A	C	583	0.64	0.36	ns	525	0.65	0.35	ns	346	0.64	0.36	ns
ATP2A1	rs9931989	0.35	G	C	G	591	0.64	0.36	ns	531	0.65	0.35	ns	348	0.65	0.35	ns
CACNA1S	rs10800757	0.47	T	C	T	593	0.58	0.42	ns	530	0.58	0.42	ns	337	0.75	0.25	<0.0001
CACNA1S	rs12409114	0.41	T	A	T	508	0.62	0.38	ns	471	0.62	0.38	ns	258	0.64	0.36	<0.01
CACNA1S	rs2296383	0.43	T	C	T	594	0.57	0.43	ns	532	0.57	0.43	ns	338	0.58	0.42	ns
CACNA1S	rs3767499	0.47	C	C	T	585	0.48	0.52	ns	525	0.44	0.56	ns	338	0.46	0.54	ns

CACNA1S	rs4498834	0.43	C	C	T	587	0.43	0.57	ns	532	0.45	0.55	ns	348	0.41	0.59	ns
CACNA1S	rs734881	0.42	A	A	G	590	0.37	0.63	ns	531	0.40	0.60	ns	337	0.31	0.69	<0.0001
CACNA2D1	rs10237261	0.47	A	A	G	596	0.49	0.51	ns	531	0.50	0.50	ns	347	0.49	0.51	ns
CACNA2D1	rs12536871	0.44	T	G	T	592	0.48	0.52	ns	532	0.51	0.49	ns	291	0.46	0.54	ns
CACNA2D1	rs17247184	0.46	T	C	T	593	0.55	0.45	ns	531	0.58	0.42	ns	338	0.57	0.43	ns
CACNA2D1	rs2237505	0.44	T	C	T	594	0.57	0.43	ns	529	0.56	0.44	ns	348	0.58	0.42	ns
CACNA2D1	rs2237527	0.48	T	C	T	593	0.48	0.52	ns	531	0.55	0.45	ns	342	0.54	0.46	ns
CACNA2D1	rs258677	0.4	T	G	T	590	0.62	0.38	ns	529	0.61	0.39	ns	338	0.64	0.36	ns
CACNA2D1	rs258690	0.4	C	C	T	584	0.46	0.54	ns	527	0.48	0.52	ns	347	0.46	0.54	ns
CACNA2D1	rs35985094	0.4	T	C	T	577	0.59	0.41	ns	528	0.59	0.41	ns	340	0.60	0.40	ns
CACNA2D1	rs37134	0.41	G	C	G	591	0.57	0.43	ns	530	0.58	0.42	ns	348	0.58	0.42	ns
CACNA2D1	rs4732435	0.49	A	A	G	586	0.50	0.50	<0.0001	530	0.55	0.45	ns	338	0.56	0.44	ns
CACNA2D1	rs2190232	0.41	T	T	C	136	0.81	0.19	ns	196	0.83	0.17	ns	72	0.82	0.18	ns
CASQ1	rs11265351	0.21	A	A	G	589	0.12	0.88	<0.0001	530	0.11	0.89	<0.05	338	0.08	0.92	ns
CASQ1	rs11265352	0.38	A	A	G	594	0.38	0.62	ns	531	0.41	0.59	ns	338	0.38	0.62	ns
CASQ1	rs12070418	0.26	A	A	G	593	0.28	0.72	ns	531	0.25	0.75	ns	348	0.30	0.70	ns
CASQ1	rs3747623	0.38	T	C	T	585	0.64	0.36	ns	527	0.58	0.42	<0.0001	338	0.68	0.32	ns
CASQ1	rs60043899	0.12	A	A	T	592	0.12	0.88	ns	531	0.12	0.88	ns	339	0.12	0.88	ns
CASQ1	rs617698	0.39	G	A	G	450	0.63	0.37	ns	360	0.65	0.35	ns	70	0.56	0.44	ns
CASQ1	rs686015	0.43	A	A	T	588	0.59	0.41	ns	529	0.57	0.43	ns	336	0.63	0.37	ns
CPT2	rs1056425	0.32	T	C	T	595	0.68	0.32	ns	531	0.68	0.32	ns	339	0.67	0.33	ns
CPT2	rs10888776	0.46	G	A	G	591	0.55	0.45	ns	531	0.53	0.47	ns	338	0.58	0.42	ns
CPT2	rs1799821	0.46	G	A	G	591	0.59	0.41	<0.05	529	0.58	0.42	<0.001	338	0.60	0.40	ns
CPT2	rs2062015	0.46	G	C	G	597	0.42	0.58	ns	532	0.46	0.54	ns	349	0.42	0.58	ns
CPT2	rs6692897	0.44	A	A	G	590	0.51	0.49	<0.0001	531	0.51	0.49	<0.0001	349	0.50	0.50	<0.0001
CPT2	rs737464	0.46	T	C	T	592	0.55	0.45	ns	530	0.53	0.47	ns	338	0.58	0.42	ns
CPT2	rs7539949	0.46	G	A	G	591	0.08	0.92	ns	532	0.11	0.89	<0.01	347	0.34	0.66	ns
CPT2	rs78117157	0.11	T	C	T	591	0.88	0.12	ns	531	0.88	0.12	ns	341	0.83	0.17	ns
PYGM	rs477549	0.1	A	A	G	549	0.91	0.09	ns	522	0.89	0.11	ns	317	0.91	0.09	ns

PYGM	rs506354	0.09	C	C	T	595	1.00	0.00	ns	530	1.00	0.00	ns	343	0.92	0.08	ns
PYGM	rs523200	0.11	C	A	C	577	0.89	0.11	<0.0001	518	0.86	0.14	<0.0001	346	0.90	0.10	ns
PYGM	rs547066	0.09	A	A	C	534	0.08	0.92	ns	467	0.09	0.91	ns	270	0.09	0.91	ns
PYGM	rs555974	0.09	T	T	G	597	1.00	0.00	ns	534	1.00	0.00	ns	273	1.00	0.00	ns
PYGM	rs569602	0.09	G	A	G	565	0.93	0.07	ns	523	0.91	0.09	ns	334	0.92	0.08	ns
PYGM	rs630966		C	C	G	536	0.08	0.92	ns	473	0.10	0.90	ns	296	0.10	0.90	ns
PYGM	rs592521	0.09	C	C	T	599	0.50	0.50	<0.0001	531	0.50	0.50	<0.0001	349	0.50	0.50	<0.0001
STAC3	rs10876968	0.28	T	G	T	594	0.70	0.30	ns	528	0.73	0.27	ns	339	0.70	0.30	ns
STAC3	rs11172134	0.19	A	T	A	591	0.81	0.19	ns	528	0.81	0.19	ns	342	0.81	0.19	ns
STAC3	rs3204635	0.28	T	C	T	586	0.54	0.46	<0.0001	522	0.55	0.45	<0.0001	346	0.57	0.43	ns
STAC3	rs7133915	0.48	C	T	C	538	0.07	0.93	ns	448	0.00	1.00	ns	173	0.00	1.00	ns
TRPV1	rs12936340	0.36	G	A	G	590	0.61	0.39	ns	533	0.63	0.37	ns	339	0.65	0.35	ns
TRPV1	rs161366	0.49	C	C	T	596	0.99	0.01	ns	532	1.00	0.00	ns	349	1.00	0.00	ns
TRPV1	rs182637	0.45	A	A	G	356	0.43	0.57	ns	527	0.46	0.54	ns	267	0.41	0.59	ns
TRPV1	rs224534	0.36	A	A	G	593	0.34	0.66	ns	530	0.35	0.65	ns	339	0.35	0.65	ns
TRPV1	rs224537	0.36	A	A	G	445	0.34	0.66	ns	354	0.34	0.66	ns	70	0.36	0.64	ns
TRPV1	rs224546	0.43	C	C	T	566	0.42	0.58	ns	508	0.43	0.57	ns	345	0.44	0.56	ns
TRPV1	rs8078936	0.37	T	C	T	532	0.64	0.36	ns	459	0.64	0.36	ns	315	0.63	0.37	ns

Table A.3: Hardy-Weinberg equilibrium significance values and allele frequencies for pathogenic variants. Bonferroni Corrected HWE values presented, alongside allele frequencies (AF) and total N numbers for successfully genotype-called samples in each subgroup. Minor allele frequency (MAF) presented for non-Finnish European population as reported in GnomAD v3.1.2.

Gene	Protein change	DNA change	rsID	MAF	Minor Allele	Total MHS	MHS MAF	MHS HWE	Total MHN	MHN MAF	MHN HWE	Total MHSR	MHSR MAF	MHSR HWE
ACADVL	p.G441D	c.1322G>A	rs2309689	4.41E-05	A	430	0	ns	356	0	ns	69	0.028986	ns
ACADVL	p.R459Q	c.1376G>A	rs751995154	5.88E-05	A	594	0.045455	ns	529	0	ns	348	0.021552	ns
ACADVL	p.V283A	c.848T>C	rs113994167	0.001809	C	579	0.028497	ns	531	0.000942	ns	346	0.001445	ns
AMPD1	p.M343I	c.1029G>T	rs61752478	0.004586	A	512	0.004883	ns	531	0.037665	ns	341	0.039589	ns
AMPD1	p.Q12X	c.34C>T	rs17602729	0.1323	A	509	0.105108	ns	531	0.145951	ns	338	0.093195	ns
ATP2A1	p.C675X	c.2025C>A	rs121918114	1.71E-05	A	440	0.001136	ns	351	0.035613	<0.0001	70	0.014286	ns
ATP2A1	p.E982K	c.2944G>A	rs538702357	0	A	589	0.001698	ns	531	0.00565	ns	333	0.046547	ns
ATP2A1	p.P789K	c.2366C>T	rs121918115	1.47E-05	T	595	0.047899	ns	529	0.030246	ns	344	0	ns
ATP2A1	p.R198X	c.592C>T	rs121918113	1.47E-05	T	596	0.003356	ns	530	0.033019	ns	337	0.047478	ns
ATP2A1	p.R560C	c.1678C>T	rs761592113	0	T	592	0.005912	ns	530	0	ns	337	0.01632	ns
CACNA1S	p.R1239G	c.3715C>G	rs28930069	0	C	594	0.001684	ns	530	0.000943	ns	348	0.002874	ns
CACNA1S	p.R1239H	c.3716G>A	rs28930068	0	T	595	0.108403	ns	531	0.079096	ns	348	0	ns
CACNA1S	p.R528H	c.1583G>A	rs80338777	1.47E-05	T	590	0.000847	ns	531	0	ns	348	0	ns
CACNA2D1	p.D1045A	c.3134A>C	rs35131433	0.006797	G	588	0.006803	ns	519	0.00578	ns	322	0.001553	ns
CASQ1	p.D244G	c.731A>G	rs730882052	-	G	590	0.001695	ns	533	0	ns	338	0	ns
CPT2	p.P50H	c.149C>A	rs28936375	0.000191	A	549	0.009107	<0.01	422	0.003555	ns	278	0.016187	ns
CPT2	p.S113L	c.338C>T	rs74315294	0.001999	T	586	0.006826	ns	530	0.003774	ns	339	0.007375	ns
PYGM	p.A193S	c.577G>T	rs77656150	0.002984	A	4	0	ns	5	0	ns	56	0.008929	ns
PYGM	p.G205S	c.613G>A	rs119103251	0.000397	T	439	0.022779	ns	359	0	ns	69	0	ns
PYGM	p.R50X	c.148C>T	rs116987552	0.003116	A	593	0.005902	ns	393	0.002545	ns	296	0.005068	ns
PYGM	p.W798R	c.2392T>C	rs119103258	2.95E-05	G	586	0.090444	ns	530	0.004717	ns	338	0	ns
PYGM	p.Y85X	c.255C>A	rs527236146	4.52E-06	T	559	0.004472	ns	520	0	ns	342	0	ns
STAC3	p.K288X	c.862A>T	rs371720347	0.000235	A	589	0	ns	530	0	ns	347	0	ns
STAC3	p.W284S	c.851G>C	rs140291094	5.88E-05	G	445	0	ns	358	0	ns	69	0	ns
TRPV1	p.G684V	c.2051G>T	rs759094783	2.86E-06	A	579	0	ns	433	0	ns	265	0	ns
TRPV1	p.R772C	c.2314C>T	rs1217651219	2.94E-05	A	0	0	ns	63	0	ns	0	0	ns